

**NOTTINGHAM  
TRENT UNIVERSITY**



**DEVELOPMENT OF A NOVEL 3D  
NANOFIBRE CO-CULTURE MODEL FOR  
CHARACTERISATION OF NEURAL CELL  
DEGENERATION**

**Joseph Mathew Chemmarappally  
(N0404816)**

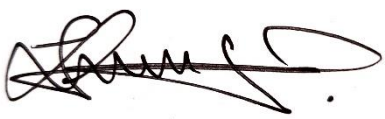
A thesis submitted in partial fulfilment of the  
requirements of Nottingham Trent University for the  
degree of Doctor of Philosophy

**Supervisor team: Prof Bob Stevens,  
Dr Luigi De Girolamo & Dr Alan Hargreaves**

**October 2019**

## **DECLARATION OF OWNERSHIP**

This submission is the result of my work. All help and advice, other than that received from tutors, has been acknowledged and primary and secondary sources of information have been properly attributed. Should this statement prove to be untrue, I recognise the right and duty of the Board of Examiners to recommend what action should be taken in line with the University's regulations on assessment contained in the Handbook

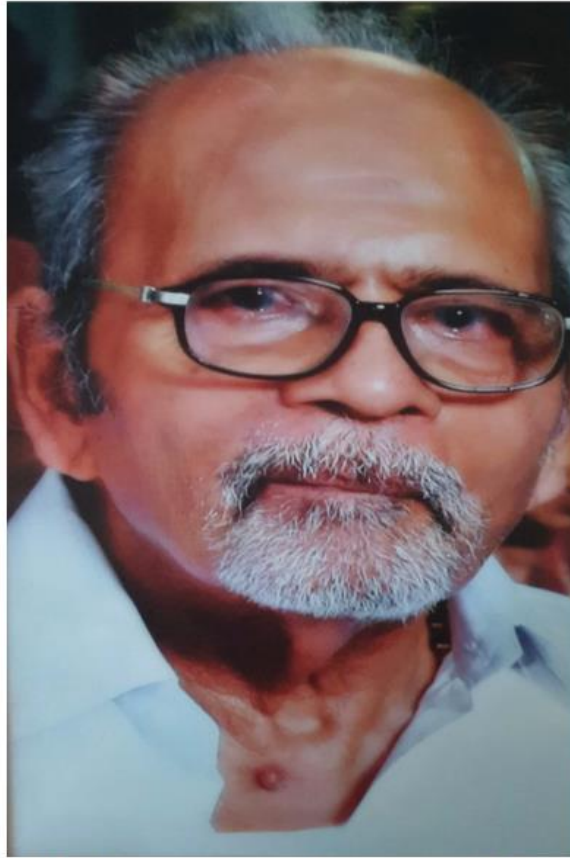
Sign.....

Date..... 28/10/2019.....

## **Copyright Statement**

This work is the intellectual property of the author, and may also be owned by the research sponsor(s) and/or Nottingham Trent University. You may copy up to 5% of this work for private study, or personal, non-commercial research. Any re-use of the information contained within this document should be fully referenced, quoting the author, title, university, degree level and pagination. Queries or requests for any other use, or if a more substantial copy is required, should be directed in the owner(s) of the Intellectual Property Rights.

## **Dedication**



**In loving memory of my grandfather  
Thomas Chandy Konnath  
30/08/1935 - 06/09/2015**

I want to dedicate my research to my loving grandfather Mr. Thomas Chandy Konnath, who sadly passed away due to Parkinson's disease. He is the reason I choose to pursue research on neurodegenerative disease, and I hope to make a difference, even in the smallest way possible.

## **Acknowledgements**

First, I want to sincerely thank my director of studies Prof Bob Stevens, for constant support and guidance throughout my PhD journey. I cannot thank enough Dr Luigi De Girolamo (Gino) and Dr Alan Hargreaves for giving me this fantastic opportunity to work alongside them. I am immensely grateful to Bob Stevens for being enthusiastic, motivating, providing thoughtful advice, being an inspiration and for being my mentor. Thanks to Dr Gino for being very supportive through every possible moment for the past 9 years and for becoming a good friend. My sincere thanks to Dr Alan for constant expert advice, guidance and support in this challenging journey. I would also like to express my gratitude to NTU QR funding, Vice Chancellor bursary and the Physics department NTU for funding my PhD studentship.

A special thanks to the Physics department and IBRC technical support team Daniel Yates, Christopher Mutton, Ryan Toms, Dr Jacob Spears, Dave Parker and Dr Kathryn Kroon for all the spontaneous help and support without any hesitation. A big thanks to Dr Sammy Cheung for helping me and training me on OCT imaging. Dr Neranga Abeywickrama, thank you for educating me on many types of equipment, helping me out every time I wanted something and for putting up with me for seven years. Dr Enzo Fornair, Dr Costas Tsakonas, Dr Demosthenes Koutsogeorgis and Dr Nikolaos Kalfagiannis thank you so much for the help and support at times and for all the fun times and laughs at iSMART. James, Jodie and Cristina, I have known you guys only for a short time but you guys have made an impact and thanks for the support at times.

A very big thank you to my closest friend Henry Pegram and Michael Cripps for all the fantastic time, motivation and for supporting me like family during this journey, you both have made this journey so easy. This would be incomplete without all my dear fantastic friends/PhD colleagues at NTU for their company and support during hard times especially, Dan, Magda, Pauline, Sarah, Anna, Anahita, Simon, Devika, Nick, Awais, Jordan, Laura, Falguni, Elisa, Grace, Charlotte, Veeru and Brijesh. Also, a big thank you to my lovely friends back in India for the push and support every time I needed one. This PhD journey has not only given me knowledge and skill but also beautiful and wonderful memories that I would cherish forever.

I must thank my lovely, sweetest best friend, my full-time accomplice and my inspiration, Dr Divya Nagarajan, for being with me through all the happiest and saddest moments. None of this would have happened if she was not there to guide me through the right path. She pushed me from being an average student to a PhD holder and made me what I am today. My path would have stayed lost without her. Finally, a very big thank you to my lovely dad, my sweet mom, my caring sister and a supportive brother-in-law for helping me and supporting me through every possible situation to achieve my goal. I hope I have made you all proud.

# Table of Contents

<b>LIST OF FIGURE .....</b>	<b>I</b>
<b>LIST OF TABLES .....</b>	<b>V</b>
<b>ABBREVIATIONS .....</b>	<b>VI</b>
<b>ABSTRACT .....</b>	<b>IX</b>
<b>CHAPTER 1: MAIN INTRODUCTION .....</b>	<b>1</b>
<b>1.1 Electrospinning .....</b>	<b>1</b>
1.1.1 Nanofibres.....	2
1.1.2 Polyacrylonitrile.....	3
1.1.3 Polyetheramines.....	5
1.1.4 Nanofibres for <i>In vitro</i> model .....	6
1.1.5 Application of nanofibres in bioscience .....	7
1.1.6 Nanofibre and tissue engineering .....	9
<b>1.2 Neurodegenerative Disease .....</b>	<b>13</b>
1.2.2 Midbrain hub of motor movements.....	16
1.2.2.1 Neurons .....	17
1.2.2.2 Glial Cells .....	18
1.2.2.3 Role of Astrocytes.....	19
1.2.4 Neurotoxins .....	23
1.2.4.1 Rotenone.....	24
1.2.4.2 MPTP .....	24
1.2.4.3 MG132 .....	24
1.2.4.4 BSO.....	25
<b>1.3 <i>In vitro</i> cell Models for neural cell degeneration.....</b>	<b>25</b>
1.3.1 Toxin Models.....	26
1.3.1.1 6-hydroxydopamine (6-OHDA) .....	27
1.3.1.2 1-Methyl-4-Phenyl-1,2,3,6-Tetrahydropyridine (MPTP) .....	27
1.3.1.3 Rotenone.....	27
1.3.2 Genetic Models.....	29
1.3.3 Pre-clinical models of neural cell degeneration .....	29
<b>1.4 3D Cell Culture.....</b>	<b>32</b>
1.4.1 Cellular Spheroids .....	34
1.4.2 Hydrogel models .....	36
1.4.3 Engineering based scaffolds for neural tissue construction .....	37
1.4.4 Microfluidic technology models .....	38
<b>1.5 Novelty of This Study.....</b>	<b>40</b>
1.5.1 Structure of this study .....	41
<b>CHAPTER 2: MATERIALS AND METHODS.....</b>	<b>43</b>

<b>2.1 Materials.....</b>	<b>43</b>
2.1.1 Cell Culture .....	43
2.1.1.1 Cell Lines.....	43
2.1.1.2 Cell Culture Reagents .....	43
2.1.1.2.1 Cell Culture Media .....	43
2.1.1.2.2 Common Cell Culture Reagents .....	44
2.1.2 Plastic, Glassware and other materials.....	44
2.1.3 Chemicals and reagents .....	45
2.1.4 Equipment.....	47
2.1.5 Antibody .....	50
2.1.5.1 Primary Antibody .....	50
2.1.5.2 Secondary Antibodies .....	51
<b>2.2 Methods .....</b>	<b>52</b>
2.2.1 Design engineering and laser cutting .....	52
2.2.1.1 Suspended random nanofibre scaffolds .....	52
2.2.1.2 Aligned nanofibre.....	54
2.2.1.3 Radial nanofibre .....	56
2.2.2 Electrospinning solution preparation .....	58
2.2.2.1 Rheometer measurement.....	58
2.2.3 Electrospinning .....	60
2.2.3.1 SEM analysis.....	63
2.2.3.2 Contact angle analysis.....	63
2.2.3.3 Optical Coherence Tomography .....	64
2.2.3.4 Nanofibre sterilisation analysis.....	65
2.2.4 Cell Culture .....	65
2.2.4.1 Clonal Cell lines .....	65
2.2.4.1.1 Human SH-SY5Y neuroblastoma.....	65
2.2.4.1.2 Human U-87 MG glioblastoma.....	66
2.2.4.1.3 Viable cell count and seeding .....	66
2.2.4.1.4 Cryo-preservation of cells.....	67
2.2.4.1.5 Revival of cryo-preserved cells.....	67
2.2.4.1.5 Neural cell differentiation .....	67
2.2.4.2 Neural progenitor cells ReNcell CX.....	68
2.2.4.2.1 Laminin coating .....	68
2.2.4.2.2 ReNcell CX maintenance medium .....	68
2.2.4.2.3 Revival of cryo-preserved cells.....	69
2.2.4.2.4 Sub-culturing of ReNcell CX cells .....	69
2.2.4.2.5 Viable cell count and seeding .....	70
2.2.4.2.6 ReNcell cell differentiation .....	70

2.2.4.3 Primary Cells.....	70
2.2.4.3.1 Preparation for tissue processing .....	71
2.2.4.3.2 Cell dissociation and seeding .....	71
2.2.5 Cell Culture on nanofibre scaffolds .....	72
2.2.5.1 Nanofibre Sterilisation before cell seeding .....	72
2.2.5.2 Clonal cells .....	73
2.2.5.3 ReNcell CX.....	73
2.2.5.4 Primary Cells.....	73
2.2.6 Cell Viability assay .....	74
2.2.6.1 Trypan blue exclusion assay .....	74
2.2.6.3 CellTiter-Glo® 3D .....	74
2.2.7 Cell Proliferation assay .....	75
2.2.7.1 MTT cell metabolic Assay .....	75
2.2.8 Effect of glial ECM on neurons .....	76
2.2.9 Sample preparation for microscopy .....	76
2.2.9.1 Methanol fixation .....	76
2.2.9.2 Immunofluorescence antibody staining .....	76
2.2.10 Protein levels identification.....	77
2.2.10.1 SDS-PAGE electrophoresis.....	77
2.2.10.1.1 Total protein cell lysate from cell grown on TCP .....	77
2.2.10.1.2 Total protein extraction from fibre .....	78
2.2.10.1.3 Protein quantification by mini Lowry.....	79
2.2.10.1.4 Preparation of resolving gel .....	79
2.2.10.1.5 Preparation of stacking gel .....	80
2.2.10.1.6 Preparation of samples for separation by SDS-PAGE.....	81
2.2.10.2 Western Blotting .....	82
2.2.10.3 Immunoprobng for proteins .....	82
2.2.10.4 Quantification of western blots.....	83
2.2.11 Toxins investigation .....	83
2.2.12 Co-Culture Model to investigate the effect of Toxins.....	84
2.2.13 Statistical analysis .....	86
2.2.13.1 Polymer absorbance analysis .....	86
2.2.13.2 Rheology measurement .....	86
2.2.13.3 Nanofibre Diameter and Pore size measurement.....	87
2.2.13.4 Proliferation and Viability analysis .....	87
<b>CHAPTER 3: NANOFIBRE FABRICATION AND ANALYSIS .....</b>	<b>88</b>
<b>3.1 Introduction .....</b>	<b>88</b>
3.1.1 Content of this chapter.....	92
<b>3.2 Results.....</b>	<b>93</b>

3.2.1 Engineered designs.....	93
3.2.2 Polymer preparation .....	94
3.2.3 Electrospinning solution rheology properties .....	95
3.2.4 Electrospinning .....	96
3.2.4.1 Random Nanofibre Scaffolds.....	98
3.2.4.1.1 SEM and FibreMetric analysis .....	98
3.2.4.1.2 Contact angle measurement .....	100
3.2.4.1.3 Scaffold thickness measurement .....	101
3.2.4.2 Aligned nanofibre.....	102
3.2.4.2.1 SEM and FibreMetric analysis .....	103
3.2.4.2.2 Contact angle measurement .....	106
3.2.4.2.3 Scaffold thickness measurement .....	107
3.2.4.3 Radial Nanofibre .....	109
3.2.4.3.1 FibreMetric analysis .....	109
3.2.5 Nanofibre sterilisation .....	111
3.2.5.1 Ethanol treatment.....	111
3.2.5.2 Ultra-violet treatment.....	114
3.2.5.3 Antibiotic treatment .....	117
<b>3.3 Discussion .....</b>	<b>120</b>
<b>3.4 Conclusion .....</b>	<b>127</b>
<b>CHAPTER 4: IMMORTALISED CELL LINE SCAFFOLD MODEL ....</b>	<b>128</b>
<b>4.1 Introduction .....</b>	<b>128</b>
4.1.1 SH-SY5Y Human Neuroblastoma.....	129
4.1.1.1 Undifferentiated and differentiated SH-SY5Y cells .....	129
4.1.1.2 Markers of Differentiation.....	131
4.1.2 U-87 MG Human Glioblastoma.....	131
4.1.2.1 Differentiated U-87 MG Cells .....	132
<b>4.2 Content of this chapter .....</b>	<b>133</b>
<b>4.3 Results.....</b>	<b>134</b>
4.3.1 Culturing and subculturing .....	134
4.3.2 Cell culture on nanofibres scaffolds .....	135
4.3.2.1 Unsuspended random nanofibre.....	135
4.3.2.2 Suspended random nanofibres scaffolds.....	137
4.3.2.3 Aligned nanofibre scaffolds.....	139
4.3.3 Cytoskeletal staining and SEM analysis .....	140
4.3.4 Cell attachment and growth .....	142
4.3.5 Investigation of U-87MG growth in DMEM .....	145
4.3.6 Cell differentiation .....	147
4.3.6.1 Immunofluorescence staining of differentiation markers .....	147
4.3.6.2 Protein expression analysis .....	152

4.3.7 Toxicology analysis on SH-SY5Y and U-87MG on both TCP and 3D nanofibres .....	157
4.3.8 Effect of the glial extracellular matrix on neurones .....	161
4.3.9 Development of a 3D co-culture model .....	164
4.3.9.1 Establishment of co-culture with neuronal cells on the 2D surface and glial cell on PJ fibre.....	164
4.3.9.2 Co-culture with glial cells on the 2D surface and neuronal cell on PAN fibre .....	165
4.3.9.3 Establishment of a 3D nanofibre based co-culture model with differentiated neuronal and glial cells. ....	166
<b>4.4 Discussion .....</b>	<b>169</b>
<b>4.5 Conclusion .....</b>	<b>175</b>
<b>CHAPTER 5: STEM &amp; PRIMARY CELLS SCAFFOLD MODEL .....</b>	<b>176</b>
<b>5.1 Introduction .....</b>	<b>176</b>
5.1.1 Neural Stem cells .....	176
5.1.2 Primary cell cultures .....	177
<b>5.2 Content of this chapter .....</b>	<b>180</b>
<b>5.3 Results.....</b>	<b>181</b>
5.3.1 ReNcells CX human neural progenitor cell line.....	181
5.3.1.1 Culturing and subculturing .....	181
5.3.1.2 Culturing on nanofibre scaffolds .....	183
5.3.1.3 ReNcell CX attachment and growth.....	184
5.3.1.4 Cell differentiation .....	186
5.3.1.5 Effects of toxins on ReNcells CX .....	188
5.3.2 Primary neurons and glial cells .....	190
5.3.2.1 Culturing of primary cells on TCP and fibres.....	190
5.3.2.2 Primary cell metabolic activity .....	190
5.3.2.3 Immunofluorescence .....	194
5.3.2.4 3D co-culture model.....	196
<b>5.4 Discussion .....</b>	<b>200</b>
<b>5.5 Conclusion .....</b>	<b>205</b>
<b>CHAPTER 6: MAIN DISCUSSION .....</b>	<b>206</b>
<b>6.1 Introduction .....</b>	<b>206</b>
<b>6.2 Electrospinning biomaterials scaffolds for in vitro cell culture and tissue engineering. ....</b>	<b>208</b>
<b>6.3 3D scaffolds vs 2D TCP on immortalised cells .....</b>	<b>211</b>
<b>6.4 Investigation of stem cell and primary cell on PAN and PJ nanofibre scaffolds .....</b>	<b>215</b>
<b>7.0 CONCLUSION AND FUTURE WORK.....</b>	<b>218</b>
<b>7.1 Conclusion .....</b>	<b>218</b>
<b>7.2 Future Work.....</b>	<b>221</b>
7.2.1 Polymers and nanofibres .....	221

7.2.2 Cells based techniques .....	222
7.2.3 Other nanofibre based studies .....	223
<b>REFERENCE .....</b>	<b>227</b>

## List of Figure

### Chapter I

Figure 1. 1 Schematic illustration of the basic electrospinning process setup. ....	2
Figure 1. 2 Chemical structure of Jeffamine® ED series. ....	5
Figure 1. 3: Schematic diagram showing Neurodegeneration pathophysiology associated pathways.....	16
Figure 1. 5: Potential neuroprotective pathways of astrocytes. ....	21
Figure 1. 6: Chemical structure for neurotoxins used in this study. ....	23

### Chapter II

Figure 2. 1: Schematic representation of random fibre design with measurements .....	53
Figure 2. 2: Random fibre cross-sectional view. ....	53
Figure 2. 3: Schematic diagram for aligned fibre template. ....	55
Figure 2. 4: Aligned fibre cross-sectional view. ....	56
Figure 2. 5: Schematic diagram Radial fibre design. ....	57
Figure 2. 6: Radial fibre cross-sectional view .....	58
Figure 2. 7: Schematic representation of HAAKE™ CaBER™ 1 .....	59
Figure 2. 8: Schematic representation of polymer filament formation and measurement using the HAAKE™ CaBER™ 1 Capillary Breakup Extensional Rheometer works.....	60
Figure 2. 9: Schematic representation of our in-house built electrospinning system .....	62
Figure 2. 10: Schematic representation of contact angle measurement to identify the hydrophobicity of a surface.....	64
Figure 2. 11: Schematic representation of the experimental setup designed to create a co-culture system.....	85

### Chapter III

Figure 3. 1: Laser speed and power settings optimisation.....	93
Figure 3. 2: PAN and PJ polymers dissolved in DMF. ....	95

Figure 3. 3: PAN and PJ viscosity measurement. ....	96
Figure 3. 4: Schematic representation of jet flow formation. ....	96
Figure 3. 5: Temperature and humidity analysis during electrospinning. .....	97
Figure 3. 6: PAN SEM and FibreMetric analysis data.....	99
Figure 3. 7: PJ SEM and FibreMetric analysis data. ....	99
Figure 3. 8: Random fibre contact angle analysis.....	101
Figure 3. 9: OCT measurement for random PAN and PJ scaffold. ....	102
Figure 3. 10: Aligned nanofibre design SEM imaging.....	104
Figure 3. 11: FibreMetric data for Aligned PAN fibre scaffold. ....	105
Figure 3. 12: Aligned fibre contact angle analysis. ....	106
Figure 3. 13: OCT measurement for aligned PAN fibre scaffold. ....	108
Figure 3. 14: SEM and FibreMetric analysis for PAN radial fibres. ....	110
Figure 3. 15 <i>Ethanol sterilisation analysis for PAN</i> .....	112
Figure 3. 16 Ethanol sterilisation analysis for PJ. ....	113
Figure 3. 17: UV Sterilisation box wavelength measurement.....	114
Figure 3. 18 UV sterilisation analysis for PAN. ....	115
Figure 3. 19 UV sterilisation analysis for PJ.....	116
Figure 3. 20 Antibiotic sterilisation analysis for PAN and PJ. ....	118

## **Chapter IV**

Figure 4. 1: SH-SY5Y and U-87MG microscope image. ....	135
Figure 4. 2: Unsuspended nanofibre on a polyester sheet.....	136
Figure 4. 3: Coomassie blue staining of cells cultured on unsuspended fibres.....	137
Figure 4. 4: Coomassie blue staining of cells cultured on random nanofibre scaffolds.....	138
Figure 4. 5: Coomassie blue staining of cells cultured on aligned nanofibre scaffolds.....	140
Figure 4. 6: Cytoskeletal protein stain to show cell attachment on nanofibre.....	141
Figure 4. 7: SEM imaging showing cell attachment on nanofibre.....	142

Figure 4. 8: SH-SY5Y proliferation on PAN, PJ fibres and plate. ....	143
Figure 4. 9: U-87 MG proliferation on PAN, PJ fibres and plate. ....	144
Figure 4. 10: U-87 MG cultured in DMEM media. ....	146
Figure 4. 11: Immunofluorescence imaging of Differentiated SH-SY5Y on PAN fibre. ....	148
Figure 4. 12: Immunofluorescence imaging of Differentiated SH-SY5Y on PJ fibre. ....	149
Figure 4. 13: Immunofluorescence imaging of Differentiated U-87 MG on PAN fibre. ....	150
Figure 4. 14: Immunofluorescence imaging of Differentiated U-87 MG on PJ fibre. ....	151
Figure 4. 15: Phosphorylated neurofilament-H (SMI 34) protein expression in differentiated SH-SY5Y cell on a plate, PAN and PJ fibre. ....	153
Figure 4. 16: $\beta$ III tubulin protein expression in differentiated SH-SY5Y cell on a plate, PAN and PJ fibre. ....	154
Figure 4. 17: Synaptophysin protein expression in differentiated SH-SY5Y cell on a plate, PAN and PJ fibre. ....	155
Figure 4. 18: GFAP protein expression in differentiated U-87MG cell on a plate, PAN and PJ fibre. ....	156
Figure 4. 19: CellTiter-Glo <sup>®</sup> 3D viability assay showing the effect of Toxins on SH-SY5Y cultured on Plate, PAN and PJ fibre. ....	159
Figure 4. 20: CellTiter-Glo <sup>®</sup> 3D viability assay showing the effect of Toxins on U-87 MG cultured on Plate, PAN and PJ fibre. ....	160
Figure 4. 21 SH-SY5Y cells cultured on U-87MG ECM feeder layer. ....	163
Figure 4. 22: Schematic representation of the experimental setup designed to create a co-culture system. ....	164
Figure 4. 23 Co-culture cell viability of SH-SY5Y and U-87 MG. ....	165
Figure 4. 24: Co-culture cell viability of SH-SY5Y and U-87 MG. ....	166
Figure 4. 25 Effect of toxins on differentiated SH-SY5Y cultured on PAN and U-87MG cultured on PJ in a co-culture model. ....	168

Figure 5. 1: ReNcell CX cell attachment on laminin-coated and uncoated light microscope image.....	182
Figure 5. 2: ReNcell culture on PAN and PJ random fibres.....	183
Figure 5. 3: ReNcell CX MTT metabolic assay on PAN, PJ and TCP....	185
Figure 5. 4: Immunofluorescence image of undifferentiated and differentiated ReNcells on PAN and PJ fibres. ....	187
Figure 5. 5: Effect of toxins on ReNcell CX cells.....	189
Figure 5. 6: MTT metabolic assay of primary hippocampal neurons cultured on PAN, PJ fibre compared to TCP.....	192
Figure 5. 7: Primary hippocampal glial cell viability assay on PAN, PJ fibre compared to the TCP.....	193
Figure 5. 8: Immunofluorescence image of primary hippocampal neurons cultured on PAN scaffolds.....	195
Figure 5. 9: Immunofluorescence image of primary glial cells from hippocampal tissue. ....	196
Figure 5. 10: Primary neurons and glial cell co-culture model.....	198
Figure 5. 11: Primary neuron cultured on PAN and treated with toxins. ....	199

## **Chapter VII**

Figure 7. 1: Human Osteoblast and Tenocyte cultured on hydroxyapatite-coated aligned nanofibre.....	224
Figure 7. 2: Neural cells cultured on graphene-coated coverslips. ....	225
Figure 7. 3: Neural cells cultured on graphene-coated nanofibres. ...	225

## List of Tables

Table 1. 1: Role of astrocytes associated with multiple regions and functions of the brain (Gorshkov, Aguisanda, Thorne, et al. 2018). ....	20
Table 1. 2: Neural cell models with various pathological phenotypes ..	30
Table 1. 3 3D Spheroid neural models. Adapted from (Zhuang, Sun, An, et al. 2018) .....	34
Table 2. 1: List of Primary antibodies.....	50
Table 2. 2: Preparation of acrylamide resolving gel mixes for SDS-PAGE .....	80
Table 2. 3: Preparation of acrylamide stacking gel mix for SDS-PAGE.	81
Table 3. 1: Other methods of nanofibre fabrication .....	91
Table 3. 2: Electrospinning parameters for PAN and PJ.....	98
Table 3. 3 Diameter and pore size based on electrospinning parameters .....	100
Table 3. 4: Contact angle based on electrospinning parameters.....	101
Table 3. 5: Random Scaffold thickness based on electrospinning parameters.....	102
Table 3. 6: Aligned fibre FibreMetric data based on electrospinning parameters.....	105
Table 3. 7: Aligned fibre contact angle data based on electrospinning parameters.....	107
Table 3. 8: Random Scaffold thickness based on electrospinning parameters.....	108
Table 3. 9 Method of sterilisation for both PAN and PJ .....	119

## Abbreviations

### #

2D	Two dimensional
3D	Three dimensional
6-OHDA	6-hydroxydopamine
µm	Micrometres

### A

AD	Alzheimer's disease
AIDA	Advanced image data analyser
ALS	Amyotrophic lateral sclerosis
ARE	Antioxidant response element
ATCC	American type culture collection
ATP	Adenosine triphosphate

### B

BDNF	Brain-derived neurotrophic factor
BSA	Bovine serum albumin
BSO	L-Buthionine sulfoximine

### C

CNS	Central nervous system
COMT	Catechol-o-methyl transferase
CSF	Cerebral spinal fluid

### D

DA	Dopamine agonist
dbcAMP	Dibutyryl cyclic adenosine monophosphate
DBS	Deep brain stimulation
DMA	Dimethylacetamide
DMEM	Dulbecco's modified eagle medium
DMF	Dimethyl-formamide
DMSO	Dimethylsulfoxide
DSA	Drop shape analyser

### E

ECM	Extracellular matrix
EGF	Epidermal growth factor
EMEM	Eagle's minimum essential medium

### F

FBS	Foetal bovine serum
Fgf8	Fibroblast growth factor 8
FGFb	Fibroblast Growth Factor basic

## **G**

GABA	Gamma-aminobutyric acid
GFAP	Glial fibrillary acidic protein
GS	Glutamylcysteine synthetase
GSH	Glutathione

## **I**

IF	Intermediate filament
IFN-g	Interferong
IL-1b	Interleukin 1b
iNOS	Nitric oxide synthase

## **K**

kDa	Kilo daltons
KV	Kilovolt

## **L**

LRRK2	Leucine rich repeat kinase 2
-------	------------------------------

## **M**

MAO-B	Monoamine oxidase B
MG132	Z-L-Leu-D-Leu-L-Leu-al
MPP+	1-methyl-4-phenylpyridinium ion
MPTP	1-methyl-4-phenyl-1, 2, 3, 4-tetrahydropyridine
MTT	4, 5-dimethylthiazol-2-yl)-2, 5-diphenyltetrazoulium bromide

## **N**

NADH	Nicotinamide adenine dinucleotide hydride
NEAA	Non-essential amino acids
NF	Neurofilament
NF-H	Neurofilament heavy
nm	Nanometers
NMDA	N-Methyl-D-aspartic acid
NMR	Nuclear magnetic resonance
NSC	Neural stem cells
Nurr1	Nuclear receptor-related protein-1

## **O**

OCT	Optical coherence tomography
-----	------------------------------

## **P**

PA	Peptide amphiphile
PAA	(Poly)acrylic acid
PAN	Polyacrylonitrile
PBS	Phosphate buffered saline
PCL	Poly ( $\epsilon$ -caprolactone)
PEVA	Poly(ethylene-co-vinylacetate)
PHA	Polyhydroxyalkanoates
PHB	Poly- $\beta$ -hydroxybutyrate
PHBV	Poly(3-hydroxybutyrate-co-3-hydroxy valerate)
PINK1	PTEN-induced putative kinase
PJ	Pan/jeffamine® ed-2003
PLA	Poly(lactic acid)
PLGA	Poly(lactic-coglycolic acid)
PLL	Poly(L-lysine)
PNIPAAm	Poly(N-isopropylacrylamide)
PNS	Peripheral nervous system
PO	Propylene oxide
PPI	Pulse per inch
PRKN	Parkin rbr e3 ubiquitin protein ligase
PU	Polyurethane

## **R**

RA	Retinoic acid
RH	Relative humidity
ROS	Reactive oxygen species

## **S**

SD	Standard deviation
SDS	Sodium dodecyl sulphate
SEM	Scanning electron microscopy
SFM	Serum-free medium
Shh	Sonic hedgehog
SNCA	Alpha-synuclein

## **T**

T25/75	Tissue culture flask 25/75ml
TBS	Tris-Buffered saline
TCP	Tissue culture adherent plate
TEMED	Tetramethylethylenediamine
TLB	Total lysis buffer
TRAP-1	TNF receptor-associated protein 1

## **U**

UPS	Ubiquitin-proteasome system
-----	-----------------------------

## **Abstract**

Neurodegenerative diseases are prolonged and progressive. In general, they affect individuals in the latter stages of their lives. The pathology of neural cell degeneration is widely researched, and most current therapeutic strategies aim to delay its progression by either promoting neuronal regeneration, resurrecting the lost brain function with stimulation electrodes or by cell replacement therapies. Neuronal and glial cells are researched to better understand the physiological condition and to find a cure for degenerative diseases. In current *in vitro* techniques, cells dissociated from their natural three-dimensional (3D) tissue and cultured on flat surfaces present a significant drawback in drug discovery and cell therapy research. Communication and various signal transduction between neuronal and glial cells in the *in vivo* system are purely based on a dynamic convoluted systematic network constructed and expanded in a 3D manner. Recently, electrospun 3D nanofibre scaffolds have gained attention among researchers for their ability to mimic the natural 3D microenvironment that cells inhabit. Developing an *in vitro* system which emulates the *in vivo* 3D habitat of neural cells has been a significant challenge. This thesis reports on the advantages of using novel 3D suspended nanofibre membrane technology to create better models for both drug discovery and therapeutic implants.

In this study, we focused on developing a suitable sterile nanofibre porous membrane using Polyacrylonitrile (PAN), and Jeffamine® ED-2003 modified polyacrylonitrile (PJ) to provide favourable conditions for neuronal and glial proliferation, differentiation and survival. The study was designed, engineered and optimised three different state-of-the-art fully suspended nanofibre models that are highly multi-functional and suitable for investigating several diseases and chronic conditions. We have characterised the growth and survival of human SH-SY5Y neuroblastoma, human U-87MG glioblastoma, human ReNcell CX neural progenitor and primary neural cells from E18 rat hippocampal tissue on

both PAN and PJ nanofibre scaffolds. Our investigations and chronic studies have shown extended survival of cells on a scaffold in comparison to these cells cultured on the base of cell adherent tissue culture plates (TCP). Differentiation cell culture trials have demonstrated that both PAN and PJ are capable of supporting cell differentiation and immunofluorescence and western blot analysis has shown elevated levels of key differentiation marker proteins on the cells cultured on the suspended scaffolds compared to TCP.

Our findings indicate that the new 3D suspended nanofibre scaffolds support improved growth, survival and differentiation of both cell populations as well as increasing the sensitivity of the cells to Toxins when compared to the sensitivity of cells growth of the base of TCPs. Moreover, chronic exposures to Toxins using the novel co-culture scaffold model has shown prolonged neuronal survival in the presence of astrocytes. Together, our findings suggest the potential for the 3D nanofibre approach to improve in vitro therapeutic studies and our co-culture system, which creates a better mimic, should lead to a reduced number of animals used for pharmaceutical development and in the screening of compounds to find neuroprotective compounds to prevent degeneration of neural cells.

## Chapter 1: Main Introduction

### 1.1 Electrospinning

The process of stretching melted polymer using high voltage and fabricating continuous nanoscale fibres with a diameter ranging from sub-micrometre to nanometre is known as electrospinning. Using electrostatic force to produce ultrathin fibre structures was traced back to 100 years, and the first patent on this technology was by Formhals in 1934 (Hu, X., Liu, Zhou, et al. 2014). This ultra-fine fibre manufacturing technology coined in the 1990s from the term "electrostatic spinning" used earlier by Reneker and co-workers (Doshi and Reneker 1995; Reneker and Yarin 2008). This technology has gained considerable interest in several fields for its remarkable simplicity, versatility and potential uses in multi-disciplinary areas. Until now several notable applications of electrospinning include filtration (Gopal, Kaur, Ma, et al. 2006; Aussawasathien, Teerawattananon and Vongachariya 2008; Schreuder-Gibson, Gibson, Senecal, et al. 2002), cosmetics products (Gu and Xu ; Kusamoto and Tajima ), protective clothing for military (Lee, S. and Kay Obendorf 2006; Gorji, Jeddi and Gharehaghaji 2012), nano-sensors (Rojas and Pinto 2008; Kowalczyk, Nowicka, Elbaum, et al. 2008), wound dressing (Zahedi, Rezaeian, Ranaei-Siadat, et al. 2010; Rieger, Birch and Schiffman 2013), drug delivery (Sill and von Recum 2008; Pillay, Dott, Choonara, et al. 2013), enzyme immobilisation (Lu, T., Chen, Shi, et al. 2008; Shi, Q., Chen, Lu, et al. 2008) and tissue engineering scaffolds (Yoo, Kim and Park 2009; Hu, J., Kai, Ye, et al. 2017).

As shown in figure 1.5, the process of electrospinning makes use of a combination of mechanical and electrostatic force to spin fibre using a needle with a very fine orifice which is connected and maintained at a positive or negative charge by a high voltage DC power supply. When the intensity of the electric field has increased the fluid at the tip of the capillary tube elongates and forms a conical shape known as the Taylor cone. Further increasing the electric field the surface tension of the

polymer solution overcomes the electrostatic repulsive force, the liquid that spills out of the capillary tube elongates allowing the jet to form a fine continuous thin filament which solidifies with solvent evaporation and these filaments are collected on to a rotating or stationary grounded collector where they accumulate to form a nanofibre matrix (Greiner and Wendorff 2007; Reneker and Yarin 2008).

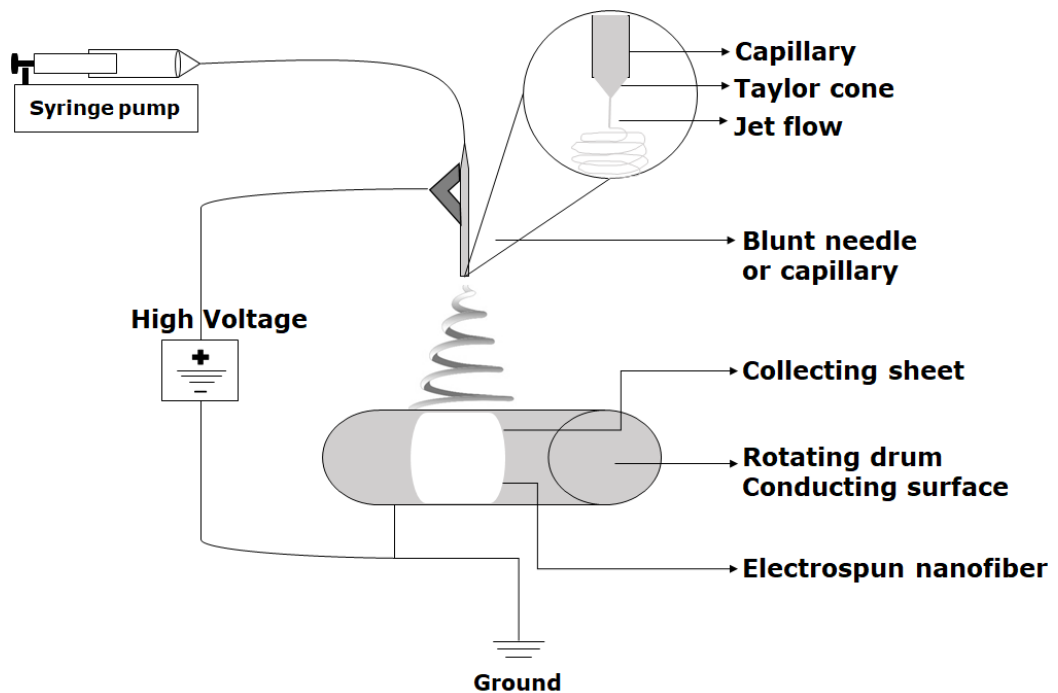


**Figure 1. 1 Schematic illustration of the basic electrospinning process setup.**

### 1.1.1 Nanofibres

Nanofibre is a final product that is obtained by the method of electrospinning of polymers. These nanoscale structures are cylindrical and can range from nanometers to several micrometres in diameter. The polymers are dissolved in various solvents based on needs (Teraoka and Teraoka 2002). Nanofibres can be made using a wide range of natural or synthetic polymers or a blend of both to enhance different physical properties to address a wide range of applications. Examples of natural polymers include keratin, silk fibroin, cellulose, collagen, gelatin chitosan and alginate (Vasita and Katti 2006; Khajavi, Abbasipour and Bahador 2016). Examples of synthetic polymers includes poly(3-hydroxybutyrate-

co-3-hydroxy valerate) (PHBV), poly(lactic acid) (PLA), poly(lactic-co-glycolic acid) (PLGA), polyacrylonitrile (PAN), polycaprolactone (PCL), polyurethane (PU), and poly(ethylene-co-vinylacetate) (PEVA)(Vasita and Katti 2006; Khajavi, Abbasipour and Bahador 2016). The diameter of nanofibres can differ based on the type of polymers used and also based on different parameters used during electrospinning (Reneker and Chun 1996). Each polymer imparts unique properties to the nanofibre mat, like a large surface area to volume ratio, different porosity, changes in mechanical strength, the difference in pore size, flexibility and functions. The above properties and functions can also be modified when polymers are blended with different additives. This study has mainly focused on a synthetic fibre PAN and blend of PAN with polyetheramines commonly known as Jeffamine

### 1.1.2 Polyacrylonitrile

PAN is a synthetic rich carbon source made as semicrystalline organic polymer resin with a linear chemical formula  $(C_3H_3N)_n$ . PAN melts at 300°C or when heated at a rate of 50°C per minute when mixed with a solvent (Gupta, Paliwal and Bajaj 1998). It is a very flexible polymer with a wide range of uses. PAN is used in making ultra-thin filtration membranes, fibres for textile and hollow fibres. Its applications even widen from high-tech uses like military purpose and also used to make commonly used products like pressure vessels and fishing rods.

In 1930, Hans Fikentscher and Claus Heuck were the first to synthesis PAN in Ludwigshafen, Germany (DE Patent No. 654989). Later in 1931, Herbert Rein identified that PAN could be dissolved using ionic liquid and in 1938 he spun the first PAN-based fibre using aqueous solutions of quaternary ammonium sodium thiocyanate and aluminium perchlorate (DE Patent No. 631756). The first mass production of PAN was in 1946 and was identified that PAN is readily soluble in polar solvents like dimethylformamide (DMF), dimethylacetamide (DMA), ethylene and propylene carbonates, sodium thiocyanate, zinc chloride and nitric acid

(Wu, Chen, Wan, et al. 2012). Electrospun fibres made using PAN are highly-hydrophobic (Feng, Li, Li, et al. 2002).

From all the major applications of PAN, one of the interesting use is its prominent role in tissue engineering and biomedical application, including replacement of damaged tissue. From a clinical study published on June 11, 1955, PAN has been used for replacing a portion of the abdominal aorta of a dog. The same team has demonstrated several times how PAN could be used to create different prostheses and used these in implant therapies (Kinmonth, Taylor and Lee 1955). Other research showed that four clinical patients who had patch grafting with PAN between 1958 and 1960 were followed up for a minimum of 17 years and all patients exhibited excellent health condition and recovery. Three of these patients were successfully reoperated upon, but the fourth patient died 17 years after patch grafting because of rupture of an aneurysm. Microscopy in three patients showed varying degrees of degenerative changes in the aortic wall opposite the patch. There was no evidence of infection or foreign body reaction in these parts of the aortic walls (Bergdahl and Ljungqvist 1980). The follow-up investigation showed the potential medical application along with the robust and inert nature of PAN.

Carbon-based materials like PAN have been extensively used to investigate several cell culture studies. In tissue engineering and regenerative medicine scaffolds are typically required to have a 3D structure to provide larger surface area and space for cell adhesion, migration and tissue formation (Crowder, Prasai, Rath, et al. 2013). PAN had exhibited high carbon yield when compared to other precursors without alteration in its basic structure when electrospun to fibres or made into other products (Wangxi, Jie and Gang 2003). Also, its physical properties, morphology and dimensions can be easily modified and optimised during fabrication (Chen, J. C. and Harrison 2002). When prepared PAN nanofibres have shown high surface-to-volume ration as well as interconnected pores and modifiable surface, all of which are

preferred cues for tissue engineering and identification of regenerative medicines (Xu, C., Inai, Kotaki, et al. 2004).

### 1.1.3 Polyetheramines

Polyetheramines/jeffamine is a highly versatile polymer containing primary amino groups attached to the end of a polyether backbone generally based on propylene oxide (PO), ethylene oxide (EO) or a mixture of both ([Huntsman, UK](#)) (Figure 1.6). Based on use and different properties, jeffamine comes in various forms as monoamine, diamines and triamines. Jeffamine polymer is commonly used as a copolymer to alter chemical and physical properties of other polymers. It comes in a broad range of molecular weights and amine functionality. Jeffamine offers excellent scope to design new compounds and mixtures. It has been used as an additive in the full variety of fields and studies to enhance the property of the chosen polymers.

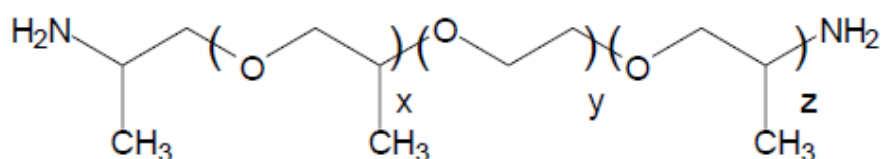


**Figure 1. 2 Chemical structure of Jeffamine® ED series.**

In a plant biology study, jeffamine-ED was used as an additive to enhance the property of a polymer which proved to be efficient in remedying iron-deficient maize plants. They exhibited very low-antibacterial activity against non-pathogenic soil bacteria. The combination of these properties renders these new synthetic macromolecular chelating agents promising for agricultural applications (Mladenova, Ignatova, Manolova, et al. 2002). Another study showed that jeffamine was used as a copolymer with Poly(N-isopropylacrylamide) (PNIPAAm) for investigations on glioblastoma cells. In the study, the authors have demonstrated the use of jeffamine as an additive and have shown a combination of the two polymers offers a significant opportunity for studying the

microenvironmental regulation of clinically relevant models of glioblastoma models *in vitro* (Heffernan, McNamara, Borwege, et al. 2017). Jeffamine has a wide range of molecular weight, amine functionality, oxide type and distribution. Compounds made from Jeffamine reagents provides flexibility in synthetic design. For the most part, Jeffamine Reagent products undergo typical amine reactions and are low viscosity liquids, exhibiting low vapour pressure. Jeffamine reagents originated chemically at the Texaco Chemical Company as lubricants and fuel additives and are now most frequently used in manufacturing adhesives, coatings, epoxies, and curing agents ([Hampton Research](#)). Jeffamine was also used in several other application; Alexander McPherson published the use of Jeffamine Reagents in a crystallisation publication (McPherson 1992). The first protein structure solved using Jeffamine reagents was that of Xylose Isomerase in the publication by (Lloyd, Gallay, Akins, et al. 1994).

#### **1.1.4 Nanofibres for *In vitro* model**

Producing nanofibre scaffolds with a diameter ranging from 100-1000nm was introduced to tissue engineering by the method of electrospinning during the '90s (Doshi and Reneker 1995; Reneker and Yarin 2008). Also, electrospun nanofibres are capable of providing nanomechanical and biodegradation properties allowing embedded cells to proactively interact with the provisional functionalised matrix, thus remodelling it to resemble natural extracellular matrix (ECM). Traditionally, *in vitro* neuronal cell cultures have been performed using two dimensional (2D) monolayer cultures which do not provide a native environment for healthy cell growth. Successful engineering of desired tissue has been the ultimate goal of tissue engineering where engineering technology and principles of biology are applied together to mimic the ECM and the environment. Cells were grown on 2D surfaces, such as solid polystyrene tissue culture plastic results in remodelling, characterised by changes in gene expression, rearrangement of the internal cytoskeleton and altered cell

morphology (Vergani, Grattarola and Nicolini 2004). A modelled environment similar to a natural habitat can potentially have a significant effect on cell performance and also influence the results of biological assays. The advantages of using a 3D nanofibre scaffold to mimic the *in vivo* environment are:

- 1) It enhances the structure of the cell and physiological relevance of experiments performed *in vitro* (Knight and Przyborski 2014)
- 2) Provides greater cell-cell contact, resulting in increased intercellular cell signalling (Vasita and Katti 2006),
- 3) Supports the cells to differentiate into more complex structures and facilitates the development process (Vasita and Katti 2006),
- 4) Provides a greater surface area, porosity, enhancing greater cell adhesion, and improved access to metabolites, nutrients and removal of metabolic waste. Currently, no model is capable of replicating all the hallmarks of neural cell degeneration (Peng, Oo and Andersen 2010)

However, in this study, we have created two distinct 3D natural habitats with nanofibres that are capable of harbouring neuronal and glial the two primary cells involved in neurodegenerative disease. Also, during this study, we were able to investigate three different significant hallmarks and create a cell model that does not include animals and may be used for examining more hallmarks and screen more drugs.

### **1.1.5 Application of nanofibres in bioscience**

The exploitation of interactions between biomaterials to create functional nanostructures have given rise to an exciting platform for tissue engineering. The creative assembly of nanoscaffolds composed of peptides, nucleic acid or biopolymers with precise size, shape and spatial orientation has allowed researchers to observe the remarkable capability of nanofibres regarding exhibiting molecular recognition, interaction and compatibility with a variety of cells both *in vitro* and *in vivo*. Their

therapeutic applications have been investigated hugely over recent years leading to a wide range such as nucleic-acid based novel structures for drug delivery (Li, H., Labean and Leong 2011), tissue regeneration using biomaterials, bioengineering for stem-cell-based organogenesis, neural tissue engineering, scaffolds for dental pulp tissue engineering. Furthermore, several types of research show the use of electrospun nanofibres to regenerate various soft tissues such as skin, blood vessel, tendon/ligament (Kumbar, James, Nukavarapu, et al. 2008).

The functional recovery of neurodegenerative diseases through compelling treatments has been difficult due to the unique challenges presented by the complex physiology of the central nervous system. Current therapeutic strategies aimed at delaying the progression of neurodegenerative diseases by a) reducing inflammation for neuroprotection to prevent secondary cell death b) replacement of damaged neuron supplemented with appropriate factors c) restoration of original neuronal structures by promoting neurite regeneration (Bian, Wang, Aibaidoula, et al. 2009). Given the limitations of CNS recovery due to the poor regenerative capacity of neural tissues, investigations of researchers lead to an excellent approach called tissue engineering that may provide an opportunity for reconstruction of injured tissues. The principle of tissue engineering is based on the general hypothesis that mimicking ECM *in vitro* will provide an intimate interface between individual cells that is conducive for various cellular activities from adhesion, proliferation and differentiation (Liang, Hsiao and Chu 2007). Nanofibrous constructs can be altered based on the application by controlling the morphology of the scaffold with suitable biochemical cues using a variety of biodegradable and biocompatible components that promotes regeneration. The possibility of tailoring artificial scaffolds has extended their application in chemical therapy as drug carriers as they provide a permissive substrate for cell penetration leading to enhanced drug uptake. Cellularised nanofibrous scaffolds have several promising advantages for brain tissue reconstruction to bridge structural gaps by

re-knitting of injured sites and facilitating endogenous cell migration and axonal elongation (Guo, Leung, Su, et al. 2009). Currently, several techniques are available for fabricating nanofibres: electrospinning, phase separation and self-assembly. The versatility of the electrospinning technique has allowed a wide range of tissue engineering platforms from cardiovascular to stem cell engineering (Li, Wan-Ju, Tuli, Huang, et al. 2005). Several research groups have investigated the feasibility of using electrospun scaffolds for neural tissue engineering in various models, including murine neuronal cells and neuronal stem cell lines. Although these findings based on previous research have indicated electrospun scaffolds as potential candidates for nerve repair application, research conducted by Dr Samuel Stupp on the design of injectable nanostructures in spinal tissue has shown that they can self-assemble to rescue damaged neurons and rapidly re-grow in a paralysed mouse model. This demonstration has encouraged several scientists that someday nanotechnology self-assembly will allow researchers to tailor and develop personalised treatments for patients in previously unimaginable ways. For the use of 3D-scaffolds in regenerative medicine, for purposes such as *in vivo* engraftment or *in vitro* culture of any progenitor stem cells, optimisation of model systems with matrix parameters are essential for the fate of the cells. Studies suggest that cell survival and differentiation can be hugely influenced by the matrix composition and concentration of compounds that interact to promote growth patterns. Given that 3D microenvironment provided by scaffold composition can increase the survival rate of embedded cells, a study on human neuronal progenitor cells showed enhanced differentiation and survival on 3D scaffolds functionalised by laminin compared to 2D-cultures (Ortinou, Schmich, Block, et al. 2010).

### **1.1.6 Nanofibre and tissue engineering**

Among the multiple uses of this technology, tissue engineering is one of the most promising areas. The use of biomaterials processed by the

electrospinning technique has gained considerable interest for neural tissue engineering applications. The underlying rationale based on the biomimetic principle that they mimic the physical structure of major constructive elements in the native ECM as biologically, almost all of organs and tissues are hierarchically organised and synthesised into the fibrous form of dimensions down to nanometre scale. It can also provide nanomechanical and biodegradation properties allowing embedded cells to proactively interplay with the provisional functionalized matrix, thus remodelling it to resemble innate ECM (Vasita and Katti 2006). In a tissue engineering approach, specific cells loaded on an engineered scaffold may promote functional recovery. Well-designed scaffolds can achieve signals for cell growth, differentiation, and subsequent tissue formation with suitable surface and bulk properties similar to the environmental cue in the extracellular matrix. Cell behaviour has been observed to be influenced by surface physicochemical properties like topography, surface charge and protein adsorption/immobilisation and release (Lee, Y. and Livingston Arinzeh 2011). Due to the function of mimicking the naturally occurring protein fibrils in the extracellular environment, electrospun nanofibres have gained great interest. Each nanofibre has a high surface to volume and aspect ratio allowing more surface area contact of the scaffold with the cell (Lee, Y. and Livingston Arinzeh 2011). Based on the type of material used for electrospinning, the physical and biological properties of a scaffold can be determined. Properties like surface wettability, mechanical properties and degradation can be manipulated by copolymerization or by polymer blending of various synthetic and natural, non-biodegradable/ biodegradable materials.

Scaffolds composed of specific and accurate biomaterials with nano-scale features have a high potential of providing structural support that mimics natural extracellular ambience facilitating an intimate interface between individual neuronal cells in culture. Several biomaterials have been tested recently to achieve the purpose, including poly(l-lactic-co-glycolic acid) polymer sponges (Darice Y, Scott J, Paul H, et al. 2007), collagen,

hyaluronic acid hydrogels (Cui, Tian, Hou, et al. 2006) polycaprolactone (PCL) and polydimethylsiloxane-tetraethoxysilane scaffold in animal models as brain implants with variable results. Results of (Pan, H., Jiang and Chen 2006) show use of PLAGA-dextran to support fibroblast attachment and migration within the artificial architecture while (Bhattacharai, Bhattacharai, Yi, et al. 2004) produced similar results with poly (p-dioxane-co-L-lactide)-PEG. In 2008, a study by (Novikova, Pettersson, Brohlin, et al. 2008) showed that poly- $\beta$ -hydroxybutyrate (PHB) graft seeded with Schwann cells could support & promote spinal cord repair. In several cases of CNS injuries, researchers have studied neural stem cells (NSC) to possess tremendous therapeutic potential in CNS regeneration treatments. For the successful differentiation of NSC, a variety of biomaterials have been investigated. Bian et al. demonstrated the use of non-cytotoxic and biodegradable implants composed of biopolymers such as Polyhydroxyalkanoates (PHA) developed as nerve conduits with co-polymers PHBHHx consisting of 3-hydroxybutyrate and 3-hydroxyhexanoate to repair peripheral nerve damage *in vivo* animal models (Bian, Wang, Aibaidoula, et al. 2009). Evaluation of nanofibres composed of biomaterials such as PLA and polyhydroxyalkanoates (PHA) have shown similar results indicating strong potentials of PHA matrices with PHBHHx for neuronal differentiation of NSC for CNS repair (Xu, X., Li, Peng, et al. 2010) Electrospun scaffolds composed of copolymers  $\epsilon$ -caprolactone (PCL) and ethyl ethylene phosphate encapsulated with differentiating agents have resulted in enhanced neuronal differentiation (Low, Rujitanaroj, Wang, et al. 2013). Comparison between electrospun nanofibres composed of PCL and collagen-PCL blend shows that blend of natural and synthetic polymers could promote migration of glial cells and axonal outgrowth suggesting use as artificial nerve implant (Schnell, Klinkhammer, Balzer, et al. 2007).

The benefit of using 3D nanofibres to regulate specific lineage from stem cells as compared to the 2D surface is based on topographical cues applied in conjunction with biochemical signals. This was confirmed by

(Christopherson, Song and Mao 2009) who suggested that larger diameter reduced proliferation and differentiation of rat NSCs into neuronal lineage even in the presence of differentiation conditions and with smaller diameters higher degree of neuronal differentiation was observed in comparison to 2D surfaces.

A study by (Tysseling-Mattiace, Sahni, Niece, et al. 2008) has demonstrated that 3-D peptide amphiphile (PA) nanostructures displaying neuroactive epitopes can inhibit glial scar formation and also facilitate axon regeneration after spinal cord injury. (Min, Jung, Kim, et al. 2013) Showed that PCL nanofibre encapsulated with Spirulina extract promoted astrocyte activation that could be used in astrocyte tissue engineering for neuronal regeneration. Nanofibres that are designed with bioactive peptide epitopes have been used for the selective differentiation of neural progenitor cells into neurons (Silva, Czeisler, Niece, et al. 2004).

In another study, Meiners, et al. 2007 reported that surface modification of 3D electrospun nanofibres with neuroactive peptides derived from human tenascin-C significantly enhanced neuronal cell adhesion, neurite growth and survival *in vitro* as compared to poly(L-lysine)-coated coverslips. A study demonstrated that vertically aligned carbon nanofibre to deliver an electrical-neural interface to culture PC12 neural cells that are suitable for use as implants (Nguyen-Vu, Chen, Cassell, et al. 2007). Highly aligned multi-layered nanofibre constructs supplemented with astrocytes for neuroprotective effects provide a repair-mediating environment guiding axonal growth and bridge lesions (Weightman, Jenkins, Pickard, et al. 2014). Several more groups have demonstrated *in vitro* culture of Schwann cells on electrospun aligned nanofibres than randomly oriented fibres emphasising on orientation cues ideal for nerve regeneration (Subramanian, Krishnan and Sethuraman 2011). An investigation showed similar results with neurite expansion from DRG explants on Poly-L-lactate nanofibres of high, intermediate and random alignments showed robust neurite growth on highly aligned compared to

random fibres (Corey, Gertz, Wang, et al. 2008). Research also suggests that sustained delivery of differentiating agents such as retinoic acid and brain-derived neurotrophic factor (BDNF) together with synergistic effects of electrospun nanofibre topography enhances neuronal differentiation of neural progenitor cells (Low, Rujitanaroj, Wang, et al. 2013).

Neural cell proliferation and differentiation through axonal growth has been drastically influenced by the degradation rate and mechanical performance of synthetic polymeric scaffolds. Synthetic polymers such as polydioxanone (PDS) and PAN- poly (acrylonitrile-co-methyl acrylate) have shown to support neural cell growth (Guo, Leung, Su, et al. 2009), but proliferation and survival were reported to differ due to orientations of the constructs. The study also indicated the significant role of topographical cues that influence nerve regeneration. Addressing neuron-fibre interactions is critical to allow nanoscaffolds for a range of regeneration purposes to be fabricated. Reports also indicate the use of polymerisable Polylactic acid (PLA) as a suitable material for synthesising neural scaffolds, via 3D soft lithography, as they have shown sustained proliferation of human SH-SY5Y cells after photocuring (Koroleva, Gill, Ortega, et al. 2012). The ability of PLLA nanofibre substrates on coverslips pre-coated with PLGA (poly(lactic-co-glycolic acid) were studied to facilitate the growth of primary motor and sensory neurons at low plating densities where neuronal alignment on PLLA surpassed neurite alignment from explants (Corey, Gertz, Wang, et al. 2008).

## 1.2 Neurodegenerative Disease

According to the Medical research council, around 50 million people live with dementia worldwide - with one new case every 3 seconds. 850,000 people are estimated to be living with dementia in the UK with numbers set to rise to over 1 million by 2025. This will increase to 2 million by 2051. This accounts for a rising number of 127,000 people in the UK diagnosed with Parkinson's ([NHS](#)) and there are over 40,000 people with

early-onset dementia (onset before the age of 65 years) in the UK. Most people with neurodegenerative diseases start to express symptoms after the age of 50, although 1 in 20 people experience symptoms under age of 40 and slightly more common in men than women (De Lau and Breteler 2006). With a continuous ageing population people affected by neurodegenerative disease, it is predicted to rise from 22% to 29% in 2033 and 31% by 2058 ([AgeUK](#)). An individual life affected with neurodegenerative disorder will cause dramatic changes in their quality of life and affect the life of the family members too. The economic burden is estimated at £26 billion annually ([Imperial College, London](#)). The cost of illness escalates as the disease progresses. The value has varied from country to country, but the significant contribution to the price is towards patient care and nursing.

Neurodegenerative disease is a common term used for various range of illness that affects the primary functions of neuronal and glial cells in the brain. The condition is a chronic progressive loss of the function or death of neurons that has caused a very significant disability and reduced quality of life for almost 4 million people worldwide (Dorsey, Constantinescu, Thompson, et al. 2007; Scott, Dawson and Dawson 2017). Some of the common neurodegenerative diseases include amyotrophic lateral sclerosis, Parkinson's disease, Alzheimer's disease, and Huntington's disease. The neurodegenerative disorder has become an increasing burden to patient, families and the healthcare system (Chrischilles, Rubenstein, Voelker, et al. 1998; Nussbaum and Ellis 2003). Amyotrophic lateral sclerosis is a specific disease that causes the death of neurons controlling voluntary muscles (Rubert Sánchez 2018). Parkinson's Disease is the death of neurons in the substantia nigra a region of midbrain resulting in the low supply of dopamine, which is responsible for chemical signalling and several other functions in a brain (Sadek, Mohammed, Abunbehan, et al. 2019). Alzheimer's is a chronic neurodegenerative disease that usually starts slowly and gradually worsens over time. It is the cause of 60–70% of cases of dementia and

the most common early symptom is difficulty in remembering recent events (Burns and Iliffe 2009). Huntington's disease also known as Huntington's chorea, is an inherited disorder that results in the death of brain cells. The earliest symptoms are often subtle problems with mood or mental abilities (Dayalu and Albin 2015). Many kinds of research have been performed to study and understand the risk and protective nature of the disease. Studies have reported that neurodegenerative pathophysiology can only be identified after 70% death of the cells (Davie 2008). The neuronal degradation can also be observed along with the death of astrocytes and the activation of the microglia. The disease is known to affect the motor system causing several obvious early symptoms like shaking, rigidity, slowness of movement and difficulty in walking (Sargetis 2016). At later advanced stages of dementia, depression, and anxiety, emotional and sleeping problems (Sveinbjornsdottir 2016). The actual cause of the disease is still unknown, but several studies believe that it might be genetic and several environmental factors (Kalia and Lang 2015). Currently as it stands these diseases are incurably resulting in a slow degeneration of neural cells. With the current advancement in research many similarities have been identified that related these diseases to one another on a sub-cellular level. There are many parallels between different neurodegenerative disorders including atypical protein assemblies as well as induced cell death (Bredesen, Rao and Mehlen 2006; Rubinsztein 2006). Discovering further relevance and similarities can offer hopes to develop therapeutic advance that could treat many diseases simultaneously.

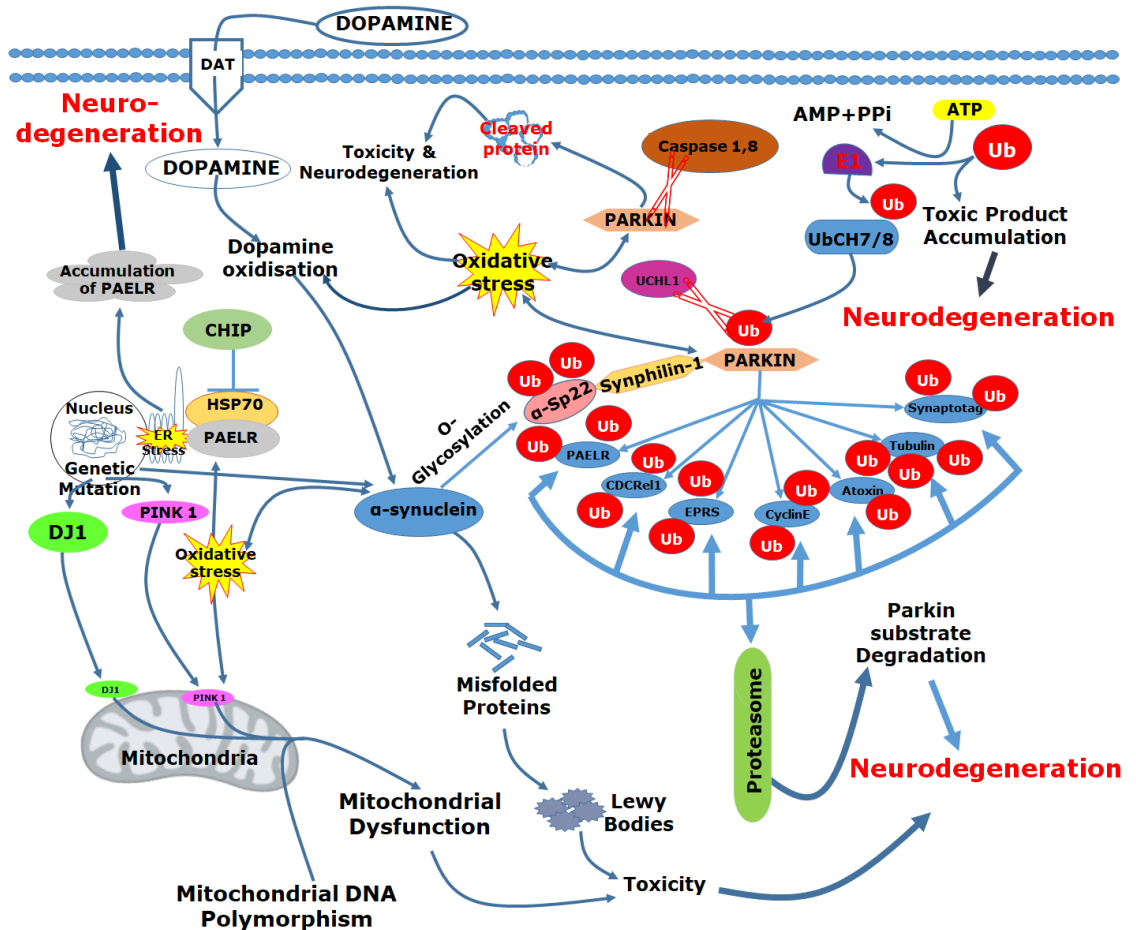


**Figure 1. 3: Schematic diagram showing Neurodegeneration pathophysiology associated pathways.**

Idea obtained and recreated from ([Qiagen Pathway](#))

### 1.2.2 Midbrain hub of motor movements

The Midbrain is one of the essential parts of the human brain, consisting of motor neurons involved in several activities in the body (Breedlove, Rosenzweig and Watson 2007). Midbrain acts as a conduit connecting the forebrain above and the cerebellum below. This part of the brain is one of the most complicated and superior in terms of complexity and function when compared to other regions (Tovote, Esposito, Botta, et al. 2016). In the Midbrain, the substantia nigra is a small basal ganglia structure that is responsible for motor movements. Due to the high levels of neuromelanin and dopaminergic neurons this region of the midbrain appears considerably darker (Rabey and Hefti 1990). It consists of two regions pars compacta and pars reticulata with very different functions and connections. Both of these regions are responsible for the supply of

dopamine to several areas of the brain. Pars compacta are formed of dopaminergic neurons, and disease like Parkinson's is characterised by the death of neurons in this region (Kim, S. J., Sung, Um, et al. 2003).

### **1.2.2.1 Neurons**

Inability to control movements, cases of dementia, problems with mood or mental abilities and loss of memory are the common symptoms observed in Neurodegenerative disorders. Neuronal cells are the primary source of signal transport in the central nervous system of mammals and loss of this particular substance in the brain leads to catastrophic disorders in the brain. The exact reason for cell loss is still unknown (Kalia and Lang 2015). There are roughly about 100 billion neurons in the human brain which is responsible for several pathological disturbances caused by neurodegenerative diseases. Neurons that are responsible for the cause of Parkinson's disease alone accounts for 2-5% of the total population, and they are primarily found in the Midbrain. These neurons are called the dopaminergic neurons and are found less in number and are found confined to small areas of the brain with projections into various parts of the brain (Schultz 2007), even though at such low numbers these neurons play a critical role in different brain functions including voluntary movements several behavioural processes like mood, addiction, reward and stress. Identification and localisation of the brain dopamine cell were initially done by Falck-Hillarp histofluorescence methods (Falck, Hillarp, Thieme, et al. 1962). The central part of mesencephalon contains approximately 90% of the total number of brain dopaminergic neurons. Humans have been known to have 590,000 dopaminergic neurons followed by 165,000 in macaque monkeys and 45,000 in the rat brain; in the early sixties, the number in humans drops to 350,000. (Bogerts, Häntschi and Herzer 1983; German and Manaye 1993).

### 1.2.2.2 Glial Cells

Glial cells are non-neuronal cells in the CNS and are also known as neuroglia. They are the most abundant cells found in the CNS, ranging between 33% and 66% depending on the mammalian species (Herculano-Houzel 2014; Jäkel and Dimou 2017). As being a part of the CNS, glial cells do not play a direct role in synaptic interaction and electrical signalling but they help to define synaptic contacts, maintain the signalling ability of neurons, maintain homeostasis, form myelin and provide support and protection for neurons (Jessen and Mirsky 1980; Wolosker, Dumin, Balan, et al. 2008). Glial cells were identified in 1856 by a pathologist Rudolf Virchow. A differentiated form of glial cells includes oligodendrocytes, astrocytes, ependymal cells, and microglia found in CNS whereas the satellite cells and Schwann cells are found in the peripheral nervous system (PNS) (Purves, Augustine, Fitzpatrick, et al. 2001). Oligodendrocytes are mainly responsible for the Myelin sheath coating in the CNS, providing the insulation required by neuronal cells for efficient electrical signalling (Baumann and Pham-Dinh 2001). Astrocytes are the most abundant type of microglia in the CNS. In early days, these star-shaped astrocytes were known to be a space filler in the brain but later identified that they play a significant role in secretion, absorption, neural transmission and maintenance of the blood-brain barrier (Kolb and Whishaw 2009). Studies have also shown that both oligodendrocytes and astrocytes are directly linked to neurodegenerative diseases (Papuć, Kurzepa, Kurys-Denis, et al. 2014). Ependymal cells function as a neural stem cell that lines the spinal cord and the ventricular system of the brain; and also plays a part in the creation and secretion of cerebral spinal fluid (CSF) (Johansson, Momma, Clarke, et al. 1999). Schwann cells play a similar role as oligodendrocytes in the PNS and are responsible for clearing debris that allows regrowth of PNS neurons (Jessen and Mirsky 2005). Cells that surrounds the neurons in sensory, sympathetic and parasympathetic ganglia are mostly the satellite glial cells (Hanani 2005). Satellite glial cells are also responsible for regulating the external

chemical environment and like the astrocytes, they interconnect the gap junctions in the PNS. They are very sensitive to injury and inflammation and contributes to chronic pain (Ohara, Vit, Bhargava, et al. 2008). All types of glial cells are responsible for several activities, and functioning of a mammalian brain, but astrocytes especially play a direct, active and a very critical role in several neurodegenerative diseases (Rappold and Tieu 2010; Booth, Hirst and Wade-Martins 2017).

### **1.2.2.3 Role of Astrocytes**

Astrocytes also are known as astroglia are star-shaped cells found abundant in the brain, covering 20-40% of the total glial population (Verkhratsky and Butt 2013). Even though an actual number of astrocytes present in the brain is still disputed, several studies have clearly shown the role of astrocytes in neurodegenerative diseases. Studies on amyotrophic lateral sclerosis (ALS) have demonstrated the neuroprotection role of astrocytes “in which the removal of glutamate from the extracellular space by astrocytes confers neuroprotection, whereas astrocytic release of toxic soluble molecules promotes neurodegeneration” (Rappold and Tieu 2010). In recent years the dual role of astrocytes which cause damage and protection has been thoroughly researched in several experimental models and for a potential target for drug discovery (Gorshkov, Aguisanda, Thorne, et al. 2018).

One of the significant roles of astrocytes in the maintenance of neurotransmitters such as glutamate and gamma-aminobutyric acid (GABA) (Schousboe, A., Bak and Waagepetersen 2013). They are the primary source of enzymes which are needed for neuronal synthesis and metabolism. Lack of this can lead to an increased propensity for neuron glutamate excitotoxicity and subsequent cell death (Gorshkov, Aguisanda, Thorne, et al. 2018). Through several secreted factors like prostaglandins, nitric oxide, and arachidonic acid astrocytes regulates blood flow in the brain (MacVicar and Newman 2015). They are also responsible for guiding the formation and maturation of synapses;

secreted molecules like apolipoproteinE and thrombospondins by astrocytes significantly promotes synapse formation shown *in vivo* and *in vitro* studies (Risher and Eroglu 2012; Clarke and Barres 2013). Targeting control synaptogenesis using astroglia could be a new method to target several neurodegenerative diseases. Astrocytes are responsible for the regulation of reactive oxygen species (ROS); high amounts of ROS are usually generated in the brain due to the high rates of oxidative metabolism. Glutathione derived from astrocytes is an essential antioxidant that has demonstrated protection against neuronal cell death (Drukarch, Schepens, Stoof, et al. 1998; Gorshkov, Aguisanda, Thorne, et al. 2018) whereas other studies have also shown that the activation of immunological cytokines, such as interferon (IFN- $\gamma$ ) and interleukin 1 $\beta$  (IL-1 $\beta$ ) in astrocytes, can generate harmful ROS causing damage to neurons (Sheng, Hu, Feng, et al. 2013). Table 1.1 provides a summary of several functions and the role of astrocytes in CNS.

**Table 1. 1: Role of astrocytes associated with multiple regions and functions of the brain (Gorshkov, Aguisanda, Thorne, et al. 2018).**

Functions and Role	Biological process	Reference
CNS Development	<ul style="list-style-type: none"> <li>• Neurons develop first, and then astrocytes develop.</li> <li>• Guides the migration of neural progenitors.</li> <li>• Supports Synapsis formation.</li> <li>• Produces and maintains Myelin.</li> </ul>	(Clarke and Barres 2013)
Barrier Function	<ul style="list-style-type: none"> <li>• Forms the blood-brain barrier.</li> <li>• Gap Fillers</li> <li>• Includes barrier properties in cerebral and endothelial cells</li> </ul>	(Kimmelberg and Nedergaard 2010; Sofroniew and Vinters 2010)
Homeostasis	<ul style="list-style-type: none"> <li>• Specialised mechanism to regulate fluids</li> <li>• Channels neurotransmission</li> </ul>	(Schousboe, I. and Winther-Lindqvist 2013)

	<ul style="list-style-type: none"> <li>• Glutamate and GABA regulations</li> </ul>	
Metabolic support	<ul style="list-style-type: none"> <li>• Glucose regulation in CNS</li> <li>• Releases molecules to directly activate synapsis</li> </ul>	(Sofroniew and Vinters 2010)
Synaptic transmission	<ul style="list-style-type: none"> <li>• Can modulate neuronal excitability via their <math>Ca^{2+}</math></li> <li>• Growth factors can regulate synaptic transmission over an extended period</li> </ul>	(Clarke and Barres 2013)
Neurovascular Support	<ul style="list-style-type: none"> <li>• Connects with blood vessels</li> <li>• Releases second messengers</li> <li>• In response to electrophysiological activity, regulates changes in blood flow.</li> </ul>	(Gordon, Mulligan and MacVicar 2007; Attwell, Buchan, Charpak, et al. 2010; MacVicar and Newman 2015)

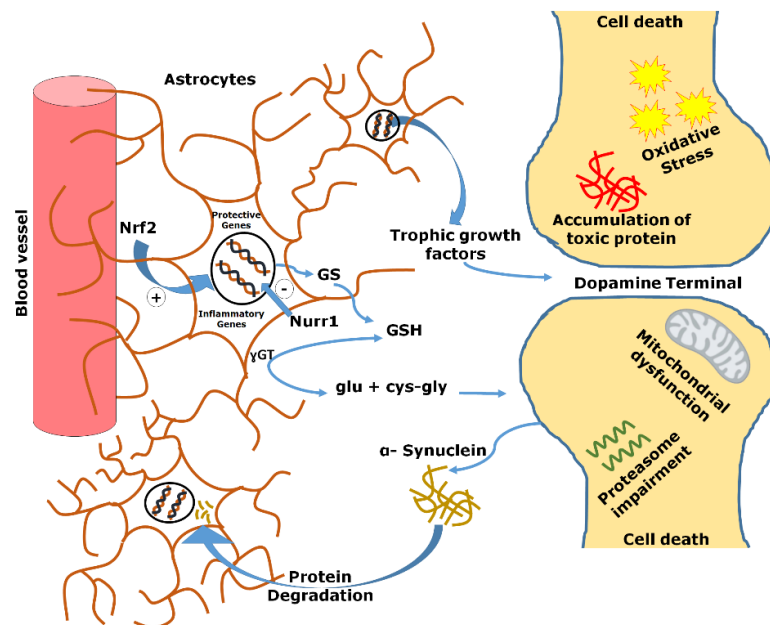


**Figure 1. 4: Potential neuroprotective pathways of astrocytes. Recreated from (Rappold and Tieu 2010).**

Multiple factors can influence a neuron cell death. Conditions like a genetic mutation, environmental toxins or maybe combinations of both through mitochondrial dysfunction, protein degradation, and oxidative

stress can lead to cell death. It has been predicted that astrocytic neuroprotection can be through the following pathways

1) The release of glutathione (GSH) which is then cleaved by  $\gamma$ -glutamyltranspeptidase on the astrocyte plasma membrane to generate glutamate and cysteinylglycine, which serves as a precursor of neuronal GSH synthesis.

2) The release of neurotrophic growth factor.

3) Activation of the transcription factor Nrf2 leads to expression of genes containing the antioxidant response element (ARE), including glutamylcysteine synthetase (GS), which is involved in GSH synthesis.

4) Activation of the transcription factor Nurr1, which suppresses the production of inflammatory cytokines.

5) Removal and degradation of cytotoxic molecules, such as  $\alpha$ -synuclein. (Rappold and Tieu 2010).

The cytoplasm of astrocytes contains intermediate filaments that produce a distinct protein called glial fibrillary acidic protein (GFAP) which is a significant component of these cells. Astrocytes protect the neuronal cells, and meaningful activities of these cells are found intertwined neurons, myelin and the axons (Benarroch 2005). Post-mortem studies of neurodegenerative disease patient brain showed a low density of astrocytes expression and GFAP levels when compared to a healthy human brain. (Hirsch and Hunot 2009). Several attempts have been made to study the neuroprotective property of astrocytes. A recent study targeted 5-HT<sub>1A</sub> receptors in astrocytes to protect neurons in mice models. The study was performed in a co-culture of astrocyte cells and neuronal cells, and the results showed that astrocytes via 5-HT<sub>1A</sub> receptors protected neurons against oxidative stress when treated with 8-OH-DPAT (Miyazaki, Asanuma, Murakami, et al. 2013). A similar study on functional engraftment of human ES cell-derived neurons enriched by

co-culture with telomerase-immortalised midbrain astrocytes has also proved the importance of astrocytes for the survival of neurons under various conditions. In the case of several neurodegenerative diseases, investigations on the neuroprotective property of astrocytes have suggested that survival of astrocytes play an important role directly or indirectly in the survival of neurons. Rappold and his co-workers have recently demonstrated the possible astrocytic pathway involved in neuronal protection, as shown in figure 1.2. A study has also demonstrated that extensive damage caused to astrocytes can extend its effect to the loss of neuronal cells thus leading to neurodegeneration (Rappold and Tieu 2010).

### 1.2.4 Neurotoxins

Neurotoxins, as the name implies, can prove neurologically toxic with their specific ability to damage neural components. Below are the four major types of neurotoxins that are used in this study to mimic neurodegenerative diseases pathophysiology.

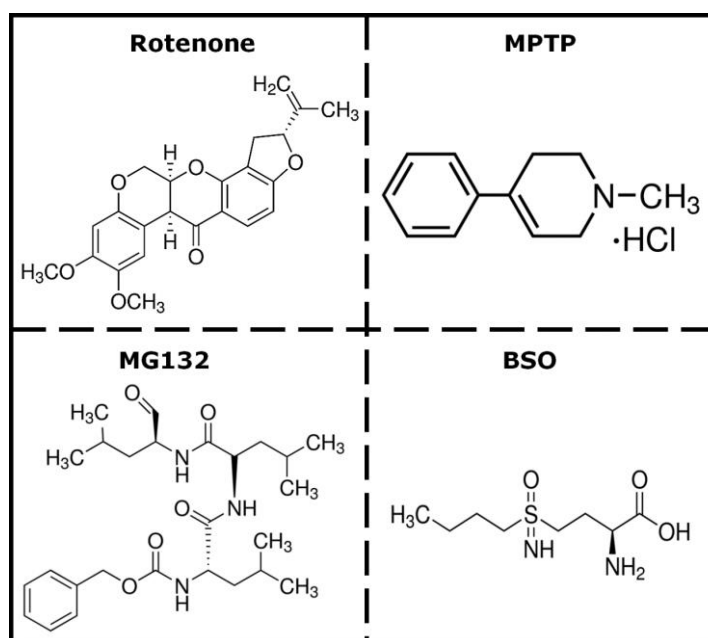


**Figure 1. 5: Chemical structure for neurotoxins used in this study.** Commonly used to simulate neural cell degeneration pathophysiology in several studies. Image obtained from Sigma Aldrich [Rotenone](#), [MPTP](#), [MG132](#), and [BSO](#)

#### **1.2.4.1 Rotenone**

Rotenone is one of the neurotoxins that have been used cause damage to the mitochondria in experimental models to explore the aspects of neural degeneration. Previous investigations have proposed several mechanisms for rotenone toxicity such as complex I inhibition, increased ROS production and effect on mitochondrial DNA replication. Several other toxins seem to induce apoptosis by its ability to open the mitochondrial transition pore that releases cytochrome-c and consequent ATP depletion (Cassarino, Parks, Parker Jr, et al. 1999).

#### **1.2.4.2 MPTP**

1-Methyl-4-phenyl-1,2,3,6-tetrahydropyridine hydrochloride (MPTP) is another toxin that causes a syndrome similar to core neurological symptoms and neurodegeneration by inducing oxidative stress and mitochondrial respiration defect together with an aggregation of proteins (Dauer, et al. 2003). Both rotenone and MPTP have been studied to behave as respiratory chain inhibitors of mitochondria while MPTP results in nerve cell death. A study showed that Ca<sup>+</sup> induced mitochondrial stress which is associated with inhibition of complex-I as an essential factor in neurodegeneration. It demonstrated that Ca<sup>+</sup> did not stimulate ROS to increase in rotenone-treated rat mitochondria with the presence of complex-I (Sousa, et al. 2003).

#### **1.2.4.3 MG132**

Z-L-Leu-D-Leu-L-Leu-al (MG132) is another type of proteasome inhibitor toxin used in many different studies, and it is a peptide aldehyde which blocks the proteolytic activity of the 26S proteasome complex (Han, Moon, You, et al. 2009). It is capable of reducing ubiquitin-conjugated protein degradation in mammalian cells with no changes in its ATPase and isopeptidase activity (Kim, D., Kim and Li 1999).

#### 1.2.4.4 BSO

L-Buthionine sulfoximine (BSO) a type of glutamylcysteine synthetase inhibitor. It contains Sulfoximine a chemical compound containing sulphur double bonded to nitrogen. It reduces glutathione a metabolite which plays a significant role in the protection of cells against oxidative stress and also plays a minor role in chemotherapy for the treatment of cancer (Defty and Marsden 2012).

#### 1.3 *In vitro* cell Models for neural cell degeneration

Due to limitations of live brain tissues, our understanding of neural cell degeneration is restricted to studies using post-mortem samples which represents the end-stage of disease. Despite interspecies differences, several aspects of the pathology displayed in such examples do not exactly necessarily mimic the disease phenotype at cellular levels. This highlights the importance of modelling of disease phenotype *in vitro* using defined cell populations to make it possible to study neurological disorders such as Amyotrophic lateral sclerosis, Parkinson's disease, Alzheimer's disease, and Huntington's disease.

The pathogenesis of neurodegenerative diseases is concurred by multiple factors and use of *in vitro* models using established cell lines, and primary cell cultures allow exploring genes/proteins involved in single pathogenic mechanisms by offering favourable controlled environment. To improve the understanding of neural cell degeneration at cellular levels, researchers focus on neurotoxicity (MPP+, 6-OHDA, BSO), excitotoxicity (NMDA, glutamate), mitochondrial dysfunction and defects in protein degradation. For neurodegenerative diseases like amyotrophic lateral sclerosis, Parkinson's disease, Alzheimer's disease, and Huntington's disease the major hallmark is the progressive loss of neural cells, and hence the development of *in vitro* models of these cell types could enable the study of neurodegeneration and novel preventative therapeutics. Although there is the only limited availability of human neurons from

foetal samples, direct examination of toxicity or protective effects in such neurons has been a challenge. Under such scenarios, pluripotent stem cells and neural stem cell progenitors are an excellent alternative source to ex vivo cultures of immortalised cell lines.

Besides stem cells, neuronal cell models in particular human neuroblastoma SH-SY5Y lineages have been employed due to its catecholaminergic neuronal properties (not strictly dopaminergic) and ease of maintenance during preclinical validations in neural cell degeneration research. SHSY5Y cells have been extensively used for differentiating into neuronal cells to characterise of neuronal features induced and as a cell model for toxicity studies. Retinoic acid (RA) differentiation of SHSY5Y cells demonstrated low proliferation rates with pronounced neuronal morphology with expressions of genes related to synaptic vesicle cycle, dopamine synthesis/degradation, transporter and was found to be more sensitive to 6-OHDA. Use of inhibitors of dopamine transporters induced protection against oxidative damage in RA-differentiated SHSY5Y cells (Lopes, Fernanda M., da Motta, De Bastiani, et al. 2017). A recent study indicated that MiR-124-3p could play a neuroprotective role in 6-OHDA treated SHSY5Y cells by targeting annexinA5 that mediates apoptosis and caspases activity (Dong, Zhang, Tai, et al. 2018). Different aspects of neural cell degenerative disease progression and novel treatments can be studied by employing appropriate experimental animal models. Although current animal models do not completely mimic these diseases, major types such as toxin models and genetic models have contributed extensively to knowledge on neurodegenerative diseases. Several invertebrates such as *Drosophila*, *C. Elegans* and snail and vertebrates like zebrafish, monkey, rat and mouse have been used to research the disease pathogenesis.

### **1.3.1 Toxin Models**

A range of toxin models based on neurotoxins has been studied over the years to test neuronal degeneration. Main characteristics of neurotoxins

such as 6-OHDA, MPTP, rotenone and paraquat have been extensively studied on recapitulating hallmarks of neural cells degeneration

#### **1.3.1.1 6-hydroxydopamine (6-OHDA)**

Neurotoxin-based neural cell degeneration model using intracerebral injections of 6-ODHA have shown to be neurotoxic by inhibiting the activities of mitochondrial respiratory complexes I and IV (Prajapati, Garabadu and Krishnamurthy 2017) along with the production of free radicals that induce oxidative stress and mitochondrial dysfunction (Hwang 2013). 6-ODHA can also trigger a decrease in glutamine in the striatum and an increase in glutamate thereby shifting the steady-state equilibrium of Gln-Glu cycle between neurons and astrocytes (Lei and Powers 2013)

#### **1.3.1.2 1-Methyl-4-Phenyl-1,2,3,6-Tetrahydropyridine (MPTP)**

Intravenous injections of MPTP could cross the blood-brain barrier (BBB) and be shown to induce parkinsonism by being metabolised by mono-amino oxidase in glial cells and transported into neurons in the form of MPP<sup>+</sup> (1-Methyl-4-Phenylpyridinium Ion). Further, MPP<sup>+</sup> results in reduced ATP production and ROS accumulation (Yan, Wang and Zhu 2013). Besides, MPTP can elevate levels of glutamine and other key enzymes of Glu-Gln cycle in the striatum that result in the loss of neurons and impaired motor function (Lu, Y., Zhang, Zhao, et al. 2018). Thus, MPTP administrations represent to be a classic toxin model.

#### **1.3.1.3 Rotenone**

Rotenone, a plant root extract is hydrophobic and could cross the BBB, independent of dopamine transporters. Like MPTP, rotenone inhibits mitochondrial complex I, leading to ROS production and thus mitochondrial dysfunction (Terron, Bal-Price, Paini, et al. 2018). A model developed by Betarbet showed that intravenous infusions of low doses of rotenone in Lewis rats caused selective degeneration of nigrostriatal

neurons (Betarbet, Sherer, MacKenzie, et al. 2000) while another group showed multisystem degeneration including loss of 54% and 28.5% of striatal fibres and neurons respectively (Höglinger, Féger, Prigent, et al. 2003). The progressive degeneration of neurons in brain might involve the contribution of a cascade of neuroinflammatory events that have been identified in several *in vivo* studies. Studies highlight the importance of identification of cellular and molecular events associated with neuroinflammation in neural cell degenerative models. Cellular responses such as oxidative stress and cytokine-receptor mediated apoptosis might not only allow us to understand disease progression but also to develop therapeutic strategies to downregulate the inflammation process and other deleterious events to the slow progression of these diseases (Hirsch and Hunot 2009).

Chronic midbrain slice culture *in vitro* model was used to determine the relevance of rotenone-induced damage to neurons. It was shown that treatments with  $\alpha$ -tocopherol and coenzyme Q10 attenuated rotenone-induced oxidative damage. This relevance was also determined *in vivo* models by systemic rotenone infusion that led to increased oxidative damage in particular dopamine-rich brain regions known to degenerate in brains the patients (Sherer, Betarbet, Testa, et al. 2003). A study conducted by (Malagelada, Jin, Jackson-Lewis, et al. 2010) reported that neuronal cell death was protected by rapamycin by blocking translation of RTP801 protein that is induced in cell and animal models and in affected SN neurons of the patients that leads to neuronal death due to dephosphorylation of Akt kinases, which is crucial for maintaining cell survival.

### 1.3.2 Genetic Models

Virtually all Alzheimer's disease models are based on the use of transgenic methodologies targeting APP, presenilin, tau or APOE genes, mostly in mice. Amyotrophic Lateral Sclerosis targeted genes include those encoding superoxide dismutase 1 (SOD1), (TAR)-DNA-binding protein 43 (TDP-43) and DNA/RNA binding protein Fused in Sarcoma (FUS). Transgenic models targeting the huntingtin (Htt) gene have been developed, providing new experimental opportunities for studying on Huntington disease. Since the identification of the huntingtin gene and the characteristic expanded CAG repeat/polyglutamine mutation, multiple murine genetic models and one rat genetic model have been generated. In addition to the different model to investigate neural cell degeneration, transgenic worm models using the Nematode *C. Elegans* has been used to study genes that are positively linked to familial neurodegenerative disease. Genes such as SNCA/ PARK1/ PARK 4,  $\alpha$ -synuclein, Leucine rich repeat kinase 2 (LRRK2), Parkin RBR E3 Ubiquitin Protein Ligase (PRKN), PTEN-induced putative kinase 1 (PINK1), DJ-1 (Protein Deglycase), ATP13A2 (ATPase Cation Transporting 13A2) have been found to be mutated during neural cell degeneration are widely studied using *C. Elegans* with their homologs LRRK-1, PDR-1, PINK-1, DHR-1.1/1.2, CATP-6 respectively. *C. Elegans*, a microscopic roundworm, have orthologs for 60-80% of human disease-causing genes including genes implicated in neurodegenerative disease thus indicating the use of this model organism in studying particular genes and generation of genetic models of several neurodegenerative disorders (Cooper and Van Raamsdonk 2018).

### 1.3.3 Pre-clinical models of neural cell degeneration

Acceleration of neural cell degeneration research depends on robust and promising preclinical models. Michael J. Fox Foundation has generated models that support progress in neurodegenerative disease research. Below is the list of models that displays various pathological phenotypes.

**Table 1. 2: Neural cell models with various pathological phenotypes**

<b>Model</b>	<b>Advantage</b>	<b>Disadvantage</b>
Genetically modified	<ul style="list-style-type: none"> <li>• Near physiological expression levels and standard spatiotemporal expressions.</li> <li>• Suitable for targeting clinically relevant pathways.</li> </ul>	<ul style="list-style-type: none"> <li>• Pathology is either absent or present only in advanced age.</li> <li>• Lack of motor deficits in several models.</li> </ul>
Viral vector-mediated overexpression/knockdown	<ul style="list-style-type: none"> <li>• Rapid onset of motor deficits with spatiotemporal control of progressive nigral lesions.</li> <li>• Facilitates the designing of internal control and adaptability to multiple species.</li> </ul>	<ul style="list-style-type: none"> <li>• Major drawback includes the use of supra-physiological expression levels.</li> </ul>
$\alpha$ -synuclein pre-formed fibrils ( $\alpha$ SynPFFs)	<ul style="list-style-type: none"> <li>• Spatiotemporal control of progressive nigral lesions with protracted time course.</li> <li>• Suitable for targeting extracellular <math>\alpha</math>-synuclein and its seeding hypothesis.</li> </ul>	<ul style="list-style-type: none"> <li>• Supra-physiological expression levels, less robust motor deficits and uncertainty of relevance of <math>\alpha</math>-synuclein species with human pathology.</li> </ul>
Neurotoxins	<ul style="list-style-type: none"> <li>• Spatiotemporal control of progressive nigral lesions with rapid onset.</li> <li>• Robust stereotyped motor deficits and oxidative stress.</li> </ul>	<ul style="list-style-type: none"> <li>• Lack of robust alpha-synuclein pathology and clinical relevance.</li> </ul>

Yeast/  
zebrafish/  
Drosophila

- High-throughput screening of therapeutics.

- Insufficient modelling of the human brain and complexity.
- Findings from these models require further replications in mammalian systems to understand its human relevance.

Other models include knockout models of transcriptional factors such as sonic hedgehog (SHH), pituitary homeobox 3 (Pitx3), nuclear receptor-related protein-1 (Nurr1) and engrailed 1 (EN1) that are key to the development and stability of nigrostriatal system (Gonzalez-Reyes, Verbitsky, Blesa, et al. 2012; Zhang, Le, Xie, et al. 2012). Disruption of mitochondrial transcriptional factor A has resulted in impaired motor function and neuronal death, due to degeneration of intraneuronal inclusions and nigrostriatal pathways (Good, Hoffman, Hoffer, et al. 2011). Studies have also suggested that defects in VMAT2 (vesicular monoamine transporter) might be an early mechanism leading to neuronal death (Taylor, Alter, Wang, et al. 2014), as VMAT2- knockout mice demonstrated enhanced MPTP toxicity while VMAT2-overexpressors displayed neuroprotection from MPTP toxicity (Lohr, Bernstein, Stout, et al. 2014).

Mimicking of neurodegenerative disease phenotype in animal models could be achieved by combining both toxin and genetic-based models as a multigene modulated transgenic model. Involvement of miRNA or siRNA to the appropriate model system could allow the development of a robust model. Use of primary cell culture models to mimic slow the progression with cellular damage phenotype could also help in drug discovery, but the use of these cells in a 2D tissue culture plastic may give findings that may not be entirely true. Every cell model discovered in the past has always

involved the use of animals or *in vitro* tissue culture experiments, yet there is not a significant model that has explained the full nature of neural cell degeneration or sufficiently reduced the progression without any side effects. Methods like cell replacement therapies and models using embryonic cells have always focused on replacing the lost neurons by injecting engineered cells directly into the affected area without providing the support or guidance for cells to grow (Björklund and Lindvall 2000; Björklund, Sanchez-Pernaute, Chung, et al. 2002). These techniques have only shown partial improvements or caused further damage in the rodent models. In this study, we have demonstrated the two primary cells that form the human brain can be cultured in a 3D nanofibre matrix that is capable of providing natural habitat. This model is capable of creating an *in vivo* like study in an *in vitro* environment allowing researchers to understand and analyse the pathophysiology conditions similar to a natural state, thus reducing the number of unsuccessful animal and human trials. The scaffold embedded with matured embryonic stem cells or pre-mature cell may also provide a robust platform in cell replacement and implant therapies shortly. Also, the development of a fully conductive scaffold and tissue model can help us to understand the electrical activity of these cells and improve investigations like DPS.

#### **1.4 3D Cell Culture**

Cell cultured and studied on two dimensional TCP has been a routine practice in many research groups worldwide. Cells cultured in 2D is arguably primitive and does not represent the anatomy or physiological conditions of a cell in its natural form. Using 3D cultures becomes more relevant but requires a multidisciplinary approach, and with advanced 3D systems, it becomes more relevant to human and animal physiology, leading to possibilities of complex co-culture systems. The use of a 3D cell culture system can vary widely based on the purpose which can range from tissue engineering for clinical purposes thorough to development of implant therapies and models of drug screening. Eukaryotic cell cultures have been in practice for more than 40 years, and the most common

substrate used for cell growth have been made using polystyrene or glass forcing the cells to form of a flat two-dimensional surface (Freshney 2015). Thousands of published studies ranging from drug screening through to developmental molecular biology have relied on 2D surfaces for the growth of adherent cells. It has been an assumption that animal or human physiology can be accurately reproduced using cellular monolayers; however, a 2D surface cannot represent an ECM found in native tissue (Haycock 2011). During the point of intercellular communication, many 2D culture experiments fail to consider the interplay between different cell types, with many cultures being of a single cell type. 2D co-cultures overcome some of these problems but mostly not easy to handle and inaccurately reproducing cellular function observed within a tissue (Haycock 2011).

A number of 3D methods have been developed in recent years for a range of issues in which the cell culture environment is taking the spatial organisation of the cell into account (Abbott 2003; Lee, J., Cuddihy and Kotov 2008). The aim is to bridge the gap between the use of whole animal and monolayer cell cultures. It is, therefore, necessary to create a growth environment that can mimic the native tissue as close as possible. However, 3D systems are complex and have several parameters to be considered. One critical criterion is the choice of material for the scaffold and the source of the cell. Not all three-dimensional culture models require a scaffold; however, the use of scaffolds for 3D models has certainly increased considerably in the past ten years. Examples include highly oriented 3D collagen scaffold to promote directed axonal growth, with dorsal root ganglia explants creating a 3D model for peripheral nerve regeneration (Bozkurt, Brook, Moellers, et al. 2007), Another study demonstrated grow embryonic, postnatal, and adult neural stem and progenitor cells on a collagen and hyaluronan scaffold (Brännvall, Bergman, Wallenquist, et al. 2007). A 3D scaffold made of poly(lactic-co-glycolic acid)/poly(L-lactic acid) were used for differentiating human embryonic stem cells (Levenberg, Huang, Lavik, et

al. 2003). Finally, one study compared the viability of hippocampal neurons and astrocytes grown on 2D conditions with 3D scaffold prepared from the coralline exoskeleton, showing better results for the 3D cultures (Peretz, Talpalar, Vago, et al. 2007). Three-dimensional culture models can be grouped into the study of whole animals and organotypic explant cultures (including embryos), cell spheroids, microcarrier cultures, and tissue-engineered models, hydrogels, scaffold-based and bioprinted models.

#### 1.4.1 Cellular Spheroids

Cellular spheroids are simple three-dimensional models that can be generated from a wide range of cell types and form due to the tendency of adherent cells to aggregate. Cellular spheroids are created from single culture or co-culture techniques using conventional methods like hanging drop, rotating culture, or concave plate methods (Castañeda and Kinne 2000; Timmins, Harding, Smart, et al. 2005; Pampaloni, Reynaud and Stelzer 2007). Scaffolds are not required for culturing spheroids and can be readily imaged using a microscope. Spheroids have been commonly used for high throughput screening and modelling solid tumour growth and metastasis studies (Ivascu and Kubbies 2006).

**Table 1. 3 3D Spheroid neural models. Adapted from** (Zhuang, Sun, An, et al. 2018)

Cell Type	Evaluation	Reference
<b>Mimicking neuronal networks formation</b>		
<b>Rat cortical</b>	Neurons within the spheroids were electrically active. Formation of synaptic networks Laminin secretion	(Dingle, Boutin, Chirila, et al. 2015)

<b>Rat cortical cells and hippocampal cells</b>	Functional networks were observed inside the NBB The synaptic connection between NBBs	(Kato-Negishi, Morimoto, Onoe, et al. 2013)
<b>Rat primary NPC</b>	Satellites spheroid were found around the host spheroids. Bundle networks were found between host spheroid and satellite	(Jeong, Chang, Park, et al. 2015)
<b>Understanding of neuropathology</b>		
<b>Human medulloblastoma cell line and human neural stem cells</b>	Feasibility study, Spheroid (co-culture of tumor cell and stem cell) was treated with Etoposide indifferent levels, led to ratio change of tumor cell and stem cell	(Ivanov, Parker, Walker, et al. 2014)
<b>NT2 cells</b>	Differentiated neurospheres enriched in mature neurons Functional astrocytes were obtained by stirred suspension culture	(Terrasso, Pinto, Serra, et al. 2015)
<b>Rat cortical cells</b>	Disrupted synaptic integrity in Abreacted group Decreased	(Choi, Yoon Jung, Park and Lee 2013)

	acetylcholine amount in Abreacted group	
<b>SH-SY5Y cell line</b>	Neural differentiation Increased levels of degeneration were achieved compared to 2Dsystem	(Seidel, Krinke, Jahnke, et al. 2012)
<b>Human midbrain- derived NPC</b>	Spheroids contained mature neurons with abundant synaptic connections. Functional neurons were observed.	(Simao, Pinto, Piersanti, et al. 2014)

#### 1.4.2 Hydrogel models

One of the significant challenges of treating neurodegenerative disease involves transplantation of foetal ventral mesencephalon grafts that survive post-transplantation with restored motor functions. It is reported that only 20% of these survive (Brundin, Karlsson, Emgård, et al. 2000) and researchers have been investigating methods to improve the survival of such neuronal grafts post-transplantation. Injectable scaffolds such as *in situ* hydrogels have been assessed to test their efficacy as a delivery platform to improve graft survival. An ideal scaffold would enhance cell engraftments by providing a supportive microenvironment for cell adhesion, deliver growth factors locally and prevent an attack from host neuro-immune cells (Orive, Anitua, Pedraz, et al. 2009). Collagen hydrogels are popular scaffolds with abundant natural ECM that is widely used for several applications such as cartilage engineering (Chattopadhyay and Raines 2014), dentistry (Patino, Neiders, Andreana, et al. 2002) nucleic acid delivery to balance inflammation and angiogenesis (Browne, Monaghan, Brauchle, et al. 2015). A study showed that encapsulation of primary neurons in GDNF-enriched collagen

hydrogel could significantly improve the survival and functional efficacy after intra-striatal transplantation in a rat model (Moriarty, Pandit and Dowd 2017). Hydrogels composed of type I collagen and low molecular weight hyaluronic acid and polyethylene glycol were used to deliver secretome from rat adipose tissue-derived MSCs in an active state and counteracted 6-OHDA by upregulation of SIRT3, an active protein in oxidative stress that positively regulates ROS detoxifying enzyme (Chierchia, Chirico, Boeri, et al. 2017). Neuroprotective agents such as activins have been studied for their potential neuroprotective effects by loading onto hydrogels for implantation into the striatum of a mouse model. Activin B loaded hydrogel was shown to significantly reduce inflammatory responses and provide substantial cellular protections and improved behaviour in mice post-surgery (Li, Juan, Darabi, Gu, et al. 2016). These studies suggest the potential applications of biomaterials in brain repair and neural transplantations for degenerative diseases.

#### **1.4.3 Engineering based scaffolds for neural tissue construction**

Materials like hydrogel and Matrigel has been frequently used in tissue engineering approaches. However, few studies suggest that these materials are poorly defined and have variations between each batch and several types of research have been notably carried out in replacing these materials (Lancaster, Renner, Martin, et al. 2013; Dixon, Shah, Rogers, et al. 2014; Caiazzo, Okawa, Ranga, et al. 2016). Extensive materials have also been investigated and modified to incorporate diverse chemical or physical cues to reconstruct tissue environment with enhanced authenticity. solid materials, such as PLGA, PLLA, PCL, Gelatine, Collagen, alginate, polyethylene glycol, silk fibroin have been widely explored for constructing neural tissue models. Compared to gel-like structures engineered solid materials are easily amendable according to the topographic and physiological cues. Depending on the specific biological interest, both natural and synthetic materials have been carefully defined to mimic the physiological conditions, and each material has its pros and cons. A study demonstrated synergistic effects of matrix and signalling

molecules on mESC differentiation comparing neuronal response when cultured on 2D substrates vs 3D scaffolds made of type 1 collagen and Matrigel, gelatine and peptide-RAD16-II. Robust neural differentiation and neurite outgrowth was observed in 3D scaffolds, and the study leads to instructive guidance for engineering 3D neural tissue environment (Kothapalli and Kamm 2013). Another study used highly porous layered silk protein-based scaffold to mimic the cerebrum and coated it with polylysine to represent the grey matter. Then the structure was combined with collagen gel to fill up the central zone of the silk to mimic the white matter. After optimising several parameters, the research group was able to maintain viable and functional macroscopic neural tissue blocks for nine weeks with robust axonal development and network interconnectivity were detected in the silk-collagen region, and random disperse of neurons were seen in the pure collagen region. The results demonstrated the critical effects of matrix mechanical stiffness on neural network formation. Models based on cell biology depends on cell organisation and response whereas engineering-based models are based on piecing together the necessary components to represent the microenvironment of tissue with high complexity and fidelity. By incorporating well-defined components necessary chemical and physical cues for a cell survival, 3D engineering-inspired models are capable of presenting the cells with a more consistent and control able microenvironment (Irons, Cullen, Shapiro, et al. 2008; Ren, M., Du, Acero, et al. 2016).

#### **1.4.4 Microfluidic technology models**

Microfluidic based 3D models are a multidisciplinary approach which is developed at an intersection of biotechnology, nanotechnology, biochemistry, physics, chemistry and engineering. The system has a designed for practical applications for low volume of fluids for automation, multiplexing and high-throughput screening. This technique is a very different form of the 3D culture system. The System manipulates the fluid flow to define the culture environment. Complex methods like co-culture of cells, control over cell patterning, perfusion flow, ECM/material organisation and soluble factor gradients generation can be achieved via

microfluidic platforms (Bhatia and Ingber 2014; van Duinen, Trietsch, Joore, et al. 2015). Microfluidics is made with high lithography resolution, good optical clarity and excellent repeatability (van Duinen, Trietsch, Joore, et al. 2015). The technique has been widely used in recapitulating the predominant features of neurological diseases, mimicking the cortical structure, modelling brain environment like the BBB and directing neurite growth (Kunze, Giugliano, Valero, et al. 2011; Park, JiSoo, Lee, Jeong, et al. 2015; Bang, Na, Jang, et al. 2016). Mimicking gradients of ECM involves the components, mechanical stiffness, signalling factors that can have a great impact on the process of the tissue. A study demonstrated an effective gradient form an effective path for cell survival and cell density. The study combined a 3D model with a spatially gradated hydrogel and u-87 cell to create a model to study the heterogeneous nature of glioma microenvironment. The system was designed with two parts, a micro-fluidic diffusive mixer and a connected mould (Pedron, Becka and Harley 2015). Similarly, another study demonstrated mimicking neuronal network formation. The group created a 3D microfluidic model filled with Matrigel to represent a primary rat cortical neuronal circuit. The study showed higher rate of neurite elongations resulting in approximately 1500µm long axonal bundles (Bang, Na, Jang, et al. 2016).

Many similar studies have been reported using the microfluidic technology 3D models, which offers high fidelity and possibility of control over culture conditions. Despite the advantages, several limitations remain. The fluid flow needs to be well balanced and controlled; if not, the system suffers bubble formation compromising cell viability. The intricate design of the fluid flow is facilely manipulated *in vitro*, and it may be difficult to introduce to *in vivo* or clinical applications (Bhatia and Ingber 2014; Zhuang, Sun, An, et al. 2018).

### 1.5 Novelty of This Study

The human brain is a highly complicated 3D structure made of the neuronal and glial cell population that is yet to be fully discovered and understood (Herculano-Houzel 2009). Understanding the dynamics of the electrical activity that constitutes the primary signalling method of the brain, how nerve cells make connections creating circuits for multiple purposes, how recall of memories work and how signals are translated to movements and behaviours. The tiniest error in the system can affect the entire network both chemically and morphological leading to several brain-related issues. Several neurological disorders have been identified that are caused by such changes in the brain, but the reason for the changes remains unknown or are not fully understood for several neurodegenerative disorders. It is clear that these diseases is caused by the loss of neural cell function in the brain, but the reason for the death of the cells is still under debate, and the cause not yet identified. The most important unresolved issue is the development of a neuroprotective therapy capable of slowing, reversing or stopping the process of neurodegeneration. As described previously, current treatments are only useful in controlling the symptoms in the early stages, but these are accompanied by irreversible side effects. All the current research in neurodegenerative diseases are focusing efforts to either identify the actual cause or to replace the lost and damaged cells. Scientists have been trying to meet these through both *in vitro* and *in vivo* animal study. *In vitro* studies on protein misfolding, abnormal autophagy, Ubiquitin-proteasome system (UPS) dysfunction, oxidative stress, mitochondrial dysfunction, altered protein phosphorylation and other targets have always been investigated using 2D cell cultures for a disease that exists in a 3-dimensional structure (Gai, Yuan, Li, et al. 2000; Ghosh, Mondal, Mohite, et al. 2013; Covell, Robinson, Akhtar, et al. 2017). Several types of research are being conducted to identify new drugs or to modify existing drugs. Most drug-related studies are conducted on animals and demand a high usage of animals with high research costs and as yet have

had poor outcomes. Several animal models have been developed to investigate novel treatments to identify factors associated with the cause, stop or slow the disease. However, most models are unsuccessful in meeting their intended target (Duty and Jenner 2011; Blesa and Przedborski 2014). Significant types of animal model for neurodegenerative diseases are toxic models addressing the hallmarks and genetic models. Toxic models are endpoint studies leading to the death of animals, and genetic models involve causing overexpression or knockouts. Unfortunately, these diseases are multi-faceted, and just one model cannot be a complete model to fully understand or investigate the condition (Jackson-Lewis, Blesa and Przedborski 2012). Current research focuses on developing strategies to delay disease progression by replacement of damaged neurons using stem cells or restoration of original neuronal architecture or by promoting neurite regeneration. Currently, there are no drugs that are capable of stopping the slow loss of neurons in a patient, and there are no a suitable *in vivo*, *in vitro* or *in silico* models to study these diseases for drug discovery.

### **1.5.1 Structure of this study**

This study has focused on investigating how various electrospun nanofibres composed of synthetic polymers such as polyacrylonitrile (PAN), PAN/Jeffamine (PJ), support cell adhesion and proliferation. To demonstrate how the model can be suitable for different types of neurodegenerative research, different types of cells that are commonly used in neurodegenerative disorder investigations were examined. The first was human SH-SY5Y neuroblastoma cell line, the second human U-87MG glioblastoma cell lines, and the third human RenCellCX a neural progenitor stem cell line and finally embryonic neurons and astrocytes from rat brain. The nanofibre materials were evaluated for their ability to provide better cell growth, support survival and were further used to develop a suitable cell model for the investigation of several

neurodegenerative diseases and a model to identify endpoints that are suitable for screening neuroprotective compounds

The main aims of the project were:

1. Use the electrospinning technique to produce bio-active scaffolds which include mixtures of aligned and non-aligned fibres, where the fibre consists of chosen polymers.
2. Identify a suitable method to sterilise the bio-active nanofibre scaffold while maintaining integrity and function.
3. Optimise nanofibre compositions to support the growth and survival of neuronal and glial from 3 different cell types
4. Investigate the effect of neural cell degeneration paradigms using the 3D system in comparison to conventional 2D culture processes.
5. Evaluate cell to nanofibre interaction and development of a 3D microenvironment
6. Develop a co-culture model and identify suitable endpoints of relevance to neuronal function, differentiation and survival that can be monitored within the 3D setup.
7. Identify suitable in-vitro designs which deliver endpoints which track those measured or observed *in vivo*, and that can be measured with a high throughput system.
8. Assess and integrate a range of known and novel neuroprotective agents with 3D nanofibre cell model to promote neuronal survival and enhance neurotrophic support and prevent neurodegeneration.

## Chapter 2: Materials and Methods

### 2.1 Materials

#### 2.1.1 Cell Culture

##### 2.1.1.1 Cell Lines

Human SH-SY5Y neuroblastoma, (CRL-2266) American type culture collection (ATCC), UK

Human U-87 MG glioblastoma, (HTB-14) ATCC, UK

Human ReNcell CX neural progenitor cells, (SCC007) Merck Millipore, UK

Primary neurons and glial derived from E18 C57 Mouse hippocampal brain tissue, BrainBits, UK

##### 2.1.1.2 Cell Culture Reagents

###### 2.1.1.2.1 Cell Culture Media

SH-SY5Y- Dulbecco's Modified Eagle Medium (DMEM) F-12 (1:1) mix with 15mM HEPES, L- Glutamine – (BE12-719F) Lonza, Berkshire, UK

U-87 MG- Eagle's Minimum Essential Medium (EMEM) w/o L-glutamine (BE12-127F) – Lonza, UK

ReNcell CX- Knockout DMEM /F-12 (12660012) GIBCO/Life Technologies (UK), Recombinant Human Fibroblast Growth Factor Basic (FGFb), (PHG0024) GIBCO/Life Technologies (UK), Recombinant Human Epidermal Growth Factor (EGF), (PHG0311) GIBCO/Life Technologies (UK), Stempro neural supplement, (A1050801) GIBCO Life Technologies (UK),

Primary neurons: Hibernate® EB (HEB; Hibernate E®/B27®/GlutaMAX™), Neurobasal®/B27®/GlutaMAX™. 4500 BrainBits, UK, papain (BrainBits® PAP 6 mg), Hibernate E-Ca (HE-Ca)

Primary astrocytes: NbASTRO BrainBits, UK

**2.1.1.2.2 Common Cell Culture Reagents**

Accutase, (A6964) Sigma-Aldrich, UK

Foetal Bovine Serum, (11573397) Invitrogen Gibco

Hybridmax filter sterilised Dimethylsulfoxide (DMSO) (D2650) – Sigma Aldrich, UK

Laminin from mouse EngelbrethHolm-Swarm (EHS), (11243217001) Sigma-Aldrich, UK

MEM non-essential amino acid solution (M7145) – Sigma Aldrich, UK

Penicillin-Streptomycin (DE17-603E) - Lonza, UK

Phosphate Buffered Saline without  $\text{Ca}^{2+}$  and  $\text{Mg}^{2+}$  (BE17-516F) - Lonza, UK

Sodium Pyruvate Solution 100 mM (BE13-115E) - Lonza, UK

Trypan blue solution [0.4% (v/v) solution] (T8154) – Sigma Aldrich, UK

Trypsin-EDTA (BE02-007E) - Lonza, UK

**2.1.2 Plastic, Glassware and other materials**

9" silanized Pasteur pipette to an opening of  $\sim 0.5$  mm (BrainBits, UK).

10 ml syringe tube luer-lok tip, Becton and Dickinson, UK

15 ml and 50 ml red capped tubes – Sarstedt, UK

21 gauge tube grade 304 cuts to length 100mm with back point one end, Stainless Tube and Needle Company, UK

3M 425 Conductive Aluminium Tape (R06933), RS Components

6 well, 12well, 24well and 96 well sterile tissue culture plates – Sarstedt, Leicester, UK

Cell culture flasks (T25, T75 and T175) – Sarstedt, UK

Corona discharged Polyester Sheets 600mm X 300mm clear polyester 75microns thick, Nano Products, UK

Cryovials - Sarstedt, UK

Leit Adhesive Carbon Tabs 12mm (AGG3347N), Agar Scientific, UK

Leit Adhesive Carbon Tabs 25mm (AGG3348N), Agar Scientific, UK

Pipette filter tips (10  $\mu$ l, 200  $\mu$ l and 1000  $\mu$ l) – Dutscher Scientific, France

Polypropylene sterilin tubes – Sarstedt, UK

PTFE tubing 1/31 inch bore size, Altec, UK

SEM Specimen Stubs, 12.5mm dia (AGG301), Agar Scientific, UK

SEM Specimen Stubs, 25mm dia (AGG399), Agar Scientific, UK

SLS Coverslips No 0 15mm Dia (MIC3278) Scientific laboratory supply, UK

Sterile serological pipettes (5ml, 10ml and 25ml) - Sarstedt, UK

### **2.1.3 Chemicals and reagents**

3-(4,5-dimethylthiazol-2-yl)-2,5-diphenyltetrazolium bromide (MTT) (M2128) – Sigma Aldrich, UK

Accugel 29:1 (40% solution) acrylamide (A20068) – GeneFlow Ltd UK

Adenosine 5'-triphosphate, ATP (A3377) - Sigma Aldrich, UK

B27 Supplement 50X, (17504001) ThermoFisher, UK

Bicinchoninic Acid (BCA) kit (BCA1-1KT)

Bovine serum albumin (A2153) – Sigma Aldrich, UK

Cell Counting Slides for TC10™/TC20™ Cell Counter, Dual-Chamber (1450015) BioRad, UK

Cell Titer Glo 3D cell viability assay kit (G9681), Promega, UK

CoolBlue MAX protein gel stain (R2034A) – Interchim Ltd, UK

Copper phthalocyanine 3, 4', 4'', 4''' tetrasulphonic acid tetrasodium salt (245356) – Sigma Aldrich, UK

Copper (II) Sulphate (451657), Sigma-Aldrich, UK

Dibutyryl-cAMP (D0627) Sigma-Aldrich, UK

Dimethylformamide (D1331) Fisher Scientific, UK

Folin & Ciocalteu's phenol reagent (F9252) Sigma-Aldrich, UK

Hexafluoro-2-propanol (105228) Sigma Aldrich, UK

Instant Blue™ protein stain (ISB1L) – Expedeon Ltd, UK

Jeffamine® ED-2003 Polyetheramine  $M_w$ 2000, Huntsman, USA

L-Buthionine-sulfoximine, (B2515) Sigma-Aldrich, UK

Marvel milk powder, Marvel, UK

MG132 (M8699) Sigma-Aldrich, UK

Nitrocellulose 0.22  $\mu$ m pore size (WP2HY00010) – Labtech Ltd, UK

Phalloidin conjugates with TRITC (P2141) - Sigma Aldrich, UK

Polyacrylonitrile  $M_w$ 150,000 (181315) Sigma-Aldrich, UK

Polycaprolactone  $M_n$ 80,000 (440744) Sigma-Aldrich, UK

Poly-L-lysine solution, (P4707) Sigma-Aldrich, UK

Precision Plus protein all blue standards (161-0376) - Bio-Rad Laboratories Ltd, UK

Protease inhibitor cocktail (P8340) – Sigma Aldrich, UK

Retinoic acid (R2625) Sigma-Aldrich, UK

RIPA Buffer (R0278) Sigma-Aldrich, UK

Rotenone (R8875) Sigma-Aldrich, UK

SDS PAGE Tank Buffer (10 X) Tris-Glycine SDS (9-0032) - Geneflow Ltd, UK

Sodium bicarbonate (S5761), Sigma-Aldrich, UK

Sodium butyrate (B5887) Sigma-Aldrich, UK

Sodium dodecyl sulfate (L3771), Sigma-Aldrich, UK

Sodium hydroxide (S8045), Sigma-Aldrich, UK

Tetramethylethylenediamine (TEMED) (T9281), Sigma-Aldrich UK

Tris Base (Tris-Ro), Sigma-Aldrich, UK

Tris-Glycine Electroblothing Buffer (10X) (B9-0056) – Geneflow Ltd, UK

TritonX (X100), Sigma-Aldrich, UK

Tween 20 (P1379), Sigma-Aldrich, UK

VECTASHIELD® mounting medium with DAPI (H-1500) – VECTOR Laboratories, UK

VECTASHIELD® mounting medium with propidium iodide (H-1300) – VECTOR Laboratories, UK

#### **2.1.4 Equipment**

Aida image analyser software (version 4.03) - Raytek Scientific Ltd, Germany

Automated Cell Counter (TC20™), BioRad, UK.

BioRad model 680 microplate reader - Bio-Rad Laboratories Ltd, UK

CBS isothermal liquid nitrogen storage system 2300 series – Sanyo medical division, UK

CO<sub>2</sub> laser cutter, (SP500), Trotec, UK

Eppendorf research pipettes (P10, P100 and P1000)

ES sputter coater (Q150R), Quorum Technologies, UK

Euromex camera (CMEX 5), Euromex microscopes, Holland

Farnell L3OB stabilised power supply, Farnell, UK

FLUOStar OPTIMA - BMG Labtech, UK

FujiFilm FLA-5100 gel scanner - Fujifilm Life Sciences Products, Sheffield, UK

Fujifilm intelligent dark box - Fujifilm Life Sciences Products, Sheffield, UK

Glassman high voltage power supply, Glassman Europe Ltd, UK

iblot – Invitrogen Lifesciences Ltd, UK

iMark microplate reader spectrophotometer, BioRad, UK

Leica CLSM laser confocal scanning microscope - Leica, Germany

MIKRO 22R microcentrifuge – Hettich Ltd, Germany

Mini wet blotting apparatus – Geneflow, UK

MiniClima humidity control EBC 11, MiniClima, Austria

Mini-Protean III - Bio-Rad Laboratories Ltd, UK

Mini-Protean tetra - Bio-Rad Laboratories Ltd, UK

Nanodrop 8000 – Labtech International Ltd, UK

NE-1002X Syringe pump, New Era Syringe Pump Systems Inc, USA

Nikon digital net camera DN100 – Nikon Ltd, Japan

Nikon Eclipse TS 100 inverted microscope – Nikon Ltd, Japan

Nikon Eclipse TS 100 inverted microscope - Nikon, Japan

Ohaus Scout Pro balance - Fisher Scientific Ltd, UK

Olympus BX51 fluorescence microscope – Olympus, Japan

Olympus CK ULWCD light microscope – Olympus Ltd, Japan

Olympus microscope (CKX31), Olympus, UK

Phenom ProX TM G2 PRO desktop Scanning Electron Microscope by Lambda photometrics, UK

Philips pH meter model PW9409 – Pye-Unicam, UK

Power Pac 3000 power supply - Bio-Rad Laboratories Ltd, UK

Protean IEF cell – Bio-Rad Laboratories Ltd, UK

REVCO Ultima II -80 °C Freezer – Biocold Laboratories, UK

Rotor-gene 3000 Thermal cycler – Corbett Research Ltd, Germany

Sanyo CO2 incubator MCO-17AIC - Sanyo Gallenkamp PCL, Leicestershire, UK

Sanyo Harrier 18/80 refrigerated centrifuge - Sanyo Gallenkamp PCL, Leicestershire, UK

Scanning Electron Microscope (JSM – 7100F), JEOL, UK

SM1 magnetic stirrer – Stuart Scientific Ltd, UK

Soniprep 150 - MSE Scientific instruments, UK

Stuart Heating block model SBH10D – Geneflow Ltd, UK

Stuart orbital shaker model SSL1 – Geneflow Ltd, UK

Stuart vortex mix model SA7 - Geneflow Ltd, UK

Telesto II OCT, Thor Labs, UK

Ultrasonic welder, China

Ultra flex III TOF/TOF mass spectrophotometer – Brucker Daltonics Ltd, UK

Walker class II safety cabinet – Walker safety cabinets Ltd, UK

Water bath 20 -90 °C – Grant Ltd, UK

## 2.1.5 Antibody

## 2.1.5.1 Primary Antibody

Table 2. 1: List of Primary antibodies

Antibody Name	Molecular Weight KDa	Host Species	Application	Supplier
Monoclonal anti $\alpha$ - Tubulin	50	Mouse	IF - 1:200 WB 1:10,000	Sigma Aldrich (T 6074)
Polyclonal anti-Actin	42	Rabbit	IF - 1:200 WB 1: 5000	Sigma Aldrich (A 2066)
Polyclonal anti GFAP	50	Rabbit	IF- 1:1000 WB-1:5000	GeneTex (GTX108711)
Monoclonal anti neurofilament- H (Phosphorylation independent)	200	Mouse	IF- 1:400 WB- 1:1000	Sigma- Aldrich (N0142)
Phosphorylated anti- Neurofilament H (NF-H), SMI34-	200	Mouse	IF- 1:500 WB-1:500	BioLegend (835504)
Monoclonal anti- Synaptophysin	37	Rabbit	IF- 1.1000 WB- 1:5000	Abcam (ab32594)
Monoclonal anti- $\beta$ III tubulin	50	Mouse	IF- 1:500 WB- 1:1000	Abcam (ab52623)

Monoclonal anti- $\beta$ actin	42	Mouse	IF- 1:500 WB- 1:1000	Abcam (ab8226)
Monoclonal anti vinculin	110	Rabbit	IF- 1:500 WB- 1:5000	Abcam (129002)

### 2.1.5.2 Secondary Antibodies

Polyclonal horse anti-mouse IgG HRP conjugated antibody (#7076) – Cell Signaling Technology, UK

Polyclonal goat anti-rabbit IgG HRP conjugated antibody (#7074) – Cell Signaling Technology, UK

Polyclonal bovine anti-goat IgG HRP conjugated antibody (805-035-180) – DakoCytomation Ltd, UK

Alexa Fluor 488 donkey anti-mouse IgG (A21202) - Invitrogen Ltd, UK

Alexa Fluor 488 donkey anti-goat IgG (A11057) – Invitrogen Ltd, UK

Alexa Fluor 488 donkey anti-rabbit IgG (A-21206) – Invitrogen Ltd, UK

Alexa Fluor 568 goat anti-mouse IgG (A11004) - Invitrogen Ltd, UK

Alexa Fluor 568 donkey anti-rabbit IgG (A10042) – Invitrogen Ltd, UK

Alexa Fluor 647 donkey anti-rabbit IgG (A31573)- Invitrogen Ltd, UK

Alexa Fluor 532 goat anti-mouse IgG (A11002)- Invitrogen Ltd, UK

## **2.2 Methods**

### **2.2.1 Design engineering and laser cutting**

The first step of this study was engineering a suitable design that can be used to form different orientations of nanofibres. Models to produce suspended nanofibre scaffolds were designed using AutoCAD 3D software which was then converted a file supported by Corel Draw for the laser cutter. The constructed design was loaded into a Trotec CO<sub>2</sub> laser cutter which was later implemented and cut to accurate measurements on a polyester sheet. Three different models were carefully designed suitable for various type of studies, each with its unique orientations. Each design was made for producing a random nanofibre, aligned nanofibre and radial nanofibre. Details on each design explained below, but this study was majorly performed on random nanofibre models.

#### **2.2.1.1 Suspended random nanofibre scaffolds**

The design and process fabricates fully suspended random nanofibre scaffolds. The design was built on a 600mm X 300mm layout with an array on 10mm circles spaced at 20mm centre to centre as shown and explained in Figure 2. 1. The design was made on a 75 µm thick polyester sheet using a Trotec Co<sub>2</sub> laser at 100% speed 28% power and 1000 pulse per inch (PPI). The model consists of two sheets a bottom sheet on which the fibres are collected and an identical top layer which is used to secure the fibre. After the fibres are spun, the sheets were ultrasonically tack welded and secured in place before cutting into the desired size to fit appropriate well plates. The fibres were laser cut at 80% speed and 50% power to create 20mm circular discs to fit in 12 well plates, as shown in Figure 2. 2.

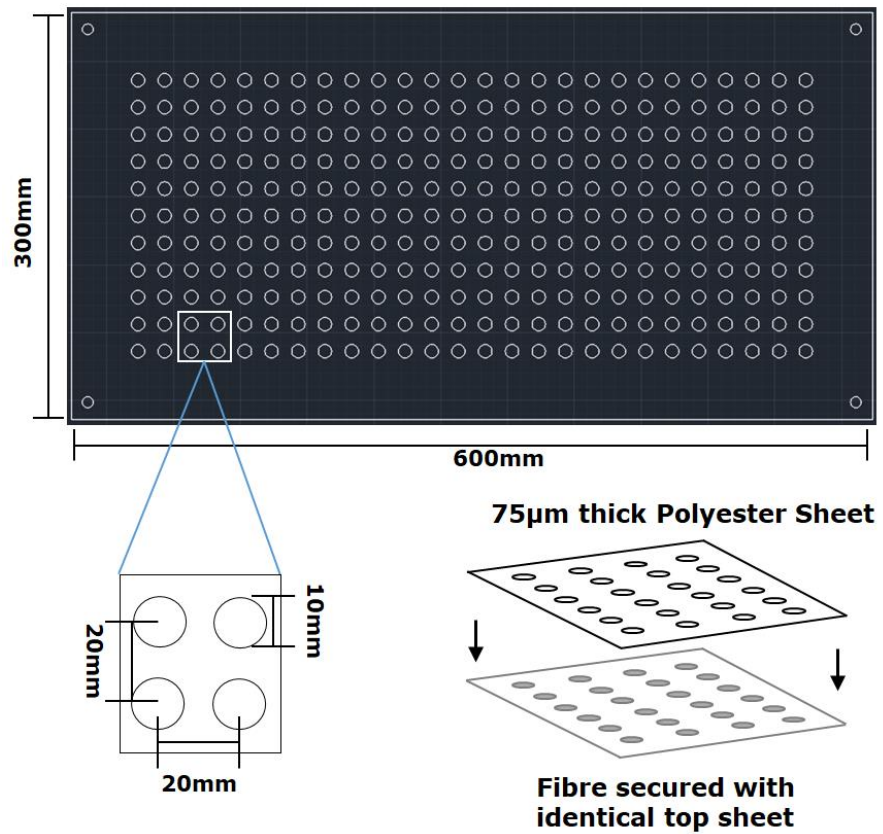


**Figure 2. 1: Schematic representation of random fibre design with measurements**

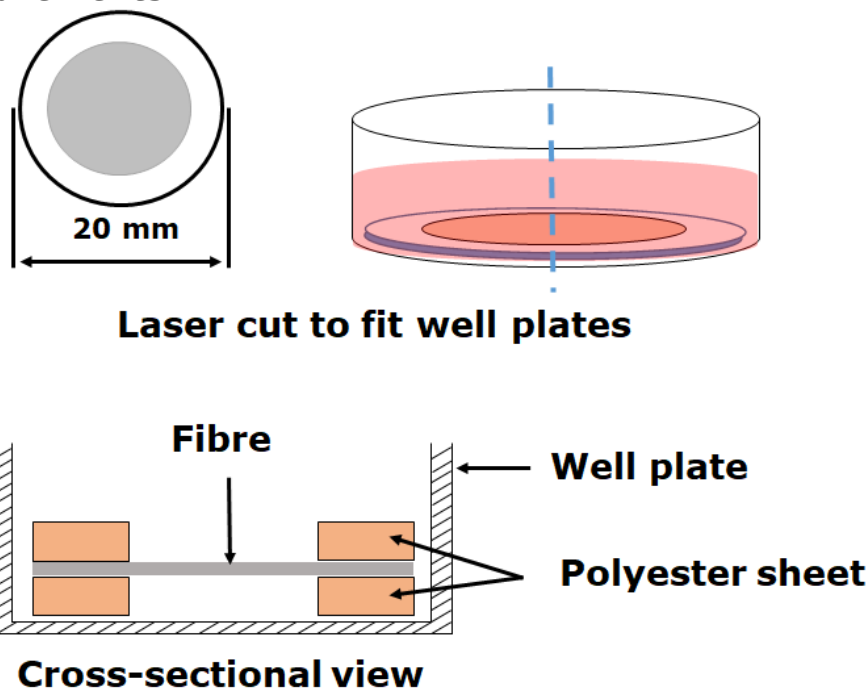


**Figure 2. 2: Random fibre cross-sectional view.**

### 2.2.1.2 Aligned nanofibre

This method of fabricating fully suspended aligned nanofibre design was developed in-house and has been filed for a patent (UK patent application number GB2553316A). The design is capable of containing both random and aligned fibre in a single scaffold. The design was engineered on AutoCAD and was made on a 75  $\mu\text{m}$  thick polyester sheet using a Trotec CO<sub>2</sub> laser at 100% speed 28% power and 1000 PPI. The design comprises of three layers of 600mm X 300mm polyester sheet. Two identical top layers to secure the fibre and a modified bottom layer to create aligned orientation of fibres. The top sheet Figure 2. 3A consists of an array of two parallel rectangles with an ellipse in the middle and the bottom sheet Figure 2. 3B with just the rectangles matching the dimensions as the top sheet. The design was built based on the aspects as described in Figure 2. 3. The top and the bottom layers were ultrasonically welded together before electrospinning. The combined sheet was placed on a rotating collector with the top sheet facing upwards. After the electrospinning, the bottom sheet was detached, and the top layer was secured with an identical sheet to secure the fibres. The sheets were ultrasonically tack welded and secured in place before cutting into the desired size to fit appropriate well plates. The final layer was laser cut at 80% speed and 50% power to a 20mm circular discs to fit in a 12 well plate Figure 2. 4.

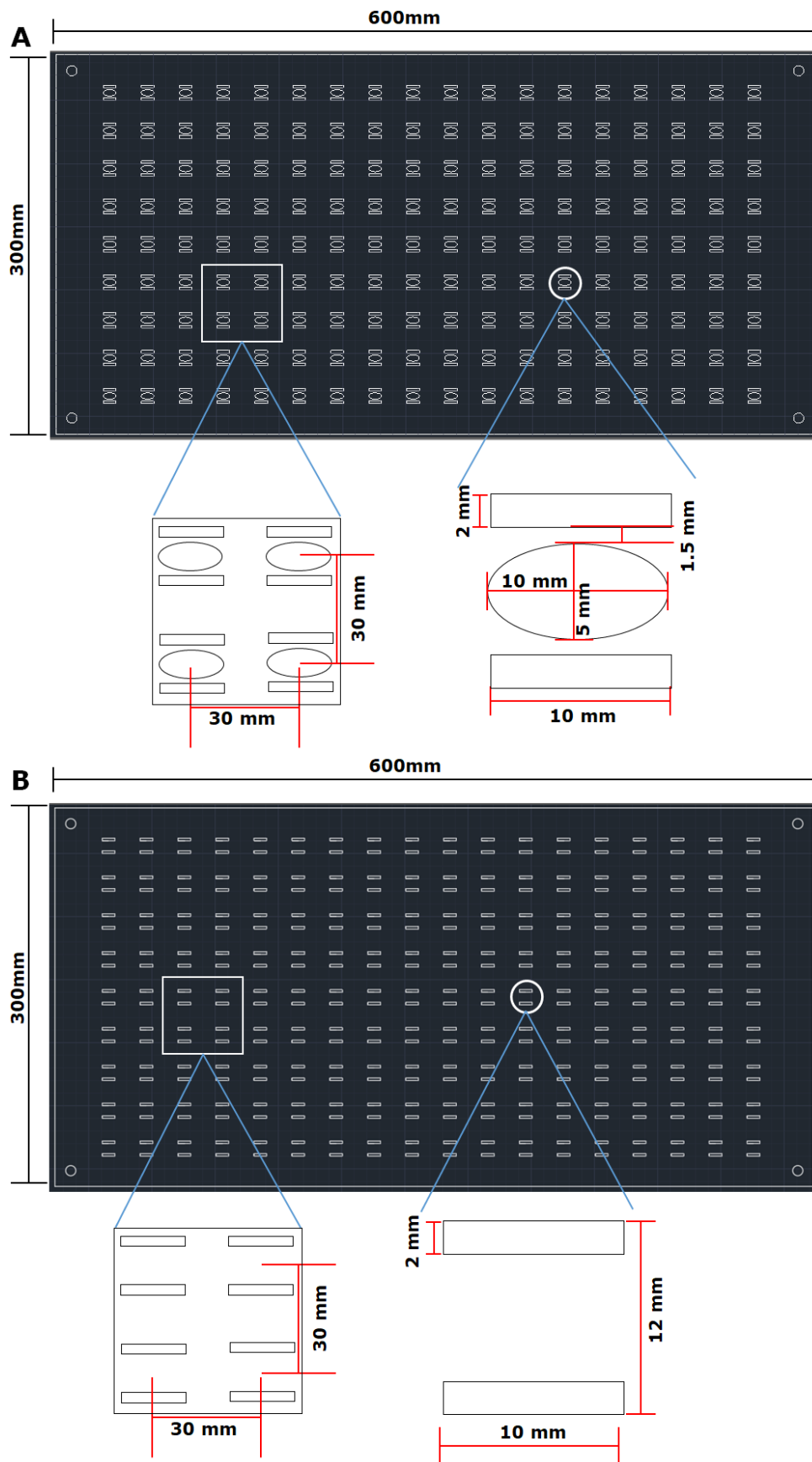


**Figure 2. 3: Schematic diagram for aligned fibre template.**  
*A Top sheet and B bottom sheet design used for obtaining aligned fibre.*

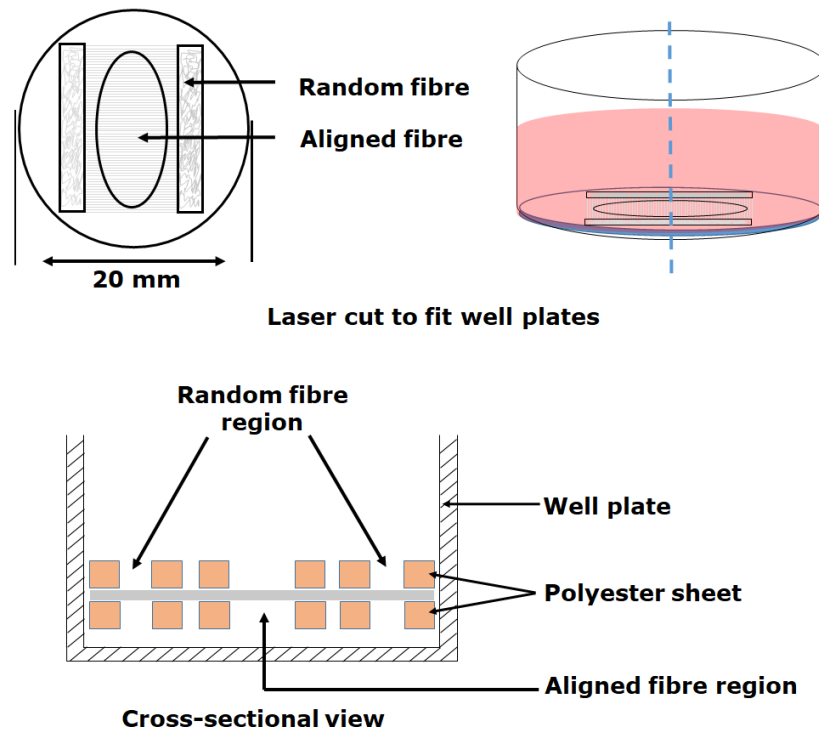


**Figure 2. 4: Aligned fibre cross-sectional view.**

### 2.2.1.3 Radial nanofibre

The radial nanofibre design was constructed based on the same principle as the aligned fibres. To obtain this type of orientation of fibre, it requires three layers; two top sheets and one bottom layer sheet. The design comprises two outer circles and one inner circle. Further details and the dimensions of the model are explained in Figure 2. 5 A and B. With the design, and it was possible to build fibres that were random orientation within the outer circle and radially aligned to the concentric centre circle of random fibres, forming an eye-shaped structure. The top and the bottom sheets were ultrasonically welded together before electrospinning. The combined sheet was placed on a rotating collector with the top layer facing upwards. After the electrospinning, the bottom sheet was detached, and the top layer was secured with an identical sheet to secure the fibres. The sheets were ultrasonically tack welded and secured in place before cutting into the desired size to fit appropriate well plates. The final layer was laser cut at 80% speed, and 50% power to produce 20mm circular discs to fit in 12 well plates Figure 2. 6.

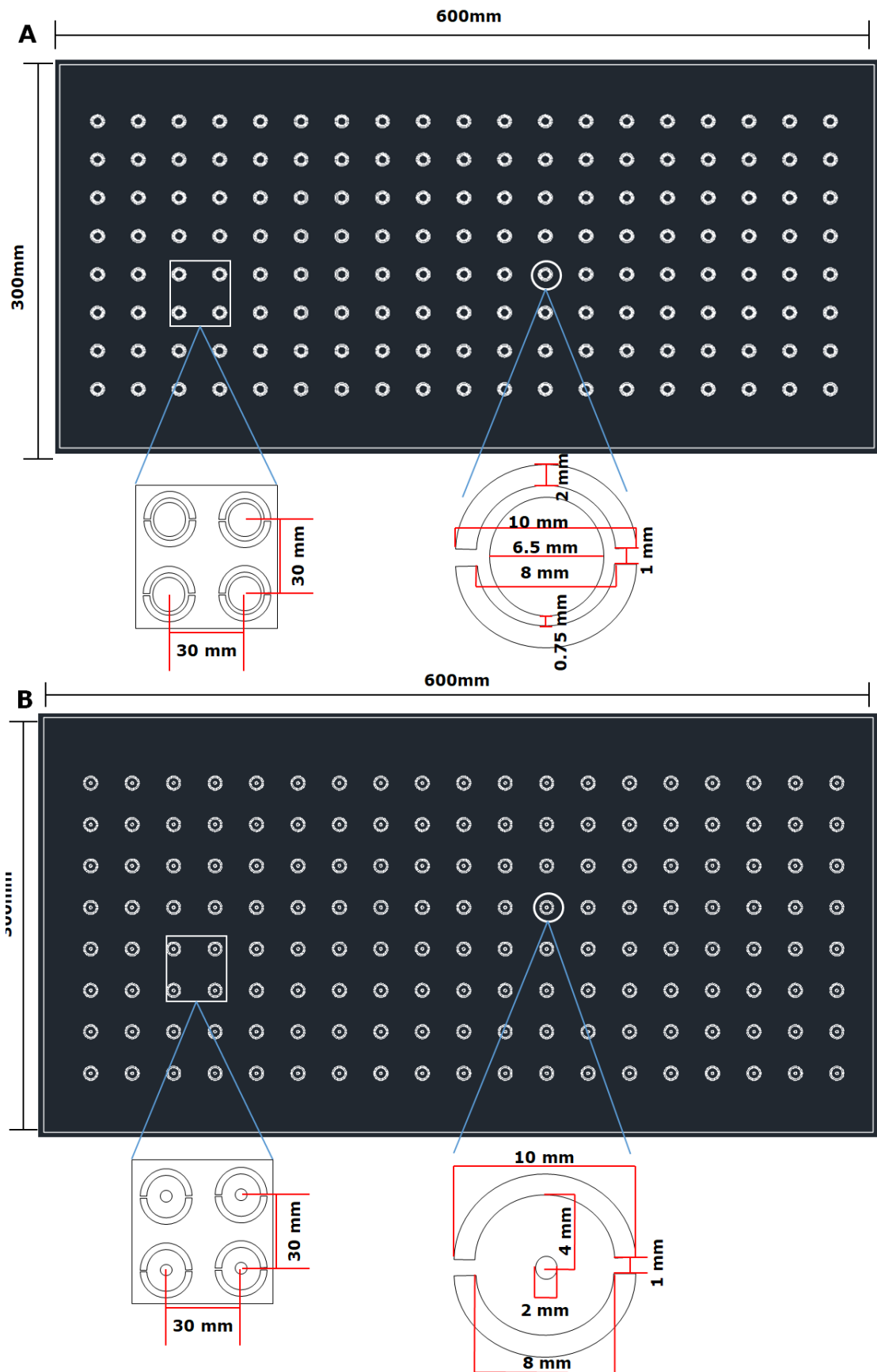


**Figure 2. 5: Schematic diagram Radial fibre design.**  
*A Top sheet and B bottom sheet design used for obtaining radial fibre.*

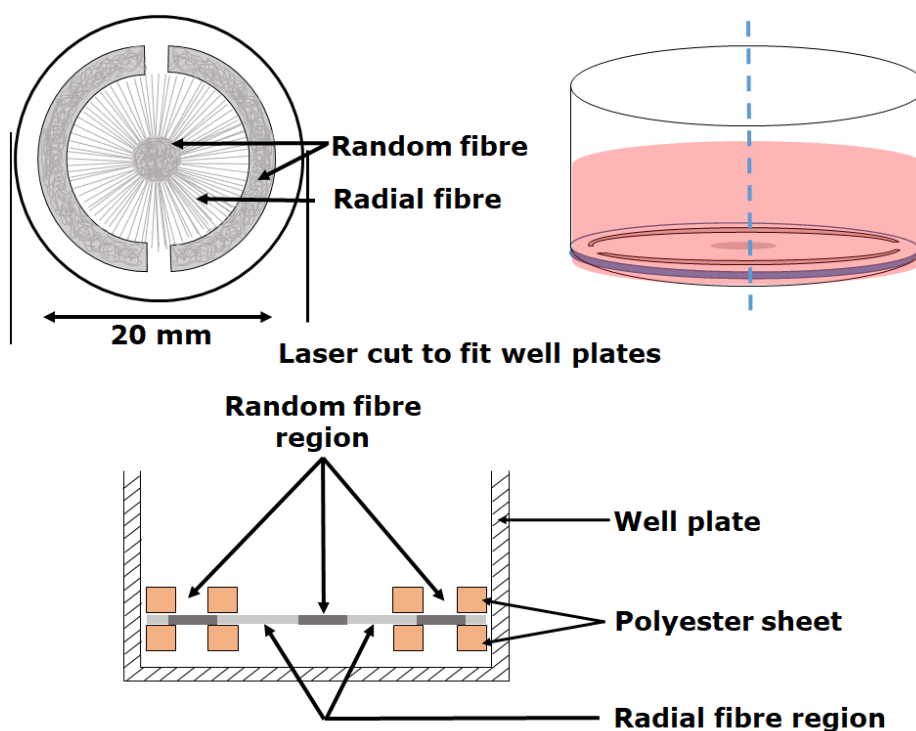


**Figure 2. 6: Radial fibre cross-sectional view**

### 2.2.2 Electrospinning solution preparation

Polyacrylonitrile (Mw 150,000) and Jeffamine<sup>®</sup> ED-2003 were dissolved in N, N-dimethylformamide (DMF). These two polymers were used to spin nanofibres in this study. Considering the density of DMF is 944kg/m<sup>3</sup>, to make 10wt% of PAN in DMF, 2g of PAN was dissolved in 19ml of DMF. Jeffamine was used as a dopant with PAN to control the degree of hydrophilicity; to make 5wt% Jeffamine in 10wt %PAN in DMF, 0.117g of Jeffamine<sup>®</sup> along with 2.22g of PAN was dissolved in 20 ml of DMF. The polymers were prepared in a glass bottle and were heated at a 50°C overnight with constant stirring. After the polymers were completely dissolved in the solvent and before electrospinning, each batch of polymers was tested for viscosity using a Capillary Breakup Extensional Rheometer

#### 2.2.2.1 Rheometer measurement

The extensional and breakup time of the polymeric solutions were measured using a HAAKE<sup>™</sup> CaBER<sup>™</sup> 1 Capillary Breakup Extensional Rheometer. A tiny amount of polymer (less than 0.2ml) was gently placed

between the two rods located at the centre of the machine creating a liquid bridge about  $500 \pm 50 \mu\text{m}$  in length connecting the two ends of the rod as shown in Figure 2. 7.

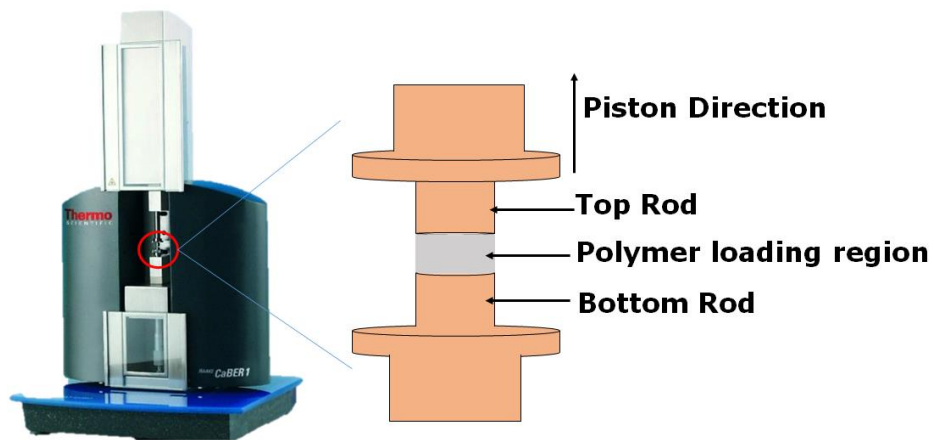


**Figure 2. 7: Schematic representation of HAAKE™ CaBER™ 1 Capillary Breakup Extensional Rheometer polymer loading region. HAAKE™ CaBER™ 1 image obtained from ([Thermo Fisher](#))**

The polymer is then exposed to a rapid extensional step by moving the upper rod upwards, therefore creating a polymer filament (Figure 2. 8). The balance of the surface tension, viscosity and elastic forces control the filament evolution as a function of time. The surface tension is trying to “pinch off” the filament while the extensional rheological properties of the fluid are trying to prevent this process. A laser micrometre measures the midpoint diameter and break time of the gradually thinning fluid filament after the upper plate has reached its final position.

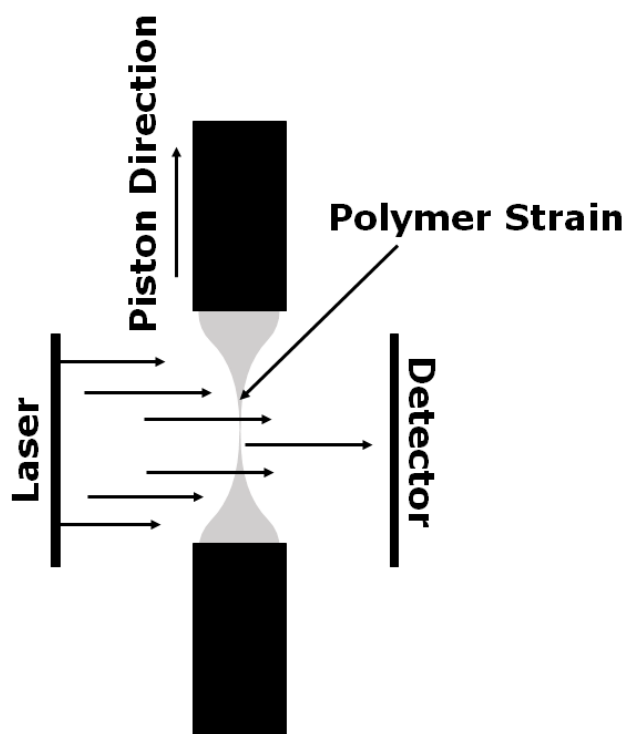


**Figure 2. 8: Schematic representation of polymer filament formation and measurement using the HAAKE™ CaBER™ 1 Capillary Breakup Extensional Rheometer works.**

### 2.2.3 Electrospinning

A schematic representation of the in-house built electrospinning set up used in this study is shown in Figure 2. 9. The entire system is secured in a well-insulated enclosure with minimum exposure on any metal apart from the grounded metal collecting drum. The chamber is also equipped with a recirculating humidity control system, as well as an activated carbon filter solvent extraction system. The main components are a syringe pump, capillary tube, blunt end needle, rotating collector drum and a high voltage supply. The required amount of polymer was filled in a 10ml Luer-Lok™ syringe and connected to a Luer-Lok™ needle. Then approximately 110cm length PTFE tubing with 1/31 inch bore size is connected to the Luer-Lok™ needle. The polymer is manually pushed through the tubing until it reaches  $\frac{3}{4}$  of the tube's length. 21 gauge size needle with one sharp and one blunt end is connected to the other side of the PTFE tube with the sharp end pushed 10mm inside the tube. The filled syringe is then loaded into the syringe pump and set at 1ml/hour

pumping speed, and the blunt end needle is guided through an acrylic holder and connected to a high voltage supply which is placed 300mm away from the surface of the collector. When a sufficiently high voltage is supplied to the polymer droplet from the needle, the surface of the polymers becomes charged. When the electrostatic repulsion overcomes the surface tension, the droplet stretches, causing a jet of fluid to be formed at the apex of the extended conical drop, also known as the Taylor cone.

The solvents desolvates and the polymer cools in flight then further elongates by an electrostatic repulsion process causing Rayleigh instability forming into the fibre. The fibres overcome the surface charge and are finally deposits on the collector rotating anti-clockwise with an assembled polyester sheet wrapped and fixed in place using aluminium tape. After the fibre have been laid the excess fibre surrounding the outside sheet is removed by cutting with a hot knife along the edges of the sheet. The drum is then set to rotate in clockwise direction, and the sheets are gradually pulled away from the drum and placed on the welding station. Depending on the type of design used the excess sheets are detached, and then the fibres are ultrasonically secured with an identical top sheet and laser cut to fit well plates. The laser-cut scaffolds were stored in a clean sealed container for further use. Multiple samples from each batch of spinning were investigated for fibre diameter, hydrophobicity and scaffold thickness using SEM, contact angle and an OCT analysis respectively.

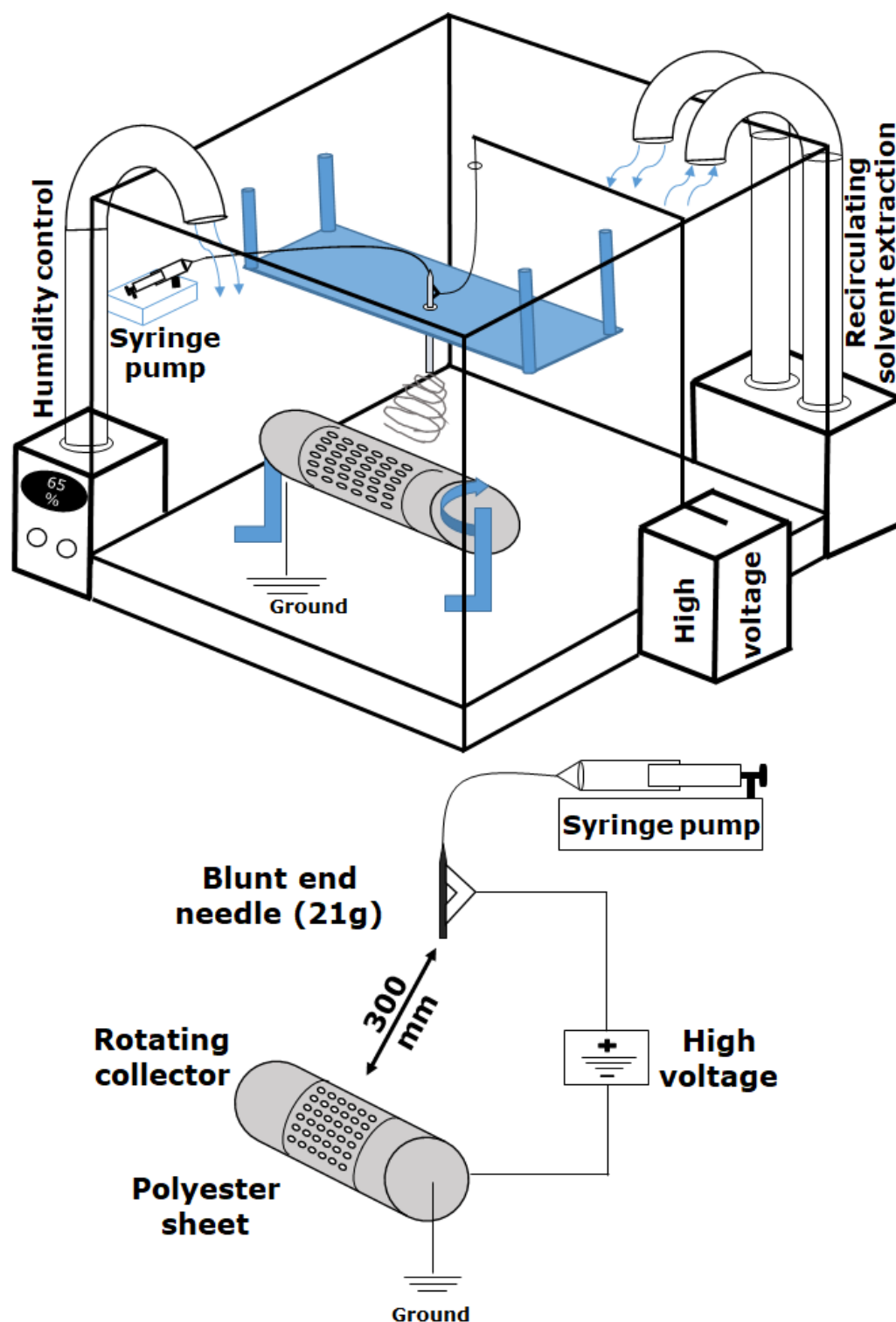


**Figure 2. 9: Schematic representation of our in-house built electrospinning system**

*With self-contained environment, needle station, controlled humidity, controlled high voltage supply, recirculating solvent extraction and rotating collector.*

### 2.2.3.1 SEM analysis

Integrity and morphology of produced fibre samples were analysed using the Phenom ProX desktop SEM. Random samples from each batch of electrospun fibres were selected and were mounted on a 25mm SEM stub using double-sided carbon tape. Fibre samples were sputter-coated with 10nm gold using an Edwards S150B sputter coater before SEM analysis. Different location of the scaffold was analysed for defects, deformations and damage at different magnification. Diameter and pore size distributions of samples were analysed using Phenom ProX FibreMetric® software. To analyse diameter and pore size multiple images at various positions and magnifications were taken then transferred into the FibreMetric® software. The software randomly chooses 100 different regions from images to measure fibre diameter and the pore sizes are examined throughout the entire image. Crossover regions overlapped fibre and fibres deep within the mat were manually deselected from the measured data. Raw data was extracted, and the mean values of the nanofibre diameters and pore size area were obtained and graphical data was produced using graph pad prism software.

### 2.2.3.2 Contact angle analysis

An angle formed with the interaction of liquid-solid and liquid-vapour interface is defined as the contact angle Figure 2. 10. It quantifies the hydrophobicity of a material's surface when a liquid drop is rested, spreads or contracts on the surface. There are several methods to determine the contact angle. In this study, we have chosen to use a user-defined baseline MATLAB code created by Dr Andrew Edwards from NTU, UK. The programme is capable of determining a contact angle with an accuracy of  $\pm 1^\circ$  for contact angles greater than  $5^\circ$ . Random samples were selected from each batch of fibres. Samples were placed on the examination station and using a pipette, distilled water (10 $\mu$ l) was dropped in the centre of the scaffold, and the dispersion of the water droplet was recorded for approximately 10 sec using a high-speed camera.

A water contact angle of fewer than 90 degrees is considered to indicate a hydrophilic surface and, if greater than 90 degrees, a hydrophobic surface (Förch, Schönherr, Schönherr, et al. 2009). There are three major parameters involved in a contact angle measurement: the solid surface, the liquid and air. When the droplet comes in contact with the surface a force ( $\gamma$ ) is exerted by the surface tension at three different interfaces: the liquid-surface (LS), liquid-vapour (LV) and solid vapour (SV) Figure 2. 10. When the droplet is in equilibrium the forces are balanced forming an equation:  $\gamma_{SV} = \gamma_{LS} + \gamma_{LV} \cos\theta$  that can be rearranged to  $\cos\theta = \frac{\gamma_{SV} - \gamma_{LS}}{\gamma_{LV}}$  to identify the contact angle.

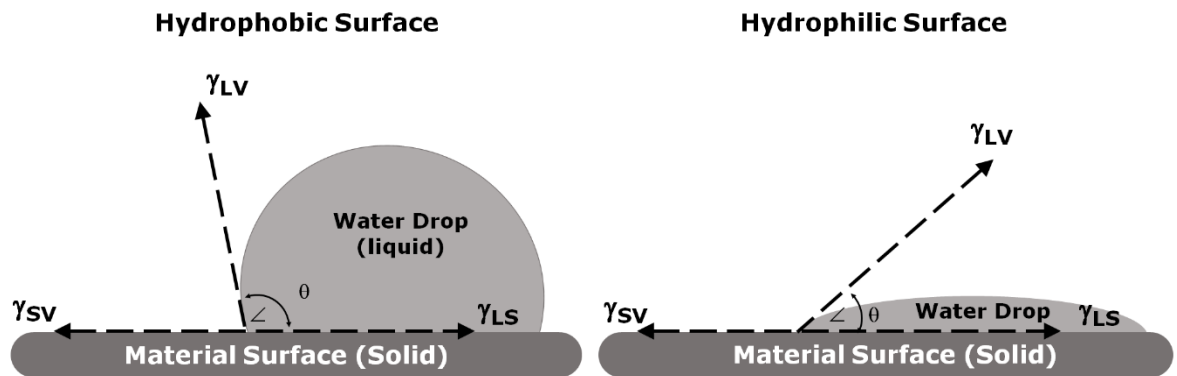


**Figure 2. 10: Schematic representation of contact angle measurement to identify the hydrophobicity of a surface.**

### 2.2.3.3 Optical Coherence Tomography

Optical Coherence Tomography (OCT) is a new imaging technique based on backscattered or back-reflected light. This technique can be used to obtain high-resolution images, a cross-sectional tomograph of samples and internal microstructure of the various material and biological systems. The OCT setup used in this study is an in-house designed system with a supercontinuum broadband laser (Telesto II from Thor Labs, UK) with a central wavelength of 1300nm and the bandwidth of the wavelength ranges from 1100nm-1500nm. The images are obtained at a resolution in the depth z-direction at 5.5 $\mu$ m and the XY direction at 20 $\mu$ m. Three randomly chosen samples in each batch were used to identify the thickness for the spun fibres. High-resolution images were obtained for

both dry and wet samples. Samples were measured suspended between two supports and wet by adding a drop (approx. 10 $\mu$ l) of ethanol causing the loose fibre strands to settle, creating a clear and better measurement.

#### **2.2.3.4 Nanofibre sterilisation analysis**

Before using the nanofibre scaffolds for cell biology experiments, it was essential to identify a suitable method of sterilisation that did not compromise the integrity and morphological properties of the fibre. The fibres were exposed to 70% (v/v) ethanol soaking, exposed to 256 nm UV light and antibiotic treatment (100 units/ml penicillin, 100 $\mu$ g/ml streptomycin). Each test was exposed for 30 minutes, 8 hours and 24 hours. Subsequently, scaffolds were transferred to a 15ml tubes with 5ml sterile distilled water under sterile conditions. The tube was vigorously vortexed to disperse any microbes present on the fibre into the sterile distilled water. Under sterile conditions, 1 ml of water from that tube was transferred to an agar plate and was evenly spread across using a sterile L-shaped glass rod. The plate was then incubated at 37 $^{\circ}$ C for 14 days to investigate any bacterial or fungal growth.

#### **2.2.4 Cell Culture**

##### **2.2.4.1 Clonal Cell lines**

###### **2.2.4.1.1 Human SH-SY5Y neuroblastoma**

SH-SY5Y cells were cultured in sterile growth medium containing DMEM/F12 supplemented with 10% (v/v) heat inactivated foetal bovine serum (FBS), 2 mM glutamine, 100 units/ml penicillin, 100 $\mu$ g/ml streptomycin and 0.1mM non-essential amino acids (NEAA) in tissue culture flasks and maintained at 37 $^{\circ}$ C in a humidified chamber of 95% of (v/v) air /5 % (v/v) CO<sub>2</sub>. When the cells were 80% - 90% confluent, they were sub-cultured by trypsinisation. Briefly, cells were washed in PBS and then incubated with 1-2ml of 1x trypsin for 5 minutes at 37 $^{\circ}$ C. Trypsin activity was neutralised by serum-containing medium. Cell detachment was aided by tapping gently on the sides of the flask. The detached cells

were transferred into a tube and pelleted by centrifugation at 300g for 5 minutes. The resultant pellet was re-suspended in growth medium and counted using a haemocytometer. The required number of cells (250,000 cells in a T25 flask and 1,000,000 cells in the T75 flask) was transferred to a sterile tissue culture flask containing pre-warmed growth medium.

#### **2.2.4.1.2 Human U-87 MG glioblastoma**

U-87 MG cells were cultured in sterile growth medium containing EMEM supplemented with 10% (v/v) heat inactivated foetal bovine serum (FBS), 2 mM glutamine, 100 units/ml penicillin, 100µg/ml streptomycin, 0.1mM non-essential amino acids and 1mM sodium pyruvate in tissue culture flasks and maintained at 37°C in a humidified chamber of 95% of (v/v) air /5 % (v/v) CO<sub>2</sub>. When the cells were at least 80% confluent, they were sub-cultured by trypsinisation. Briefly, cells were washed in PBS and then incubated with 1-2 ml of 1x trypsin for 5 minutes at 37°C. Trypsin activity was neutralised by medium with 10% serum. Cell detachment was confirmed under a light microscope, and cells that have not detached were further detached by either tapping gently on the sides of the flask or by squirting media using a pipette over the region. The detached cells were then transferred into a tube and pelleted by centrifugation at 300g for 5 minutes. The resultant pellet was re-suspended in growth medium and required number of cells (250,000 cells in a T25 flask and 1,000,000 cells in the T75 flask) was transferred to a sterile tissue culture flask containing pre-warmed growth medium.

#### **2.2.4.1.3 Viable cell count and seeding**

To estimate viable cell numbers an equal volume of diluted cell suspension and 0.4% (v/v) trypan blue solution were mixed in a microfuge tube. Viable cells (colourless cells) were counted using a haemocytometer. The cell density was estimated using the following calculation:

$$\text{Cells/ml} = \text{Average cell count (1 mm}^2\text{)} \times 10^4 \times \text{dilution factor}$$

The required number of cells to achieve a specific cell density in a known volume of growth medium was then calculated. The required cell density was seeded into an appropriate culture vessel and incubated 37°C in a humidified chamber of 95% of (v/v) air / 5 % (v/v) CO<sub>2</sub>.

#### **2.2.4.1.4 Cryo-preservation of cells**

Cells were frozen in liquid nitrogen for long-term preservation. Cells were seeded in either a T25 or T75 flask and harvested while in the log phase of growth. Briefly, cells were washed in PBS and then incubated with 250 µg/ml trypsin (100 µl for T25 flask and 500 µl for a T75 flask) for 5 minutes at 37°C and then centrifuged at 300g for 5 minutes. The supernatant was discarded, and the cell pellet was resuspended in 1 ml of ice-cold freezing medium [(10 % (v/v) DMSO in FBS)] and transferred into freezing vials. These freezing vials were moved to -80°C freezer for 24 hours and then transferred into a liquid nitrogen storage facility for long-term storage.

#### **2.2.4.1.5 Revival of cryo-preserved cells**

The freezing vial containing the Cryo-preserved cells was removed from the liquid nitrogen storage. The contents were quickly thawed in a 37°C water bath and transferred into a sterile tube containing ample growth medium to dilute the DMSO. The tube was centrifuged at 300 g for 5 minutes. The supernatant was discarded, and the pellet was resuspended in 1 ml of growth medium and transferred into a T25 flask containing appropriate growth medium. Cells were maintained according to the requirements for each cell types.

#### **2.2.4.1.5 Neural cell differentiation**

SH-SY5Y and U-87MG cells were induced to differentiate by culturing cells at 5 x 10<sup>4</sup> cells/well in growth media for 24 hours. Following attachment,

growth media was removed and replaced with serum-free media supplemented with differentiation agents. In the case of SH-SY5Y cells, media was supplemented with retinoic acid (1 $\mu$ M) and B27 supplement (1 %). Whereas U-87MG cells were supplemented with dibutyryl cyclic adenosine monophosphate (dbcAMP; 0.3 mM) and B27 supplement (1%) for up to 5 days. Cells were cultured at 37°C in 5% CO<sub>2</sub>. During differentiation, the medium was changed after every 48 hours for 5 days.

#### **2.2.4.2 Neural progenitor cells ReNcell CX**

##### **2.2.4.2.1 Laminin coating**

All tissue culture flasks and plates used to culture ReNcell CX were coated with laminin for 24 h prior to cell seeding. For coating, 1mg/ml laminin from EngelbrethHolm-Swarm murine sarcoma basement membrane (Sigma–Aldrich) was thawed at room temperature, then diluted to 20  $\mu$ g/ml final concentration in Neurobasal<sup>®</sup> medium (Gibco) alone. Sufficient laminin solution was added to cover the surface of the required tissue culture vessel (e.g. 2 ml and 5 ml volumes were used to coat a T25 and T75 flasks, respectively). Coated flasks were incubated at 37°C in a 5 % (v/v) CO<sub>2</sub> incubator for at least 4 hours before use; otherwise, flasks were pre-prepared and stored at 4°C for 24 h. before cell seeding, the laminin coating solution was aspirated and rinsed with sterile PBS.

##### **2.2.4.2.2 ReNcell CX maintenance medium**

ReNcell CX cells were maintained in KnockOut™ DMEM: nutrient mixture F-12 (DMEM/F-12) low osmolality medium without HEPES buffer. The medium (500 ml) is supplemented with recombinant human epidermal growth factor (EGF) (10  $\mu$ g/ml; Gibco), basic fibroblast growth factor (FGFb) (10  $\mu$ g/ml; Gibco), StemPro<sup>®</sup> neural supplement (10 ml; Gibco), L-glutamine (0.5 mM), penicillin (100 units/ml) and streptomycin (100 units/ml).

### **2.2.4.2.3 Revival of cryo-preserved cells**

A vial of cryopreserved ReNcell CX cells was removed from the liquid nitrogen storage and thawed quickly by incubation in a 37°C water bath for 1-2 min. The outside of the vial was wiped with 70% v/v ethanol to sterilise, and the cells were transferred into a Sterilin tube using a 2 ml sterile pipette. After the cells have been transferred into the tube, 9 ml of maintenance medium was added dropwise (pre-warmed to 37°C) to avoid osmotic shock and the consequent reduction in cell viability and was mixed gently. Then centrifuged at 300g for 5 min. Following centrifugation, the supernatant was decanted to remove any residual cryopreservation medium, and the resultant pellet was resuspended in 1 ml of pre-warmed maintenance medium using a sterile pipette. The cell suspension was seeded into a laminin-coated T25 or T75 flask containing 4 ml or 10 ml, respectively, of fresh pre-warmed maintenance medium. The cells were incubated for 24 h at 37 °C in a humidified atmosphere of 95% air/5% CO<sub>2</sub>; then the medium was changed for fresh pre-warmed maintenance medium. The monolayer was incubated until it reaches 80% confluent and the medium was changed every 48hours. Upon confluence, cells were passaged for experiments or cryopreserved for later use.

### **2.2.4.2.4 Sub-culturing of ReNcell CX cells**

ReNcell CX cells were passaged by careful removal of the maintenance medium from the coated flask and rinsing the monolayer with pre-warmed PBS for 1 min. Cells were detached by the addition of 1-2 ml of pre-warmed accutase (Gibco) according to the size of the flask (e.g. 1 ml for T25 and 2 ml for a T75 flask). The monolayer was incubated with accutase for 2 min in a 37°C incubator, and cell detachment was monitored using an inverted light microscope. Accutase's action was quenched with fresh growth medium in the proportion 2:1, and the cell suspension was transferred to a sterilin tube and centrifuged for 5 min at 300g. The resultant pellet was resuspended in 1 ml of maintenance

medium by pipetting gently back and forth to break up the pellet. Using a Pasteur pipette, one-fifth of cell suspension was placed in a laminin-coated T25 flask containing 4 ml of maintenance medium (or 10 ml in a T75 flask). The flasks were then incubated at 37°C in a humidified atmosphere of 95% air/5% CO<sub>2</sub> and monitored until the cells reached 70-80% confluence

#### **2.2.4.2.5 Viable cell count and seeding**

Upon reaching 80% confluency, cells were detached and harvested by centrifugation at 300g for 5 min as described in section 2.2.4.2.4. The cell pellets were resuspended in 1 ml of maintenance medium and counted using an automated cell counter. Briefly, 10µl of cell suspension and 10µl of trypan blue (0.4% v/v) solution was mixed at room temperature. A 10µl aliquot of the mixture was loaded into a chamber of TC20 counting slide which was then carefully inserted into the cell counter. The total viable cells count were calculated and displayed based on 1:1 cell dilution. The cell density per ml value was obtained to determine the volume of suspension necessary to seed.

#### **2.2.4.2.6 ReNcell cell differentiation**

Prior to the induction of ReNcell CX cell differentiation, cells were seeded and maintained at 37°C in a humidified atmosphere of 95% air/5% CO<sub>2</sub> for 24 h to allow cell recovery. Maintenance medium was then carefully removed by aspiration and replaced with neural cell differentiation medium containing StemPro<sup>®</sup> neural supplement (10 ml; Gibco), L-glutamine (0.5 mM), penicillin (100 units/ml) and streptomycin (100 units/ml) with no mitogens.

#### **2.2.4.3 Primary Cells**

Embryonic rat brain tissue samples were obtained from BrainBits, UK. Neural cell populations were obtained from embryonic day 18 rat hippocampal tissues. The tissue samples were shipped as vials containing

Hibernate EB (HEB; 2ml) medium; a combination of Hibernate E/B27/GlutaMAX medium. The company did not disclose concentrations of each component in the media. For an optimal neural cell yield, the tissue was used immediately upon delivery although it could be stored for 1 week at 4-8°C.

#### **2.2.4.3.1 Preparation for tissue processing**

The tissue culture wares were prepared by coating with poly-L-lysine (PLL) (50µg/ml) and incubated at 37°C for 1-4 hours for immediate use or stored at 4°C for later use. Before using, the PLL was aspirated, and the surface was rinsed with ddH<sub>2</sub>O and dried under a laminar hood. The cell dissociation solution was prepared by dissolving 6 mg (2mg/ml) sterile papain in 3 ml of Hibernate E-Ca (HE-Ca) without B27 medium and incubated for 10min at 30°C.

#### **2.2.4.3.2 Cell dissociation and seeding**

The same method of cell dissociation was used to obtain both neurones and astrocytes. Using the silanised Pasteur pipette, the HEB solution was carefully removed and saved in a sterile tube for later use. A 2ml aliquot of cell dissociation solution was added to the tissue vial and incubated for 10 min at 30°C with gentle agitation for 5 min. The cell dissociation solution was carefully removed without disturbing the tissue sample and replaced with HEB solution. Using the silanised Pasteur pipette, the tissue was triturated for 1 minute and left undisturbed for a 1 min to allow cell aggregates to settle. The supernatant containing the dispersed cells were transferred to a 15ml sterile tube and centrifuged at 200g for 1 minute. The supernatant was decanted, and the pellet was resuspended in NbActive media for neurons and NbAstro media for astrocytes. A 20µl aliquot of cell suspension was mixed with 80µl of trypan blue (1:5 dilution), and cell number was determined using an automated cell counter. The desired number of cells were calculated and seeded in PLL coated plates or flask and incubated at 37°C in a humidified atmosphere

of 95% air and 5% CO<sub>2</sub>. For the first 4 days of culture, the cells were maintained in the appropriate media with 1% (v/v) gentamycin and 1% (v/v) glutamate. Following 4 days of growth, the medium was replaced with NbActive medium alone for neurones and NbAstro medium alone for astrocytes. Every 4-5 days, half of the old medium was replaced with appropriate fresh growth media.

### **2.2.5 Cell Culture on nanofibre scaffolds**

Fibres made from PAN, PAN with Jeffamine<sup>®</sup> (PJ) were the two types used to make scaffolds used for the study. All the experiments were performed using scaffolds in a 12 well tissue culture plate with 5 X10<sup>4</sup> cells/well, i.e. 3 x10<sup>5</sup> in each 12 well plate unless mentioned otherwise. Also, as a comparison to 2D cultures, the same number of cells were seeded in separate 12 well plates with round coverslips in each well. The same method of culturing was followed through the study for all the type of fibre orientations and cell types.

#### **2.2.5.1 Nanofibre Sterilisation before cell seeding**

Each nanofibre scaffolds were sterilised before using it for cell culture. For the entire study scaffolds were sterilised using 70% ethanol. The scaffolds were exposed to 256nm UV light during spinning and laser cut to fit 12 well size tissue culture plates. The scaffolds were stored in a clean, sterile container. Under a laminar flow hood, the scaffolds required for an experiment were picked using sterile tweezers and transferred into a sterile pot with lid containing 70% ethanol (10-20ml). The substrates were soaked in ethanol for 30 minutes with a gentle swirl every 10 minutes. To neutralise the ethanol, the substrates were then washed in PBS gently three times for five-minute periods on a shaker. After that, the PBS was decanted and replaced with the culture medium for equilibration and stored for immediate use.

### 2.2.5.2 Clonal cells

Both SH-SY5Y and U-87 MG cells were maintained either in a T25 or a T75 flask throughout the study. The maximum passage number used for experiments was no more than P30. Before seeding the cells on fibres, the cells from the flask were harvested by trypsinisation and centrifuged at 300g to obtain a pellet as described in section 2.2.4.1. Meanwhile, nanofibre scaffolds were sterilised in 70% ethanol as described in section 2.2.5.1. Each scaffold was picked using a sterile tweezer and placed into a 12 well plate. After obtaining a pellet, the required number of cells were counted and calculated as described in section 2.2.4.1.3. Total volume from the cell suspension was determined and was transferred to 12 ml of culture media and was gently mixed. From the mixture, 1 ml ( $5 \times 10^4$  cells/well) was transferred to plates with scaffolds and coverslips. The plate was then incubated at 37°C in a humidified atmosphere of 95% air and 5% CO<sub>2</sub>.

### 2.2.5.3 ReNcell CX

ReNcell CX was cultured and maintained in a T25 flask throughout the study. The maximum passage used for the experiment was maintained below P10. The cells were subcultured as described in section 2.2.4.2.5. Fibres were sterilised with 70% ethanol as described in 2.2.5.1. After obtaining a pellet, the required number of cells were counted and calculated as described in section 2.2.4.2.4. Total volume from the cell suspension was determined and was transferred to 12 ml of culture media and was gently mixed. From the mixture, 1 ml ( $5 \times 10^4$  cells/well) was transferred to plates with scaffolds and coverslips. The plate was then incubated at 37°C in a humidified atmosphere of 95% air and 5% CO<sub>2</sub>.

### 2.2.5.4 Primary Cells

Rat primary E18 neural cells were directly seeded on fibres and coverslips. As these cells cannot be passaged, the cells were not maintained in flasks for further use. The cells were dissociated from rat brain tissue samples

as described in section 2.2.4.3.2. After obtaining a pellet, the required number of cells was calculated as described in section 2.2.4.3.2. Total volume from the cell suspension was determined and was transferred into 12 ml of culture media and was gently mixed. From the mixture, 1 ml ( $5 \times 10^4$  cells/ml) was transferred to plates with scaffolds and coverslips. The plate was then incubated at 37°C in a humidified atmosphere of 95% air and 5% CO<sub>2</sub>

## **2.2.6 Cell Viability assay**

### **2.2.6.1 Trypan blue exclusion assay**

The trypan blue exclusion assay is an indicator of cell membrane integrity and is excluded by viable cells. Trypan blue was used to measure the viability of cells treated in the presence or absence of several different agents for a defined time period or during cell passaging to determine the total number of viable cells. The cell suspension was mixed with 1:1 with trypan blue (0.4% (v/v)) and counted in a haemocytometer chamber. In each case, total and dead cells (stained blue) were counted. The mean viable cell number was expressed as a percentage of the total cell count.

### **2.2.6.3 CellTiter-Glo® 3D**

The Cell Titer-Glo 3D is an ATP dependent homogenous method to determine the number of viable cells in a 3D cell culture. This is a ready-to-use reagent from Promega which monitors and detects the metabolic activity of a viable cell through its ATP production. When added to the cells the homogeneous mixture results in cell lysis and generation of a luminescent signal proportional to the amount of ATP expressed which is directly proportional to the number of viable cells in the culture. Cell Titer-Glo 3D is capable of robust penetration into microtissues and 3D cultures with greater sensitivity. CellTiter-Glo® 3D is used at several stages of this study to investigate treatment-based analysis. Cell Titer-Glo 3d is added in equal volume as the media in each well. After the required treatments, 500µl of media is removed from each well and replaced with 500µl of Cell

Titer-Glo 3D. To induce cell lysis, the cultured cells were vigorously mixed for 5-10 min on a plate shaker. The plate was then incubated at room temperature for 30 minutes, and the luminescence was recorded.

### **2.2.7 Cell Proliferation assay**

To understand the level of attachment and proliferation of the cell types, cells were harvested and seeded at  $5 \times 10^4$ /well on both PAN and PJ nanofibre scaffolds. After 48 hours, cell laden fibres were methanol fixed and stained with Coomassie Brilliant Blue dye to visualise cell attachment. To monitor the level of proliferation and prolonged survival, each cell types were cultured on each fibre type for 11 days alongside 2D tissue culture plastic surface (control) with media changes every 48 hours. All samples were tested for cell viability using the MTT assay after each 48-hour period.

#### **2.2.7.1 MTT cell metabolic Assay**

Cell metabolism were assessed by MTT (3-(4, 5-dimethylthiazol-2-yl)-2, 5-diphenyltetrazolium bromide) reduction assay (Mosmann 1983; Berridge, Herst and Tan 2005). MTT can be accumulated by viable cells and reduced by mitochondrial dehydrogenase enzyme to form formazan crystals. The accumulated formazan is then solubilised in DMSO and detected using a spectrophotometer at 570nm. Tetrazolium dye reduction is generally assumed to be dependent on NAD(P)H-dependent oxidoreductase enzymes largely in the cytosolic compartment of the cell (Berridge, Herst and Tan 2005). Therefore, reduction of MTT and other tetrazolium dyes depends on the cellular metabolic activity due to NAD(P)H flux. Cells with a low metabolism reduce very little MTT and in contrast, rapidly dividing cells exhibit high rates of MTT reduction. The assay conditions can alter metabolic activity and thus tetrazolium dye reduction without affecting cell viability.

Throughout this study, MTT assay was used to investigate the increase in the metabolic activity of the cells in the proliferation of cells on fibre study

and investigation of toxins on cells. When the assay was performed for the cell on fibre, the scaffolds were transferred to a fresh plate before adding MTT. 100  $\mu$ l of 5 mg/ml MTT was added to each well to make a final concentration of 0.5mg/ml. The plate was incubated for 1 hour at 37 °C in humidified atmosphere of 95 % of (v/v) air / 5 % (v/v) CO<sub>2</sub>. The medium was removed from the wells, and 100  $\mu$ l of DMSO was added into each well to solubilise the formazan product. The absorbance was measured at 570nm using a microplate reader. The results were expressed as percentage change in MTT reduction compared to control

### **2.2.8 Effect of glial ECM on neurons**

The U-87MG cells were cultured, and upon reaching 80% confluency, the cells were washed several times with PBS to remove any trace of the media. Then 3-5ml of sterile distilled water was added to each well and incubated in room temperature for 5-10 minutes. The cells absorb the water and undergo osmotic shock causing the cell walls to rupture and explode, leaving the ECM intact. The lysed cells were confirmed under a light microscope, and the cell debris was removed by several washes with distilled water.  $1 \times 10^3$  cells of SH-SY5Y were seeded into the same plate and in a fresh plate (control). Both plates were then incubated at 37°C in a humidified atmosphere of 95% air and 5% CO<sub>2</sub> for 14 days. The cell growth was monitored every 48 hours.

### **2.2.9 Sample preparation for microscopy**

#### **2.2.9.1 Methanol fixation**

All cell types were seeded in individual 12 well plates with PAN fibres, PJ fibres and coverslips at a density of 50,000 cells per well. Following treatment, cells were washed with PBS and fixed with ice-cold 90 % (v/v) methanol/1X Tris-Buffered saline (TBS) for 20 minutes at - 20 °C.

#### **2.2.9.2 Immunofluorescence antibody staining**

Following the methanol fixation, the Cells were then permeabilised for 10 minutes using 1% Triton X-100 in TBS at room temperature and were

blocked with 3 % (w/v) BSA/TBS-Tween (0.1 %) for 1 hour at room temperature. The plates were then incubated with the relevant primary antibody diluted in 3 % (w/v) BSA/TBS-Tween (0.1(v/v) %) and incubated overnight at 4 °C in a humidified chamber. The following day slides were washed thoroughly with 0.1 % (v/v) Tween-20 in TBS. The slides were then incubated with Anti-IgG alexafluor conjugated secondary antibody diluted in 3 % (w/v) BSA/TBS-Tween [0.1% (v/v)] for 2 hours. The slides were then washed to remove all unbound secondary antibody. Each sample from each well was removed and placed on glass slides with anti-fade mountant vectorshield containing DAPI or propidium iodide nuclear stain and covered with a glass coverslip. The coverslip was sealed with clear nail varnish, and slides were viewed using an Olympus fluorescence microscope.

### **2.2.9.3 Scanning electron microscopy**

SEM microscopy was used to examine and analyse cell attachment and morphology on nanofibre and coverslips at greater magnification and higher resolution. After the completion of experimental incubations, cells were fixed in 90% (v/v) methanol in TBS at -20°C for 30 minutes. After fixation, cells were dehydrated by sequential incubation in ethanol at 30% (v/v), 50% (v/v) 70% (v/v) 80% (v/v), 90% and 100% for 10 min with gentle agitation (Braet, De Zanger and Wisse 1997; Parameswaran and Verma 2011). After the final dehydration step, samples were air-dried for 15 min before mounting on SEM carbon stubs and sputter-coated to a 10 nm thick gold layer. Samples were characterised with a Phenom ProX desktop SEM at 10kV.

### **2.2.10 Protein levels identification**

#### **2.2.10.1 SDS-PAGE electrophoresis**

##### **2.2.10.1.1 Total protein cell lysate from cell grown on TCP**

Total protein cell lysates were prepared from an entire 12 well plate to ensure parity with nanofibre samples. Samples (12 wells) were pooled to

obtain sufficient protein for analysis. To prepare total protein extracts, cells were scraped from the monolayer using a cell scraper, pooled and transferred to a 15ml tube. The cells were pelleted at 300g for 5 minutes and washed twice in PBS. Dependent on pellet size, the sample was resuspended in total lysis buffer (100-200 $\mu$ l) containing 1% (v/v) protease inhibitor cocktail and transferred to a pre-cooled microfuge tube. The total protein extract was heated to 100 °C for 5 minutes in a heating block and subsequently sonicated (3 x 5-second bursts on power setting no.6) on ice. Lysates were then centrifuged at 300g for 5 minutes at 4°C to pellet insoluble material. The supernatant was carefully pipetted to a fresh microfuge tube and stored at -20°C for quantification. The protein content of each sample was quantified using Mini Lowry's method (Lowry, Rosebrough, Farr, et al. 1951).

#### **2.2.10.1.2 Total protein extraction from fibre**

Similarly, to culture plates, nanofibres from an entire 12 well plate were pooled to obtain enough protein for analysis. Cell laden nanofibre scaffolds from each well were transferred to a 15ml tube with ice-cold PBS. Nanofibres were centrifuged at 300g for 5 minutes and resuspended in ice-cold PBS. The step was repeated a few times to remove any trace of media. After the final centrifugation, PBS was decanted and total lysis buffer (approx.100-200 $\mu$ l) with 1% (v/v) protease inhibitor cocktail was added and transferred into a pre-cooled microfuge tube. The samples were then subjected to heat and cold shock treatment by boiling at 100 °C for 5 minutes in a heating block and immediately placed on ice. The samples were then sonicated (3 x 5-second bursts on power setting no.6) in ice and centrifugation at 300g for 5 minutes at 4°C. The supernatant containing all the protein was carefully pipetted to a fresh microfuge tube and stored at -20°C for quantification. The protein content of each sample was quantified using Mini Lowry's method

### 2.2.10.1.3 Protein quantification by mini Lowry

The protein concentrations were calculated by performing a Mini Lowry assay. Bovine serum albumin (BSA) standards were prepared to generate a standard curve for estimating the protein concentration of the cell lysates. BSA (1mg/ml) standards of required dilutions were made from a stock solution of 1mg/mL as given shown in table 2.2. 10 $\mu$ L of cell extract was taken and made up to 100 $\mu$ L using distilled water. All samples and standards were thoroughly mixed by vortexing. Aliquots of 1mL Lowry reagent (100ml sodium carbonate Na<sub>2</sub>CO<sub>3</sub>/ sodium hydroxide solution NaOH+ 2ml of 1 % Copper sulphate solution and 2ml of 2.7% Sodium tartrate solution) was added to all the tubes & incubated at room temperature for 15 minutes. Then 100 $\mu$ L of Folin-Ciocalteau (diluted 1:1 with distilled water) reagent was added to all the tubes, vortexed before incubation at room temperature for a minimum of 30min. Development of blue colour was observed based on the amount of protein present. After 30 minutes, 100 $\mu$ L from each sample was transferred to a 96 well plate to measure the absorbance at 750nm. The amount of protein present in each experimental sample was calculated by comparing to a standard curve generated from the BSA standards.

### 2.2.10.1.4 Preparation of resolving gel

As per the manufacture's guidelines, the gel was prepared using the Bio-Rad protean III or tetra apparatus. For the separation of proteins of interest, a 10 % (w/v) polyacrylamide gel was used. A total volume of 10 ml polyacrylamide gel was made as described in table 2.2. Just before the gel was poured into the gel casting set up 50 $\mu$ l of 10 % (w/v) ammonium persulphate (APS) and 10 $\mu$ l of N, N, N', N'-Tetramethylethylenediamine (TEMED) was added to induce gel polymerisation. The casting setup consisted of 2 glass plates arranged with the short plate facing forward. The gel was poured (approx. 7.5 ml) between the two-plate leaving approximately 2 cm at the top for the application of a stacking gel. The gel was overlaid with isopropanol (IPA)

to create a smooth gel interface. The resolving gel was left to polymerise at room temperature for 1 hour. The separation of proteins within a sample is varied depending on the percentage of acrylamide within the resolving gel. The table below details the composition and preparation of the resolving gels.

**Table 2. 2: Preparation of acrylamide resolving gel mixes for SDS-PAGE**

<b>Reagents</b>	<b>7.5% (w/v) gel</b>	<b>10.0% (w/v) gel</b>	<b>12.5% (w/v) gel</b>	<b>15.0% (w/v) gel</b>
40% Acrylamide (29:1)	1.9 ml	2.5 ml	3.0 ml	3.75 ml
1.5 M Tris buffer pH8.8	2.5 ml	2.5 ml	2.5 ml	2.5 ml
10% (w/v) SDS	100 µl	100 µl	100 µl	100 µl
Distilled water	5.5 ml	4.9 ml	4.4 ml	3.65 ml
<b>Total</b>	<b>10 ml</b>	<b>10 ml</b>	<b>10 ml</b>	<b>10 ml</b>
APS			<b>50 µl</b>	
TEMED			<b>10 µl</b>	

#### 2.2.10.1.5 Preparation of stacking gel

Once confirming the resolving gel had polymerised, the IPA was washed and removed using a filter paper. A total volume of 50ml 4% (w/v) stacking gel was prepared as described in table 2.3, and 2.5ml was used to prepare each gel. 12.5µl of 10 % (w/v) APS and 5 µl of TEMED were added to 2.5 ml of stacking gel mix per gel. Immediately, starting from one corner of the plate, the comb was placed slowly and carefully within the gel to form wells avoiding any air bubbles or deformation. The stacking gel was left to polymerise for approximately 30- 45 minutes at room temperature. Once the gel had polymerised, the comb was removed. The gel was then placed into a Bio-Rad SDS-PAGE protein separation

apparatus which was filled with SDS-PAGE running buffer (2.5 mM Tris pH 8.3; 192 mM glycine; 0.1 % (w/v) SDS).

**Table 2. 3: Preparation of acrylamide stacking gel mix for SDS-PAGE**

Reagents	4% (w/v) gel
40% Acrylamide (29:1)	10 ml
0.5 M Tris buffer pH 6.8	25 ml
10% (w/v) SDS	1 ml
Distilled water	14 ml
<b>Total</b>	<b>50 ml</b>
<i>APS (for every 2.5ml)</i>	12.5 $\mu$ l
<i>TEMED (for every 2.5 ml)</i>	5 $\mu$ l

#### 2.2.10.1.6 Preparation of samples for separation by SDS-PAGE

Mini Lowry determined the total volume of the sample required to load 20 $\mu$ g of protein. The known volume of sample was diluted with an equal volume of 2X concentrated reducing sample buffer (0.2 M Tris-HCl pH 6.8; 8 % (w/v) SDS; 40 % glycerol; 200 mM dithiothreitol; 0.02 % (w/v) bromophenol blue) heated to 100°C for 5 minutes in a heating block. The total mixture was then loaded to each well with 10 $\mu$ l of molecular weight marker loaded in one of the wells for each gel. The proteins were separated by one-dimensional SDS-polyacrylamide gel electrophoresis (SDS-PAGE) using the BIO-RAD protean III or tetra kits. Initial voltage was set to 80V until the samples reached the interface between stacking and resolving gel then the voltage was set to 130V for 1-1.5 hours.

### 2.2.10.2 Western Blotting

Western blotting is a common technique used to transfer protein from an SDS-PAGE gel to a nitrocellulose membrane to identify a protein of interest. Two types of western blotting techniques were available; wet blotting was preferentially used for transferring high molecular weight proteins, and semi-dry blotting was used for lower molecular weight proteins. The proteins of interest in this study ranged between 30-200 kDa, so the experiment was conducted using a wet blotting transfer. The proteins were electrophoretically transferred into a 0.22 $\mu$ m pore nitrocellulose membrane (Towbin, Staehelin and Gordon 1979). After separating the proteins using the SDS-PAGE gel was completed, the two glass plates were separated, the gel was carefully transferred to distilled water in a tray. Four pieces for the filter paper, one nitrocellulose membrane was cut to the same size as the gel and pre-soaked in Tris-glycine along with two wire mesh. The entire set was assembled as a blotting sandwich starting from cathode side with the cloth mesh then two filter papers then the nitrocellulose and the gel on top of the membrane which was then followed by two more filter papers and the mesh. The assembly was secured and submerged in a tank with a blotting buffer with the membrane facing the anode. The transfer was set at 30 V for 16 hours. The transfer of proteins was evaluated by staining the nitrocellulose membranes with 0.05 % (w/v) copper-phthalocyanine 3, 4',4'',4''' tetrasulphonic acid tetrasodium salt in 12 mM HCl. The copper stained membrane image was captured using a Fujifilm CCD camera, and then the membrane was destained with 12 mM NaOH solution.

### 2.2.10.3 Immunoprobng for proteins

After the transfer procedure, the nitrocellulose membranes were blocked with 5% (w/v) marvel/TBS-tween (0.1% v/v) at room temperature for 1 hour. Then, the blot was immersed in primary antibody diluted in 3% (w/v) marvel/TBS-Tween (0.1% (v/v)) at the relevant concentrations as listed in Table 2.1. The blot was then incubated overnight with gentle

shaking on an orbital shaker at 4 °C in the cold room. Blots were then washed 4X15min with TBS-tween. The blots were then probed with appropriate HRP conjugated secondary antibody diluted in 3% (w/v) marvel/TBS-Tween (0.1% (v/v) for 2 hours at room temperature with gentle shaking followed by four 15min washes with TBS-Tween. After washing, the blot was placed on a black laminated sheet and sprayed with Merck RapidStem™ enhanced chemiluminescence reagent. Following the one-minute incubation, the excess reagent was removed using a filter paper. The blot was then placed into the Fuji dark box and developed using FUJIFILM CCD camera.

#### **2.2.10.4 Quantification of western blots**

The intensity of protein immunoblot bands was quantitatively analysed using an Aida image analyser. The pixel intensity of equal-sized area around the bands was obtained and quantified depending on the number and intensity of pixels in each area. Changes in the sample loading were corrected against a housekeeping protein (loading control), and the corrected protein bands were expressed as a percentage of the control.

#### **2.2.11 Toxins investigation**

The biochemical changes and physical abnormalities as seen in neural cell degeneration were mimicked by the addition of various toxins which could impair normal cell functionality (Sherer, Betarbet, Stout, et al. 2002). The investigation was conducted on both traditional 2D culture surfaces and on nanofibre scaffolds to establish the adverse effect of these toxins. Four different toxins capable of causing different biochemical changes were used to conduct this study. Rotenone and MPTP, to induce complex 1 inhibition; MG132, to induce proteasome inhibition; and BSO, a glutamylcysteine synthetase inhibitor to reduce glutathione levels. Both neuronal and glial cells were seeded at a density of 50,000 cells/well on nanofibres and tissue culture plates (TCP). After 24 hours, the fibres were transferred to a fresh plate to avoid cells that may not have attached to

the fibre. All samples were incubated for an additional 24 hours at 37 °C with 5% CO<sub>2</sub>. 48 hours later, the media from both TCP were replaced with media containing Toxins at final concentrations as shown: Rotenone, 0.5 µM and 2.5 µM; MPTP, 10 µM and 100 µM; MG132, 0.1 µM and 0.5 µM; and BSO, 2 mM. After the addition of toxins, all samples were incubated under the same conditions for 72 hours. Following incubation, both TCP were tested for cell viability using the MTT and CellTiter-Glo® 3D viability assays as described in section 2.2.6.

### **2.2.12 Co-Culture Model to investigate the effect of Toxins**

A co-culture system of neuronal and glial cells using both traditional 2D cultures and nanofibres was utilised. Cells were initially cultured individually on different surfaces prior to constructing a mixed co-culture and incubating the neural populations in the same well. The co-culture model consisted of two layers as described in Figure 2. 11. The construct was either made with the 2D surface (layer 1) then a spacer and then a scaffold (layer 2) or with scaffold as both layers separated by a hollow spacer.

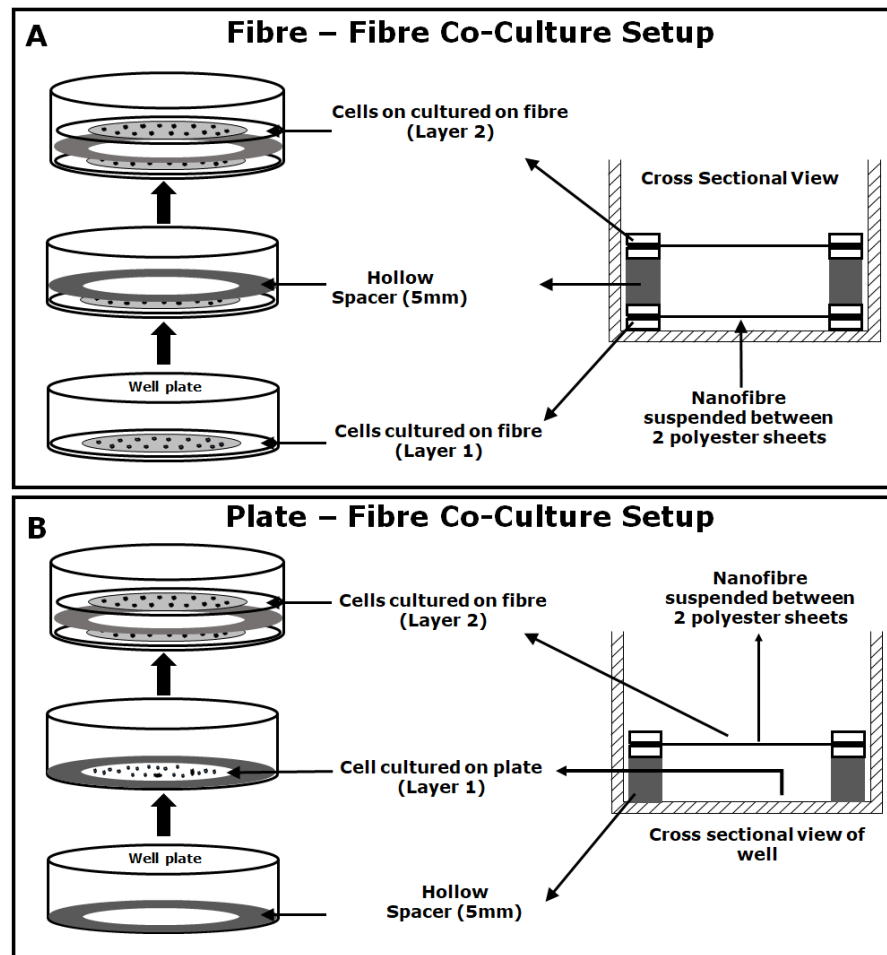


**Figure 2. 11: Schematic representation of the experimental setup designed to create a co-culture system.**

Each layer harboured a different neural cell type with three different experimental setups;

1. The neuronal cells on the plate and glial on fibre
2. Glial cells on the plate and neuronal cells on the fibre and
3. Both neuronal and glial cells on individual fibres.

Based on the three-experimental set, both neuronal and glial were seeded individually at a density of 50,000 cells/well, cultured for 48 hours and induced to differentiate with B27 supplement for five days at 37°C with 95 % air and 5% CO<sub>2</sub> supply. After five days the experiment was arranged as shown in figure 2.14. Also, 0.5µM rotenone, 0.1µM MG132 and 2 mM BSO were added to the co-culture, which was incubated at 37°C with 95 % air and 5% CO<sub>2</sub> supply for 20 days to recreate a longer-

term, chronic model. Every 72 hours the co-culture was separated, and the fibres were transferred from each well into a fresh culture dish to measure viability, and fresh media with toxins were replaced for the remaining wells. Cell viability was examined individually for each scaffold and plate using CellTiter-Glo® 3D viability assay kit.

### **2.2.13 Statistical analysis**

The data was generally presented as mean  $\pm$  the standard deviation (SD). Statistical analysis was performed on all datasets, and all analysis was conducted using the Graph Pad Prism for Windows Version 7.02. P-values  $<0.05$ ,  $<0.01$  or  $<0.001$  were considered statistically significant and were indicated within figures as \*  $p<0.05$  , \*\* $p<0.01$  or \*\*\* $p<0.001$ .

#### **2.2.13.1 Polymer absorbance analysis**

The absorbance data obtained was statically analysed using unpaired two-tailed T-test. The data obtained were normally distributed (as ascertained by the Kolmogorov-Smirnov Test for Normality). The data consists of a distinct control and test set with a clear statistical intention to test for differences within these two populations. The critical area of a distribution is two-sided testing whether a sample is greater than or less than a certain range of values. The data were represented as one control which was independently compared to two variables showing a significant difference compared to the control.

#### **2.2.13.2 Rheology measurement**

In this data, two-parameter were analysed to include Strain diameter vs time and Strain diameter vs strain rate for both PAN vs PJ polymer. The statistical analysis chosen for this study was Unpaired t-test with Welch's correction due to the two variables (PAN and PJ) have normal distributions with equal variance. The Welch's t-test was used for unequal variances, but the assumption of normality was maintained.

**2.2.13.3 Nanofibre Diameter and Pore size measurement**

One hundred different measurements were analysed for each sample. The data is represented in an even mean distribution among the one hundred measurements with standard error and standard error mean ( $\pm$ ).

**2.2.13.4 Proliferation and Viability analysis**

Throughout the study, values obtained for proliferation and viability assessments were converted to a percentage of the corresponding control, thereby assigning the control values as 100%.

The data obtained were normally distributed (as ascertained by the Kolmogorov-Smirnov Test for Normality). Statistical analysis was performed using the Two-Way ANOVA with Sidak's multiple comparisons tests. The two-way ANOVA compares the mean differences between groups that have been split into two independent variables (Plate and Fibre) and the Sidak multiple comparisons was applied to and compare each time point against the two variables.

P-values for significance were indicated within figures as \*  $p < 0.05$  , \*\* $p < 0.01$  or \*\*\* $p < 0.001$ .

## Chapter 3: Nanofibre fabrication and analysis

### 3.1 Introduction

The synthesis of nanofibres fabrication dates back over four centuries (Tucker, Stanger, Staiger, et al. 2012; LF Nascimento, S Araujo, R Cordeiro, et al. 2015). However, the first attempt to manufacture nanofibre by electrospinning occurred between 1934 and 1944 by the scientist Anton Formhals (Tucker, Stanger, Staiger, et al. 2012). The words nanofibre and electrospinning came to light and was started to be commonly used among scientist and researchers only by the late 20<sup>th</sup> century (LF Nascimento, S Araujo, R Cordeiro, et al. 2015). In this current modern scientific world, nanofibre manufacture has taken many turns, and the methods of fabrication have been significantly revised. Over the years, the number of applications of and research with electrospun nanofibre has dramatically with many different methods of forming nanofibres being developed to meet production requirements. Table 3.1 summarises the recent developments in nanofibre fabrication methods along with each methods advantages and disadvantages (Nayak, Padhye, Kyratzis, et al. 2012).

All the electrospun nanofibre scaffolds used in this study were produced using a purpose-built electrospinning system. It consists of an interlocked humidity-controlled chamber with recirculating airflow. The organic solvents used to dissolve polymers to form electrospinning solutions are removed using activated carbon filters. This helps to maintain a stable environment needed to produce high-quality nanofibres. The set up within the chamber is relatively simple; it consists of a blunt-end needle which is fed with a polymer solution and connected to the high voltage positive supply. The needle is held at a fixed distance from a metallic cylindrical drum which can be rotated about its axis. This research set up has several advantages such as consistent diameter, controlled pore size, controlled fibre mat thickness, environment-friendly, and can be used to coat up to B1 size laser cut plastic sheets.

<b>Method</b>	<b>Fibre diameter</b>	<b>Advantages</b>	<b>Disadvantages</b>	<b>Reference</b>
<b>Needless Electrospinning</b>	200–800 nm	Higher production rate	The vast spread of fibre diameter	(Yarin and Zussman 2004)
<b>Bubble Electrospinning</b>	No information available	Low cost, high production rate. Clogging free	The solvent used cannot be recovered, excessive use of solvents	(Liu, G., Qiao and Guo 1996; Liu, Y. and He 2007)
<b>Electroblowing</b>	40–120 nm	Higher production rate	Solvent recovery	(Wang, X., Um, Fang, et al. 2005)
<b>Cylindrical porous hollow tube</b>	300–600 nm	Higher production rate	The intricate design of the setup	(Varabhas, Chase and Reneker 2008)
<b>Microfluidic manifold</b>	85–350 nm	Simple, spin multiple polymers, control over the deposition	Solvent recovery	(Srivastava, Loscertales, Marquez, et al. 2008)
<b>Roller electrospinning</b>	144 nm Avg.	Higher production rate	Not possible low mol. Weight polymers	(Cengiz and Jirsak 2009)

<b>Melt electrospinning (Electrical heating)</b>	16 ± 10.7 mm for molten fibres and 560nm ± 90 nm for solid fibre	Solvent-free approach	Mostly amorphous fibre, thermal degradation	(Zhou, Green and Joo 2006)
<b>Coaxial melt electrospinning</b>	Avg. 150 nm	Encapsulation, suitable for a wide range of materials	Complex setup	(McCann, Marquez and Xia 2006)
<b>Melt electrospinning (LASER heating)</b>	Avg. ~1 mm	No electric discharge, suitable for a polymer with a high melting point, less thermal degradation	Amorphous fibres, unstable.	(Ogata, Yamaguchi, Shimada, et al. 2007)
<b>Meltblowing</b>	Less than 500 nm	Higher production rate	Breaking of fibres and bead formation	(Brang, Wilkie and Haggard 2008; Bodaghi and Sinangil 2009)
<b>Melt extrusion</b>	Avg. diameter 150 nm–400 nm,	Consistent fibre diameter	Short lengths of fibre, fibre length: 60 µm	(Li, Huayi, Ke and Hu 2006)
<b>Flash-spinning</b>	500 nm	Higher production rate	Short lengths of fibre	(Nayak, Padhye, Kyratzis, et al. 2012)

<b>Drawing</b>	60 nm	Simple, long and continuous fibre	The lower production rate and no uniform diameter	(Tong, L. and Mazur 2008; Xing, X., Wang and Li 2008)
<b>Pressurised gas</b>	less than 3000 nm	Suitable for spinnable fluids	Complex process	(Reneker, Chun and Ertley 2002)
<b>Force spinning</b>	Micron and submicron	The lower electric field, simple process, high production rate	High temperatures required	(Lozano and Sarkar 2009)
<b>Jet-blowing</b>	10 nm to 50 mm	Formation of composites does not require the use of harsh solvents	Complex process	(Sen, Bedding and Gu 2005)
<b>Melt-spinning</b>	Less than 1000nm	Suitable for many solvents and polymers, simple	Degradation of polymers during spinning	(Huang, Marshall, Armantrout, et al. 2012)

**Table 3. 1: Other methods of nanofibre fabrication**

**3.1.1 Content of this chapter**

In this chapter, we have demonstrated the use of two synthetic polymers Polyacrylonitrile and Jeffamine® to fabricate biocompatible nanofibre scaffolds that allow cells to attach, proliferate, and survive. In support of this chapter, the engineering designs, method of polymer preparation, electrospinning parameters, and the range of fibre orientations which can be produced using a patented method will be explained. This chapter will also focus on the quantification of the nanofibre and scaffolds produced and explain the different and most suitable methods for nanofibre sterilisations. Although the work developed routes to produce scaffolds with three different nanofibre orientations, namely random, aligned and radial, the scaffolds used to develop the neurodegenerative in vitro model was random non-woven scaffolds.

## 3.2 Results

### 3.2.1 Engineered designs

Random, aligned and radial fibres designs developed in this study were made on the 75 $\mu$ m thick polyester sheet. The laser focus was positioned to the surface of the sheet or 15mm from the focusing lens on the Trotec laser cutter. Arrays of the aperture design were laser cut, and the speed and power combinations were adjusted to identify the settings which produced dimensionally accurate and clean cuts to the polyester sheets. This optimisation process determined that a laser cutting setting of 80% of the maximum speed and 28% of maximum power produce acceptable dimension control and clean edges on a Trotec SP500 laser cutter

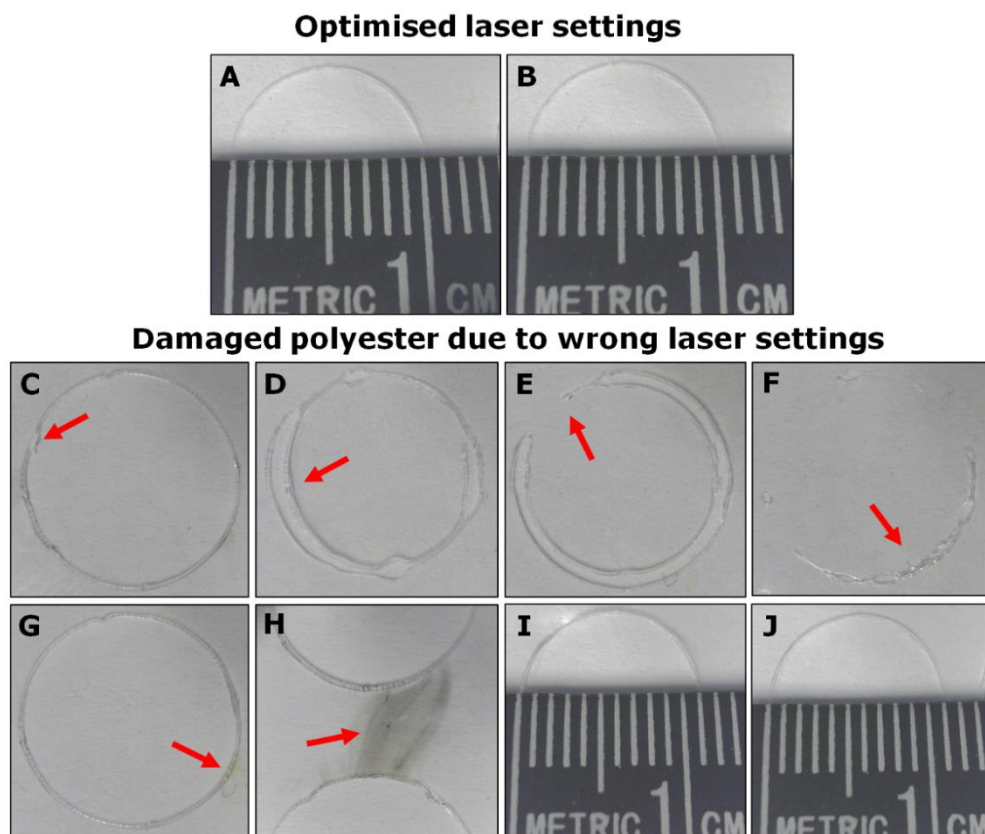


**Figure 3. 1: Laser speed and power settings optimisation.**

The figure shows the microscope image of designs made on the polyester sheet using a CO<sub>2</sub> laser cutter with different power and speed. The arrows indicate the damage caused on the polyester sheet due to the incorrect parameter for the laser

In Figure 3. 1, A and B show a design cut with fully optimised laser setting with accurate dimensions and clean-cut edges. C-J shows the various type of damage that can be caused to the design when wrong laser settings are applied. Faults like excessive melting (C), improper cutting (D, E, and F), shape deformation (G), deposition caused due high laser power (H), and change in the measurement of the design is the common damage observed due to incorrect laser settings.

### 3.2.2 Polymer preparation

Two synthetic polymers, polyacrylonitrile (PAN) and Jeffamine<sup>®</sup> ED 2003 were dissolved in DMF. 10wt% (w/w) PAN and 10wt% PAN with 5wt% Jeffamine<sup>®</sup> ED-2003 (PJ) were used to make nanofibre for this study. The mixture was heated at 50°C overnight with constant stirring. When the fully dissolved electrospinning solutions have no contaminants, the PAN solutions will be very pale-yellow, and PJ will be pale red (Figure 3. 2). Consistency among a different batch of the polymer was measured using a spectrophotometer. The absorbance of both PAN and PJ was measured by adding 100µl of both polymers and solvent in a 96 well plate, and an endpoint measurement was obtained at 540nm. Compared to DMF, 10wt% PAN had an average absorbance of 40%±2% and adding 5wt% Jeffamine<sup>®</sup> the average absorbance was measured to be at 75%±2% of PJ polymer (Figure 3. 2). In general, the dissolved polymer was stored at 4°C in a sealed container for up to 4 weeks and heated to room temperature before use.

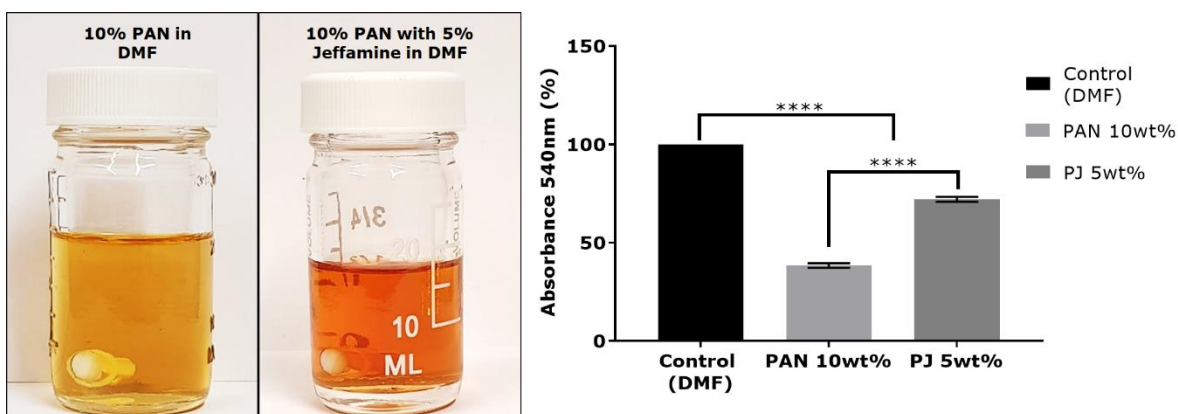


**Figure 3. 2: PAN and PJ polymers dissolved in DMF.**

The figure shows when PAN and PJ are entirely dissolved in DMF; PAN appears in pale yellow, and PJ appears in pale red. The absorbance of both polymers was measured at 540nm compared to the DMF. Obtained values were converted to percentage setting control values to 100%. Results are expressed at the mean ratio + SEM  $n=5$  \* $P<0.001$  against polymer vs solvent determined by unpaired two-tailed Student-T test.

### 3.2.3 Electrospinning solution rheology properties

After the PAN and PJ polymer formulations were prepared overnight by constant stirring at 50°C, the viscosity of both types of polymers was measured using the HAAKE™ CaBER™ 1 Capillary Breakup Extensional Rheometer. The polymers were brought to room temperature before a small volume of each polymer was loaded on the Rheometer as described in section 2.2.2.1. Shear viscosity and strain breakup time were measured. For PAN the shear viscosity was measured to be  $7.102 \text{ E}^{-1} \pm 1 \text{ Pa.s}$  with a calculated breakup time of  $2.98\text{E}^{-1} \pm 0.5$  seconds, and for PJ polymer solution the shear viscosity was measured to be at  $7.030 \text{ E}^{-1} \pm 1 \text{ Pa.s}$  with a calculated breakup time of  $2.18 \text{ E}^{-1} \pm 0.5$  seconds for PJ formulation (Figure 3. 3). A minor change was observed to the breakup time of PJ compared to PAN. Consistent data were obtained from every new batch.

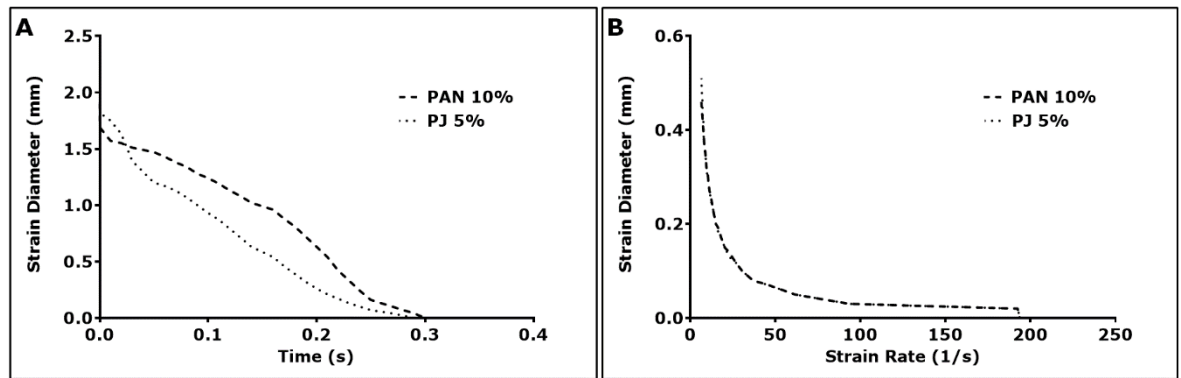


**Figure 3. 3: PAN and PJ viscosity measurement.**

Graph A show both PAN and PJ polymers change in strain diameter Vs time and graph C shows the strain diameter vs the strain rate. Results are expressed at the mean ratio  $\pm$  SEM  $P < 0.05$  against PAN 10% vs PJ5% determined by Unpaired Welch's Two-tailed student-T tests.

### 3.2.4 Electrospinning

After investigating the viscosity of PAN and PJ polymer solution, each polymer is loaded into a 10 ml syringe for electrospinning as explained in section 2.2.3. When the high voltage is applied the polymer stretches creating nanofibres. To obtain continuously spun nanofibres, it is essential to form a continuous jet flow which was achieved by optimising the high voltage supply (Figure 3. 4).

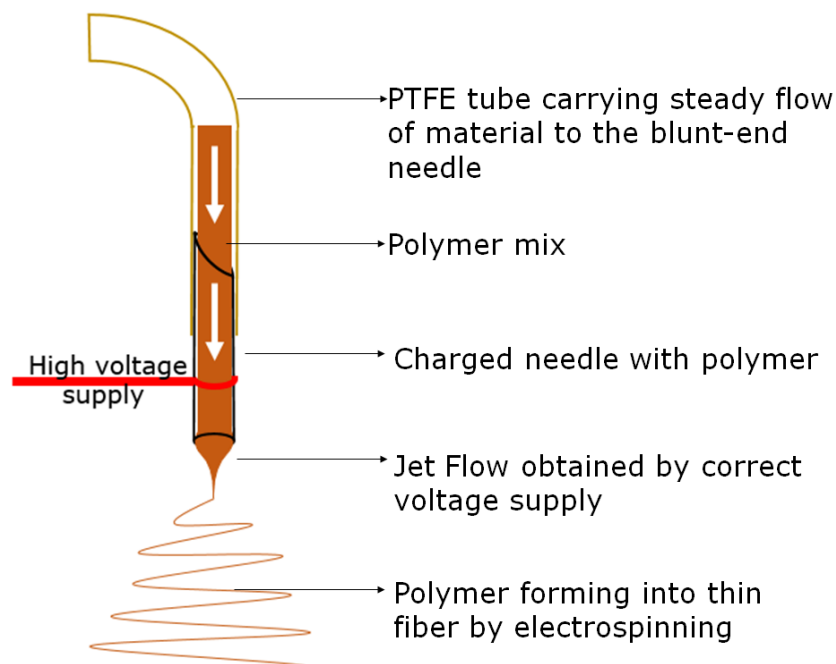


**Figure 3. 4: Schematic representation of jet flow formation.**

Depending on the viscosity and the flow rate of each polymer solution the voltage can vary. Both PAN and PJ was spun at 1ml/ hour flow rate, and the fibres were obtained at 21kV and 18kV for PAN and PJ respectively. The distance between the needle and the collector was set continuously to 30cm. During the electrospinning process, the relative humidity (RH) was 65%, and the air temperature was 21°C the stability over a typical electrospinning deposition run is shown in Figure 3. 5. The spun sheet was carefully detached from the collector, and the fibres were secured with an identical top sheet. The sheets were securely stored and were laser cut to fit well TCP. From every batch, the sample was randomly chosen to investigate fibre diameter, pore size, contact angle analysis, and membrane thickness.

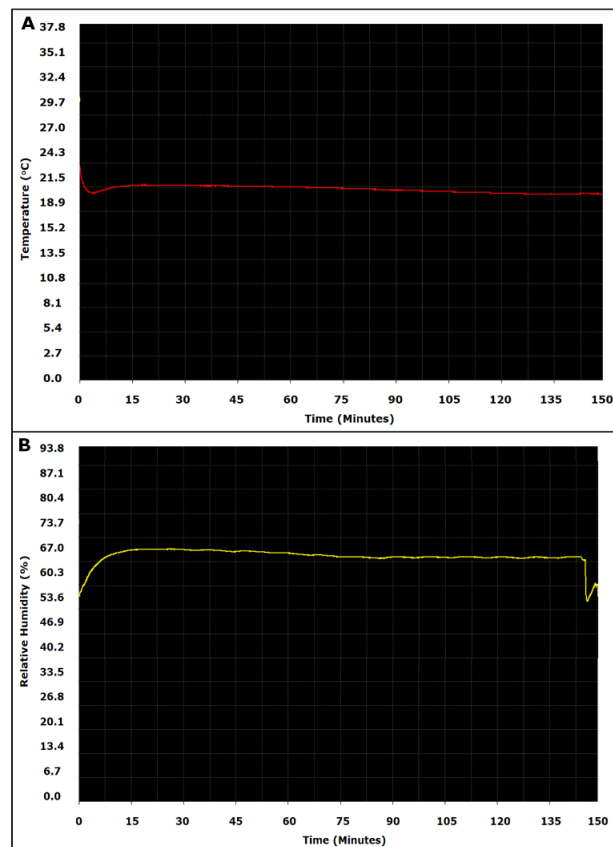


**Figure 3. 5: Temperature and humidity analysis during electrospinning.**

*The data is obtained from the Extech RHT10 temperature and humidity analyser that records the information throughout the electrospinning process. Graph A show the temperature recorded at 21°C for 2.5 hours and Graph B shows the humidity maintained at 65% throughout the process.*

**Table 3. 2: Electrospinning parameters for PAN and PJ**

<i>Polymer</i>	Needle to Collector distance	Flowrate	Voltage	RH	Temp	Total vol
<i>PAN</i>	30 cm	1ml/hr	21 kV	65%	21°C	2.5 ml
<i>PJ</i>	30 cm	1ml/hr	18 kV	65%	21°C	2.5 ml

### 3.2.4.1 Random Nanofibre Scaffolds

To obtain random fibres, the design was engineered on the polyester sheet as explained in section 2.2.1.1. A single sheet with an array of laser cut 1cm hole was used to obtain fully suspended random fibres. To improve the sterility, the laser cut sheets, and the collector was wiped with 70% ethanol before the electrospinning process. The sheet was wrapped around the collector and secured with aluminium tape. The electrospinning was set according to the parameters shown in *Table 3. 2*, and a total volume of 2.5 ml of the polymer was collected in the form of fibres on the design.

#### 3.2.4.1.1 SEM and FibreMetric analysis

The distribution of the nanofibre diameter and the pore size and orientation of the nanofibre scaffolds were analysed by processing the Phenom ProX SEM images with FibreMetric image analysis software available in the Phenom Suite on the Phenom desktop SEM. Selected samples were coated with 10nm of gold and prepared for SEM as described in section 2.2.3.1. The fibre bed was thoroughly examined for any form of defects or damage in multiple areas. Images obtained at 6000X magnification are transferred into FibreMetric software to analyse for fibre diameter and pore size as explained in section 2.2.3.1.

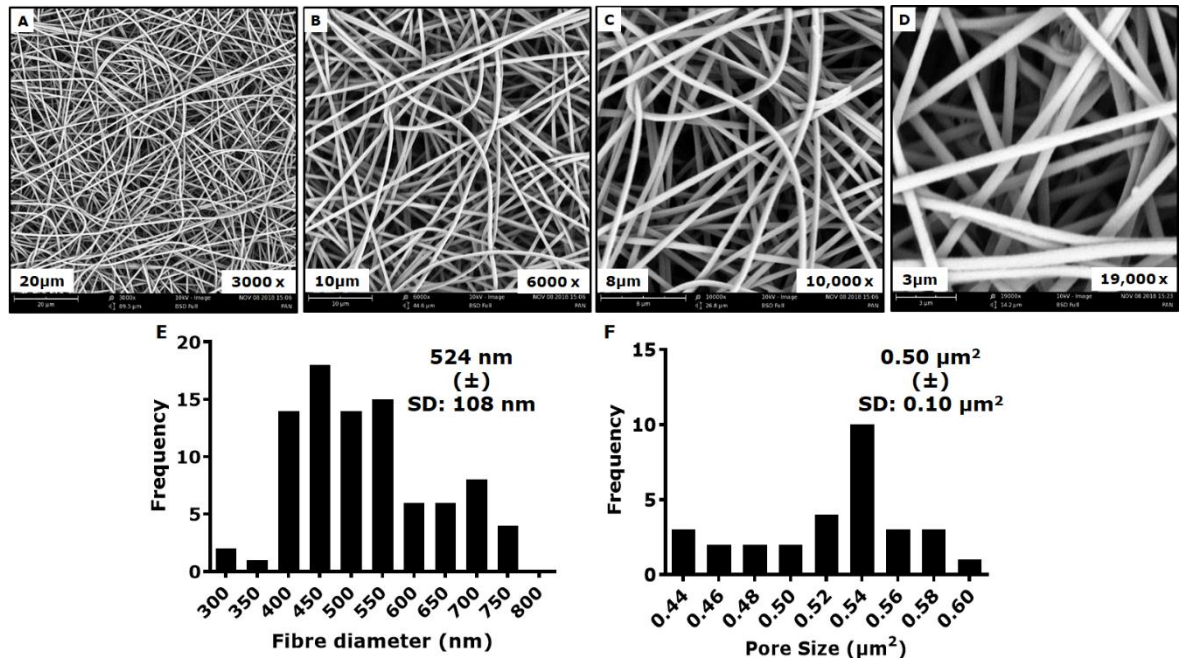


**Figure 3. 6: PAN SEM and FibreMetric analysis data.**

Image A-D show SEM analysis for damage on the fibre at different magnification of a chosen area. Graph E shows the fibre diameter and F represents the pore size. The frequency of the distribution for fibre diameter and pore size was calculated along with mean and standard deviation (SD) using graph pad prism

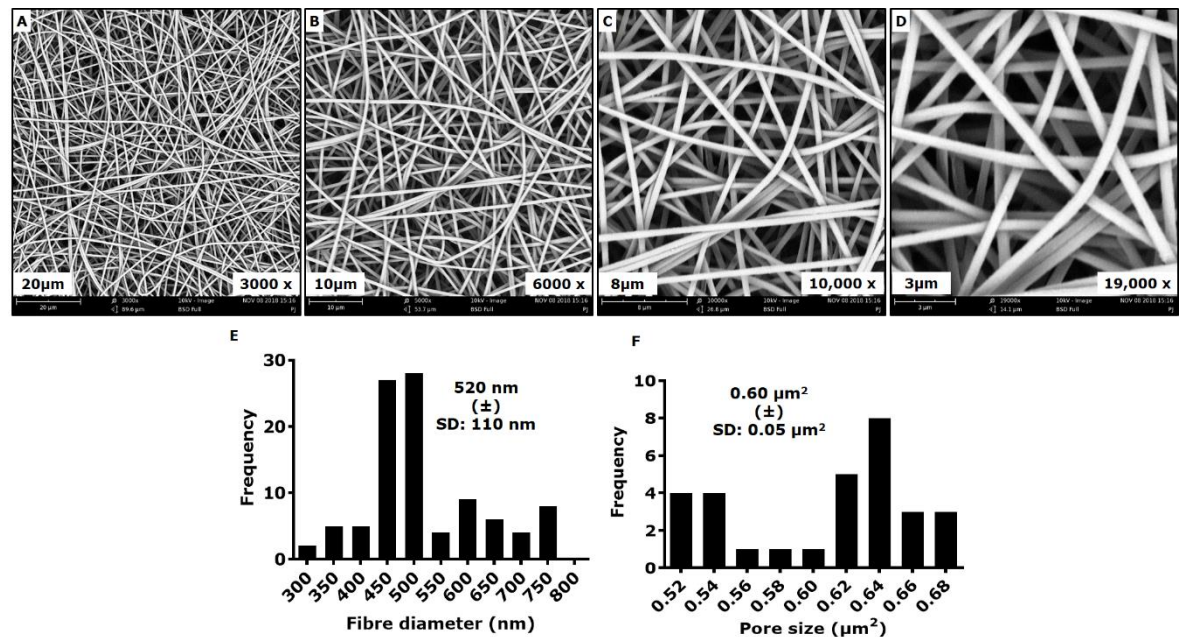


**Figure 3. 7: PJ SEM and FibreMetric analysis data.**

Image A-D show SEM analysis for damage on the fibre at different magnification of a chosen area. Graph E shows the fibre diameter and F represents the pore size. The frequency of the distribution for fibre diameter and pore size was calculated along with mean and SD using graph pad prism

The average diameter for a 10% PAN Electrospun at 1ml/hour rate in 21kV with 2.5ml of total deposition was  $524\text{nm} \pm 108\text{nm}$  with pore size of  $0.50 \mu\text{m}^2 \pm 0.10 \mu\text{m}^2$  (Figure 3. 6) and the average diameter of 10% PAN with 5% Jeffamine<sup>®</sup> electrospun at 1ml/hour rate at 18kV was  $520\text{nm} \pm 110\text{nm}$  with a pore size of  $0.60 \mu\text{m}^2 \pm 0.05 \mu\text{m}^2$  (Figure 3.7)

**Table 3. 3 Diameter and pore size based on electrospinning parameters**

<i>Polymer</i>	Flowrate	Voltage	Total volume	Diameter (nm)	Pore size ( $\mu\text{m}^2$ )
<i>PAN</i>	1ml / hr	21 kV	2.5 ml	524±SD:108	0.50±SD:0.10
<i>PJ</i>	1ml / hr	18 kV	2.5 ml	520±SD:110	0.60±SD:0.05

### 3.2.4.1.2 Contact angle measurement

The hydrophobic properties of both PAN and PJ fibre scaffolds were tested using contact angle analysis as described in section 2.2.3.2. A high-speed camera video was set to run for 10 sec, and a drop of water was placed on the centre of random fibres scaffold. The wetting dynamics of the scaffold was video recorded and measured for 10 sec. The Drop Shape Analyser (DSA) software measure the changes in the shape of the droplet for the recorded period and calculates an average contact angle for 10 sec. The DSA determined that random fibre scaffold made with PAN was hydrophobic with an average contact angle of  $112.7^\circ$ . The addition of 5% Jeffamine<sup>®</sup> made the scaffold hydrophilic and with complete wetting. The PJ scaffold average contact angle was measured to be at  $0^\circ$  at the end of 10-sec measurement (Figure 3. 8)

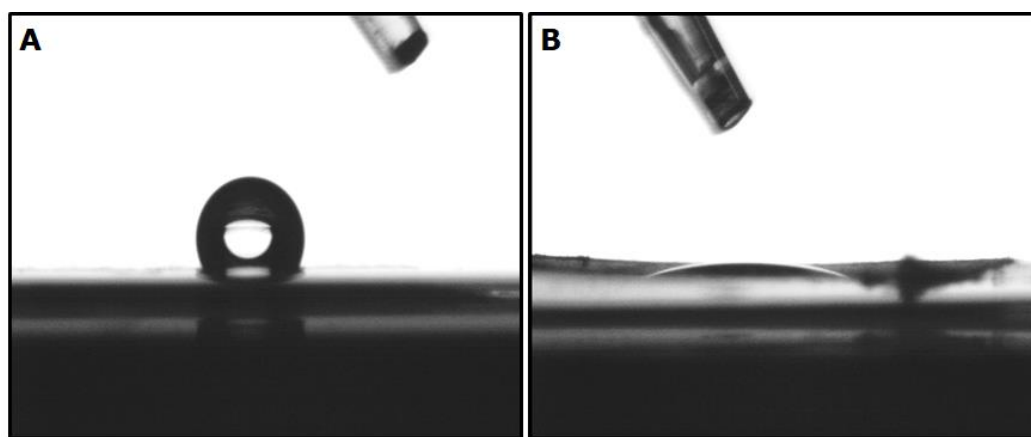


**Figure 3. 8: Random fibre contact angle analysis.**

Image A shows PAN fibre is hydrophobic with the water droplet staying stagnant on the surface of the scaffold and Image B shows PJ fibre is hydrophilic where the water droplets wet into the scaffold. The image was obtained from a screenshot of a 10-sec high-speed video recording, and the average data was obtained with DSA for the 10sec video recording.

**Table 3. 4: Contact angle based on electrospinning parameters**

Polymer	Flowrate	Voltage	Total vol	Contact angle
PAN	1ml / hr	21 kV	2.5 ml	112.7°
PJ	1ml / hr	18 kV	2.5 ml	0°

### 3.2.4.1.3 Scaffold thickness measurement

OCT is capable of internal imaging structure of a material or generating a cross-sectional tomographic image of a thin low light scattering sample. An OCT instrument describes in section 2.2.3.3 was used to determine the total thickness of the scaffold membrane. Randomly chosen scaffolds were tested for thickness in both dry and wet state as described in section 2.2.3.3. Analysis of the image was performed on wet samples as wetting the samples created an upper and lower liquid interface, and this provided a better structure to measure with less scattering. The thickness was measured using image J software at three different locations as shown in figure 3.9. The thickness of the scaffolds was measured to be an average of 33.5  $\mu\text{m}$  for PAN and 30  $\mu\text{m}$  for PJ (Figure 3. 9).

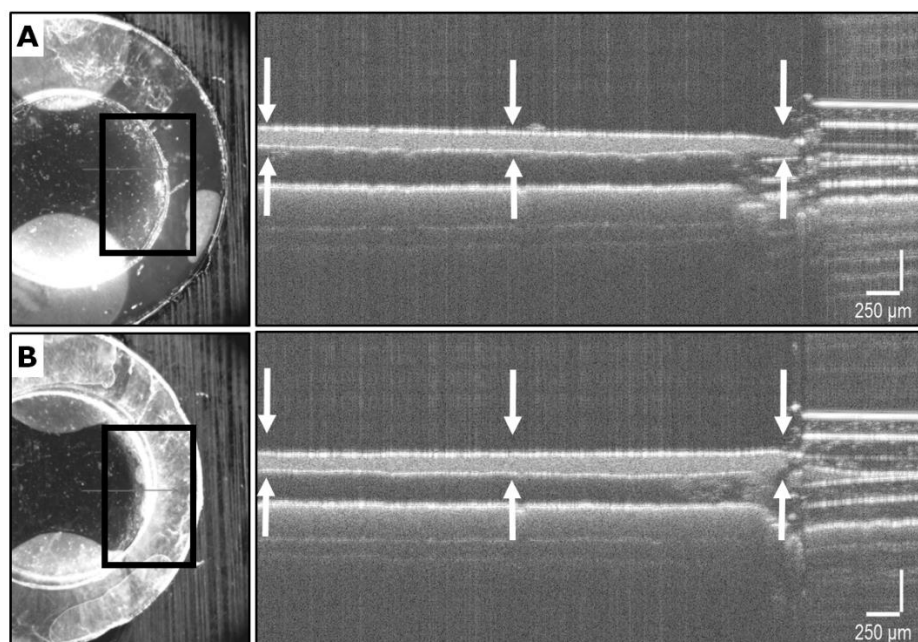


**Figure 3. 9: OCT measurement for random PAN and PJ scaffold.** Image A shows the region of PAN scaffold measured using OCT and image B shows PJ scaffold. Both samples were wetted with ethanol prior to obtaining the OCT image. The area between the arrows indicates the suspended fibre. The arrows represent the point of measurement for each scaffold using image J software.

**Table 3. 5: Random Scaffold thickness based on electrospinning parameters**

<i>Polymer</i>	Flowrate	Total volume	Membrane thickness	Total thickness
<i>PAN</i>	1ml / hr	2.5 ml	33.53 $\mu\text{m}$	183.53 $\mu\text{m}$
<i>PJ</i>	1ml / hr	2.5 ml	30.02 $\mu\text{m}$	180.02 $\mu\text{m}$

### 3.2.4.2 Aligned nanofibre

Aligned nanofibre scaffolds were manufactured using our patented process as explained in section 2.2.1.2. Accordingly, two laser-cut sheets were ultrasonically tack welded together and placed on the rotating drum with the top sheet outermost. Both PAN and PJ fibres were deposited during separate runs to form aligned nanofibres. Both fibre types were electrospun with 1ml/hour flow, with 2.5 ml of the solution being

converted to fibre. Electrospinning parameters were the same as those used for random fibre scaffolds, notably 21kV for PAN and 18kV for PJ.

#### **3.2.4.2.1 SEM and FibreMetric analysis**

The samples were coated with 10nm of gold and prepared for SEM as described in section 2.2.3.1. At different magnifications, the fibre bed was thoroughly examined for defects and damage. Images obtained were transferred into FibreMetric software to analyse for fibre diameter and pore size as explained in section 2.2.3.1. The patent-pending process creates aligned fibre scaffold inserts which have three regions, an aligned fibre region and two random fibre regions (Figure 3. 10). Diameter and pore size was measured for each type. For PAN the average diameter and pore size for the random region of the scaffold was 570nm  $\pm$  SD: 124nm and 0.57 $\mu\text{m}^2$   $\pm$  SD: 0.05  $\mu\text{m}^2$  respectively. The average diameter and pore size for the aligned region was 424 nm  $\pm$  SD: 50 nm and 0.22  $\mu\text{m}^2$   $\pm$  SD: 0.09  $\mu\text{m}^2$  respectively (Figure 3. 11). Similar to PJ the average diameter and pore size for the random region of the scaffold were 550nm  $\pm$  120nm and 0.56 $\mu\text{m}^2$   $\pm$  0.05  $\mu\text{m}^2$  respectively. The average diameter and pore size for the aligned region was 439 nm  $\pm$  50 nm and 0.24  $\mu\text{m}^2$   $\pm$  0.09  $\mu\text{m}^2$  respectively (data not shown).

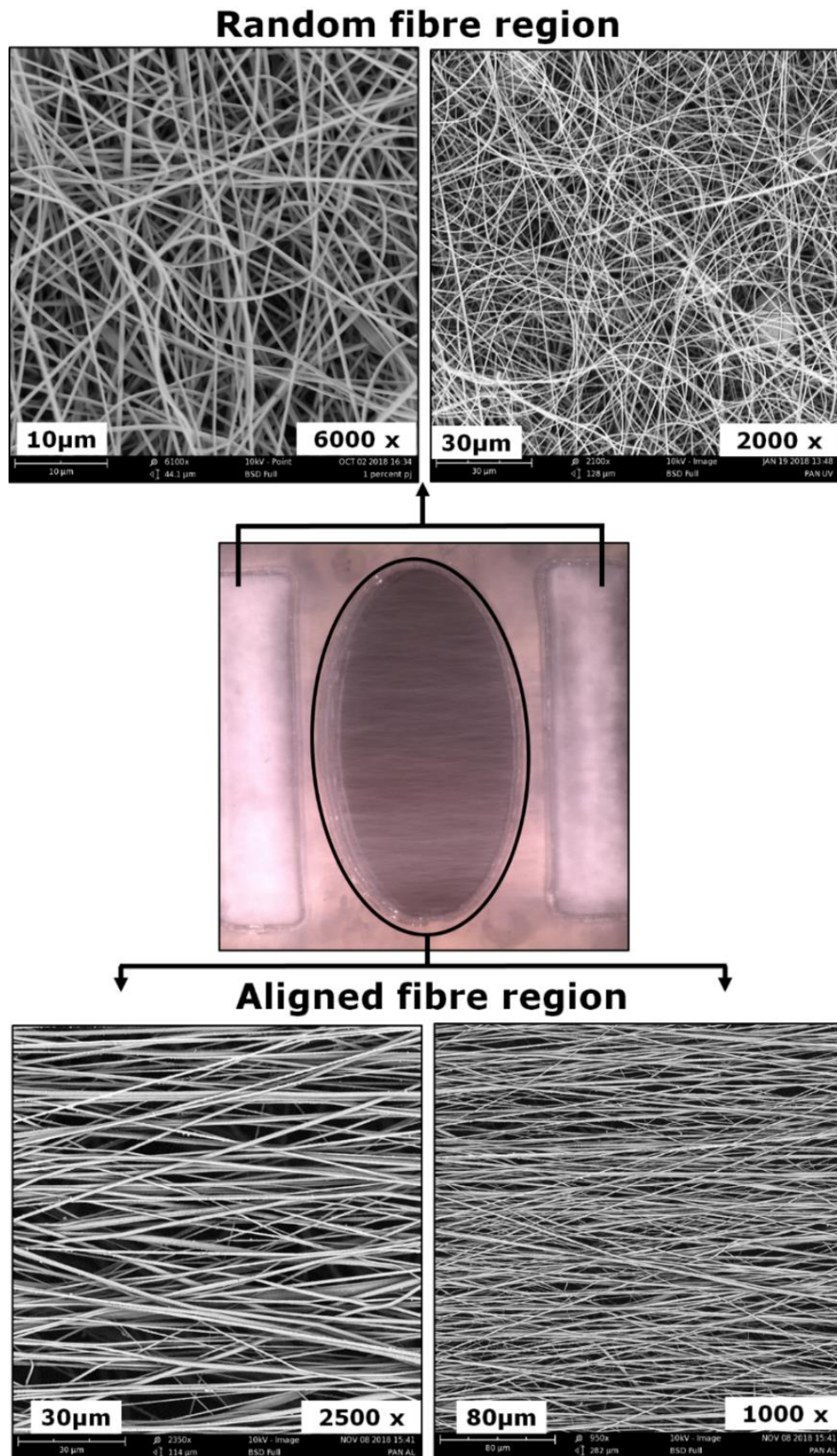


**Figure 3. 10: Aligned nanofibre design SEM imaging.**

The design consist of two regions. The two rectangle region forming random fibres and the centre ellipse region harbouring the aligned fibres.

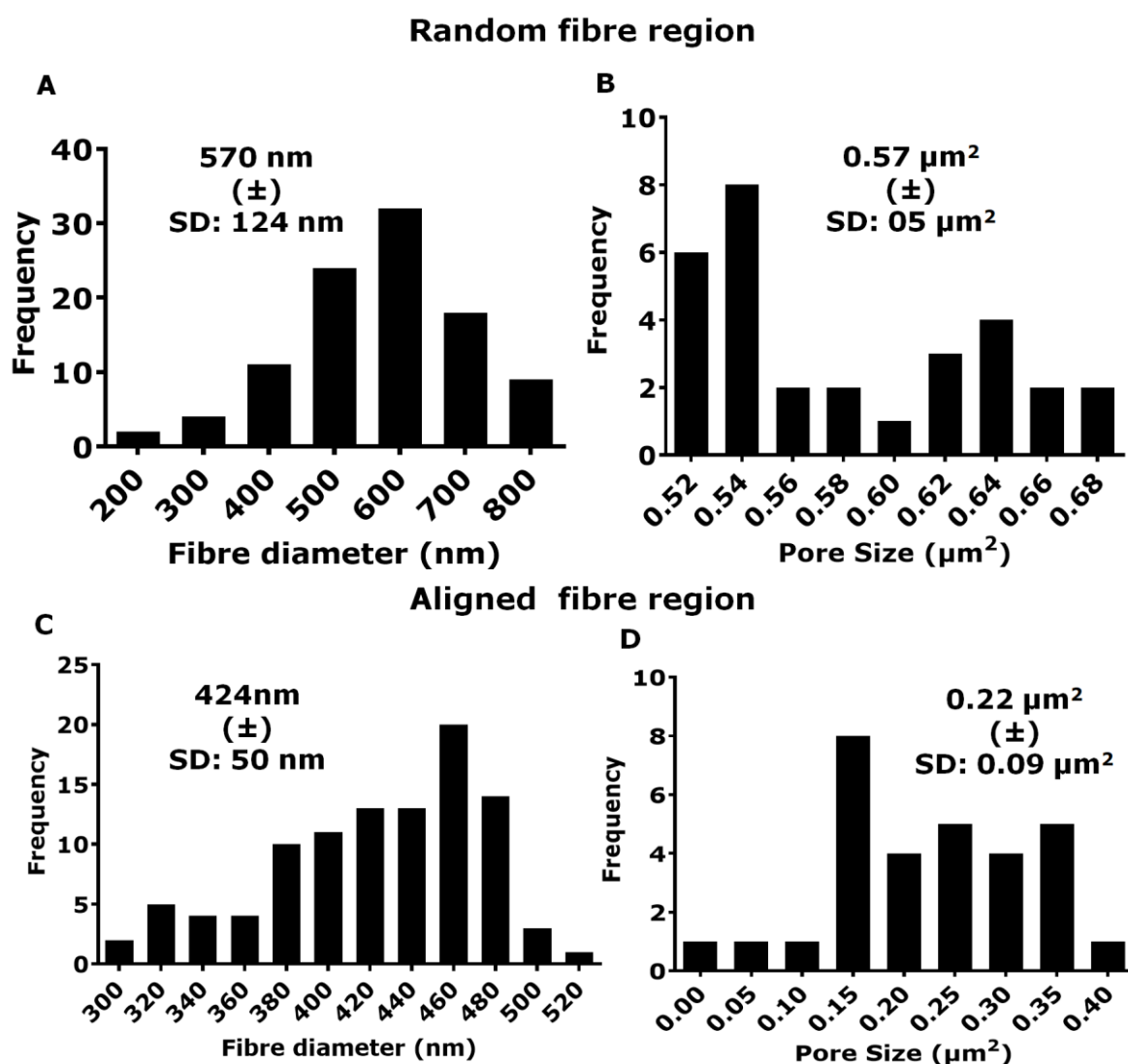


**Figure 3. 11: FibreMetric data for Aligned PAN fibre scaffold.**

In this image Graph, A and B show the diameter and pore size of the random fibre region and Graph C and D represents the diameter and pore size of the aligned fibre region receptively.

**Table 3. 6: Aligned fibre FibreMetric data based on electrospinning parameters**

Polymer	Flow rate	Total volume	Random region		Aligned region	
			Diameter (nm)	Pore size ( $\mu\text{m}^2$ )	Diameter (nm)	Pore size ( $\mu\text{m}^2$ )
PAN	1ml / hr	2.5 ml	570 ± SD:124	0.57 ± SD: 0.05	424 ± SD: 50	0.22 ± SD: 0.09
PJ	1ml / hr	2.5 ml	550 ± SD:120	0.56 ± SD: 0.05	439 ± SD: 50	0.24± SD: 0.09

### 3.2.4.2.2 Contact angle measurement

Both aligned PAN and PJ were tested using contact angle analysis as described in section 2.2.3.2. The aligned fibre inserts consist of two types of region, and the hydrophobic nature of both was tested using DSA. For PAN aligned fibre inserts the random region showed hydrophobic nature with a contact angle measured to be at  $110.8^\circ$  (Figure 3. 12 A) and in the aligned region the contact angle was measured to be at  $130.2^\circ$  (Figure 3. 12 C). When aligned fibre made with PJ fibre, the contact angle for the random region and the aligned region was measured at  $0^\circ$  at the end of the 10sec reading (Figure 3. 12 B and D). Aligned PJ fibre expressed a higher wetting rate compared to the random PJ whereas aligned PAN showed a high hydrophobic nature compared to random PAN

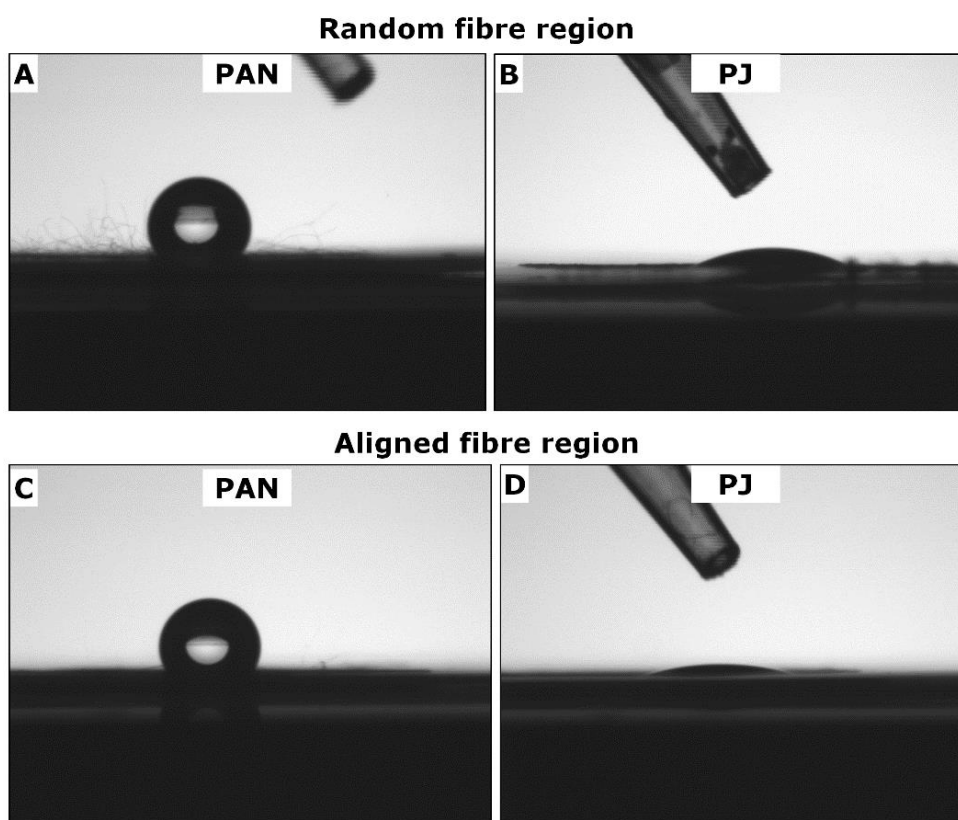


**Figure 3. 12: Aligned fibre contact angle analysis.**

The scaffold consists of two regions. Image A and B shows analysis of the random region for PAN and PJ fibre respectively and Image C and D show the analysis of the aligned region of PAN and PJ respectively. The image was obtained from a screenshot of a 10-sec high-speed video recording, and the average data was obtained with DSA for the 10sec video.

**Table 3. 7: Aligned fibre contact angle data based on electrospinning parameters**

<i>Polymer</i>	Flow rate	Total volume	Random region	Aligned region
<i>PAN</i>	1ml / hr	2.5 ml	110.8°	130.2°
<i>PJ</i>	1ml / hr	2.5 ml	0°	14.2°

### 3.2.4.2.3 Scaffold thickness measurement

Similar to the random design the thickness of the aligned fibre membrane was analysed using OCT. The total thickness of the scaffold sandwiched between two polyester sheets was measured using the OCT. Three randomly chosen scaffolds were tested for thickness in both dry and wet state as described in section 2.2.3.3. Each region of the aligned fibre design was measured separately. The rectangles on either side were carefully cut, and the OCT was performed on both rectangles and the ellipse region of the design. The thickness was measured using image J software at three different locations as shown in Figure 3. 13. For PAN fibre the thickness of the two rectangular random areas was 33.5 $\mu$ m and 34.2 $\mu$ m. The average thickness of the aligned area was measured to be at 26.7 $\mu$ m. Both PAN and PJ fibres showed similar thickness in the membrane when spun at 1ml/hour rate with a total deposition of 2.5ml.

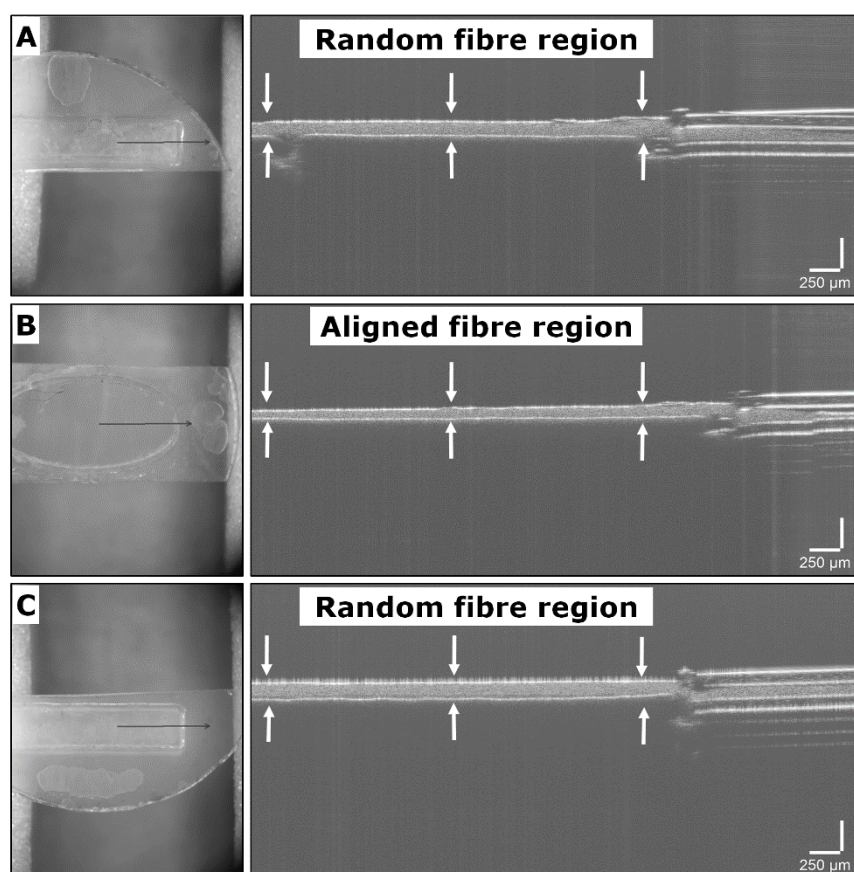


**Figure 3. 13: OCT measurement for aligned PAN fibre scaffold.** Image A and C show the random region of the aligned fibre design and image B shows the aligned region of the design. Each area was individually measured under OCT and analysed individually. The area between the arrows indicates the suspended fibre. The arrows represent the point of measurement for each scaffold using image J software.

**Table 3. 8: Random Scaffold thickness based on electrospinning parameters**

Polymer	Flow rate	Total volume	Membrane thickness		
			Random region	Aligned region	Random region
PAN	1ml / hr	2.5 ml	33.5 µm	26.7 µm	34.2 µm
PJ	1ml / hr	2.5 ml	32.6 µm	26.2 µm	32.9 µm

### 3.2.4.3 Radial Nanofibre

The radial nanofibres were achieved by a two-sheet design made based on similar principle as the aligned fibre design. Two sheets made as described in section 2.2.1.3 were ultrasonically welded and wrapped around the collector drum. The radial fibre design is an innovative model that holds a random fibre at the peripheral area with radially aligned fibre travelling to the centre forming into a region of random fibre at the epicentre. Both PAN and PJ polymers were electrospun on the radial fibre design using the standard parameters used with every other design in this study. Post spinning the sheet was carefully removed from the collector and secured with an identical top sheet; then the base sheet was detached carefully. The design was laser cut to well plate size and was examined using a Phenom ProX SEM.

#### 3.2.4.3.1 FibreMetric analysis

Multiple samples were chosen and sputter coated with 10nm gold for SEM analysis. The samples were analysed the radial formation using a light microscope and SEM analysis (Figure 3. 14). Similar to the aligned fibre design, the radial fibre design also consists of regions with different orientation of fibres. The outer and centre region hold random fibres, and the space between the two had radial fibre formation. Diameter and pore size was measured for both regions. The diameter of fibres in the random region was measured at  $458\text{nm} \pm 170\text{nm}$ , and the radial region had a fibre diameter of  $245\text{nm} \pm 68\text{nm}$  and bother regions had variable pore size.

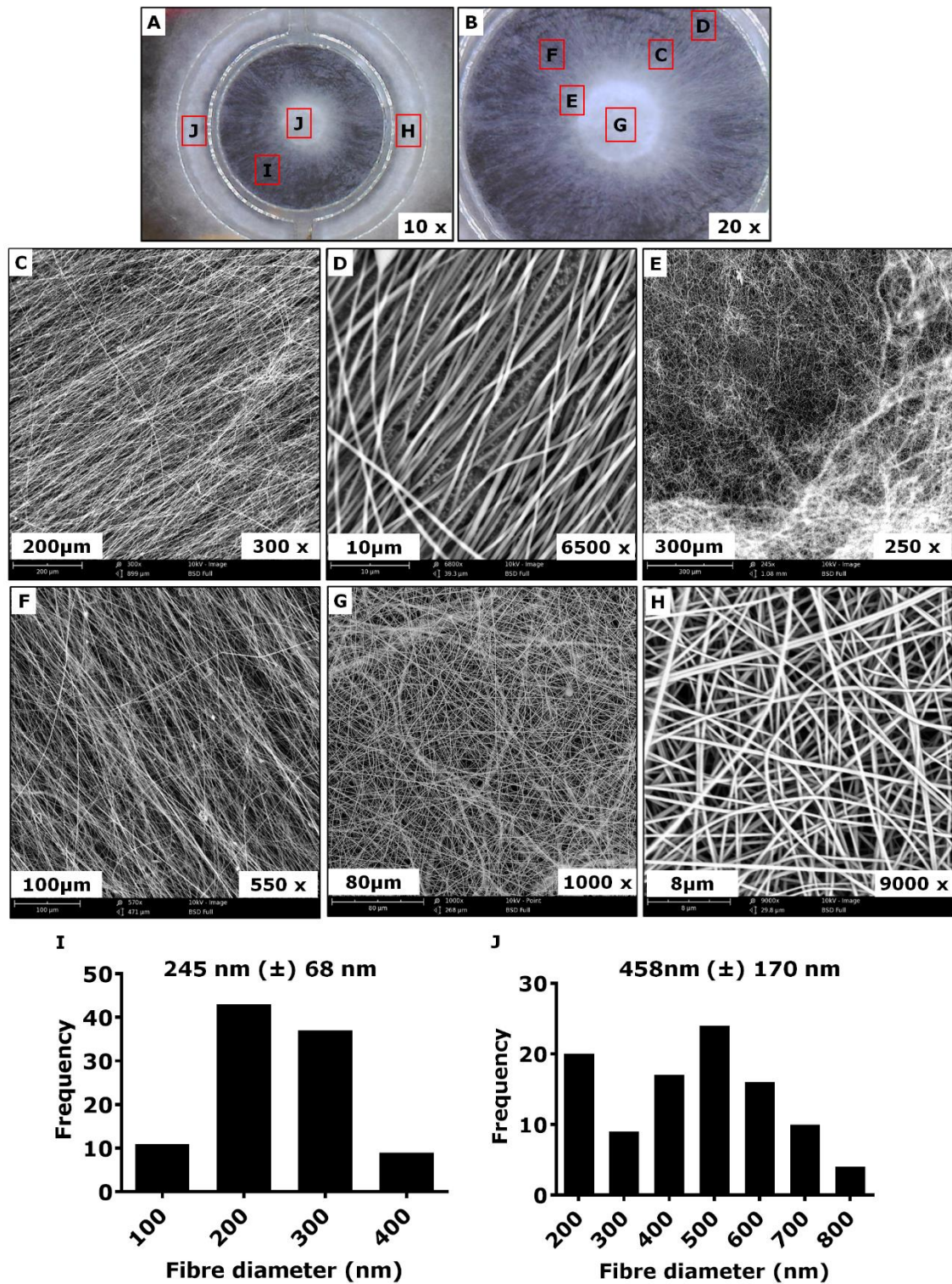


**Figure 3. 14: SEM and FibreMetric analysis for PAN radial fibres.** In this panel, image A and B shows a light microscope image of the scaffold and C-H shows the different regions analysed under the SEM. The graph I shows the fibre diameter for radial region and Graph J shows fibre diameter for the random regions in the radial design. The regions at which the image and measurement were taken has been indicated accordingly on image A and B.

### 3.2.5 Nanofibre sterilisation

Following the electrospinning of fibres and laser cutting the scaffolds, it was essential to sterilise the fibre scaffolds before introducing it to biological samples. The nanofibres were not manufactured in a sterile environment and may contain contaminants that can cause interference and fungal or bacterial contaminations when introduced to biological samples. Several techniques are available for nanofibre sterilisation, but each method of sterilisation can vary based on the material. It was essential to identify the most suitable method that does not compromise the properties and morphology of the fibres.

#### 3.2.5.1 Ethanol treatment

Ethanol is a commonly used disinfectant that is very safe and effective to use. A 70% ethanol concentration is capable of killing single-celled organism as diluted alcohol causes coagulation of protein at a slower rate than absolute alcohol thus penetrating the cell before being blocked causing the entire cell to coagulate leading to the death of the cell. From each batch few scaffolds sample were soaked in 70% ethanol for 30 minutes, 8 hours and 24 hours then tested for the presence of any microbes in an agar plate for 14 days as described in section 2.2.3.4. Few fibres were soaked under same conditions then washed in sterile distilled water and were investigated for any changes in the physical and morphological properties using SEM, FibreMetric analysis, contact angle and OCT. No Microbial growth was observed for 14 days at all three-time points but samples exposed for more than 30 minutes showed surface damage like a crack in fibre surface, brittleness, rough and a substantial increase in the fibre diameter. Similar results were observed on both PAN (Figure 3. 15) and PJ (Figure 3.16) fibre scaffolds.

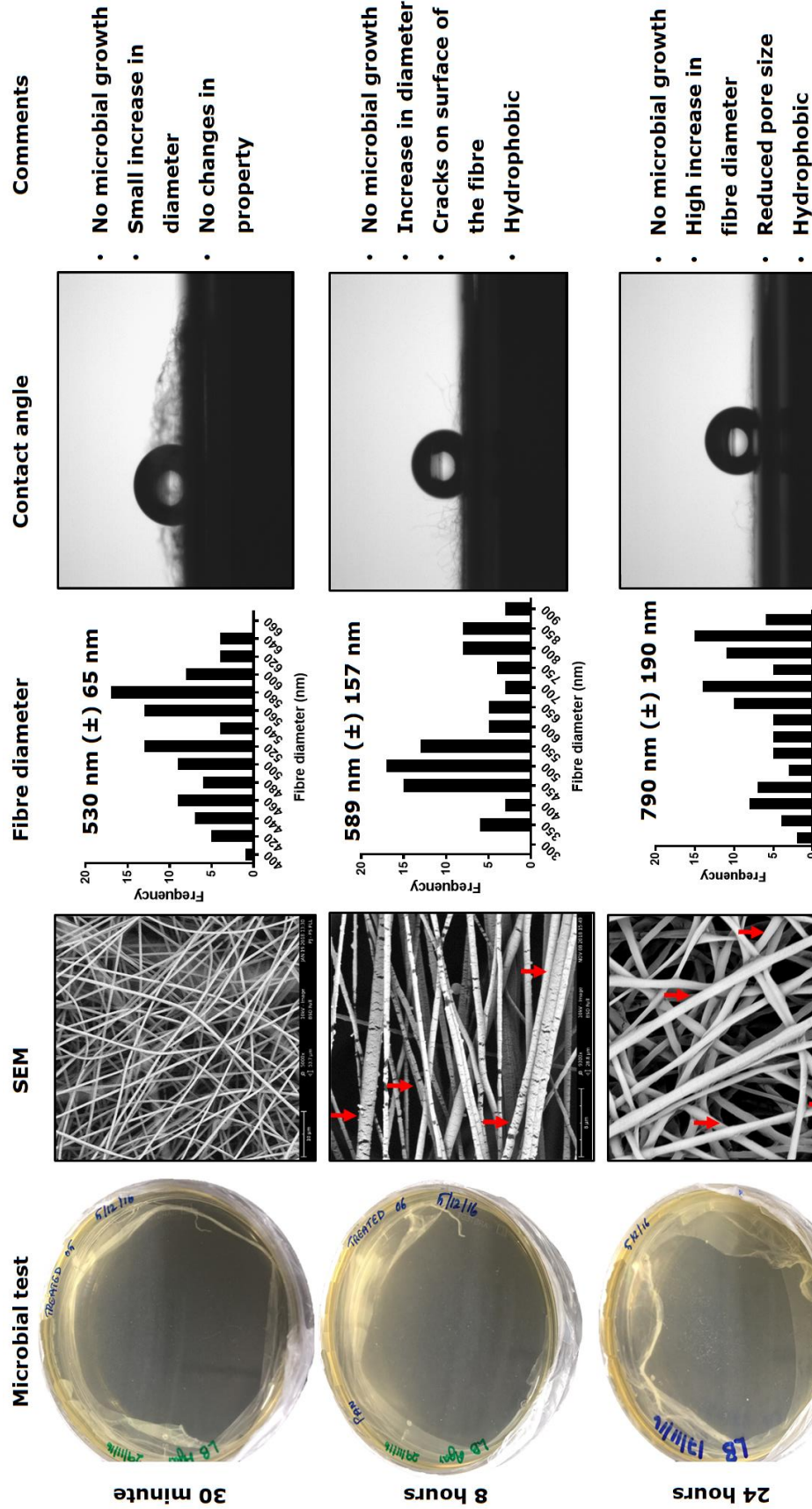


**Figure 3. 15 Ethanol sterilisation analysis for PAN.**

The image represents 70% ethanol treatment at three different time points. For each time point the fibres were tested for microbial growth, checked for morphological changes under SEM, fibre diameter measurement and surface property. The red arrows on the SEM image indicates the damages and increase in the fibre diameter caused due to longer exposure

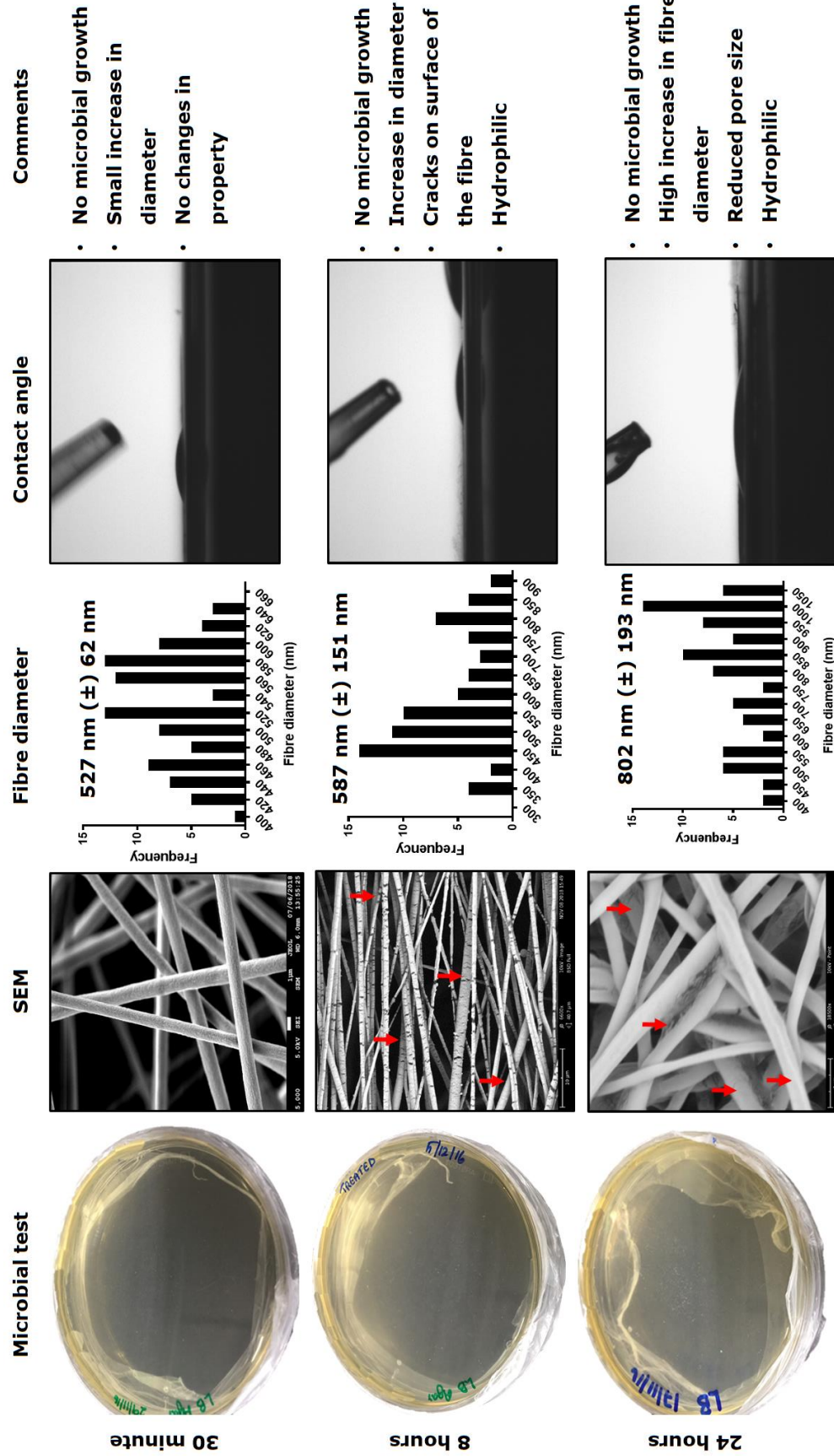


**Figure 3. 16 Ethanol sterilisation analysis for PJ.**

The image represents 70% ethanol treatment at three different time points. For each time point the fibres were tested for microbial growth, checked for morphological changes under SEM, fibre diameter measurement and surface property. The red arrows on the SEM image indicates the damages and increase in the fibre diameter caused due to longer exposure

### 3.2.5.2 Ultra-violet treatment

UV is another commonly used method of sterilisation source that is widely used to disinfect materials and surfaces. A UV light box with a wavelength of 256 nm peak output (figure 3.17) was used to investigate the UV sterilisation of nanofibres. The fibre scaffolds were exposed for 30min, 8 hours and 24 hours and the further tested for microbial growth on agar TCP for 14 days as described in section 2.2.3.4. Few samples were exposed under the same conditions and analysed for damage and any changes in the physical properties. Fungal and bacterial contamination was observed on 30-minute exposure and 8-hour exposure for both PAN (figure 3.18) and PJ (figure 3.19) scaffolds. Reduction in nanofibre diameter was observed on both PAN and PJ when exposed over 30 minutes, and DSA analysis demonstrated PAN samples exposed for 8 hours and 24 hours have transformed from hydrophobic to hydrophilic.

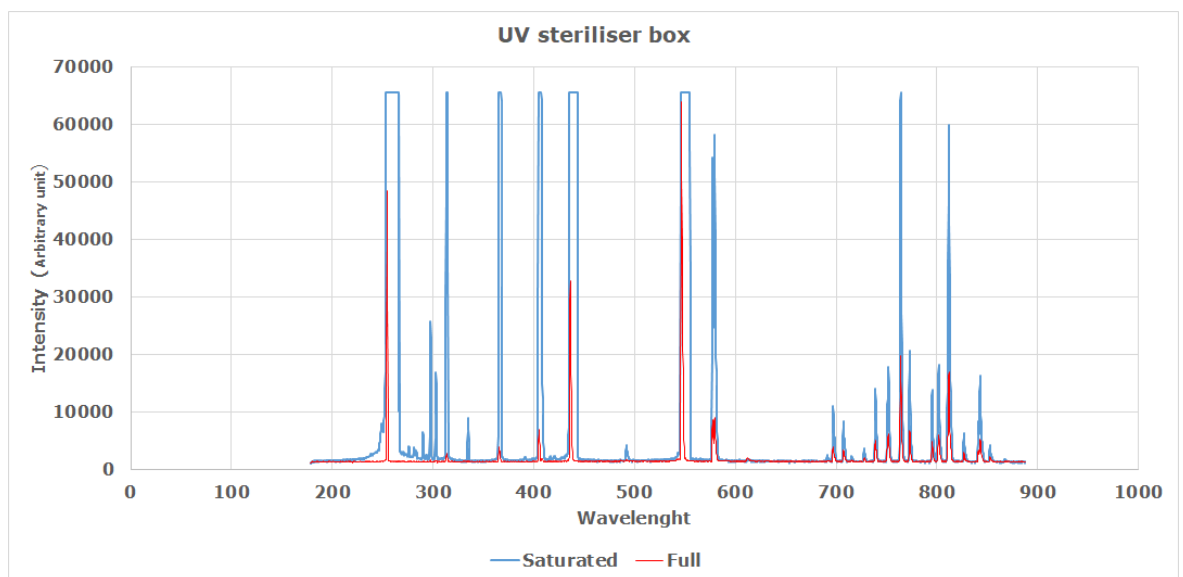


**Figure 3. 17: UV Sterilisation box wavelength measurement.**

The wavelength was measured using an Ocean Optics spectrometer USB2000 with Ocean Optics Spectra suit.

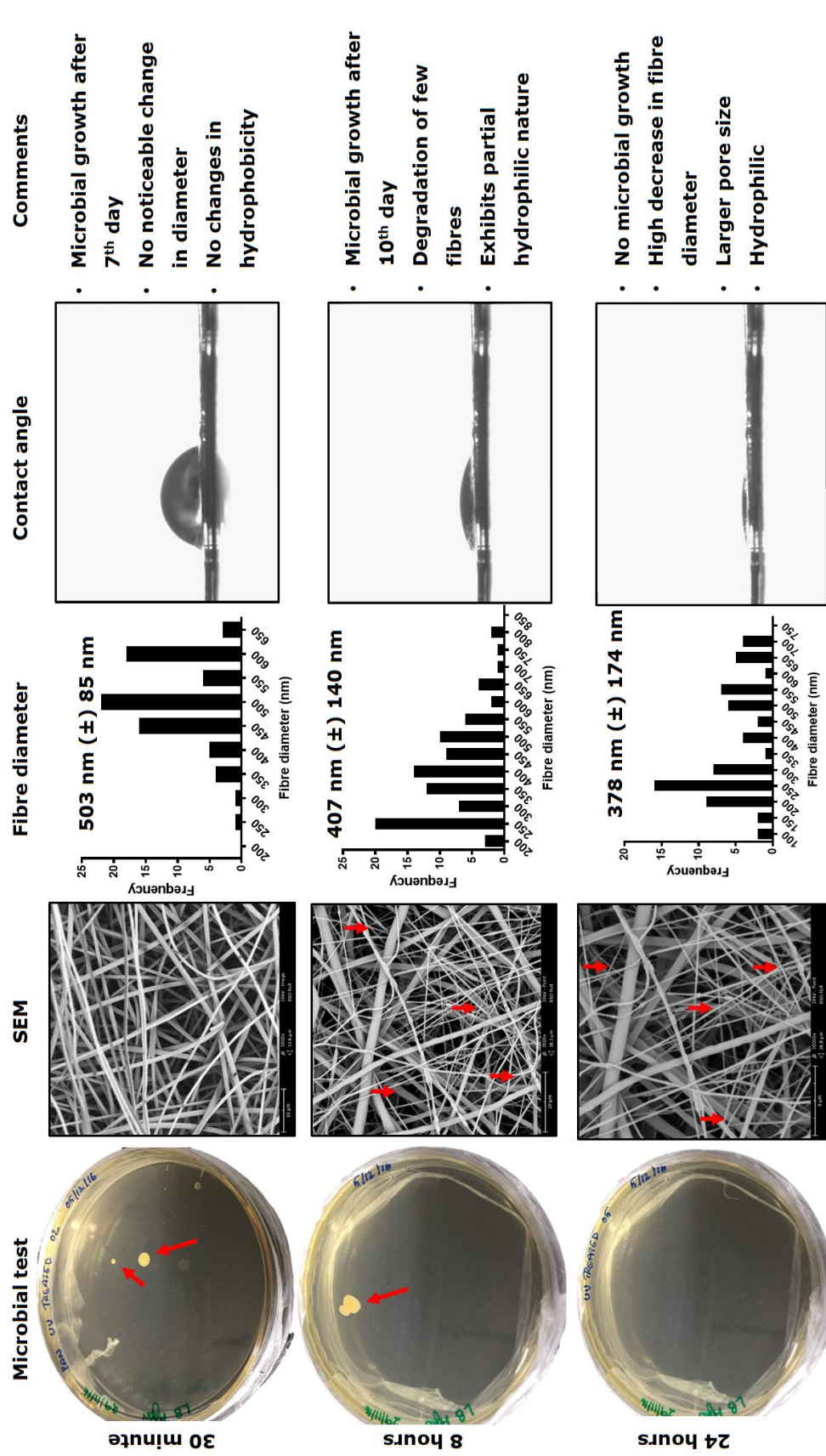


**Figure 3. 18 UV sterilisation analysis for PAN.**

The image represents UV treatment at three different time points. For each time point the fibres were tested for microbial growth, checked for morphological changes under SEM, fibre diameter measurement and surface property. The red arrows on the agar plate show the microbial contamination and the arrows on the SEM image indicates the damages and decrease in the fibre diameter caused due to longer exposure

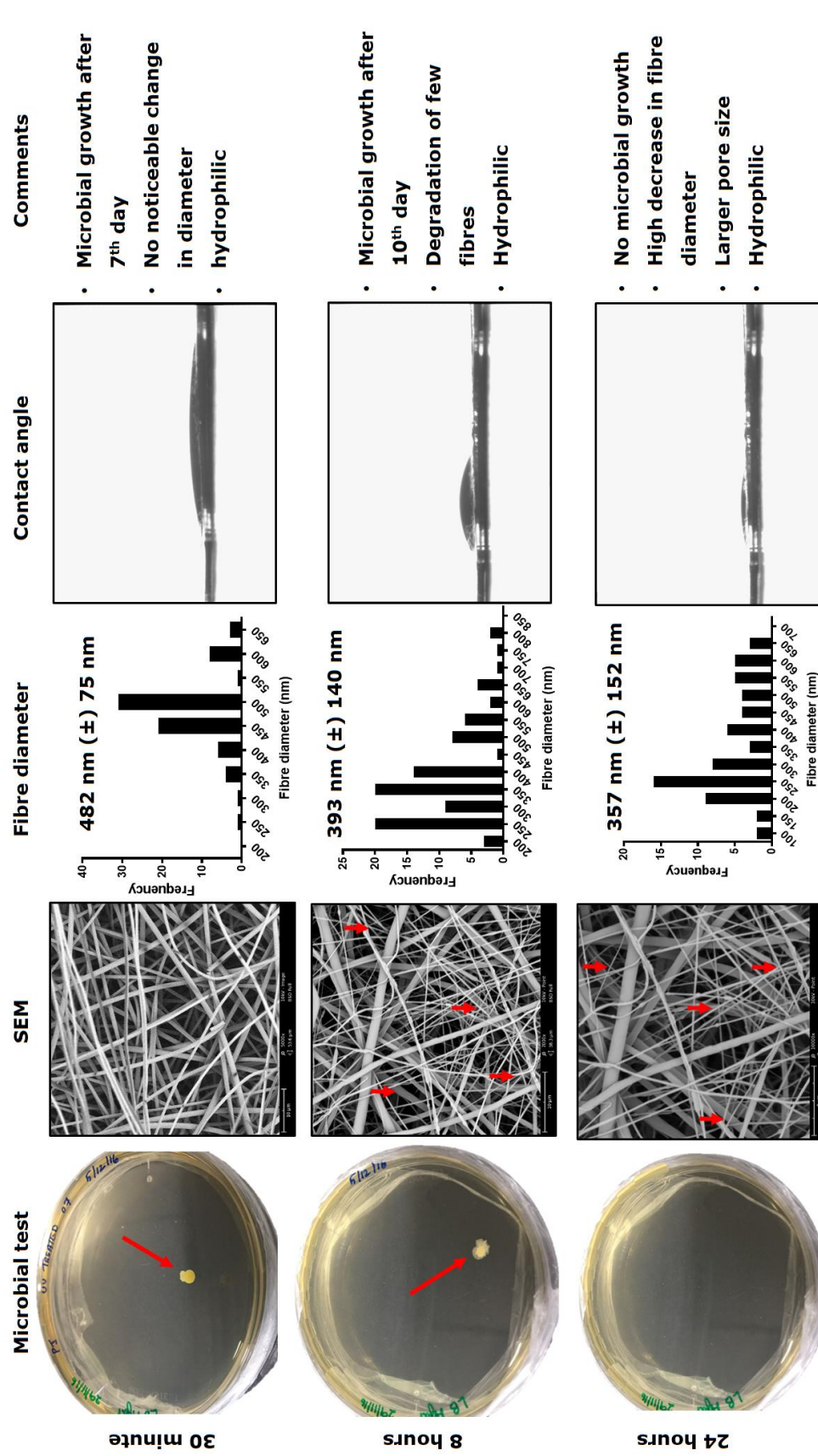


**Figure 3. 19 UV sterilisation analysis for PJ.**

The image represents UV treatment at three different time points. For each time point the fibres were tested for microbial growth, checked for morphological changes under SEM, fibre diameter measurement and surface property. The red arrows on the agar plate show the microbial contamination and the arrows on the SEM image indicates the damages and decrease in the fibre diameter caused due to longer exposure

### 3.2.5.3 Antibiotic treatment

Antibiotics are commonly used in cell culture media to prevent any microbial growth. Penicillin or streptomycin for antibacterial and amphotericin B for antifungal were used to treat nanofibres. Both antibiotics were mixed in a 50:50 ratio and the scaffolds were soaked for 30 minutes, 8 hours and 24 hours. After the incubation period, the fibres were tested for any contamination as described in section 2.2.3.4. Simultaneously, few samples were exposed under the same conditions and analysed for any damage or change in physical properties caused due to the antibiotics. When the samples were analysed under SEM, residues from the antibiotics were seen trapped between the fibres causing damage and reduced pore size. Scaffolds treated for 24 hours were severely damaged and not suitable for further high magnification investigation, fibre diameter or contact angle investigations. The 24 hours exposed fibres were very brittle and broke at the slightest disturbance. Scaffolds treated for 30 minutes and 8 hours had bacterial contamination from the 7<sup>th</sup> and 9<sup>th</sup> day respectively (figure 3.20). No changes in the surface property were observed on both PAN and PJ scaffolds when treated for a short period.

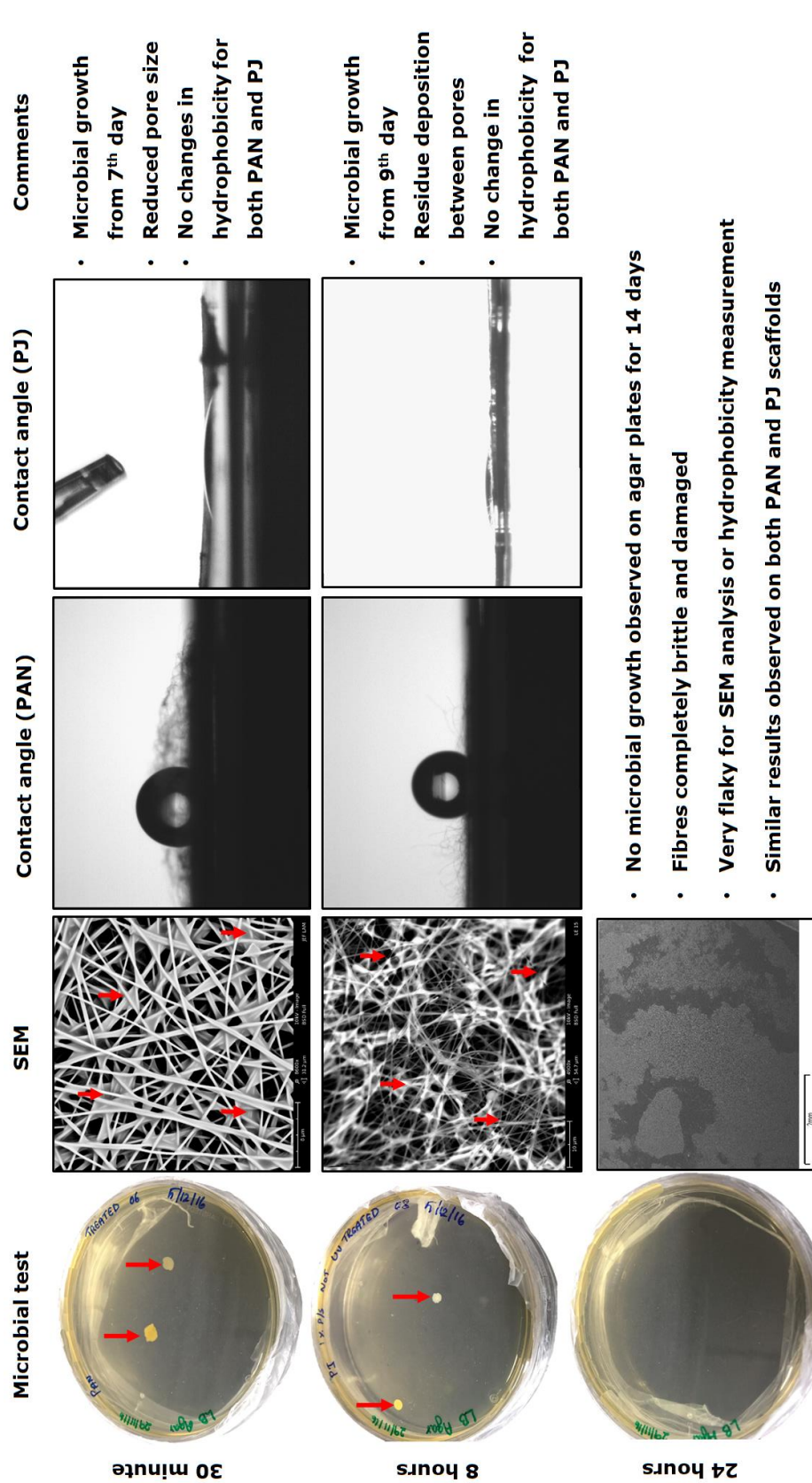


**Figure 3. 20 Antibiotic sterilisation analysis for PAN and PJ.**

The image represents Penicillin streptomycin antifungal B for antifungal in a 50:50 ratio for morphological changes under SEM, fibre diameter measurement and surface property. The red arrows on the agar plate show the microbial contamination and the arrows on the SEM image indicates the damages and decrease in the fibre diameter caused due to longer exposure

**Table 3. 9 Method of sterilisation for both PAN and PJ fibre scaffolds**

Treatment	Exposure Time	Contamination on Agar Plate			Recorded changes
		PAN	PJ	PJ	
70% Ethanol	30 Min	✓	✓	✓	<ul style="list-style-type: none"> <li>• &lt; 10% increase in thickness</li> <li>• &lt; 10% increase in thickness</li> <li>• No change in surface property</li> <li>• No change in surface property</li> </ul>
	4 Hours	✓	✓	✓	<ul style="list-style-type: none"> <li>• Increase in diameter</li> <li>• Increase in diameter</li> <li>• Cracks on surface of the fibre</li> <li>• Cracks on surface of the fibre</li> </ul>
	24 Hours	✓	✓	✓	<ul style="list-style-type: none"> <li>• Loose fibres &amp; high increase in thickness</li> <li>• Loose fibres &amp; high increase in thickness</li> <li>• Reduced pore size</li> <li>• Reduced pore size</li> </ul>
UV	30 Min	X	X	X	<ul style="list-style-type: none"> <li>• No Changes</li> <li>• No Changes</li> </ul>
	4 Hours	X	X	X	<ul style="list-style-type: none"> <li>• Cracked fibre surface</li> <li>• Reduced fibre diameter</li> <li>• Reduction in fibre diameter</li> <li>• Cracked fibre surface</li> <li>• Partial hydrophilic</li> </ul>
	24 Hours	✓	✓	✓	<ul style="list-style-type: none"> <li>• High damaged</li> <li>• Large pore size</li> <li>• Severe damage</li> <li>• Fibre degradation</li> <li>• Fibre degradation</li> <li>• Completely hydrophilic</li> </ul>
Antibiotics	30 Min	X	X	X	<ul style="list-style-type: none"> <li>• Increase in thickness &amp; hard surface</li> <li>• Increase in thickness &amp; hard surface</li> </ul>
	4 Hours	X	X	X	<ul style="list-style-type: none"> <li>• Fragile &amp; hard surface</li> <li>• Fragile &amp; hard surface</li> </ul>
	24 Hours	✓	✓	✓	<ul style="list-style-type: none"> <li>• Fiber degrades &amp; high damage</li> <li>• Fiber degrades &amp; high damage</li> </ul>

**Note: "✓" No Contamination, "X" Contaminated**

### 3.3 Discussion

First and foremost a significant part of the study was to create a robust fabrication process capable of producing sufficient high quality biocompatible suspended nanofibre scaffolds. As explained in the methods section 2.2.1, the design was laid out using AutoCAD, and DXF file formats were used to trepan a laser beam to cut out features on polyester sheets. With optimised laser settings precise apertures with sharp, well-defined edges were produced. Parameters including the focal distance, speed, and power altered the quality of the apertures drastically. Non optimised settings resulted in excessive melt back, burning, non-continuous cuts, substrate warping and dimensional changes of the design (Figure 3. 1 C-J). It was essential to use the optimised laser parameters for all the nanofibre scaffold inserts used in the project because of this sharp edge with less than 1% variation from the required dimensions (Figure 3. 1 A and B). Biomaterial scaffolds can support and provide a suitable habitat for the cells to attach, proliferate and differentiate (Chan, B. and Leong 2008). In this study, PAN, a synthetic resin, was chosen for synthesising nanofibre scaffolds based on their beneficial structural properties reported from its various applications. Jeffamine<sup>®</sup> is a synthetic molecule containing terminal amine groups at the end of a polyethene oxide polymer. This was mixed with PAN and DMF to produce PAN/Jeffamine<sup>®</sup> nanofibres. PAN is a commonly known polymer and used in many applications in different industries. Up to the late 90s, PAN was used for many medical and clinical purposes (Shiono and Usukura 1994; Okrongly, Lamons and Okarma 1994). Several recent investigations have also demonstrated the use of PAN in medical industries for blood separation and to manufacture nanocomposite composite for electrical conductivity (Kizildag, Ucar and Onen 2018; Ushiro, Takahashi and Ueno 2018). Whereas Jeffamine<sup>®</sup> range of additives is used to introduce amine groups to change the surface properties of polymers. Recently Jeffamine<sup>®</sup> has also been used for several other biological applications including the creating quantum dots

for immunoassays and to produce hydrogel to support *in vitro* cell growth (Zimmermann, Bittner, Stark, et al. 2002; Speranskaya, Beloglazova, Lenain, et al. 2014).

Both PAN and PJ polymers were widely used in this study to make suspended nanofibre scaffolds well plate inserts. The polymers were electrospun on a pre-cut design to achieve random fibres, aligned fibres and radial fibres. Each fibre orientation has its properties and unique applications. The Scaffolds were produced with our in-house built electrospinning system, which uses a blunt-end needle and a rotating collector within a controlled humidity chamber housed in a temperature controlled room maintained at 65% relative humidity and 21°C respectively (Figure 3. 5). Before electrospinning PAN and PJ, the polymers was tested for viscosity using the HAAKE™ CaBER™ 1 Capillary Breakup Extensional Rheometer. The extensional Rheometer measurements clearly showed that both PAN and PJ had a similar range of viscosity with an identical strain diameter and a slight difference in the breakup time (Figure 3. 3). This has clearly shown that the addition of a 5wt% of Jeffamine® to PAN has only caused a minor change in the viscosity of PAN. The polymers were capable of free flow when pumped at 1ml/hour rate in a PTFE deliver tube, and the fibres were obtained at 21kv for PAN and 18kv for PJ. A complex interplay of surface, rheology, shapes and electrical charges is the root for electrospinning. A combination of these factors interacts in multiples ways creating electrified jets for causing the polymer solution to stretch and form into nanofibres. When an electrical potential of the surface is increased to a sufficient value, the electrical forces act in opposition to and dominate the surface tension of the fluid causing the jet of the fluid to eject (Reneker and Yarin 2008). Another critical factor is the flow rate during the spinning. Unoptimised flow rate causes beaded fibre and thicker diameter and short drying time before landing the collator causing polymer splash. Each polymer requires an optimised flow rate based on the polymer properties and the type of fibre required. Other team

members investigated several flow rates, and both PAN and PJ were optimised and spun at 1ml/hour flow rate throughout the study.

Random fibres were made using an array of 1cm circle design on a 600X300mm polyester sheet as described in section 2.2.1.1. Using the design randomly woven nanofibres were achieved with an average fibre diameter ranging between 500-600nm for both PAN and PJ fibres with a pore size of  $0.50\mu\text{m}^2$ - $0.60\mu\text{m}^2$ . Fibre Diameter and the architecture of the surface can influence the growth of cells. A study by Chen, et al. in 2009 demonstrated that 3T3 fibroblast was able to attach and proliferate better on a 428nm diameter nanofibre scaffold than larger diameter fibres up to 1-  $1.5\mu\text{m}$ . The proliferation of cells was very slow on thicker fibres compared to the smaller fibres (Chen, M., Patra, Warner, et al. 2007). Another study also explained that fibres with a diameter of  $1.1\mu\text{m}$  showed no significant advantage for human adipose-derived stem cells regarding attachment and proliferation (Tuin, Pourdeyhimi and Lobo 2016). However, numerous studies have suggested the benefits of smaller fibre diameter when it is maintained below  $1\mu\text{m}$  (Sisson, Zhang, Farach-Carson, et al. 2010; Noriega, Hasanova, Schneider, et al. 2012).

The water contact angle measurement techniques used in this study was developed inhouse by Dr Andrew Edwards from the physics department at NTU, UK. The techniques are performed using a high-speed camera and the software measured the disperse of the water droplet using a defined MATLAB code. The first critical evaluation of liquid droplet interactions with fibres was conducted by Cassie and Baxter (Cassie and Baxter 1944). The cassie-Baxter equation in describing a liquid droplet wetting contact angle  $\theta_{CB}$  on a fibrous network containing pores was using  $\cos\theta_{CB} = f_1 \cos\theta_Y - f_2$ : where  $\theta_Y$  is the Young contact angle of liquid on a fibre,  $f_1$  is the total solid-liquid interfacial area and  $f_2$  is the liquid-air interfacial area at the contact plane with the liquid droplets ( $f_1 + f_2 = 1$ ). As considered by Cassie-Baxter regime the regular porosity and random surface roughness creates air pockets when liquid is sitting on the surface

of a fibrous network. A macroscopic contact angle between an water droplet and the irregular electrospun nanofiber network,  $\theta_{mCB}$ , can be defined from a meta-stable Cassie-Baxter consideration with a formula of  $\cos\theta = \frac{R(\pi-\theta\gamma)}{d+R} \cos\theta_{nano} + \frac{R}{d+R} \sin\theta_{nano} - 1$  where R is the nanofibre radius and d is the distance between two adjacent fibre. Our water contact angle study showed that PAN is hydrophobic, and PJ is hydrophilic. In depth investigation is required to understand the software developed by Dr Andrew and to validate the obtained contact angle values in this study. But several studies have confirmed the hydrophobicity properties of PAN as hydrophobic and Jeffamine® as hydrophilic (Kobayashi, Nagai, Wang, et al. 1996; Krakovský, Pleštil and Almásy 2006; Alarifi, Alharbi, Khan, et al. 2015). Studies have also shown PAN is a suitable polymer for surface modification and by adding 5wt% Jeffamine® to 10 wt% PAN converted the surface of PAN fibres to hydrophilic nature (Jung 2004; Shen, Li, Jiang, et al. 2009).

OCT is a technique commonly used for measuring the internal structure of the biological tissue, especially used in ophthalmology to measure the retina. It can also be used as a quality control tool for measuring the thickness of tissue scaffolds prior to cell culture (Vizzeri, Weinreb, Gonzalez-Garcia, et al. 2009; Zotter, Pircher, Götzinger, et al. 2013). Using our in-house built OCT setup, we were able to identify an average non-woven nanofibre membrane thickness of 33.5 $\mu$ m and 30 $\mu$ m for PAN and PJ respectively (Figure 3. 9). Increase in the total volume of deposition leads to an increase in the thickness of the membrane.

The aligned and radial nanofibre scaffolds are of a unique design requiring careful construction and fabrication. Scaffold inserts produce using the patent-pending method can include multiple fibre orientations in a single scaffold insert. Over the years, several methods have been used to produce aligned fibres. Some methods include coating nanofibre over two sharp and parallel knife edges (Theron, Zussman and Yarin 2001), coating finer onto plastic film on a high speed rotating drum (Sundaray,

Subramanian, Natarajan, et al. 2004), coating multiple parallel copper wire drum collector (Katta, Alessandro, Ramsier, et al. 2004), dual vertical wire collector (Chuangchote and Supaphol 2006), rotating jet (Khamforoush and Mahjob 2011), inclined gap collector (Park, Suk Hee and Yang 2011). The most current and commonly used techniques are the high-speed rotation (Haider, Al-Zeghayer, Ali, et al. 2013). All the available techniques have significant drawbacks such as high cost, significant modifications, the risk of injury, unhandleable end products, inconsistent and not suitable for cell-based studies. The invented and adopted technique only requires constructing a design as described in section 2.2.1.2 and does not require the use of high-speed drums or any other modification within an electrospinning system.

The random fibre region had an average diameter and pore size of 570nm and  $0.57\mu\text{m}^2$  respectively. The aligned region had fibres with lesser diameter and pore size, which was measured to be at an average of 424nm and  $0.22\mu\text{m}^2$  respectively. The electrostatic field which develops between two rectangular regions forces a charged fibre over one region to travel and stretch to reach the opposite region which is instantaneously at a lower potential. The stretching of the fibres creating aligned fibre scaffolds with reduced nanofibre diameter, reduced membrane thickness and pore size when compare to non-woven fibre regions. The rectangular part of the design is wholly exposed to the conducting surface. As there are two low potential surfaces on either side of the ellipse, the electrostatically charged nanofibre is drawn to one on the rectangles where it forms a bridge of nanofibre, which spans the rectangular hole. Because the bridge acts to prevent the nanofibre from reaching the surface of the low potential drum, an electrostatic charge starts to build up. At the moment when the charge build is sufficient to repel or re-direct the nanofibre, the nanofibre moves to the next nearest lowest potential region which is the other rectangle associated within the unit. The nanofibre takes the shortest path and creates a fibre, which is orthogonal to the major axis of the ellipse. This process continues for all

units. Both areas in the sheet with aligned and random fibres are suspended and can be accessed from both sides. The hydrophobicity data showed a contact angle of  $130.2^\circ$  for the aligned region of PAN, which was close to superhydrophobic a contact angle measured above  $150^\circ$  is considered as a superhydrophobic surface, and the study suggests that aligned PAN fibred can be superhydrophobic and can produce a contact angle of  $170^\circ$  (Feng, Li, Li, et al. 2002). This phenomenon may have caused due to the thin fibres and smaller pore size compared to the random region whereas PJ fibre had no changes observed in the hydrophobicity. Both regions of the design remained hydrophilic in PJ scaffolds, but the wetting rate was comparatively higher on aligned fibre than random fibres.

Similar to the aligned fibres radial fibre was designed using the same design principles. The fibre diameter in the radial region was measured to be at an average of 250nm-350nm and in the random region was measured to be at 450nm-600nm. Further investigations were not carried out as the current model as it is still under investigations and remodelling to produce a fully bioactive radial fibre suitable be for a retinal study. Minimal literature on models to create radial fibre are available. A study by Jingwei Xie, et al. 2010 showed the application of radial fibred for a wound healing and tissue regeneration application. The study used a pointed electrode surrounded by a ring electrode as a collector. The study has mentioned that the fibres were collected on a piece of aluminium foil but did not clearly explain how the fibres were transferred from the foil to a suitable scaffold based model for culturing cells (Xie, J., MacEwan, Ray, et al. 2010). Another very recent study by Jeong In Kim, et al. 2018 from Chonbuk National University created a model by modifying the collector with copper wire and metal pins creating a contact lens shaped fibre scaffold for retinal study. The study was performed using cells extracted from the whole eye of a rabbit and did not clearly explain the handling and transfer of the scaffold to a fully functional cell culture system (Kim, J. I., Kim and Park 2018). All the currently existing systems

require modification of the electrospinning procedure and do not allow an easy handling or a practical method to use the manufactured scaffolds. Our radial fibre scaffolds model were produced in large numbers (>200 per deposition run) on polyester sheets that were converted into well plates inserts suitable for easy handling and multi-stacking for *in vitro* co-culture systems which mimic *in vivo* tissue thus presenting an opportunity to reduce unnecessary testing on animals.

Sterilisation is an integral part of this study. Several techniques are currently available to sterilise nanofibres. Conventional techniques used are gamma treatment, autoclave, dry heat, vacuum, plasma treatment, ethanol, UV and electron beam treatments (Yixiang, Yong, Liao, et al. 2008; Duszyer, Koral Koc, Hockenberger, et al. 2013; Dai, Ronholm, Tian, et al. 2016; Redigueri, Sassonia, Dua, et al. 2016). Every method has its advantage and disadvantages. In this study, the fibres were tested with 70% ethanol, UV treatment and antibiotic treatment for three-time points. Fibres treated with 70% ethanol did not have any form of microbial growth when tested on agar plate, but fibres exposed over 30 minutes in ethanol showed morphological, especially increase fibre diameter and cracking due to solvent absorption, as well as a reduction in pore size of the materials. Likewise, fibre treated with UV showed no contamination for fibres treated for 24 hours, but contamination was observed on agar plates on both 30 minute and 8-hour exposures. Fibres exposed for 8 hours and 24 hours demonstrated nanofibre degradation resulting in thinner fibres, increase in pore size and changes in the hydrophobicity of PAN to hydrophilic. When the fibres were soaked in the antibiotics, fungal and bacterial contamination was observed at 30 min, and 8-hour treatment and no contamination was observed when treated for 24 hours. When examined under SEM, fibres exposed for 8 hours had modified surfaces and breaks, with residues trapped in the pores. Fibres exposed for 24 hours were very brittle and completely damaged unsuitable for performing further tests.

Based on the results from each sterilisation techniques investigated, the study was performed using a combination of all the three techniques. The collector drum and the polyester sheets were wiped with 70% ethanol before depositions. A 60W UV-C lamp was added to the electrospinning system below the collator, and the fibres were exposed to a 254nm peak output UV light as the fibre was spun and deposited on to the sheet. Before introducing the cells into scaffolds, the scaffolds were soaked in 70% ethanol for 10 minutes, washed 2-3time in PBS to normalise the ethanol then pre-soaked in the cell culture media with antibiotics for 10 minutes. Following these series of steps has maintained an absolute sterile nanofibre through the study without any compromise in the nanofibre integrity or morphology.

### **3.4 Conclusion**

In summary, this chapter has demonstrated the various steps involved in producing a functional nanofibre scaffold that can be used in the investigation of neural cell degeneration. The chapter has shown the importance of using optimised laser cutting parameters for producing sheets. The chapter has demonstrated three different designs to produce nanofibre scaffolds that can be used for a wide range of in vitro models. With the in-house built electrospinning system, designs were converted into individual, fully suspended, thin, 3D nanofibre scaffolds with either hydrophobic PAN or hydrophilic PJ fibres. The chapter has also shown the various parameters of each design including surface properties and membrane thickness measurements. From the investigation of sterilisation techniques, the chapter has demonstrated the importance of identifying a suitable sterilisation method which does not weaken or modify the desired physical or chemical properties of the scaffolds. Even though the chapter has shown three different models of nanofibre design, only the random fibre scaffold was used to create a cell model for neural cell degeneration.

## Chapter 4: Immortalised cell line scaffold model

### 4.1 Introduction

Immortalised human neural cell lines are modified cells of brain origin (e.g. neurone and glia) from that are able to continuously proliferate and grow when provided with the necessary growth factors. There are several types of immortalised human cell lines, derived primarily from primary and secondary tumours or from stem cells. Human cell lines are essential tools in research and are widely used as a model to study several complex biological systems and disease processes (Kaur and Dufour 2012). Immortalised human cells lines are often used in research in place of primary cells with several advantages, including cost-effectiveness, availability, accessibility, and to avoid potential ethical concerns (Kaur and Dufour 2012). Vaccine production, testing drug metabolism and cytotoxicity, antibody production, the study of gene function, generation of artificial tissues and synthesis of biological compounds and therapeutic proteins are currently performed with immortalised human cell lines (Macdonald 1990; Gomez-Lechon, Donato, Castell, et al. 2003; Schurr, Foster, Centanni, et al. 2009).

This part of the study has primarily focused on an immortalised SH-SY5Y human neuroblastoma and U-87 MG human glioblastoma cell line. Both SH-SY5Y and U-87MG cell line are widely used to investigate neural cell-related studies. Several studies have shown SH-SY5Y cells are capable of differentiating into matured neurons (Avola, Graziano, Pannuzzo, et al. 2018; Sang, Liu, Wang, et al. 2018) also, U-87MG can be induced to differentiate into astrocytes (Xing, F., Luan, Cai, et al. 2017) thus making these two cell line very suitable an investigation related to neural characterisation for neurodegenerative disease on nanofibre scaffolds. The preliminary aim of this study was to develop a suitable nanofibre model to characterise and investigate neural cells degeneration. Due to the reason like cost-effectiveness, readily available and easy to culture

and maintain both SH-SY5Y and U87-MG cells were chosen to perform preliminary investigations on PAN and PJ nanofibre scaffolds.

#### **4.1.1 SH-SY5Y Human Neuroblastoma**

SH-SY5Y cell line is a human-derived cell isolated from a metastatic bone tumour biopsy obtained from a four-year-old female with neuroblastoma. SH-SY5Y (ATCC<sup>®</sup> CRL-2266<sup>™</sup>) cells are a subline of the parental line SK-N-SH (ATCC<sup>®</sup> HTB-11<sup>™</sup>) which were further subcloned three times; first to SH-SY, then to SH-SY5, and finally to SH-SY5Y. SH-SY5Y were deposited to the ATCC<sup>®</sup> in 1970 by June L. Biedler (Kovalevich and Langford 2013). SH-SY5Y cells are capable of expressing dopaminergic markers and have been used to investigate several neurodegenerative disorders such as amyotrophic lateral sclerosis, Parkinson's disease, Alzheimer's disease, Huntington's disease, neurogenesis and other brain cell characterisations. One of the major limiting factors for neurones derived from primary mammalian embryonic CNS tissues is that the cells can no longer be propagated once they terminally differentiate into mature neurons. Transformed cells like SH-SY5Y neuronal-like cell line are commonly used *in vitro* studies to overcome this limitation.

##### **4.1.1.1 Undifferentiated and differentiated SH-SY5Y cells**

SH-SY5Y neuroblastoma cells are capable of possessing a more mature, neuron-like phenotype with modification of the cell culture medium; benefiting neuroscience research. As the cells were derived from human, SH-SY5Y possesses various human-specific proteins and other components that may lack in the primary animal model. Both undifferentiated and differentiated forms of these cells are used for *in vitro* studies. The choice is based on the type of study conducted. When differentiated, the cells demonstrate specific changes like the formation of neurite extensions, increases in electrophysiology activity, activated synapses that express synaptophysin and neuron-specific enzymes, neurotransmitter receptors (Påhlman, Ruusala, Abrahamsson, et al. 1984;

Adem, Mattsson, Nordberg, et al. 1987; Lopes, Fernanda Martins, Schröder, da Frota Júnior, Mário Luiz Conte, et al. 2010). Undifferentiated SH-SY5Y cells are characterised morphologically by neuroblastoma-like, non-polarized cell bodies with few, truncated processes (Kovalevich and Langford 2013). The undifferentiated cells lack mature neuronal markers and proliferate continuously and also classed as catecholaminergic neurons (Påhlman, Ruusala, Abrahamsson, et al. 1984; Xie, H., Hu and Li 2010). Depending on the method of differentiation, mature cells can produce neurite extensions and become distinctly polarised. Several methods exist for SH-SY5Y differentiation. One of the most common methods is by adding retinoic acid (RA) to the cell culture media. The retinoic acid treatment has been shown to promote survival of SH-SY5Y cells through activation of the phosphatidylinositol 3-kinase/Akt signalling pathway and upregulation of the antiapoptotic Bcl-2 protein (Itano, Ito, Uehara, et al. 1996; Lopez-Carballo, Moreno, Masia, et al. 2002). A study has also demonstrated that SH-SY5Y cells differentiated with RA had higher viability than undifferentiated cells when exposed to toxin-mediated cell death induced by 6-OHDA, MPTP, or its metabolite MPP<sup>+</sup> (Cheung, Lau, Yu, et al. 2009). Other commonly used differentiating agents include dibutyryl cyclic AMP (dbcAMP) that increases intracellular cyclic AMP levels a promoting gene expression leading to differentiation (Sanchez, Jimenez, Carrera, et al. 2004). Indeed, SH-SY5Y cells treated with dbcAMP promoted neurite extensions and high expression of GAP 43; a mature protein associated axonal processes (Kume, Kawato, Osakada, et al. 2008). Further studies have also shown that dbcAMP treatment also leads to a significant increase in tyrosine hydroxylase (TH) immunoreactivity and the cellular content of noradrenaline in a protein kinase A (PKA)-dependent manner (Itano, Ito, Uehara, et al. 1996; Kume, Kawato, Osakada, et al. 2008). According to these studies, both dbcAMP and RA differentiated SH-SY5Y cells showed similar morphological phenotypes. A few studies have also shown that B27 supplementation can influence SH-SY5Y differentiation (Kovalevich and Langford 2013).

B27 supplement is used as a part of primary neuronal cultures to support the low- or high-density growth and short- or long-term viability. These studies have shown SH-SY5Y cells were able to produce long neurite extensions and also showed high expression of some differentiation markers when supplemented with B27 (Sayas, Moreno-Flores, Avila, et al. 1999; Mathiasen, McKenna, Saporito, et al. 2004).

#### **4.1.1.2 Markers of Differentiation**

Several studies suggest different methods of differentiation. Undifferentiated SH-SY5Y cells can be characterised based on markers of proliferation like the proliferating cell nuclear antigen (PCNA) or with immature neuronal protein markers such as nestin and morphologically resembling immature catecholaminergic neurons (Cuende, Moreno, Bolanos, et al. 2008; Lopes, Fernanda Martins, Schröder, da Frota Júnior, Mário Luiz Conte, et al. 2010). A significant decrease in differentiation-inhibiting basic helix-loop-helix transcription factors ID1, ID2, and ID3 are observed when these cells are differentiated with RA (Lopez-Carballo, Moreno, Masia, et al. 2002). When differentiated, SH-SY5Y cells express several mature neuronal protein markers including  $\beta$ III-tubulin, microtubule-associated protein-2 (MAP2), synaptophysin, NeuN, synaptic associated protein-97 (SAP-97), neurofilament heavy chain (NHC) and neuron-specific enolase (NSE). Studies have also shown the increased expression of differentiation-promoting genes NEUROD6 and NEUROD1 when treated with differentiating agents (Lopez-Carballo, Moreno, Masia, et al. 2002).

#### **4.1.2 U-87 MG Human Glioblastoma**

U-87 MG human glioblastoma is a commonly used cell line for brain cancer research and some neurological disorders. Uppsala 87 Malignant Glioma (U-87 MG) consists of an epithelial morphology which was first obtained in 1966 from a 44-year-old female patient at Uppsala University (Allen, Bjerke, Edlund, et al. 2016). Initially, the cell line was handed

over to the Memorial Sloan Kettering Cancer Centre in 1973, and in 1982 it was obtained by ATCC. U-87MG cells have been used for several studies like a neurodegenerative disease, and other CNS related disease. A recent study on destabilising drug Siramesine on glioblastoma has U-87MG cell as one of the glioblastoma models to understand the effect of the drug (Jensen, Petterson, Halle, et al. 2017). Several other studies have shown that U-87MG is a good cell line to perform co-culture models with SH-SY5Y cells. A study published in 2015 has shown that Glial U87 cells protect neuronal SH-SY5Y cells from the indirect effect of radiation by reducing oxidative stress and apoptosis in a co-culture system (Saeed, Xie, Xu, et al. 2015). Moreover, another study has shown Sal-treated co-cultures of SH-SY5Y and U-87 MG cells induced remarkable proliferation of THP-1 cells in a U87 glial cell-dependent manner (Wang, F., Ni, Wang, et al. 2015). Though a study published in 2016 found that the U-87MG used from the ATCC was identified to be non-identical to its original Short Tandem Repeat STR (Allen, Bjerke, Edlund, et al. 2016) still several valid and publishable studies are still performed using U-87MG cells and is a great candidate for investigating the neurodegenerative disease.

#### **4.1.2.1 Differentiated U-87 MG Cells**

Glial cells are an essential part of the brain. They are the supportive cells in the CNS (Jessen and Mirsky 1980). Unlike neurons, they do not conduct electrical impulses, but instead, they are found between and around neurones providing neurotrophic support and physiological insulation (Wolosker, Dumin, Balan, et al. 2008). Oligodendrocytes, astrocytes, ependymal cells, Schwann cells, microglia, and satellite cells are the different types of glial cells. Human U-87 MG glioblastoma cell line is one of the commonly used cells for studies related to glial cells, and they can differentiate to glial subtypes. Studies have demonstrated that RA and dbcAMP can be used to differentiate U-87 MG cells to astrocytes (Shi, Z., Lou, Zhao, et al. 2013; Xing, F., Luan, Cai, et al. 2017). In this study, we have used dbcAMP as one of the differentiating

agents to transform U-87 MG to a more astrocytic phenotype. Cyclic AMP plays an important role in regulating cell growth, metabolic pathway signals and the cell cycle (Stork and Schmitt 2002). Studies have shown that cAMP activation results in a decrease in proliferation, reduced growth of xenografted brain tumours (Yang, Jackson, Woerner, et al. 2007; Goldhoff, Warrington, Limbrick, et al. 2008) and expression of glial fibrillary acidic protein (GFAP); an intermediate filament protein that is found highly expressed in astrocytes (Jacque, Vinner, Kujas, et al. 1978; Venkatesh, Srikanth, Vengamma, et al. 2013). This also leads to stellate-like cell structures that resemble astrocytes in vivo. Studies have shown that GFAP is expressed in U-87MG cells and it is upregulated when differentiated to a more astrocytic-like phenotype using RA or dbcAMP (Das, Karmakar, Patel, et al. 2005; Restrepo, Smith, Agnihotri, et al. 2010; Xing, F., Luan, Cai, et al. 2017). In this study we proposed astrocytic differentiation of U-87MG cells using conventional approaches but also explored the use of B27 supplementation.

#### **4.2 Content of this chapter**

In this chapter, we have demonstrated the use of PAN and PJ nanofibre scaffolds to harbour SH-SY5Y cells and U-87MG cells. We have shown the morphological changes when cultured on different models and surfaces of nanofibre scaffolds. The cells were investigated for a long period of survival, therefore, making it suitable for chronic studies. To demonstrate the prolong survival, we have investigated a proliferation viability study. The chapter also describes the outcome of multiple differentiating agents when exposed to both SH-SY5Y and U-87 MG cells cultured on both tissue culture surface and nanofibre scaffolds. The structural changes and protein expression for both cells when cultured on fibres have been thoroughly studied and compared with cell-cultured on 2D surfaces. Several microscopy techniques and protein detection analysis have been shown in this chapter as evidence for cell attachment, proliferation and differentiation. The chapter also demonstrates the effect of inhibitor that

is capable of mimicking neural cell degeneration pathophysiology on both cell type and the effect has been compared in cells cultured on the 2D surface and nanofibre scaffolds. Co-culture system using nanofibre scaffold was developed to identify suitable endpoint parameters of relevance to neuronal and glial function, differentiation and survival that can be monitored within the 3D setup.

### **4.3 Results**

#### **4.3.1 Culturing and subculturing**

Cells obtained from ATCC were stored in liquid nitrogen and revived when needed. Revived cells were cultured, harvested, bulked and preserved in liquid nitrogen for future use. Both SH-SY5Y and U-87MG cells were maintained under 30 passages. Upon reaching 30 passages, a new batch of cells was revived and cultured for experiments. Every new batch of cells was routinely examined with immunofluorescence imaging stained for neurofilament for SH-SY5Y and GFAP for U-87MG to ensure there has not been a mix-up or cross-contamination of cells. Both undifferentiated SH-SY5Y and U-87 MG cell showed a low expression of neurofilament (Figure 4. 1 C) and GFAP (Figure 4. 1 D), respectively.

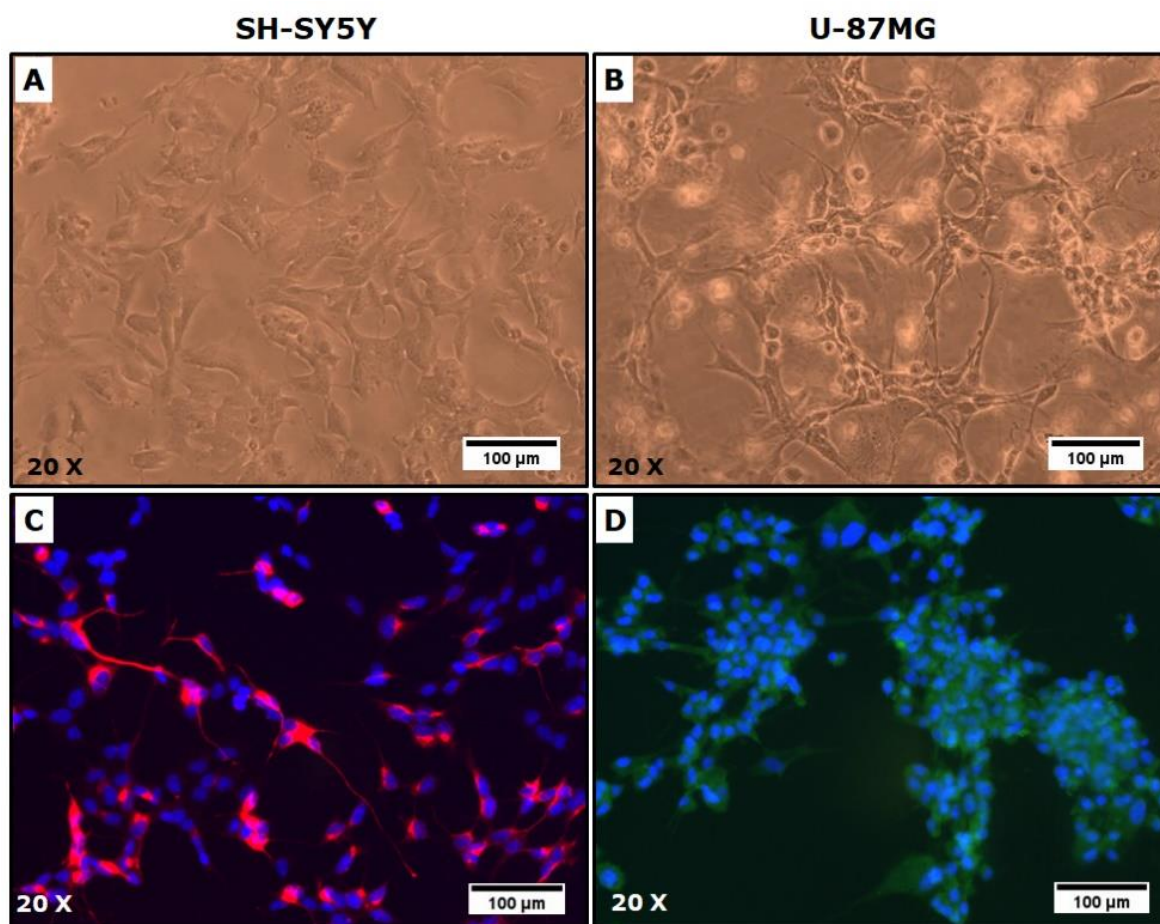


**Figure 4. 1: SH-SY5Y and U-87MG microscope image.**

(A and C) Represents SH-SY5Y human neuroblastoma and (B and D) Represents U-87MG human glioblastoma cell line. Both cells were monitored for morphological changes under a light microscope and with immunofluorescence regularly.

### 4.3.2 Cell culture on nanofibres scaffolds

Cells were cultured in tissue culture flasks, and upon reaching 80-90% confluency, the cells were trypsinised and seeded on to nanofibres as explained in section 2.2.5. Before cell seeding, the fibres were ethanol sterilised as described in section 2.2.5.1. 50,000 cells/well were seeded in each well with nanofibre scaffolds and incubated at 37°C in a humidified atmosphere of 95% (v/v) air and 5% (v/v) CO<sub>2</sub>.

#### 4.3.2.1 Unsuspended random nanofibre

Initially, the nanofibre scaffolds were obtained on an A1 size plain polyester sheets with no designs. The fibres were manufactured using electrospinning, as explained in section 2.2.3. Once the fibres were

deposited the sheets were cut into square shapes (10 mm X 10 mm) to fit into a 6 or a 12 well plate as shown in Figure 4. 2. The fibres were sterilised with 70% ethanol and placed into each well. Both SH-SY5Y and U-87MG cells were harvested and individually seeded into wells containing the nanofibre sheets. The TCP was then incubated at 37°C in a humidified atmosphere of 95% air and 5% CO<sub>2</sub> for 48 hours

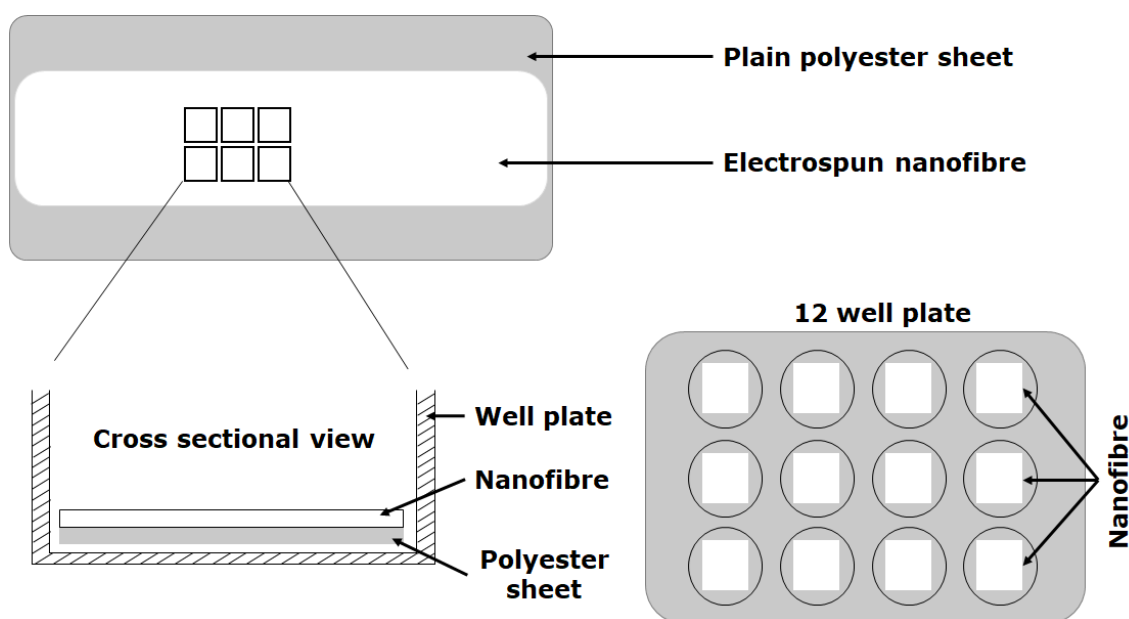


**Figure 4. 2: Unsuspended nanofibre on a polyester sheet.**

*A1 size polyester sheet wrapped around the collector drum to obtain fibre. Nanofibre sheets were manually cut with scissors to fit in a 6 or a 12 well plate for cell culture*

Following 48 hours of incubation, cells were stained with Coomassie. The fibres were moved to a fresh plate, and both fibres and the TCP were examined with light microscopy. It was observed that a number of cells accumulated on the edges of the fibre sheet and loose fibre end (Figure 4. 3). Inferior cell attachment was observed at the centre of the fibre sheets. More viable cells were found on the surface of the plate compared to the fibre sheets.

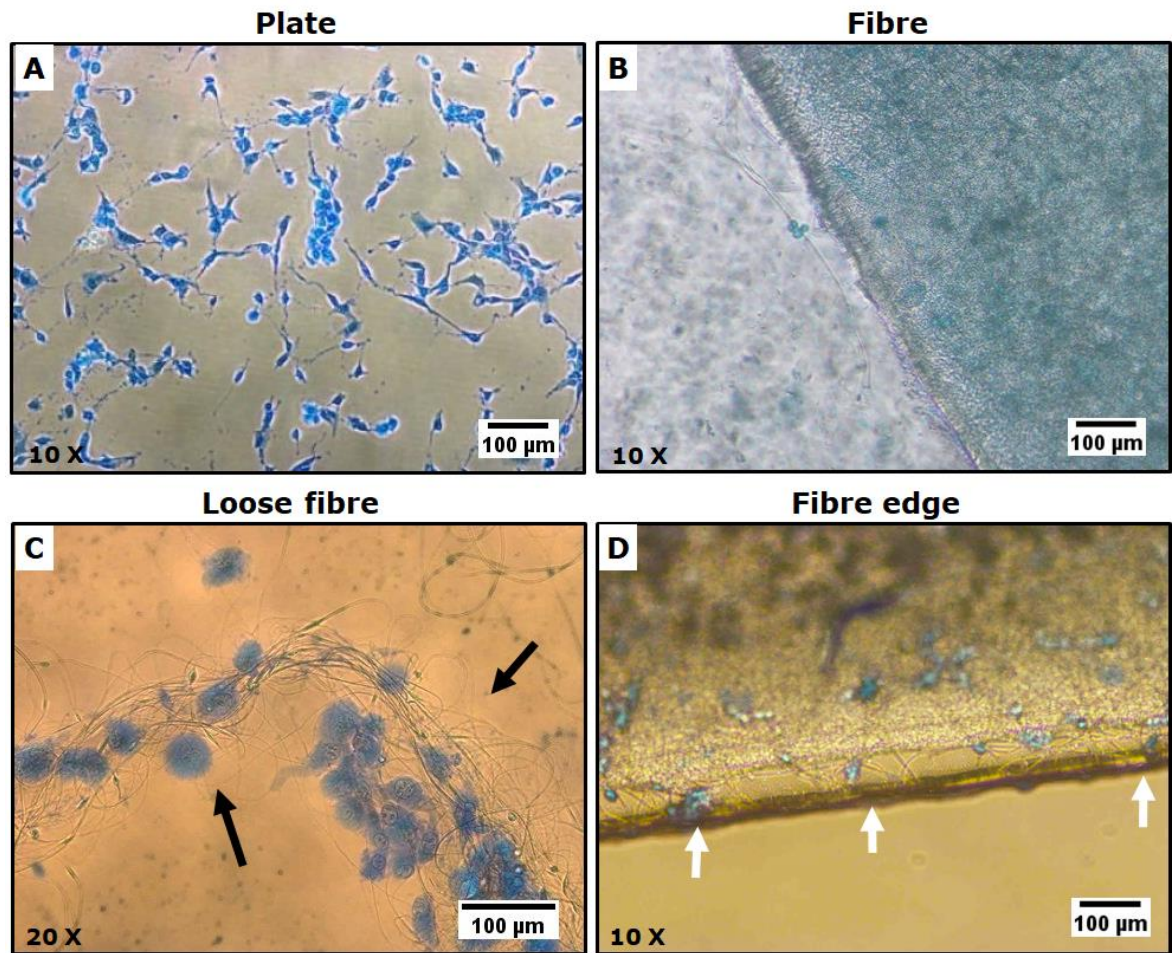


**Figure 4. 3: Coomassie blue staining of cells cultured on unsususpended fibres.**

Both SH-SY5Y and U-87MG cells were cultured on PAN and PJ unsususpended nanofibre sheets. The cells were incubated for 48 hours and stained using Coomassie blue stain. A high number of cells were found attached to the edges (white arrows) plate and loose fibre (black arrows). The images were obtained using a light microscope.

#### 4.3.2.2 Suspended random nanofibres scaffolds

As explained in section 2.2.1.1 random nanofibre scaffold designs were engineered on a 600 X 300mm polyester sheet with an array of 1cm circles cut throughout the sheet. Both PAN and PJ fibres were electrospun onto the sheet which was further secured by another identical top sheet. Each scaffold was cut to fit into a 12 well plate and sterilised with 70% ethanol as described in section 2.2.3.4. The fibres were transferred to a 12 well plate after sterilisation.

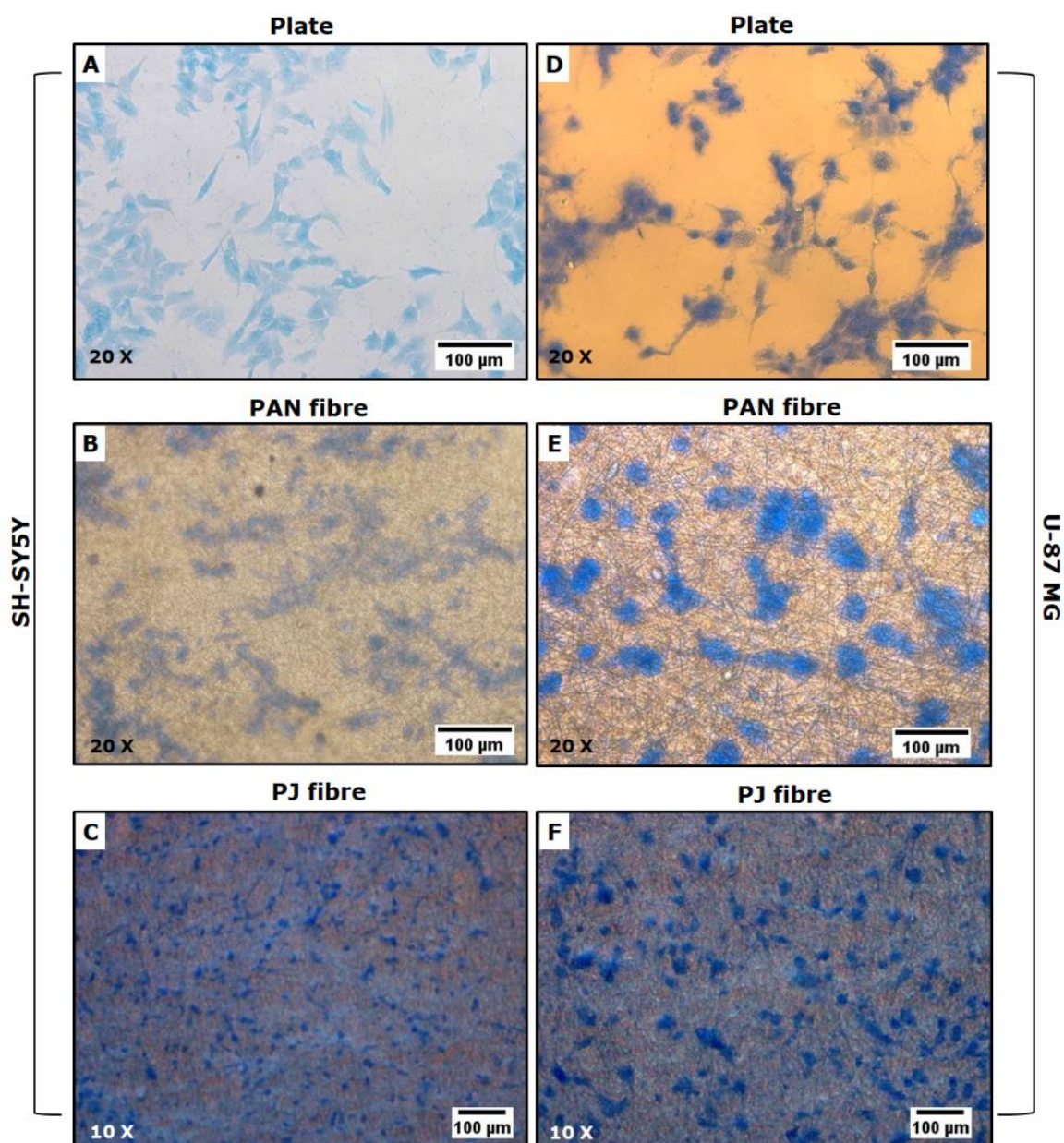


**Figure 4. 4: Coomassie blue staining of cells cultured on random nanofibre scaffolds.**

Both SH-SY5Y and U-87MG cells were cultured on PAN and PJ fibres electrospun on a random fibre design. The cells were incubated for 48 hours and stained using Coomassie blue stain. A high number of cells were found attached to the fibre than the plate. The images were obtained using a light microscope.

Both SH-SY5Y and U-87MG cells were maintained in T25 flasks prior to seeding onto random nanofibre scaffolds. Cells were seeded at 50,000 cells/well and incubated at 37°C in a humidified atmosphere for 48 hours. Following incubation, the fibres were transferred to a fresh plate, and both the original plate and the fibres were stained for total protein with

Coomassie blue for visualisation (Figure 4. 4). When observed under light microscopy, it was evident that a large number of cells were found attached to fibres compared to the plate and the fibres remained completely intact.

#### **4.3.2.3 Aligned nanofibre scaffolds**

Preliminary cell attachment investigation was performed on the aligned nanofibre design. Both PAN and PJ fibres were used to make aligned fibres using the design explained in section 2.2.1.2. Both SH-SY5Y and U-87MG cells were investigated for cell attachment on aligned fibres. Cells were seeded at 50,000cells/well in each well and incubated at 37°C in a humidified atmosphere for 48 hours. Following incubation, the fibres were transferred into a fresh plate, and both the original plate and the fibres in the fresh plate was stained with Coomassie blue (Figure 4. 5). When compared with the random fibre design and plate, both SH-SY5Y and U-87MG cells exhibited attachment and growth that allied with the fibre design pattern. The cells grew along the fibre in a uniform direction with cells aligned with the fibre direction.

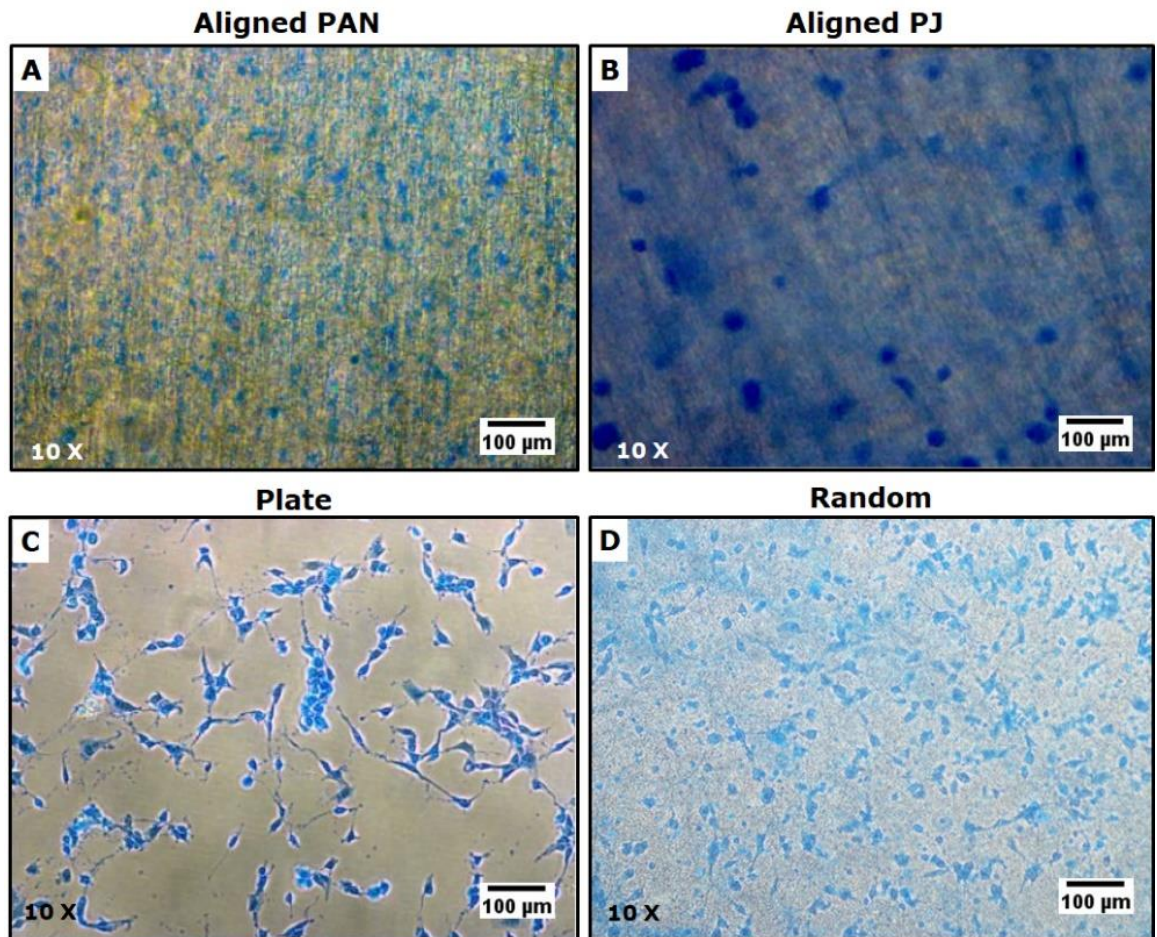


**Figure 4. 5: Coomassie blue staining of cells cultured on aligned nanofibre scaffolds.**

Both SH-SY5Y and U-87 MG cells were cultured on the aligned fibres. The cells were incubated for 48 hours and stained using Coomassie blue stain. The orientation of the cells seeded on the aligned fibre was very different from random fibre or the plate. The aligned fibres provided guidance for the cells to grow along the fibre.

### 4.3.3 Cytoskeletal staining and SEM analysis

Investigating morphological characteristics of cells cultured on fibres was essential. To achieve this, cells were dehydrated as described in 2.2.9.3 and examined in high magnification using an SEM (Figure 4. 7) and also stained for a cytoskeletal protein;  $\alpha$ -tubulin as described in section 2.2.9.2. Immunofluorescently stained fibres were mounted on a glass slide with anti-fade mountant vectorshield containing DAPI and imaged with immunofluorescence microscopy (Figure 4. 6).

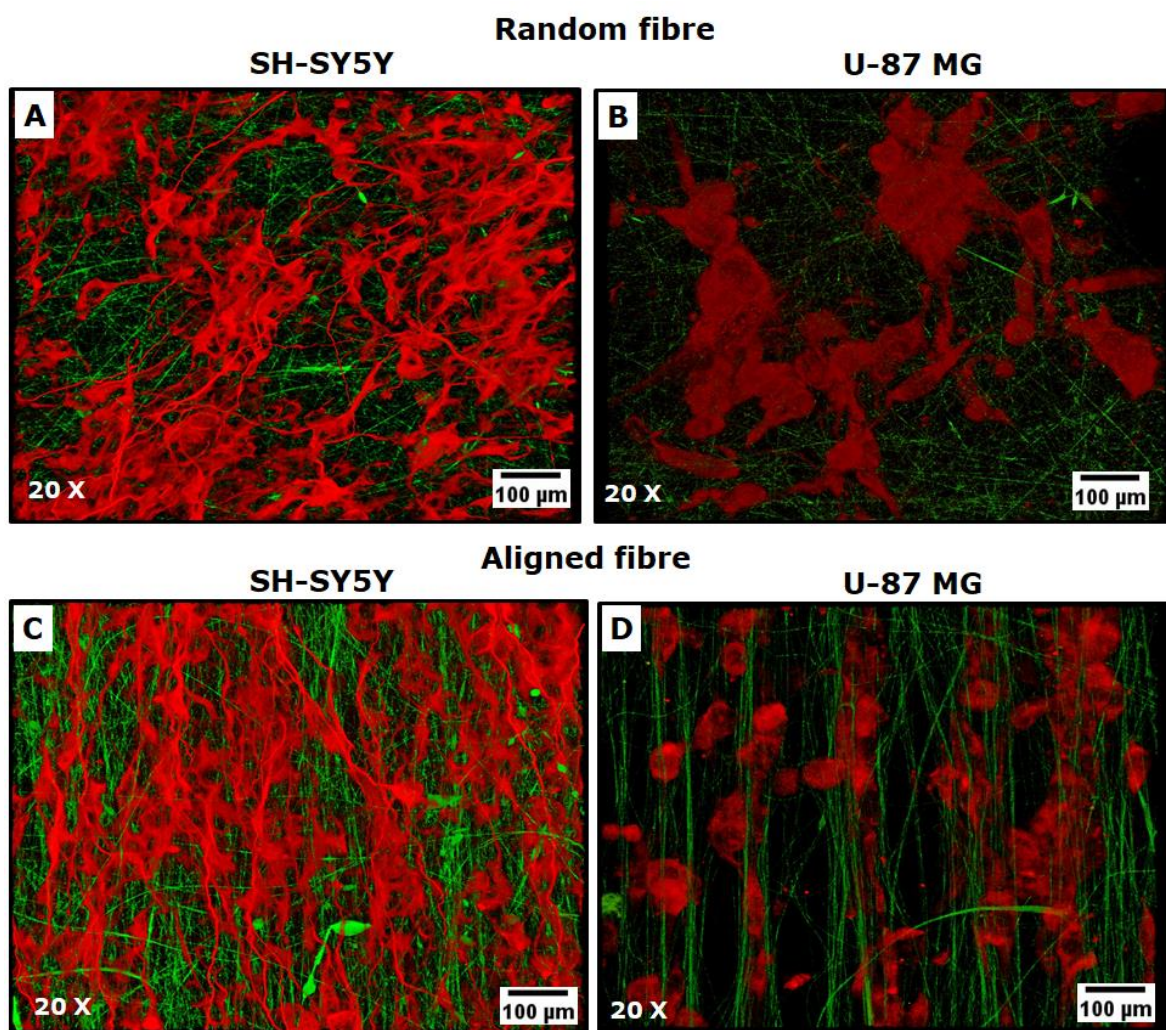


**Figure 4. 6: Cytoskeletal protein stain to show cell attachment on nanofibre.**

The cells were cultured for 48 hours, fixed and stained for  $\alpha$ -tubulin. The images were obtained using an Olympus immunofluorescence microscope. Red fluorescence -  $\alpha$ -tubulin, cytoskeletal stain, blue fluorescence - DAPI nuclei stain and green fluorescence - autofluorescence from the fibre.

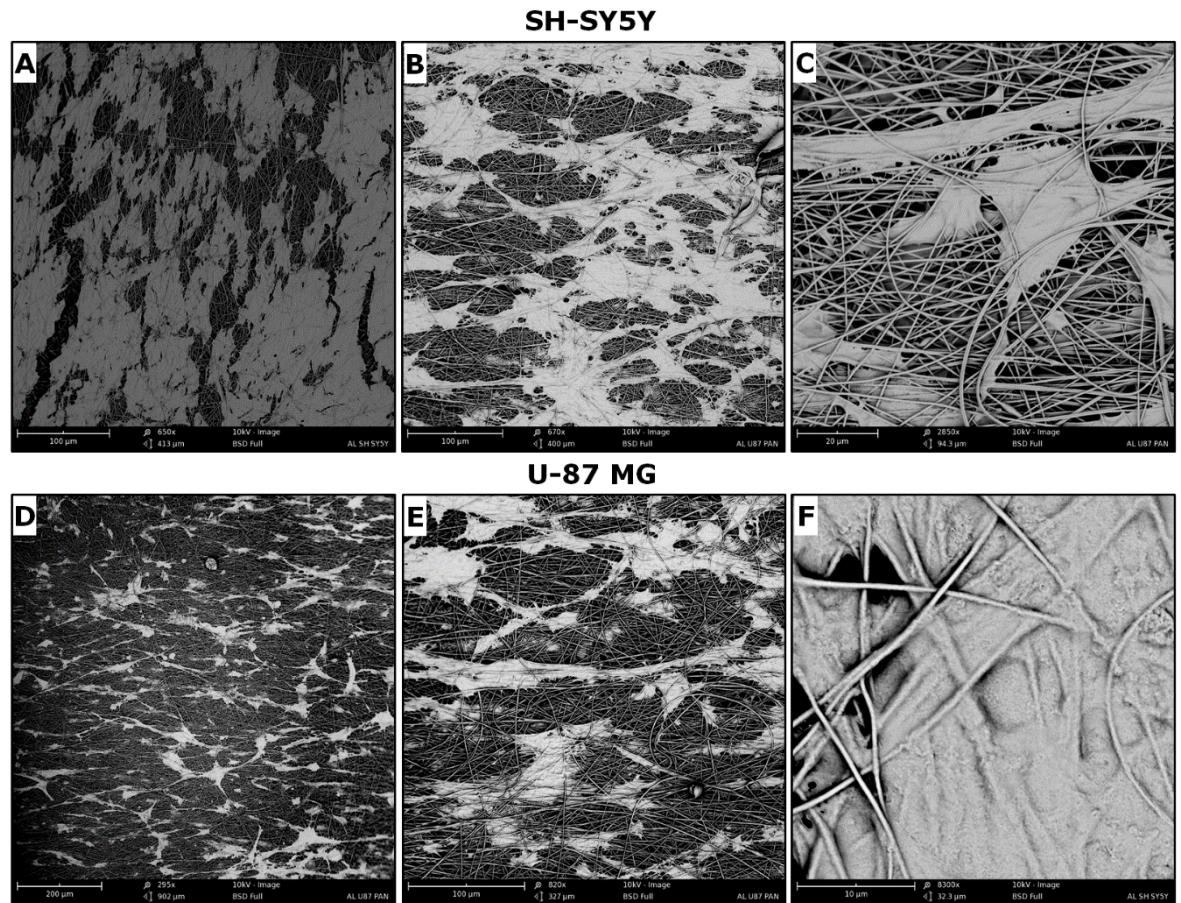


**Figure 4. 7: SEM imaging showing cell attachment on nanofibre.** The cells were cultured for 48 hours, fixed and dehydrated for SEM imaging. The cells were found wrapped and grown within the fibres. The images were obtained using the Phenom desktop SEM.

#### 4.3.4 Cell attachment and growth

In order, to investigate the level of cell attachment, growth and survival of both neuronal and glial cells on both PAN and PJ fibres, an assay that measured cell metabolic activity/proliferation was used. It was vital to understand the longevity of both cell types on the fibres. The experiment was set up as explained in section 2.2.7, and the ability of the cells to survive on fibres compared to the plate was studied by analysing cell metabolic activity/viability using the MTT reduction assay on both fibres and plate. Cells were cultured for 11 days on both plastic and fibres with viability assessed every 48 hours.

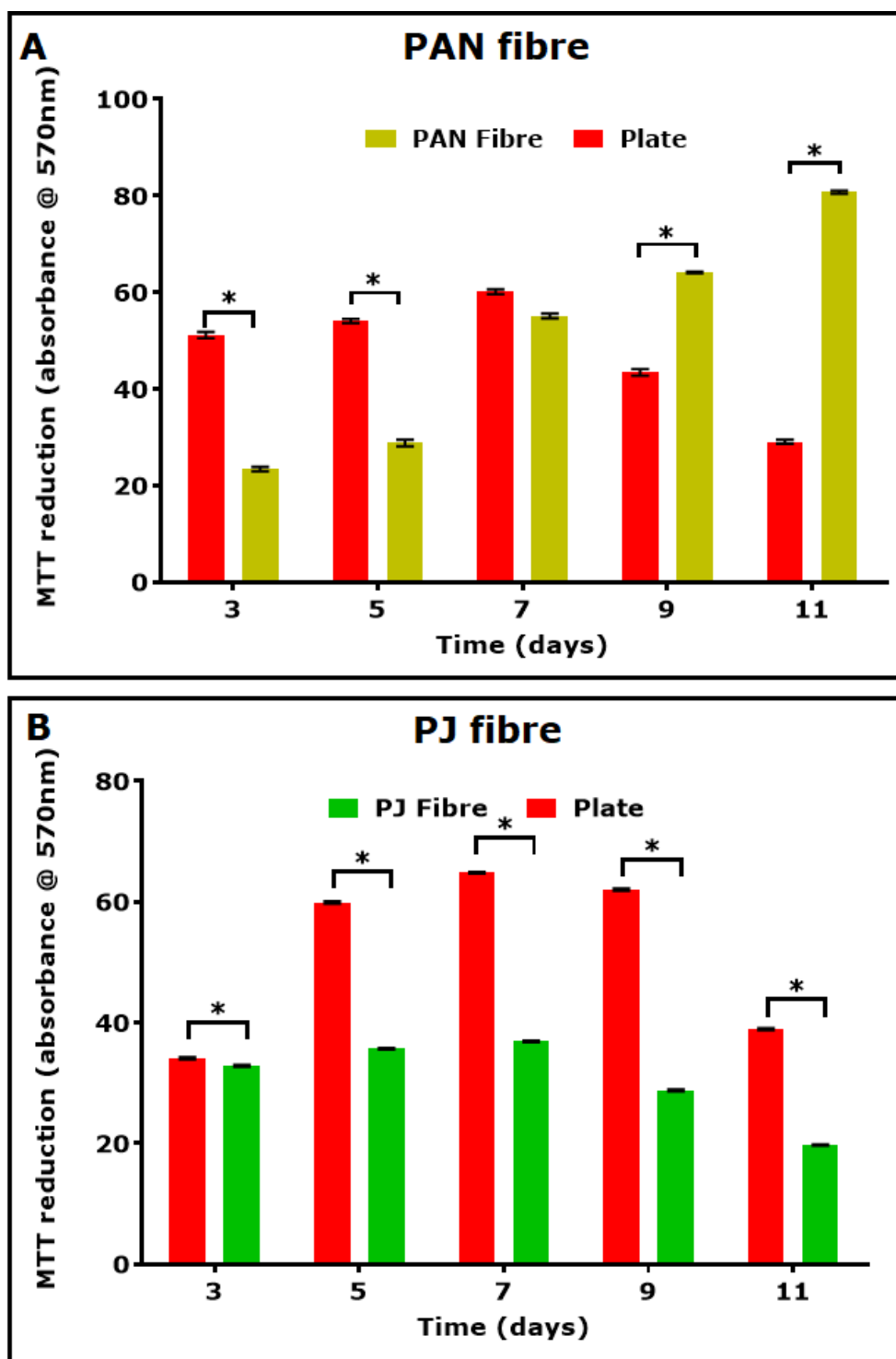


**Figure 4. 8: SH-SY5Y proliferation on PAN, PJ fibres and plate.** Panel (A) represents cell cultured on PAN compared to the plate and (B) represents PJ compared to the plate. Obtained values were converted to percentage setting control (day1) values to 100% (not shown). Results are expressed at the mean ratio  $\pm$  SEM  $n=6$  \* $P<0.005$  against plate vs fibre determined by two-tailed Student-T test and Two-Way ANOVA with Sidak's multiple comparisons tests.

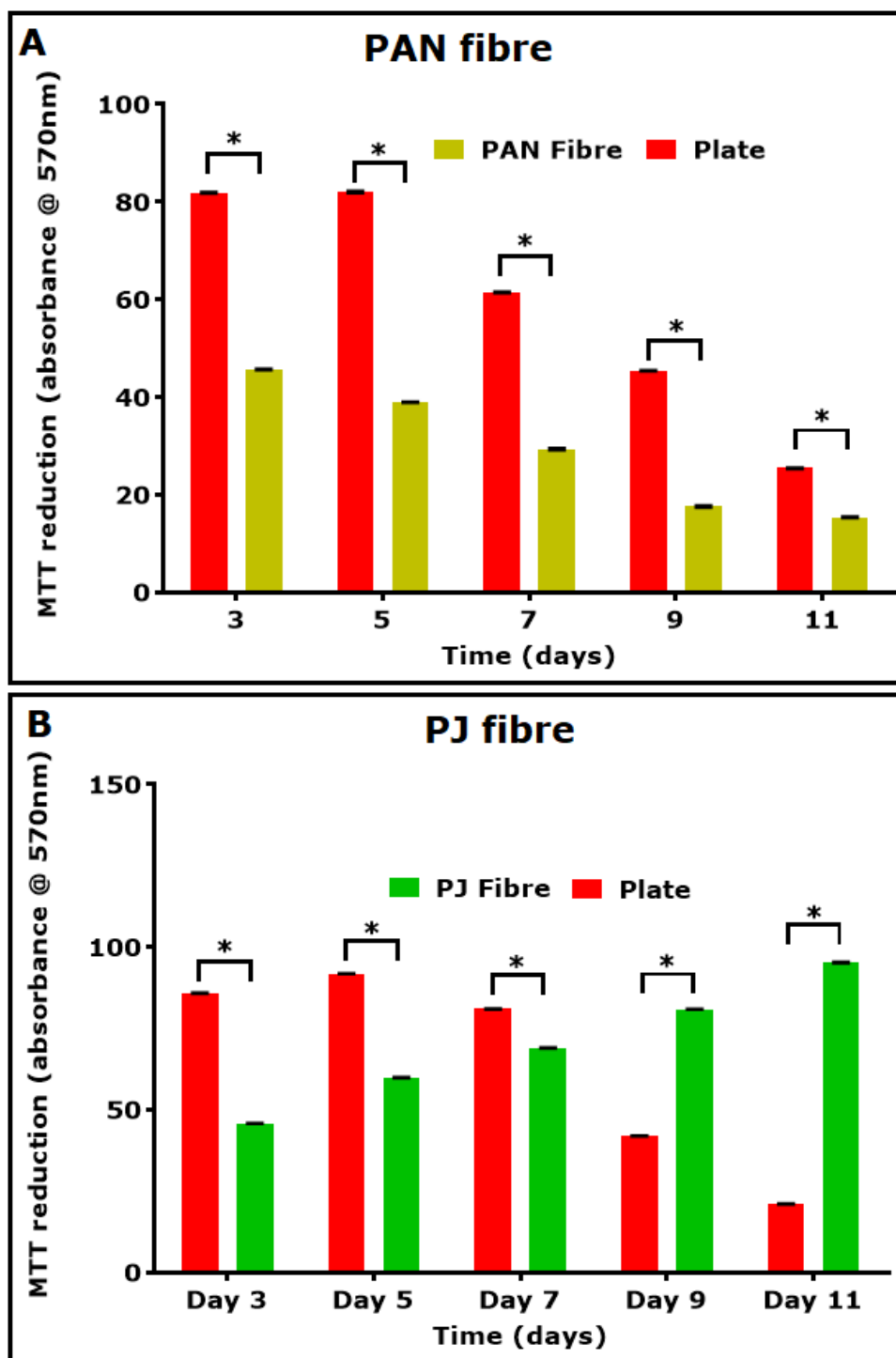


**Figure 4. 9: U-87 MG proliferation on PAN, PJ fibres and plate.** Panel (A) represents cells cultured on PAN compared to the plate and (B) represents PJ compared to the plate. Cells on plate expressed a gradual increase in cell number and viability later started decreasing after day 7 in both cases. Obtained values were converted to percentage setting control (day1) values to 100% (not shown). Results are expressed at the mean ratio  $\pm$  SEM  $n=6$  \* $P<0.005$  against plate vs fibre determined by two-tailed Student-T test and Two-Way ANOVA with Sidak's multiple comparisons tests.

The results show that SH-SY5Y cells were able to proliferate and survive longer on PAN fibre compared to PJ fibres while the rate of proliferation was reduced on fibres in comparison to culture plastic (Figure 4. 8). SH-SY5Y showed a gradual increase in cell growth and survived throughout the 11 days on PAN fibre but expressed a slower growth rate on PJ with a decrease in cell viability after day 7. Cells on plate expressed a gradual increase in cell number and viability later started decreasing after day 7 in both cases. In contrast, U-87 MG cells were able to proliferate and survive longer on PJ fibre (Figure 4. 9) compared to PAN fibre. U-87MG showed a steady survival until day 3 and gradually started to decline when cultured on PAN fibres but PJ high rate of proliferation was observed with continuous survival throughout 11 days. Similarly, the rate of proliferation was reduced on the PJ fibre compared to TCP. It was noticed that cells grown on TCP entered the log phase from day 3 and remained in the stationary phase for day 5 and 7, and subsequently began to die from day 7. A similar profile was observed for both SH-SY5Y cells cultured on PJ and U-87MG on PAN. SH-SY5Y on PAN and U-87MG on PJ showed a steady increase and continued to proliferate for 11 days.

#### **4.3.5 Investigation of U-87MG growth in DMEM**

To create a co-culture model to investigate Toxins, the investigation of growth characteristics of both cell lines in the same media was necessary. As the recommended culture media was different for SH-SY5Y and U-87 MG, it was essential to identify if both cells could be cultured with one media. U-87MG was cultured in both media (EMEM and DMEM/F12) separately, and changes in cell morphology were monitored with light microscopy.

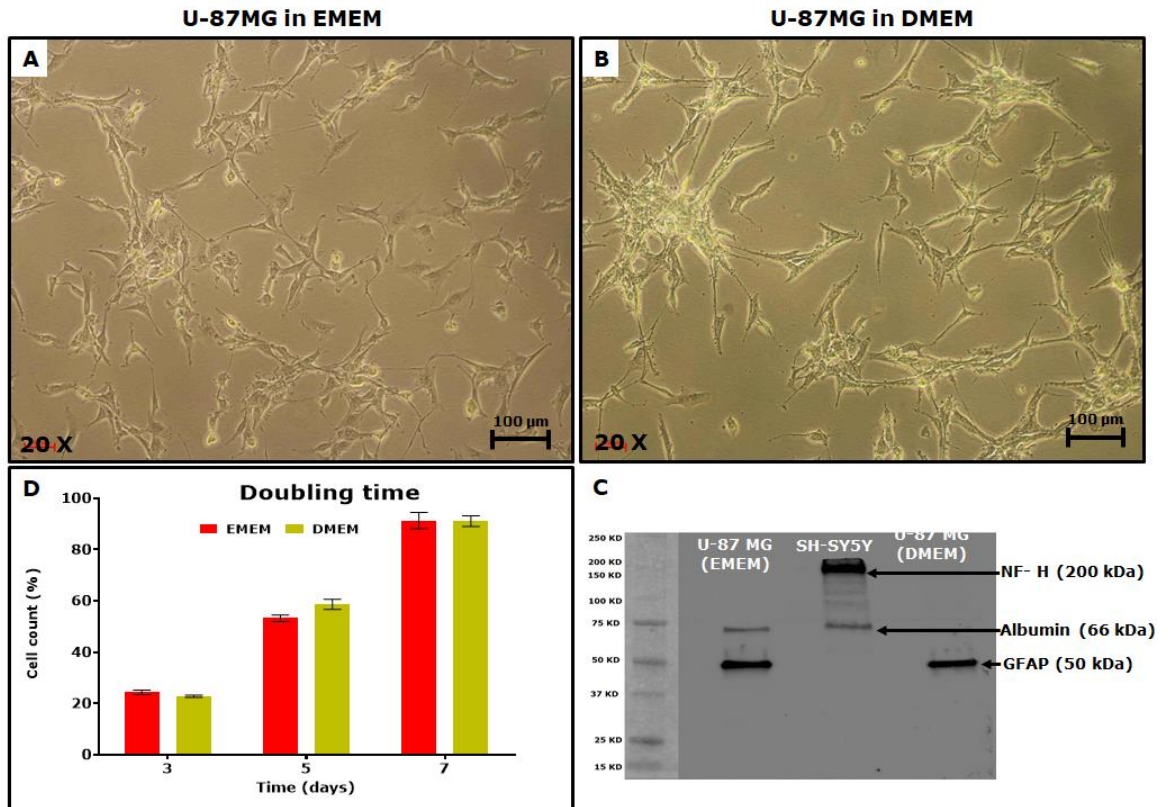


**Figure 4. 10: U-87 MG cultured in DMEM media.**

Figure A and B represents a light microscope image of U-87MG cultured in EMEM and DMEM respectively. C represents the expression Neurofilament expressed by SY-SY5Y, GFAP expressed by U-87 MG cultured in both media and Albumin from the FBS present in the media. Figure D shows the doubling time of u-87MG cells when cultured in both EMEM and DMEM. Obtained values were converted to percentage setting control (day1) values to 100% (not shown). Results are expressed at the mean ratio  $\pm$  SEM  $n=3$  \* $P<0.005$  against plate vs fibre determined by two-tailed Student-T test and Two-Way ANOVA with Sidak's multiple comparisons tests.

GFAP expression (an astrocytic protein marker) was assessed in cell cultured in DMEM or EMEM media. Protein cell lysates were prepared from cultured cells grown in respective media quantified using mini Lowry's method as described in section 2.2.10.1.3. Protein (30  $\mu$ g) was separated using SDS-PAGE, transferred to nitrocellulose and probed for GFAP as described in section 2.2.10.2. When observed under the light microscopes U-87 MG cells cultured in both EMEM and DMEM expressed similar morphology (figure 4.10 A and B) and doubling time (Figure 4.10 D). The western blot analysis confirmed the expression of GFAP for cells cultured in both media (Figure 4.10 C). These tests confirmed that U-87

MG could be cultured in DMEM with no gross changes in properties of the cell line. Future experiments in the project were conducted using DMEM/F12 based media for both SH-SY5Y and U-87 MG cells.

#### **4.3.6 Cell differentiation**

To investigate cell differentiation of the two neural cell types, SH-SY5Y and U-87MG were grown in the presence of different differentiating agents for 5 days. For SH-SY5Y, cells were grown in serum-free media supplemented with retinoic acid (1  $\mu$ M) or B27 supplement (1 % (v/v)). U-87MG cells were grown in serum-free medium supplemented with dbcAMP (0.3 mM) or B27 Supplement (1 % (v/v)). After 5 days of growth, the SH-SY5Y cells were examined for axon outgrowth and neurofilament-H protein expression representing characteristics of a maturing neuronal phenotype. U-87 MG cells were examined for stellate-like structures and GFAP protein expression representing characteristics of a maturing astrocyte phenotype. Cells cultured on both plate and fibres were fixed, and the morphological changes were examined with light microscopy. Expression of neurofilament and GFAP was analysed with immunofluorescence confocal microscopy. The level of protein expression was analysed for cells differentiated on both plate and fibre using western blotting and densitometry analysis.

##### **4.3.6.1 Immunofluorescence staining of differentiation markers**

SH-SY5Y and U-87MG were cultured on both PAN and PJ fibres in the presence of differentiating agents for 5 days. The scaffolds were fixed using 90% methanol/TBS and stained for protein differentiation markers  $\beta$ III tubulin (SH-SY5Y) and GFAP (U-87MG). Immunofluorescence images obtained from differentiating cells showed that neuronal SH-SY5Y cells were able to extend axons on PAN fibres which stained positive for  $\beta$ III tubulin; a mature neuronal marker. Both RA and B27 supplementation showed similar results with extended  $\beta$ III tubulin-positive axons

compared to the non-treated control (Figure 4.11). However, on PJ fibre SH-SY5Y cells struggled to grow and differentiate.

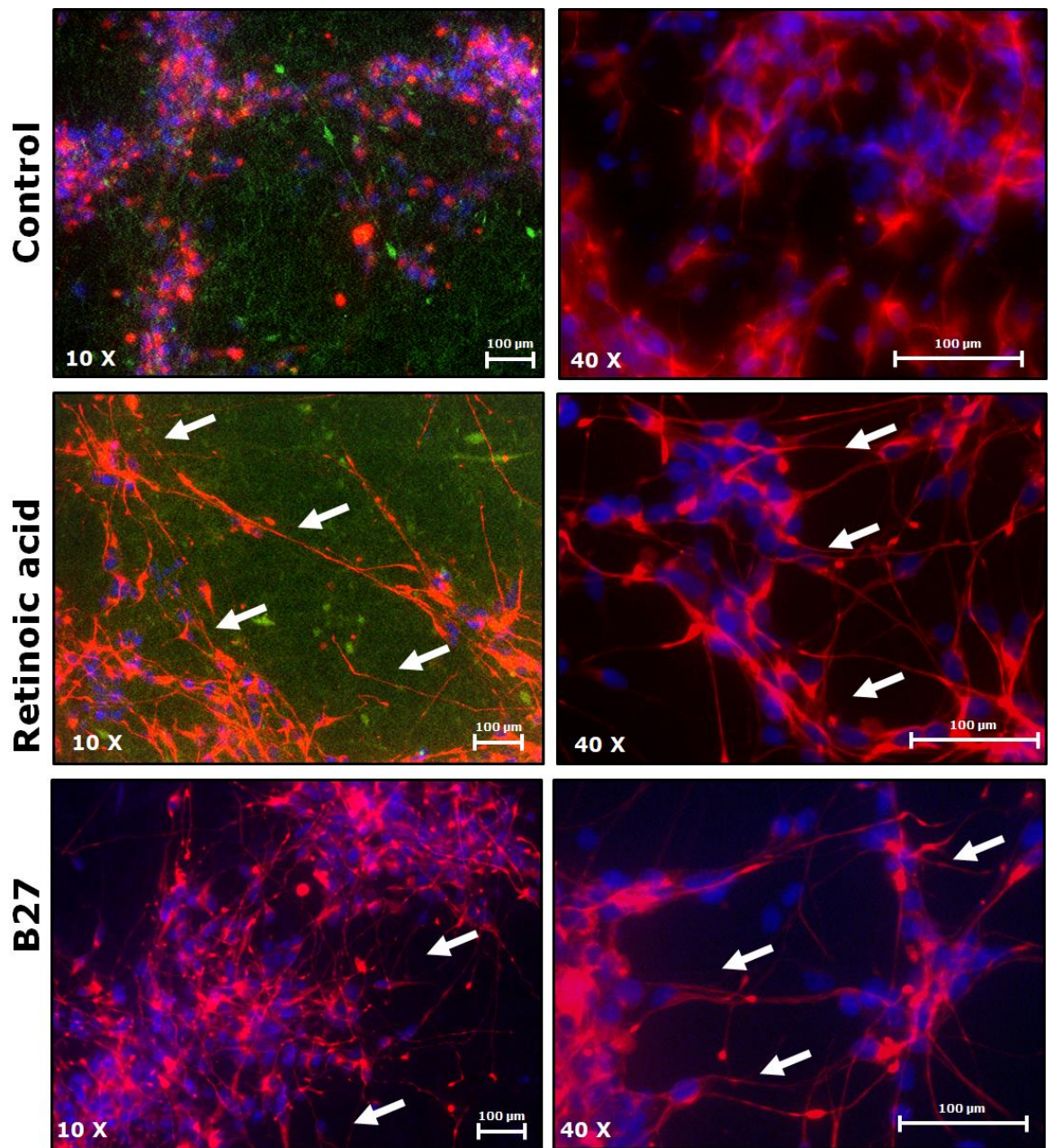


**Figure 4. 11: Immunofluorescence imaging of Differentiated SH-SY5Y on PAN fibre.**

SH-SY5Y cells were cultured on PAN for 48 hours and differentiated using RA and B27 Supplement for 5 days. Cells were fixed then stained for  $\beta$ III tubulin and imaged using a Leica confocal microscope. Neurite outgrowth was observed throughout the fibres, and high expression of  $\beta$ III tubulin was observed. Red-  $\beta$ III tubulin, blue- DAPI Nuclei stain, green- autofluorescence from nanofibres. The arrows indicate the axonal elongation in the differentiated sample.

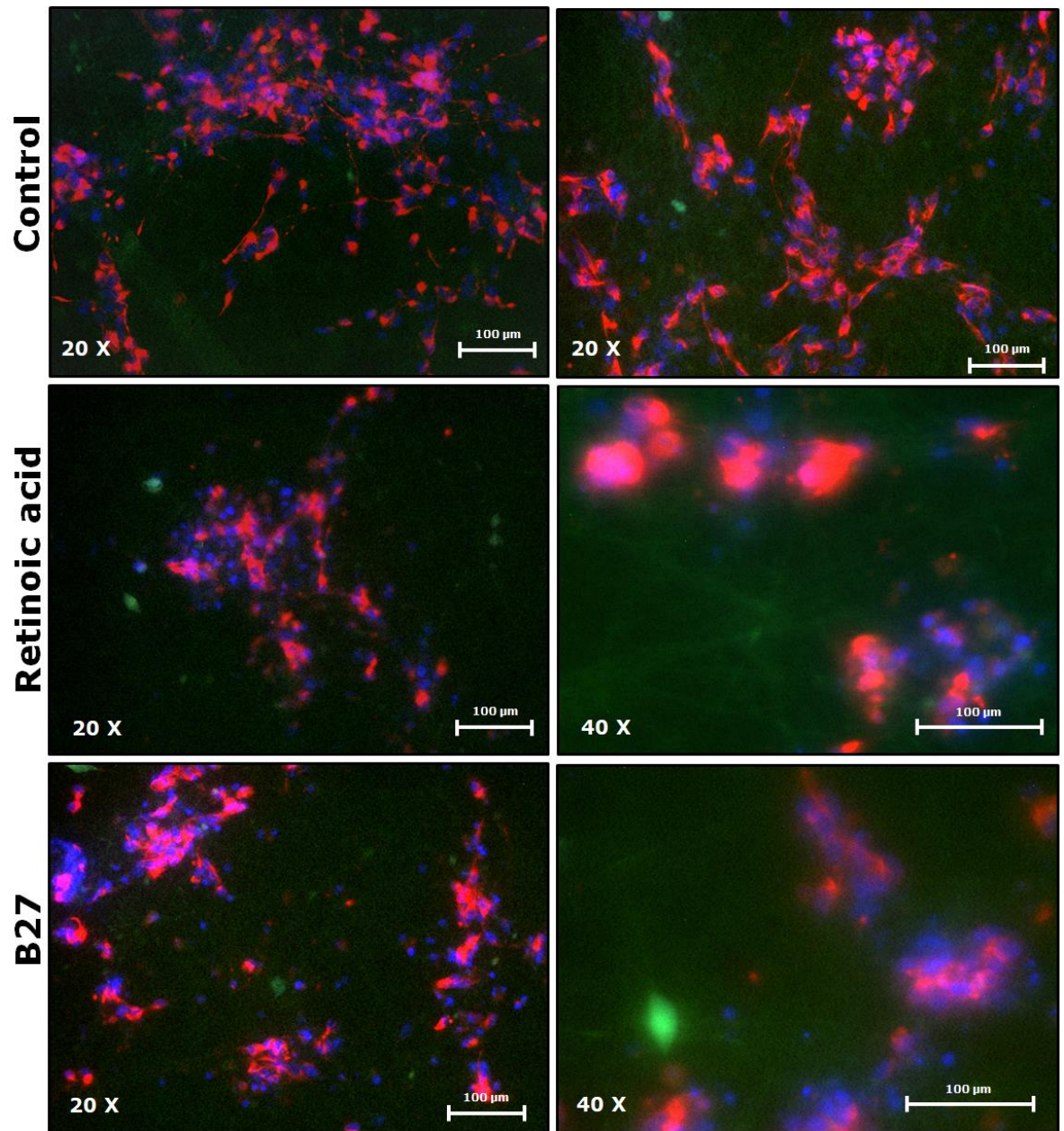


**Figure 4. 12: Immunofluorescence imaging of Differentiated SH-SY5Y on PJ fibre.**

*SH-SY5Y cells were cultured on PJ for 48 hours and differentiated using RA and B27 Supplement for 5 days. Cells were fixed then stained for  $\beta$ III tubulin and imaged using a Leica confocal microscope. Very poor neurite outgrowth and low expression of  $\beta$ III tubulin were observed. Red-  $\beta$ III tubulin, blue- DAPI Nuclei stain, green- autofluorescence from nanofibres.*

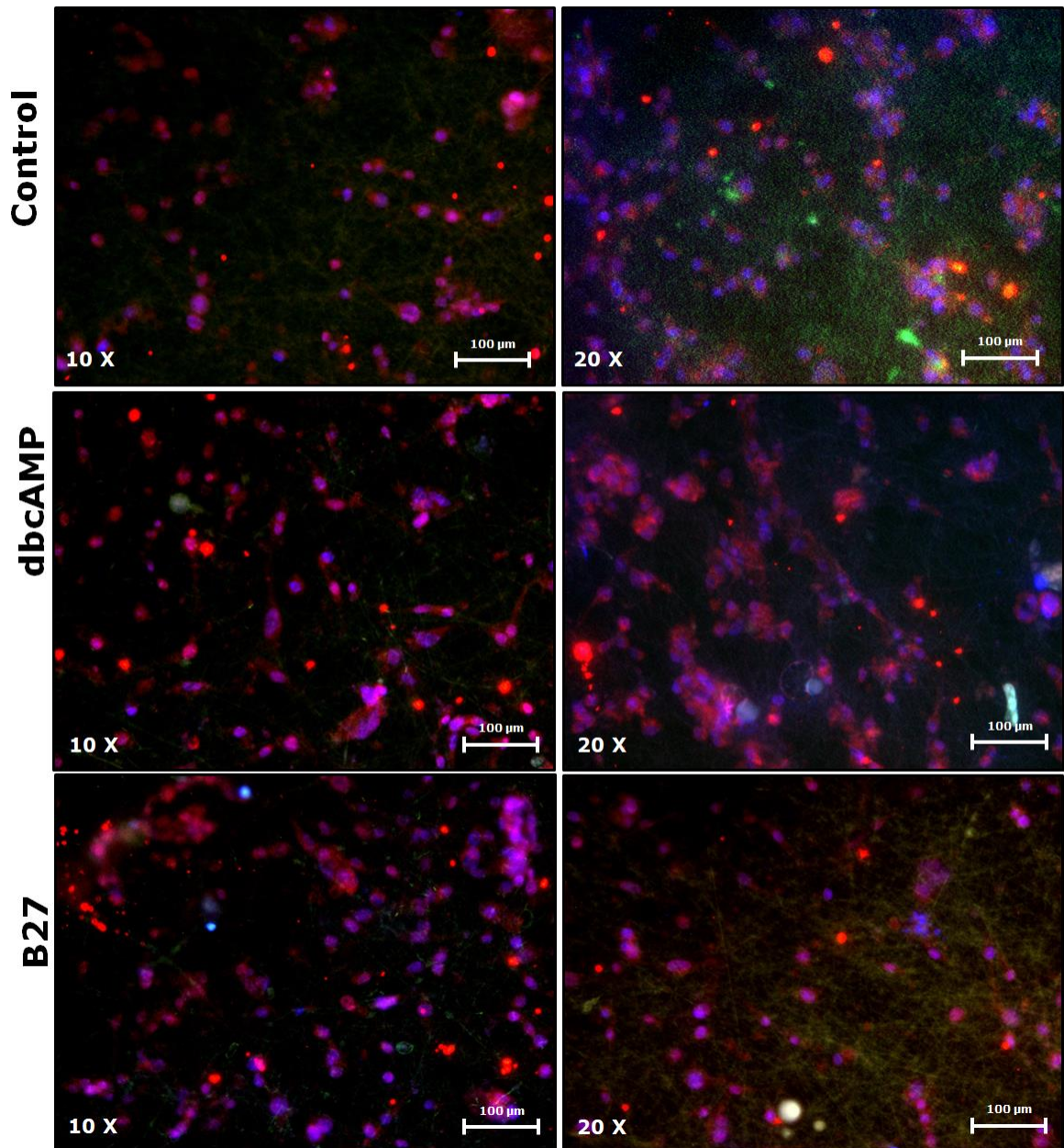


**Figure 4. 13: Immunofluorescence imaging of Differentiated U-87 MG on PAN fibre.**

*Cells were fixed then stained for GFAP and imaged using a Leica confocal microscope. Feeble expression of GFAP was observed along with many debris due to dead cells. Red- GFAP, blue- DAPI Nuclei stain, green- autofluorescence from nanofibres.*

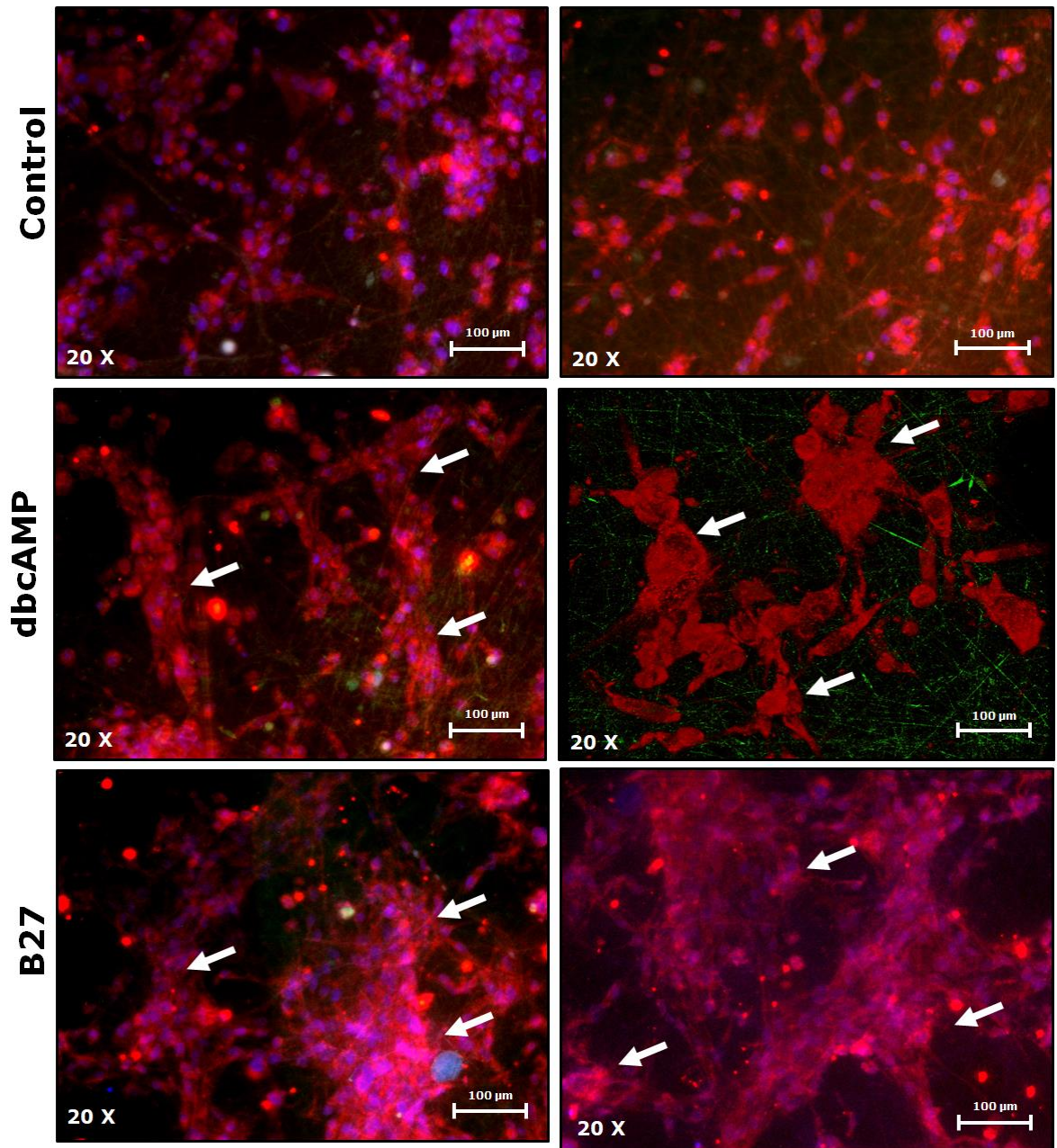


**Figure 4. 14: Immunofluorescence imaging of Differentiated U-87 MG on PJ fibre.**

Cells were fixed then stained for GFAP and imaged using a Leica confocal microscope. Differentiated cells appeared to be clustered and showed high expression of GFAP when treated with dbcAMP and B27. Red- GFAP, blue- DAPI Nuclei stain, green- autofluorescence from nanofibres. The images were obtained at multiple magnifications from multiple samples and different locations of each scaffold.

In contrast, glial U-87MG cells cultured on PJ fibre (figure 4.14) showed improved cell growth and differentiation as highlighted by GFAP positive staining of cellular extensions. U-87MG cells struggled to grow and

differentiate in PAN fibre (figure 4.13). Several cells with stable expression of GFAP were observed in U-87MG exposed to both dbcAMP and B27 supplement compared to the undifferentiated control.

#### **4.3.6.2 Protein expression analysis**

The expression of the protein was quantified using western blot analysis. Both SH-SY5Y and U-87MG cell were cultured on both fibres and plate then differentiated for 5 days. A pool of cells from an entire 12 well plate was used to extract protein from each treatment as described in section 2.2.10.1.1, 2.2.10.1.2 for plate and fibre respectively. Protein extracts were quantified using mini Lowry's protein quantification, and extracts (20µg) separated using 10% (w/v) SDS-PAGE gel electrophoresis. Separated proteins were transferred to a nitrocellulose membrane, and SH-SY5Y samples immunoprobed for phosphorylated neurofilament heavy chain (axon and neuronal maturity marker),  $\beta$ III tubulin (mature neuronal marker) and synaptophysin (synaptic and neuronal network maturity marker) while GFAP expression (mature astrocyte marker) was evaluated for U-87MG.

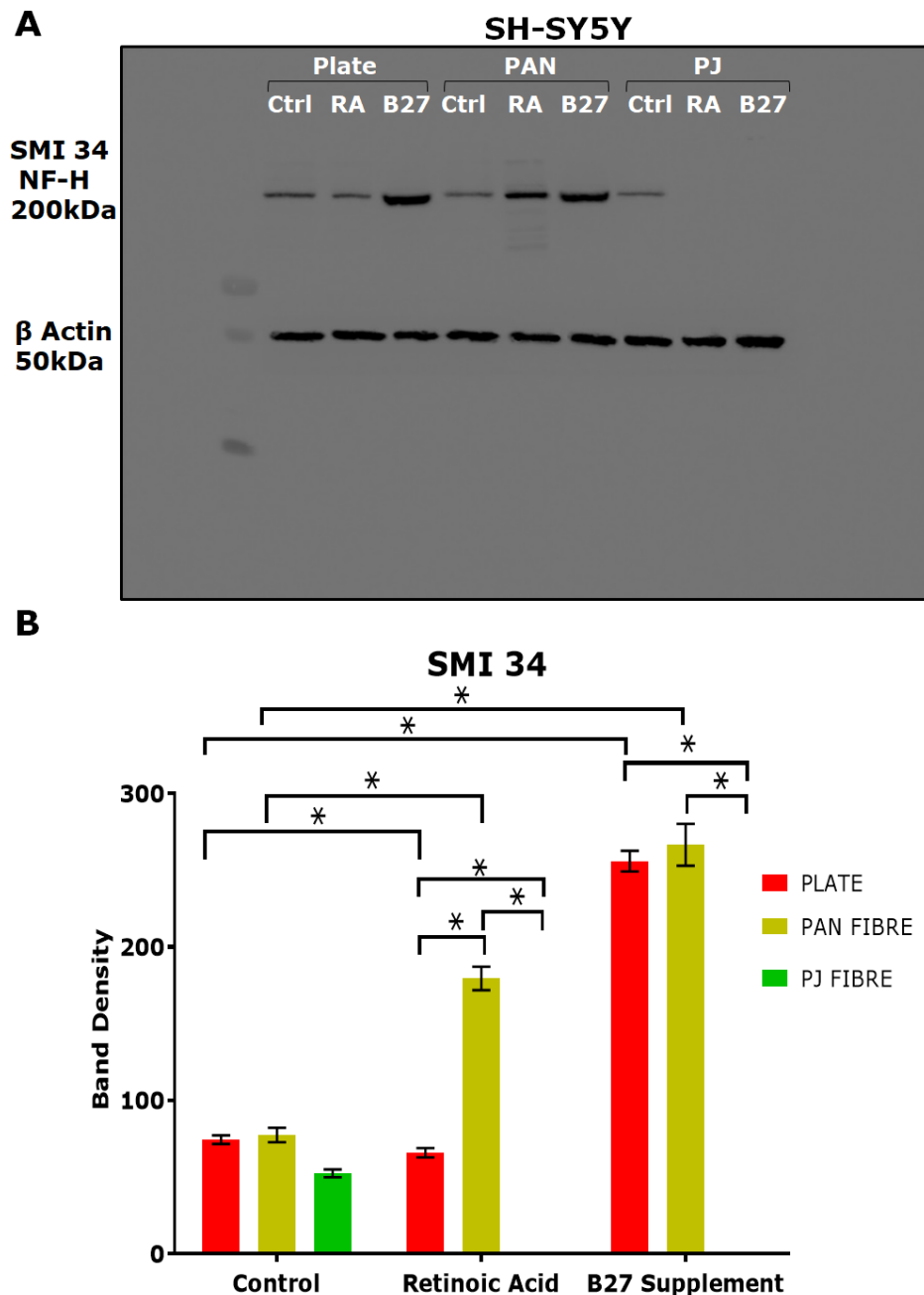


**Figure 4. 15: Phosphorylated neurofilament-H (SMI 34) protein expression in differentiated SH-SY5Y cell on a plate, PAN and PJ fibre.**

(A) Blot image obtained at 210sec exposure time and (B) Densitometry analysis of bands was performed using Advanced Image Data Analyser (AIDA) software (Fuji), and values obtained were normalised against loading control. Results are expressed as the mean percentage  $\pm$  SEM  $n=3$  \* $P<0.05$  between plate vs fibres, fibre vs fibre and treatment vs control were determined by Two-Way ANOVA Tukey multiple comparison tests.

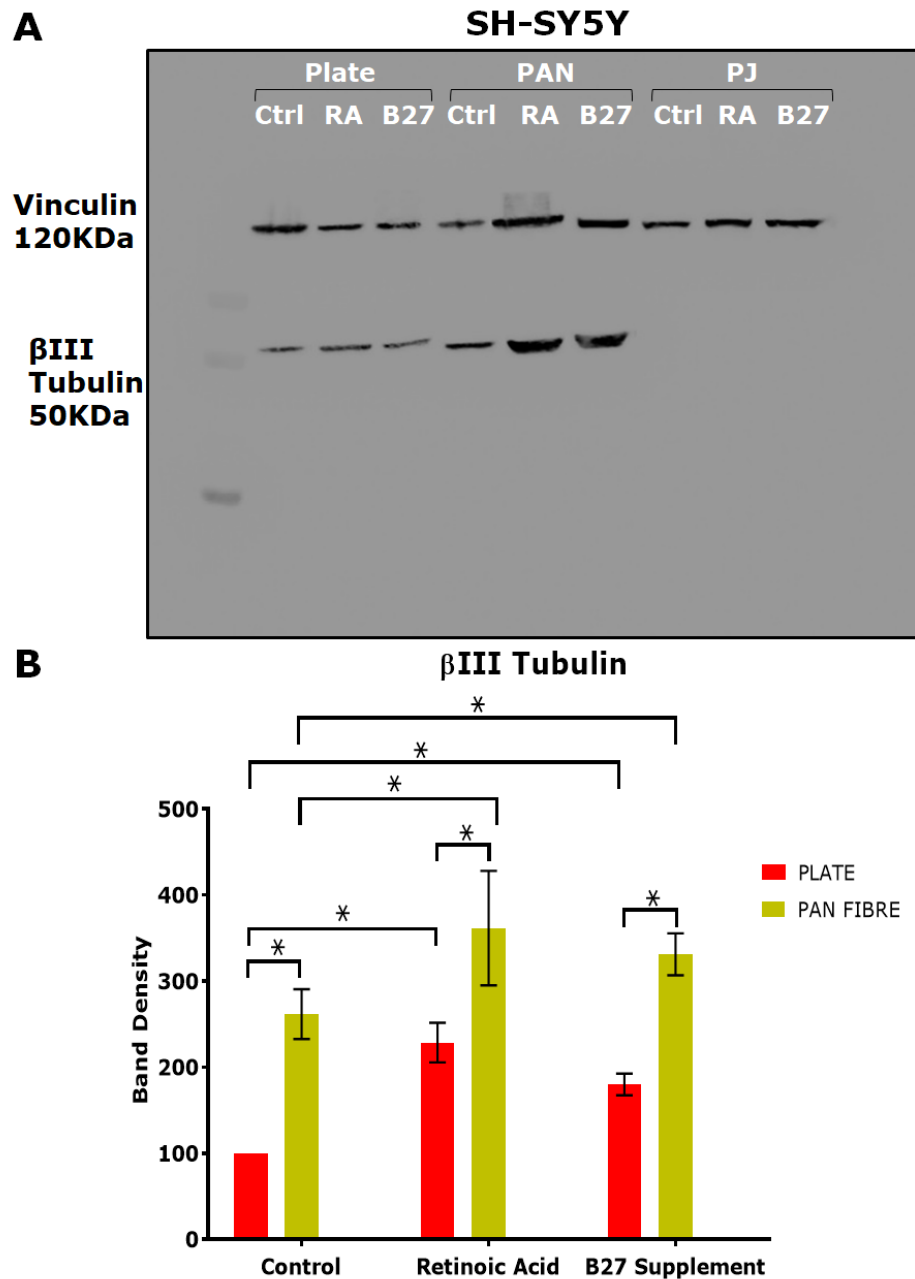


**Figure 4. 16:  $\beta$ III tubulin protein expression in differentiated SH-SY5Y cell on a plate, PAN and PJ fibre.**

(A) Blot image obtained at 150sec exposure time and (B) Densitometry analysis of bands was performed using Advanced Image Data Analyser (AIDA) software (Fuji), and values obtained were normalised against loading control. Results are expressed as the mean percentage  $\pm$  SEM  $n=3$  \* $P<0.05$  between plate vs fibres, fibre vs fibre and treatment vs control were determined by Two-Way ANOVA Tukey multiple comparison tests.

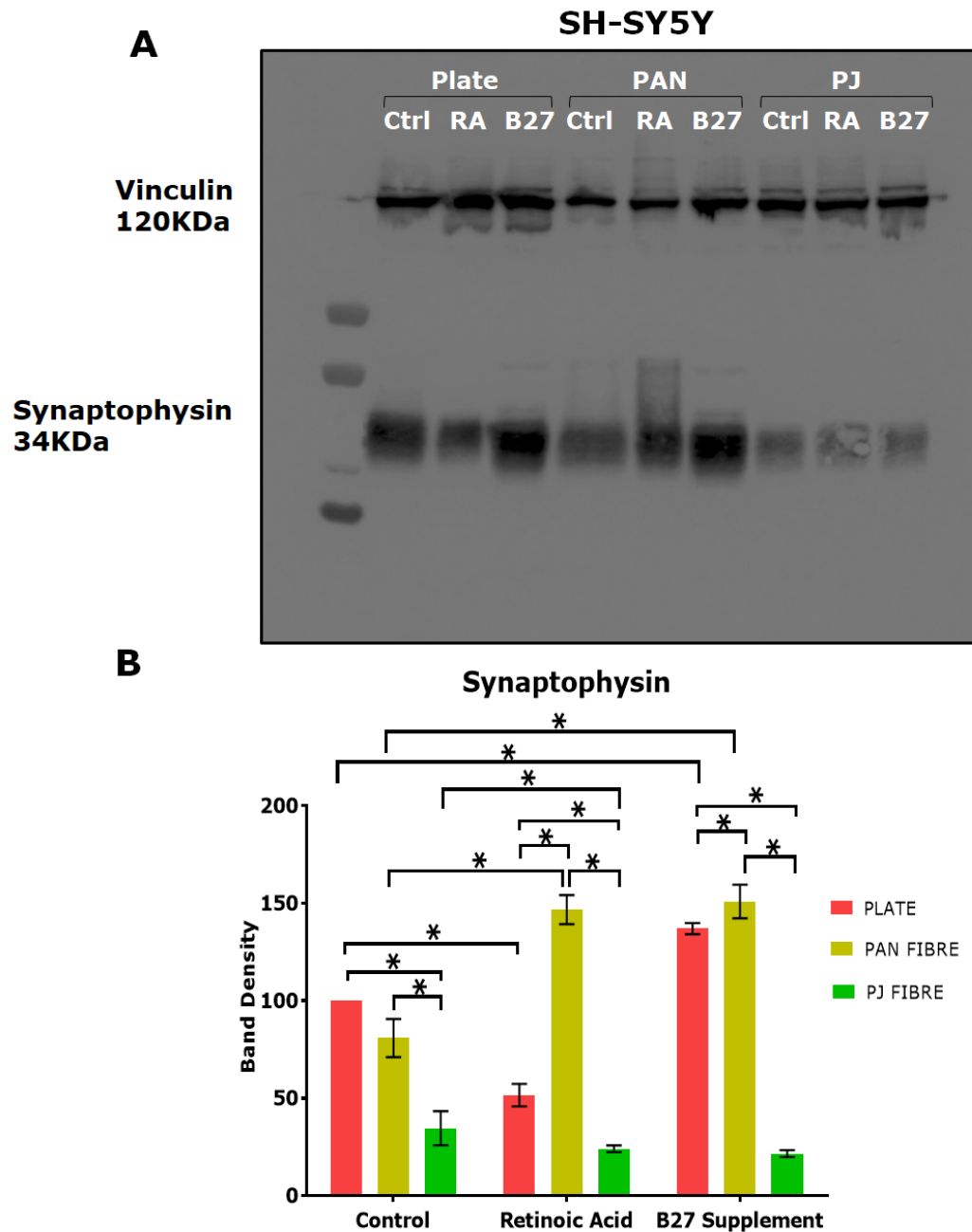


**Figure 4. 17: Synaptophysin protein expression in differentiated SH-SY5Y cell on a plate, PAN and PJ fibre.**

(A) Blot image obtained at 60sec exposure time and (B) Densitometry analysis of bands was performed using Advanced Image Data Analyser (AIDA) software (Fuji), and values obtained were normalised against loading control. Results are expressed as the mean percentage  $\pm$  SEM  $n=3$  \* $P<0.05$  between plate vs fibres, fibre vs fibre and treatment vs control were determined by Two-Way ANOVA Tukey multiple comparison tests.

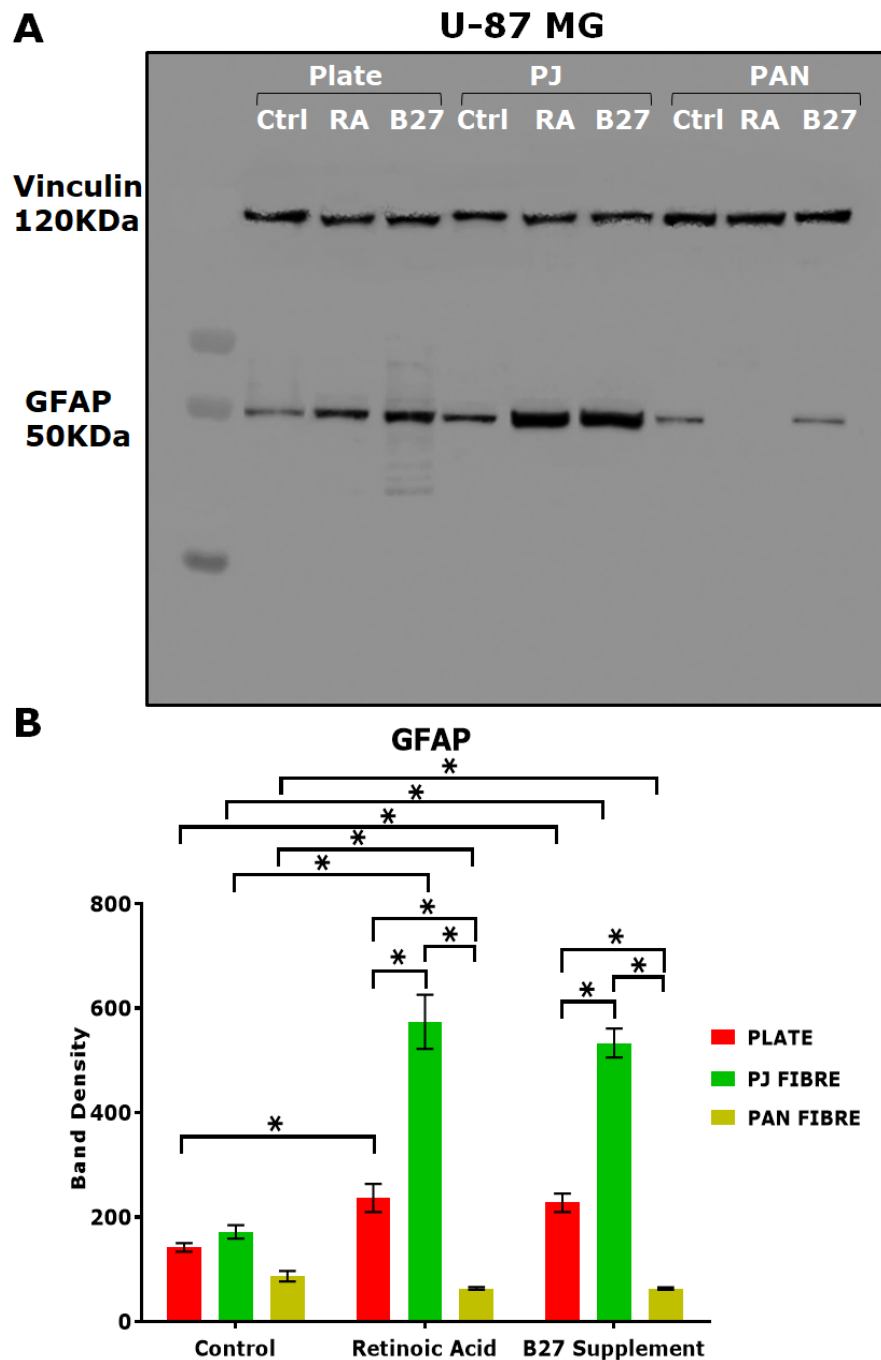


**Figure 4. 18: GFAP protein expression in differentiated U-87MG cell on a plate, PAN and PJ fibre.**

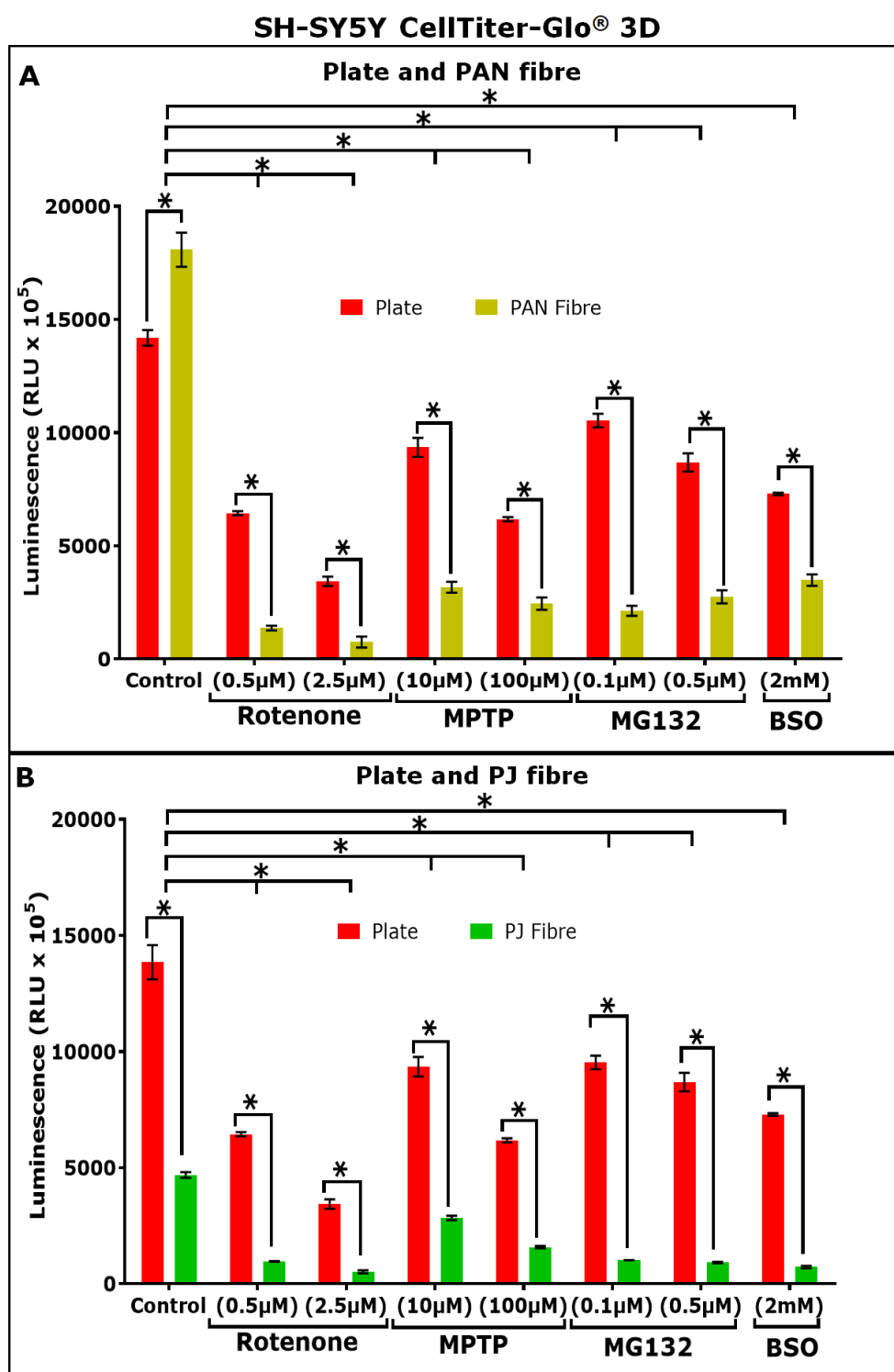
(A) Blot image obtained at 90sec exposure time and (B) Densitometry analysis of bands was performed using Advanced Image Data Analyser (AIDA) software (Fuji), and values obtained were normalised against loading control. Results are expressed as the mean percentage  $\pm$  SEM  $n=3$  \* $P<0.05$  between plate vs fibres, fibre vs fibre and treatment vs control were determined by Two-Way ANOVA Tukey multiple comparison tests.

Results obtained from the western blot analysis indicated that expression of neurofilament-H (200 kDa),  $\beta$ III tubulin (50 kDa) and synaptophysin (34k Da) significantly increased when cells were grown on PAN compared to cells cultured on the standard TCP. Weak expression or no expression of these proteins was observed from cells differentiated on PJ fibres. U-87MG cell extracts exhibited high expression of GFAP (50 kDa) on PJ fibre compared to TCP while low expression of GFAP was observed in undifferentiated (control) and feeble GFAP expression was seen for U-87MG cells cultured on PAN fibre. However, both SH-SY5Y and U-87MG showed higher levels of differentiation markers when induced to differentiate with B27 supplementation compared to retinoic acid on PAN and PJ fibres respectively. Higher expression of the protein was also seen in a cell on the plate when differentiating with B27 supplement.

#### **4.3.7 Toxicology analysis on SH-SY5Y and U-87MG on both TCP and 3D nanofibres**

In order to evaluate the efficacy of the nanofibre model, toxins capable of affecting the cells by causing mitochondrial dysfunction, glutathione depletion and impaired proteasome-mediated degradation were used. SH-SY5Y and U-87MG cells cultured on a plate, PAN and PJ fibres were exposed to different toxins for 72 hours. The effects of these toxins were compared between the cells grown on fibres and cells cultured on a plate surface. The effect of the treatments on cells cultured on both nanofibre and plate were examined by analysing cell metabolic activity and viability using MTT and CellTiter-Glo<sup>®</sup> 3D assay respectively. The results indicated that the cells exposed to treatments on nanofibres were more sensitive compared to the plate and showed increased susceptibility to cell death. At a lower concentration of treatments, it was also observed that the cells grown on fibre showed increased resistance expressing the slower rate of cell death against the effect of toxins. As shown in figure 4.19 for SH-SY5Y cells on PAN fibres mitochondrial impairment is more sensitive on the fibre than the plate. However, proteasome impairment and

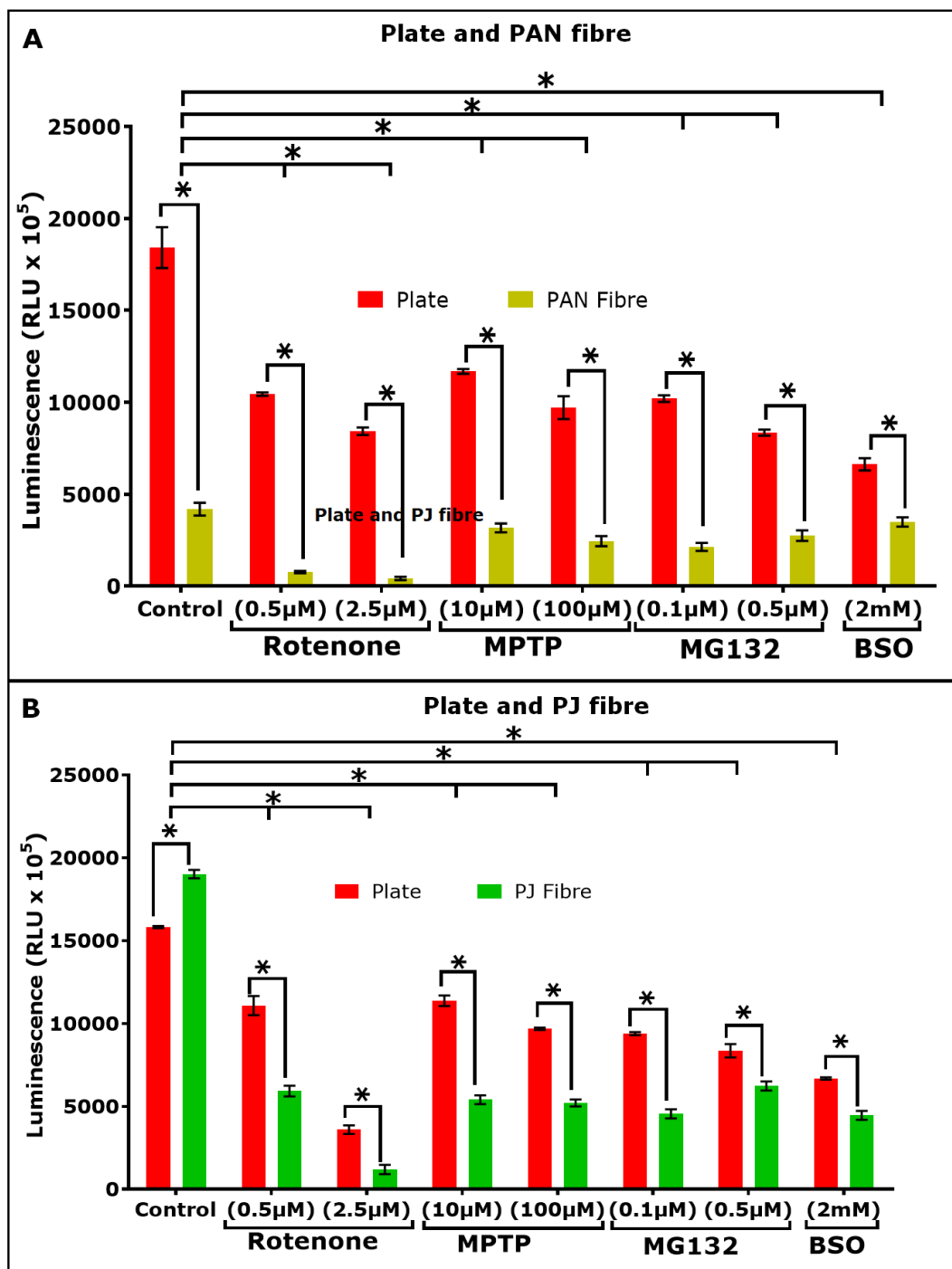
glutathione depletion between the substrates were significantly different with better cell viability compared to mitochondrial impairment. A significant difference was observed between the treatment and control of both plate and fibres. The toxins have caused a reduction in cell viability on both plate and fibres which was also further validated with CellTiter Glo® 3D viability assay. SH-SY5Y cells on PJ fibre showed extreme damage when exposed to toxins as our previous investigations suggested that PJ is not capable of supporting SH-SY5Y cell growth and this may have caused further damage causing increased cell death.



**Figure 4. 19: CellTiter-Glo® 3D viability assay showing the effect of Toxins on SH-SY5Y cultured on Plate, PAN and PJ fibre.**

Figure A represents comparison between plate and PAN fibre and Figure B shows comparison between plate and PJ fibre. Results are expressed at the mean ratio  $\pm$  SEM  $n=6$  for MTT and  $n=3$  for CellTiter \* $P<0.005$  against plate vs fibre and control vs treatment for plate and fibre was determined by Two-Way ANOVA with Sidak's multiple comparisons tests.

## U-87 MG CellTiter-Glo® 3D



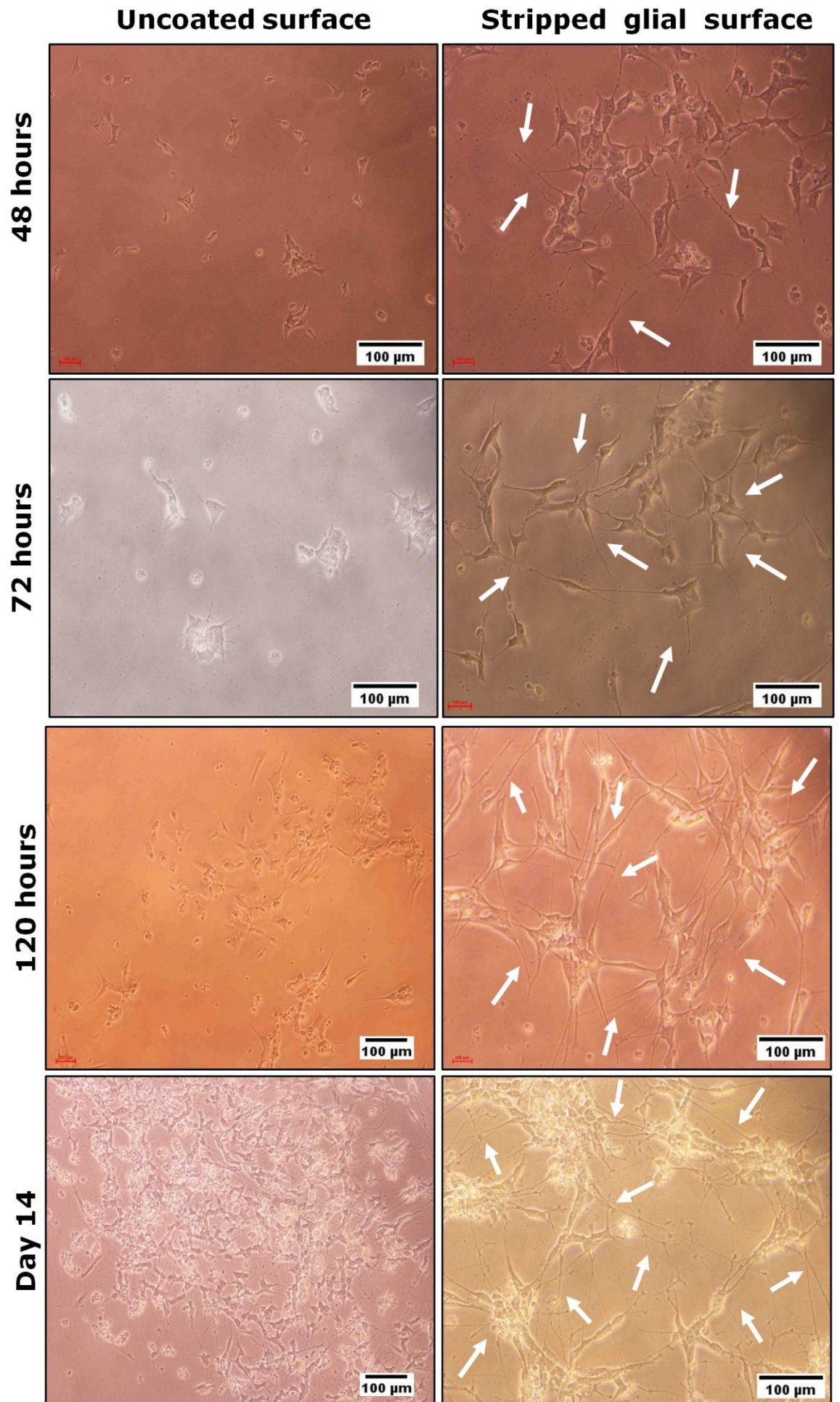
**Figure 4. 20: CellTiter-Glo® 3D viability assay showing the effect of Toxins on U-87 MG cultured on Plate, PAN and PJ fibre.**

Figure A represents comparison between plate and PAN fibre and Figure B shows comparison between plate and PJ fibre. Results are expressed at the mean ratio  $\pm$  SEM  $n=6$  for MTT and  $N=3$  for CellTiter \* $P<0.005$  against plate vs fibre and control vs treatment for plate and fibre was determined by Two-Way ANOVA with Sidak's multiple comparisons tests.

U-87 MG cells cultured on PAN showed a similar effect as SH-SY5Y on PJ. Our study has shown that PJ is the favourable material to support U-87 MG cell growth and the inhabitable surface may have caused extensive cell death. However, U-87MG on PJ fibres showed higher sensitivity to toxins at higher concentrations and a slower rate of cell death on lower concentrations. The treatments were highly significant compared to the untreated control on both plate and fibres.

#### **4.3.8 Effect of the glial extracellular matrix on neurones**

Cells from the glial cell family are known to support neuronal growth, protection and survival. To understand the effect of glial cell's ECM can have on neuronal cells we cultured glial cells on a substratum prior to stripping the cells and culturing neuronal cells on the stripped surface with no additional differentiating agents. A detailed description of the methodology has been described in section 2.2.8. The neuronal cells were cultured under standard conditions with cell culture media containing 1 % (v/v) serum for 14 days. The cells were monitored and imaged under a light microscope for every 48 hours. At the end of 14 days, the cells were fixed and stained for  $\beta$ III tubulin for immunofluorescence imaging.



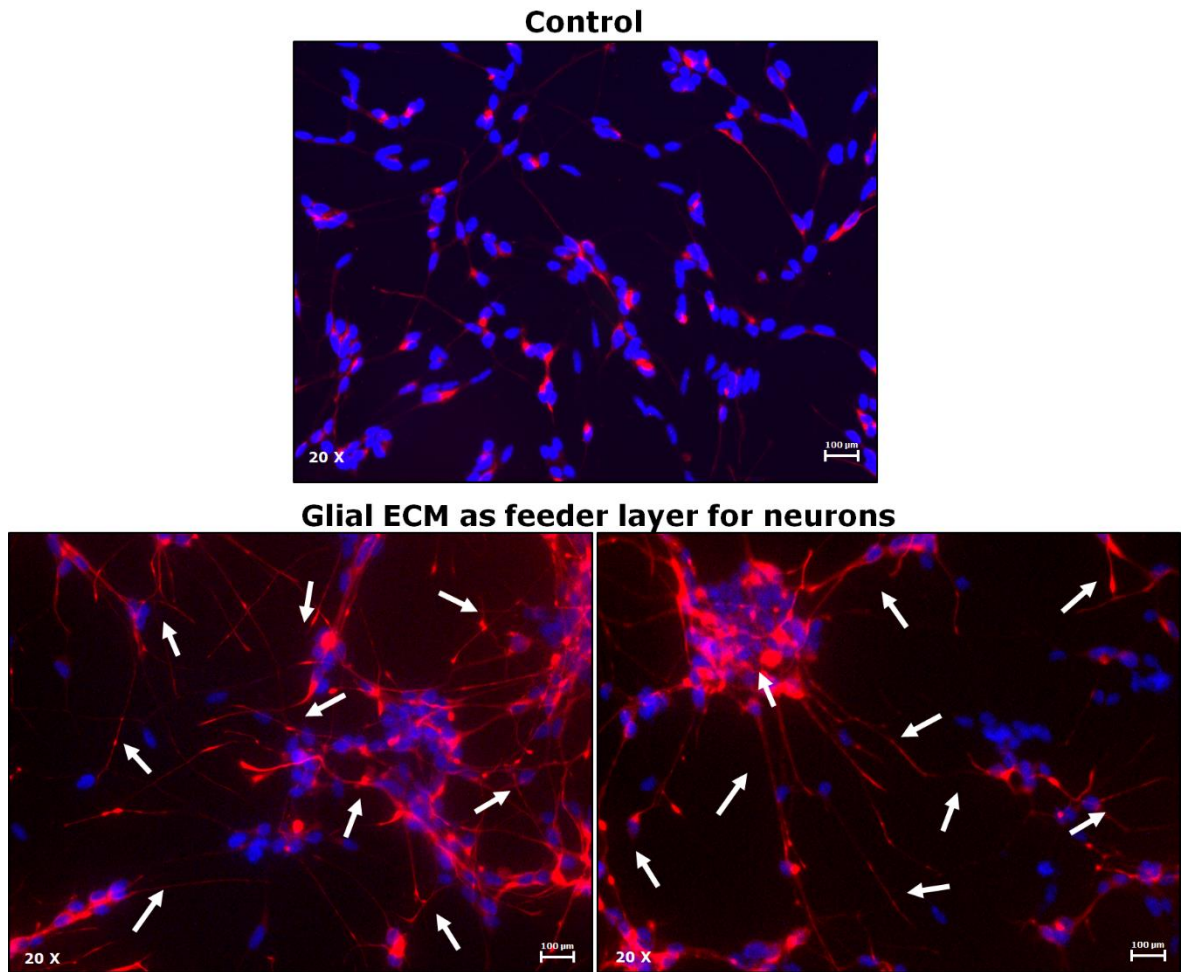


**Figure 4. 21 SH-SY5Y cells cultured on U-87MG ECM feeder layer.** SH-SY5Y cells were cultured for 14 days and was imaged under a light microscope every 48 hours. The image represents untreated surface (control) and glial stripped surface at 48 hours, 72 hours, 120 hours and day 14. At day 14 the cells were methanol fixed and stained for  $\beta$ III tubulin (red) and DAPI (blue). The white arrow on the immunofluorescence image point the neurite extension expressing  $\beta$ III tubulin with support for glial ECM. No neurite elongation was observed on untreated surface.

Within 48 hours the cells cultured on the stripped feeder layer showed faster cell proliferation with some neurites extending compared to the control. At the end of day 14, the SH-SY5Y cells showed greater morphological maturity with long axonal-like projections evident throughout the plate (Figure 4.21). The control plate with no glial stripped feeder layer expressed a slower growth rate and very few neurite extensions. The axonal extensions were confirmed by staining for  $\beta$ III tubulin and imaged under an immunofluorescence microscope.

### 4.3.9 Development of a 3D co-culture model

The 3D co-culture system was set up as described in section 2.2.12. The fibres and the 2D surface was arranged as shown in figure 4.22. The cells were cultured and differentiated individually with B27 supplement for 5 days. Three different possibilities for a co-culture was experimented to see the influence of the nanofibre and astrocytes on Neuronal cells. SH-SY5Y cell was cultured on PAN and U-87MG was cultured on PJ. The cells were also exposed to low levels of toxins and viability was measured every 72 hours using CellTiter-Glo<sup>®</sup> 3D.

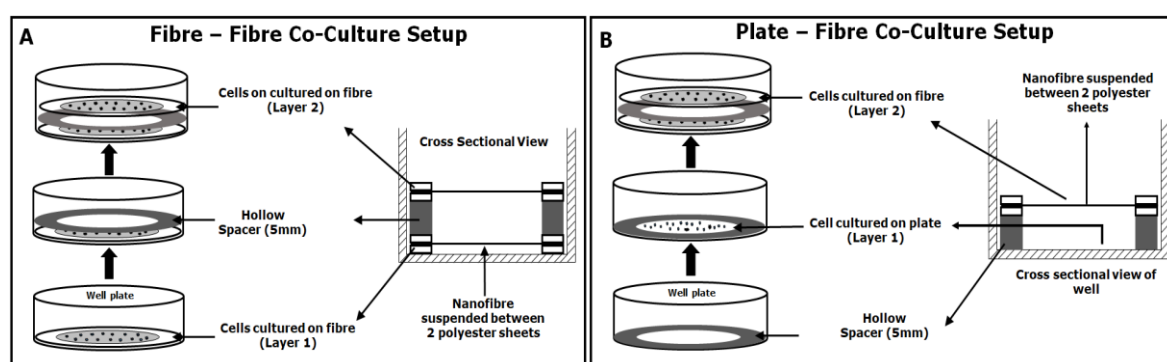


**Figure 4. 22: Schematic representation of the experimental setup designed to create a co-culture system.**

#### 4.3.9.1 Establishment of co-culture with neuronal cells on the 2D surface and glial cell on PJ fibre

In this experimental set up a two different surface was investigated. The SH-SY5Y cells were cultured and differentiated on TCP and the glial cells on PJ fibres. After 5 days of differentiation fibre grown glial cells were transferred to TCP containing neurones and incubated with growth medium in the presence of different Toxins. As shown earlier in section 4.3.4, cells cultured on TCP survive fewer days compared to cells cultured on fibres. Therefore, this co-culture experiment was only performed for 7 days, and an endpoint viability measurement was taken after the 7<sup>th</sup> day. The viability data showed that both cells cultured on plate and fibre was damaged due to the effect of toxin and expressed poor cell viability compared to untreated control. SH-SY5Y cells cultured on plate shower lower cell viability compared to the U-87MG cultured on PJ fibre (Figure

4.23 A). Though the SH-SY5Y cells expressed poor cell viability, the cells showed better resistance to the toxin in the presence of astrocytes.

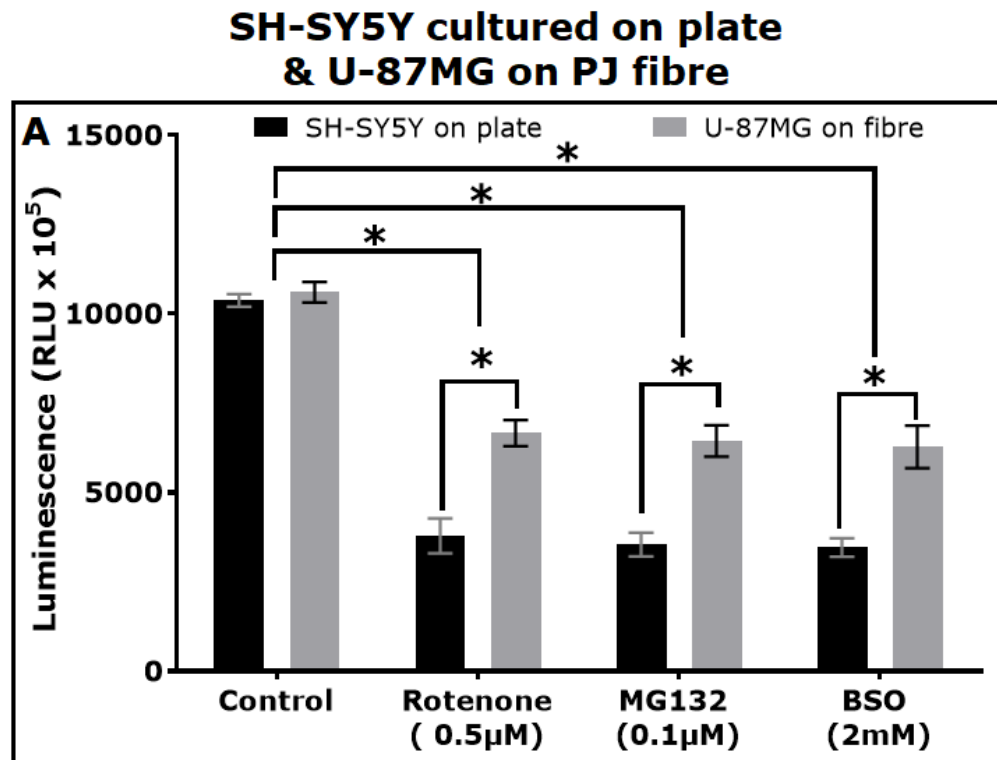


**Figure 4. 23 Co-culture cell viability of SH-SY5Y and U-87 MG** showing SH-SY5Y cells cultured on TCP and U-87MG on PJ fibre. . Both cells were differentiated and exposed to toxins Results are expressed at the mean ratio  $\pm$  SEM  $n=3$  \* $P<0.005$  against plate vs fibre and control vs treatment was determined two-tailed Student-T test and Two-Way ANOVA with Sidak's Multiple Comparison tests.

#### 4.3.9.2 Co-culture with glial cells on the 2D surface and neuronal cell on PAN fibre

In this experimental set, we assessed how astrocytes could influence the growth of neuronal cells cultured on fibres when exposed to toxins. The SH-SY5Y cells were cultured on PAN fibre, and the U-87MG cells were cultured on a TCP. Similar to the previous experiment, both cells were induced to differentiate with B27 supplement and was performed the same as the previous experiment in section 4.3.9.1.

### SH-SY5Y cultured on PAN fibre and U-87MG on plate

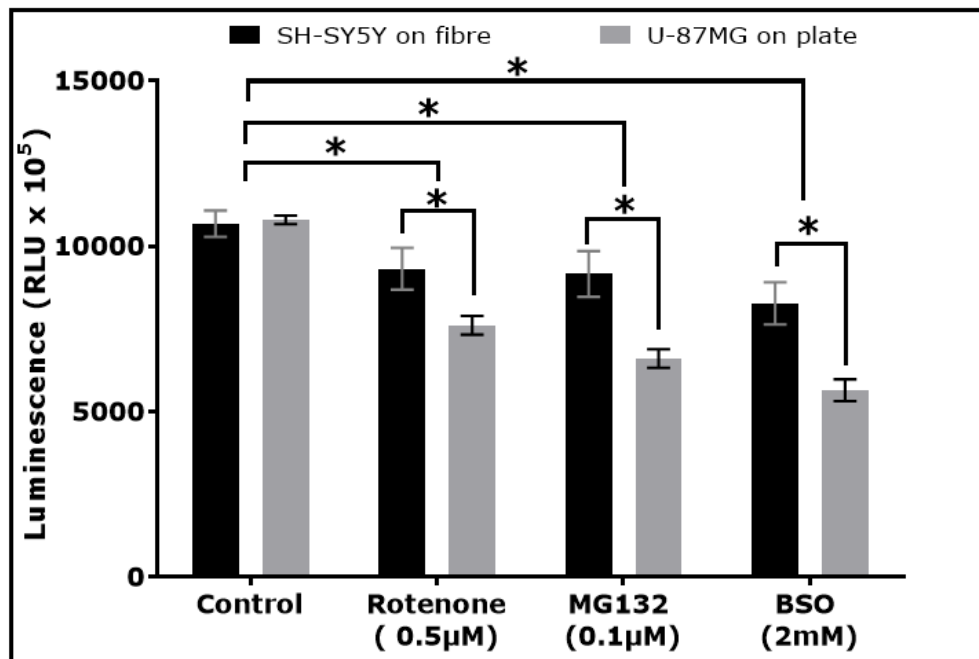


**Figure 4. 24: Co-culture cell viability of SH-SY5Y and U-87 MG.** SH-SY5Y cells cultured on PAN fibre and U-87 MG on TCP. Both cells were differentiated and exposed to toxins Results are expressed at the mean ratio  $\pm$  SEM  $n=3$  \* $P<0.005$  against plate vs fibre and control vs treatment was determined two-tailed Student-T test and Two-Way ANOVA with Sidak's Multiple Comparison tests.

Similar to the previous experimental set up (section 4.3.9.1), both SH-SY5Y and U-87MG cells showed significantly poor cell viability due to the toxin exposure compared to the control (figure 4.23 B). Presence of astrocytes may not have influenced the survival of neurons, but neurons on PAN showed slower cell death compared to neurons on a plate in the presence of astrocytes. Astrocytes cultured on the plate was more susceptible to toxins and expressed low cell viability.

#### 4.3.9.3 Establishment of a 3D nanofibre based co-culture model with differentiated neuronal and glial cells.

In this experimental set up of co-culture, both neuronal and glial cells were cultured on PAN and PJ fibres, respectively. This experiment assessed the ability of 3D scaffold and astrocytes to act together in supporting neuronal cell survival. Both cells were differentiated using

B27 for five days then arranged to form the co-culture as shown in figure 4.22 A. The neuronal cells were placed in the bottom the glial cells on the top separated with a hollow spacer and exposed to low levels of Toxins. As both cells were cultured on fibre, the experiment was continued for 20 days, and the viability of the cells was measured using CellTiter-Glo® 3D ever every 3 days as described in section 2.2.11. Our results showed that (figure 4.24), in general, neurones cultured on PAN fibre exhibited prolonged survival in the presence of toxins when cultured as a co-culture along with astrocytes. Similar effects were also observed in astrocytes cultured on PJ fibre. Both cells type showed prolonged survival for nine days and very gradual cell death after day 11. No significant difference was observed between the treatment and control up to day 11 on both SH-SY5Y (Figure 4.24 A) and U-87 MG (Figure 4.25 B). After 11 days both cell viability started to decline and expressed a significant difference between treatment and control. When differentiated SH SY5Y (Figure 4.24 C) and U-87MG (Figure 4.24 D) cells were cultured separately on nanofibre scaffolds and exposed to toxins for 72 hours, both cell types showed a loss of survival representing heightened sensitivity to the toxins. Compared to the individual culture longer survival and higher resistance to the toxins were observed in the co-culture of neuronal and astrocytes.

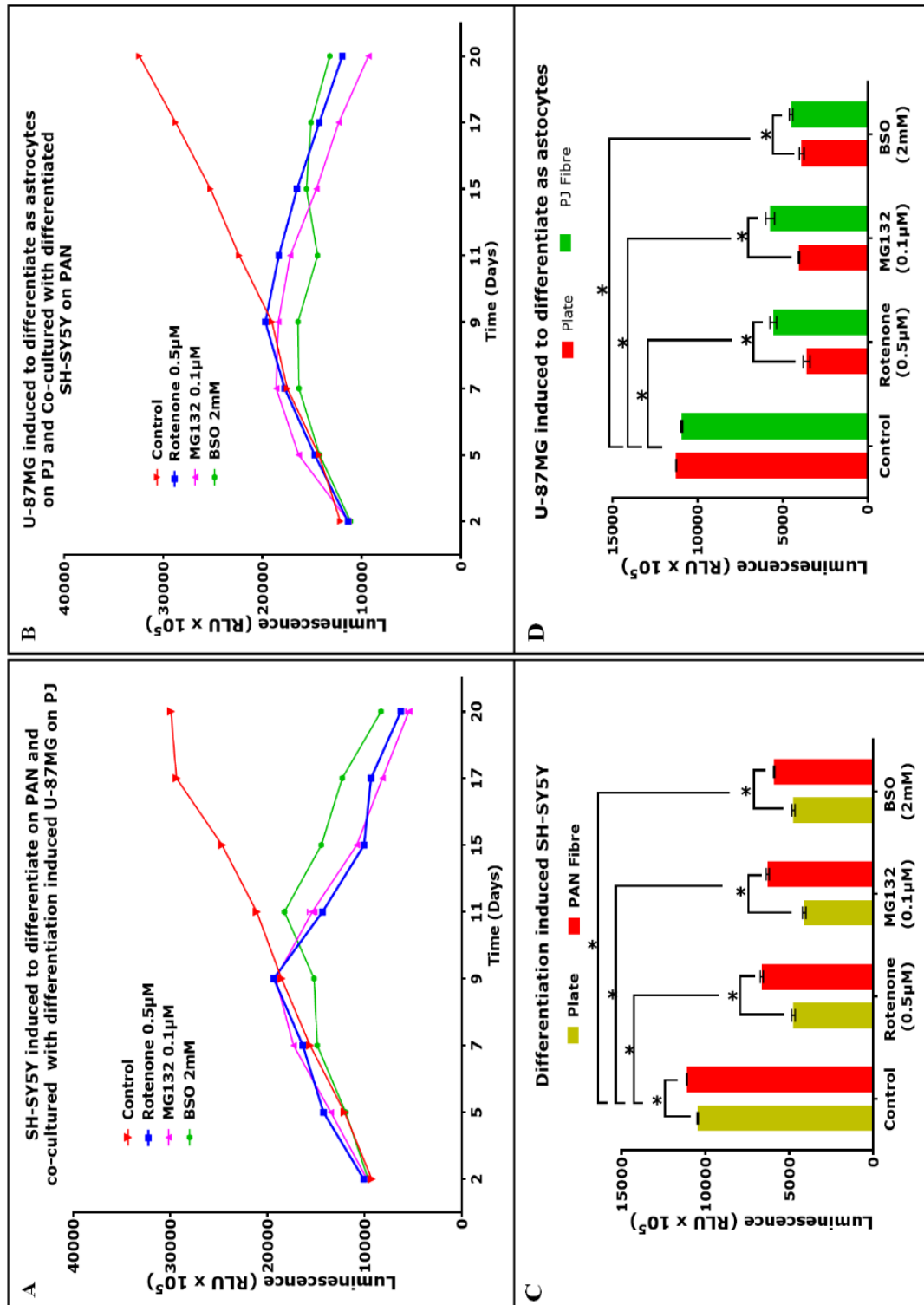


**Figure 4. 25 Effect of toxins on differentiated SH-SY5Y cultured on PAN and U-87MG cultured on PJ in a co-culture model.**

Graph A shows differentiated neuronal and graph B astrocytes viability in co-culture exposed to toxins. C and D shows individual cultures differentiated for 5days and exposed to toxins for 72 hours. Results are expressed at the mean ratio + SEM n=3 \*P<0.005 against control vs treatment for each measurement was determined by Two-Way ANOVA with Sidak's multiple comparisons test.

#### 4.4 Discussion

The principal aim of this study was to create a nanofibre scaffold that was capable of attachment, growth visualisation of cells and able to perform functional biological measurements. In the previous chapter, we demonstrated that we could manufacture different models of nanofibre scaffolds that were suitable for different *invitro* cell type models. Biomaterial scaffolds can support and provide a suitable habitat for the cells to attach, proliferate and differentiate (Chan, B. and Leong 2008). In this study, PAN, a synthetic resin, was chosen for synthesising nanofibre scaffolds based on their beneficial structural properties including strength and toughness. Jeffamine<sup>®</sup> is a synthetic compound containing terminal amine groups on polyethene oxide polymer. In this chapter human SH-SY5Y neuroblastoma and human U-87MG glioblastoma cell lines were used to investigate the ability of the synthetic nanofibre scaffolds to facilitate biological functions including cell adhesion, proliferation & differentiation. Initially, the fibres were electrospun on full-length polyester sheets which were cut into shapes to fit in well plates. When cells were cultured on these sheets of fibres, it was noticed that the cell migrated to the edges of the fibre and many cells were found attached to the loose fibre (figure 4.3) this led to an idea of fully suspended nanofibre scaffolds. A study has shown that polyester and polypropylene can be negatively charged, thus causing the cells to be repelled at loose ends of the fibre mats (Yovcheva, Avramova, Mekishev, et al. 2007). When cultured on suspended scaffolds, a number of cells were found attached to the centre of the scaffold in comparison to the plate (figure 4.4). The cell distributions and cell attachment were confirmed by Coomassie blue staining and immunofluorescence analysis.

Several studies have demonstrated that aligned fibre can promote cell alignment and guidance. Aligned fibre has been used in several studies that involve muscle regeneration, cell migration and fibre alignment for ligaments in rodent models (Ahmed and Brown 1999; Aviss, Gough and

Downes 2010; Shang, Yang, Cheng, et al. 2010). The major drawback of several studies was that it lacked the structure to hold the fibre intact throughout the study, and they were pseudo-3D scaffolds. The model developed in this study is fully suspended real 3D model that is multiple orientations in a single scaffold. We have demonstrated that the neuronal and glial cells are capable of attaching and growing on the aligned fibre model. Our immunofluorescence images have shown that the aligned fibres support a corresponding cell pattern attachment and growth organising cells along the direction of the fibres. The direction of cell growth on aligned vs random fibre was assessed with images using Fast Fourier Transform (FFT) analysis. This was performed by another team member and has been reported in his work.

This study was primarily focused only on random fibres. The results show that PAN and PJ nanofibres are suitable biomaterials to produce random nanofibre constructs that support neuronal and glial cells, respectively. The biomaterial preference for each cell type was evident in each cell type's ability to attach and grow throughout 11 days of culture on nanofibre scaffolds. In both cases, cell growth and survival were maintained for longer on nanofibre scaffolds compared to conventional tissue culture plastic. Several studies have reported the benefits and enhancement of cell metabolism when cultured on the 3-dimensional nanofibrillar surface due to its 3D structure and larger surface area-volume ratio compared to a TCP (Farzaneh, Pournasr, Ebrahimi, et al. 2010; Mahairaki, Lim, Christopherson, et al. 2010). The preferential attachment and growth of glial cells to PJ rather than PAN highlight potential differences in the ECM which promotes the adhesion and proliferation of cells (Frantz, Stewart and Weaver 2010; Hinz 2015). The composition of nanomaterials influences cell growth & survival due to topographic and biochemical cues induced by their unique physical and chemical properties (Chueng, Yang, Zhang, et al. 2016). When growing co-cultures, it is potentially more desirable to culture cells onto a multi 3D surface that is capable of mimicking the native ECM. The improved

growth and survival of both cell types could also be attributed to the physical properties of the nanofibre. Nanofibres were spun to produce a fully suspended 3D nanofibre structure allowing a greater surface area access to nutrients when cells were cultured on these scaffolds compared to pseudo-3D structures. Similarly, the flow rate was optimised to 1mL/hour for a maximum of 2 hours, since electrospinning larger volumes resulted in highly dense scaffolds. Dense fibres may help in holding cells trapped but not support cell attachment and growth, also impedes the visual monitoring of cells.

Currently, no comparative information is available for neuronal and glial cells cultured on nanofibres electrospun using PAN and PJ. Initial experiments confirm that both glial and neuronal cells are capable of attaching to PAN and PJ fibres and were able to proliferate. Results from Coomassie blue staining (figure 4.4) immunofluorescence (figure 4.6) and SEM imaging confirmed this (figure 4.7). The proliferation assay experiment suggested that SH-SY5Y cells express improved survival and proliferation on PAN than PJ fibre, while U-87MG cells were found attached to both fibre types. Furthermore, increased cell number and survival was seen on PJ than PAN for U-87MG cells. The prolonged survival of each cell on different fibre type was confirmed by culturing the cells for 11 days and investigating the cell metabolic activity. Data (Figure 4.8 and 4.9) obtained from both fibre types and plate showed that the cells were able to survive longer in fibre than the plate. This may be due to the larger surface area; a suitable scaffold material and the cells were able to utilise nutrients entirely from the media. SH-SY5Y cells showed prolonged survival on PAN and U-87MG on PJ fibre. The ability of these cells to adapt to specific surfaces opens up a wide range of possibilities including targeted cell growth, creating cell channelling and surface-specific 3D neurodegenerative disease models.

It was essential to understand the ability of both SH-SY5Y and U-87MG cells to differentiate on fibres. After identifying and confirming suitable

nanofibre, both cell types were exposed to the differentiating inducing agents, RA for SH-SY5Y and dbcAMP for U-87MG (Tiryaki, Ayres, Ahmed, et al. 2015; Korecka, van Kesteren, Blaas, et al. 2013; Fedoroff, McAuley, Houkle, et al. 1984). The B27 supplement is a commercially available product that is commonly used for the survival and maintenance of primary neurons (Roth, Zhang, Chiu, et al. 2010; Kovalevich and Langford 2013) and was used in this study as an alternative differentiating agent. Our results showed that both cell lines were capable of differentiating on fibre. SH-SY5Y cells showed extended axonal growth on PAN fibre (Figure 4.11), and U-87MG cells expressed higher levels of GFAP, but the differentiated cells appeared to form into clusters (Figure 4.14). Limited cell growth and cell differentiation were observed when SH-SY5Y and U-87MG were cultured on PJ and PAN fibre respectively. Expression of phosphorylated neurofilament H (NF-H; SMI34) (figure 4.15),  $\beta$ III tubulin (figure 4.16) and synaptophysin (figure 4.17) for SH-SY5Y cells and high levels of GFAP (figure 4.18) expression for U-87MG cells were also confirmed using western blot analysis. Indeed, western blot analysis clearly showed increased neurofilament SMI 34 levels representing a neuronal marker of maturity (Gray, Rice, Nightingale, et al. 2013),  $\beta$ III tubulin; a mature neuronal marker (Choi, S. H., Kim, Hebisch, et al. 2014), and synaptophysin; a synaptic and neuronal synaptic marker (Lee, T. T., Chana, Gorry, et al. 2015) all showed increased levels when SH-SY5Y cells were grown on PAN fibre compared to tissue culture plates and PJ fibre. Elevated levels of GFAP, a standard marker for astrocytes (Tong, J., Ang, Williams, et al. 2015), was evident in U87-MG cells grown on PJ fibre. Furthermore, these levels were elevated in response to either dbcAMP or B27 supplementation.

Once confirmation was obtained showing of both cell type was capable of nanofibre growth and differentiation, we examined the response of both SH-SY5Y and U-87MG to toxins cultured both on plate and fibre. Rotenone and MPTP are commonly used to induce complex 1 inhibition (Innamorato, Jazwa, Rojo, et al. 2010; Tanner, Kamel, Ross, et al. 2011),

MG 132 mimics proteasome inhibition (Chan, N. C., Salazar, Pham, et al. 2011) and Buthionine-Sulfoximine (BSO) promotes glutamylcysteine synthetase inhibition (Smeyne and Smeyne 2013). We, therefore, used rotenone, MPTP, MG132 and BSO to create sub-lethal conditions in SH-SY5Y and U-87MG cells cultured on both TCP and PAN / PJ fibres. Our results showed that the cells on fibre exhibited higher sensitivities to the different toxins compared to cells grown on conventional TCP. Cells cultured on both fibres showed a similar effect, but cells SH-SY5Y cultured on PJ and U-87MG on PAN showed more significant loss of cell viability due to the toxins. This may be due to the increased cell surface area in contact with the toxins on fibre compared to cells cultured on a flat 2D culture plate (Figure 4.19 and 4.20).

Several studies have also shown that glial cells are one of the essential integral functional element supporting neurons for responding to neuronal activity regulating synaptic transmission, plasticity and neuronal protection (Hillen, Burbach and Hol 2018). To examine the effect glial cells can have on a neuronal cell population we cultured neuronal cells on a plate with glial cell stripped ECM as a feeder layer. Our results show much matured axonal projection and neuronal growth after 14 days of culturing. The cells were cultured in 1% serum condition without any differentiating agents. When compared to the control the cells cultured on the feeder layer showed very long axonal projection and network connections. The matured axonal growth was confirmed with  $\beta$ III tubulin staining on an immunofluorescence microscope (Figure 4.21). Due to the limitation in time, this experiment was not performed on nanofibres, but this method could make inhabitable neuronal surfaces like PJ to become a neuron-supporting surface and can provide more natural ways for axonal elongations.

From understanding the effect of glial ECM on the neuron, we designed a 3D co-culture model that can bring both differentiated neuron and astrocytes to a proximity to provide neurotrophic factors and support

biochemically against low levels of neural toxins. Several studies have shown that astrocytes play a significant role in providing neuroprotections and a vital role in the CNS (Takuma, Baba and Matsuda 2004; Barreto, E White, Ouyang, et al. 2011; Cabezas, El-Bachá, González, et al. 2012). Our results suggest that when either of the cells was cultured on a tissue culture plastic, the cells showed very poor cell viability. The endpoint viability for SH-SY5Y cultured on a plate and U-87MG on PJ or vice versa (figure 4.23 and 4.24) showed more significant damage due to the toxins. Whereas when both cells were cultured on their favourable scaffolds, the results indicated that neuronal cells exhibit improved survival rates when culture with astrocytes. Neuronal cells showed prolonged survival against the toxins for nine days with a gradual loss of viability only seen from the 11<sup>th</sup> day was observed. A similar effect was seen in the astrocyte cell population too (Figure 4.25). The chronic co-culture model has demonstrated the prolonged survival of cells, and two different types of cell can be cultured on a different surface to recreate realistic chronic models. With the presence of astrocytes and nanofibre, the neuronal cells were able to express resistance to the lower concentrations of toxins. Astrocytes provide the neurotrophic factor (Lindahl, Saarma and Lindholm 2017) and the nanofibre provides robust structural support leading to prolonged cell survival. Several studies have also shown that glial cell line-derived neurotrophic factors can support neuronal cell line growth and very useful to study neurodegenerative diseases (Nishiguchi, Tokugawa, Yamamoto, et al. 2003; Shishkina, Mishchenko, Mitroshina, et al. 2018). A similar effect of toxins on the undifferentiated cell was also seen when differentiated SH-SY5Y and U-87MG cells were exposed to toxins individually (figure 4.24). Both cell type were sensitive to the inhibitor and showed a higher rate of cell death. They are thus showing that both astrocyte and nanofibres played a dual role in improved cell survival in the chronic 3D co-culture model. The 3D co-culture system is not just limited to just two layers. The model can hold multiple layers capable of harbouring different brain cell types in

each layer at different proximities thus creating an *in vivo* like *in vitro* brain cell populations. The system can open up to several studies that involve investigating more than one cell thus creating more realistic grounds to test drugs and several other protective agents reducing animal trails.

#### 4.5 Conclusion

In summary, this chapter demonstrated that both PAN and PJ electrospun nanofibres are capable of harbouring SH-SY5Y and U-87MG cells. More specifically we have clearly shown that SH-SY5Y cell preferably grows on PAN fibre and U-87MG prefers PJ fibre. The chapter has also demonstrated that U-87MG can be cultured in the same cell culture medium that is used for SH-SY5Y and both cells can be differentiated with multiple differentiating agents on nanofibres. Our western blot analysis showed elevated expression of the neuronal associated protein on PAN and high expression of GFAP for U-87MG cells on PJ. We have also demonstrated that toxins that are commonly used in several neural cell degeneration related studies can be used to investigate cells cultured on nanofibres too. Cells exposed to toxins individually showed greater sensitivity whereas in our 3D co-culture model cells cultured on nanofibre expressed prolong cell survival compared to cells on plate. Using 3D nanofibre scaffolds to investigate neural cell degeneration could lead to a breakthrough in understanding the importance of providing a natural habitat for the cells and the ability of nanofibres to support the survival of different cell types. Taken further, multiple treatments could be investigated and scale up the manufacture of suspended nanofibre scaffolds in well TCP would improve high content screening models used in drug discovery and to identify possible biomarkers linked to loss of neuronal cells in neurodegenerative disease.

## Chapter 5: Stem & primary cells scaffold model

### 5.1 Introduction

#### 5.1.1 Neural Stem cells

Over the last two decades, neural stem cells (NSCs) have become the main focus of interest in developing therapeutic strategies for several CNS disorders (Oh, J., Jung, Lee, et al. 2018). With a well-understood nature of degeneration, and disease like Amyotrophic lateral sclerosis, Parkinson's disease, Alzheimer's disease, and Huntington's disease has been perhaps the most widely researched condition for the use of neural stem cells (Björklund and Lindvall 2000). Other neurological diseases like Huntington's and Alzheimer's diseases also represent potential targets for such therapies (Rossi and Cattaneo 2002). Neural stem cells have mostly been derived from adult, fetal or embryonic rodent sources limiting the capacity to grow these cells while maintaining stable phenotype with the limited passage number. Similarly, human-derived neural stem cells (hNSC) have several drawbacks that include the limited donor availability, slow rate of cell proliferation and difficulties of long term expansion (Kaneko, Kako and Sawamoto 2011). The ability of hNSCs to differentiate to multiple neuronal cells types makes them a powerful tool for both research and treatment in neurological disease. Many studies have shown that it is possible to differentiate rodent stem cells and transplant them into various animal models (Conti, Reitano and Cattaneo 2006). However, only a few earlier studies using human embryonic or foetal stem cells and demonstrate truly functional differentiation into neurons (Donato, Miljan, Hines, et al. 2007). Optimised culture conditions for immortalisation with myc transcriptional factor can improve the life span and availability of hNSCs. Two such stable stem cell-like cell lines are the ReNcell CX and ReNcell VM cell lines. ReNcell CX cells were derived from the cortical region of a human fetal brain and immortalised using c-myc, whereas ReNcell VM cells were derived from ventral mesencephalon region of the human fetal brain and immortalised by retroviral transduction with the v-

myc oncogene. Cultured ReNcell line shows the ability to multiply continually and exhibit properties of hNSCs. For example, studies have shown the expression of NESTIN in an undifferentiated state, and upon withdrawal of growth factors from the medium the cells differentiate to a mixture of neuronal and glial cell types (Hovakimyan, Müller, Wree, et al. 2012). A study conducted using the ReNcell VM cell line created a 3D culture model of Alzheimer's disease (AD) with mutations in the genes encoding  $\beta$ -amyloid precursor protein, and presenilin 1, which was able to recapitulate the hallmarks of AD pathology (Kim, Y. H., Choi, D'avanzo, et al. 2015; Choi, Se Hoon, Kim, Quinti, et al. 2016). Even though ReNcells have great potential, several practical limitations are using these cells for clinical investigation and applications, as they have a high risk of uncontrolled growth leading tumour like progressions (Donato, Miljan, Hines, et al. 2007; Oh, J., Jung, Lee, et al. 2018).

### 5.1.2 Primary cell cultures

In bioscience research, cell culture studies are a valuable asset for *in vitro* and *in vivo* experiments. Cell culture techniques allow for more controlled manipulation and development of cellular functions and processes. For many decades, cell culture studies have been based on established cell lines have led to several scientific advancements; however, it has become increasingly necessary to interpret data from such cell lines with caution. Multiple studies have also pointed out the misleading, misidentified and contaminated cell lines, which has led to increased concerns and a great interest in the use of primary cell culture (Allston-Roberts, Barallon, Bauer, et al. 2010; Lorsch, Collins and Lippincott-Schwartz 2014). Many research studies are performed on cell lines due to several factors, such as they are readily available, have high proliferation capability; they are relatively easy to culture and transfect. Cell lines are often cultured and maintained over decades, forcing them to adapt to the 2D culture environment resulting in altered morphology and genetic drift making

them different both genetically and phenotypically to their tissue of origin (Alge, Hauck, Priglinger, et al. 2006; Pan, C., Kumar, Bohl, et al. 2009).

In primary cell culture, cells are isolated directly from tissue and established to grow *in vitro*. Cells isolated from a tissue have a finite lifespan depending on the cell type. Most primary cell cultures cannot be expanded whereas few may have minimal expansion capacity. Primary cells hold the morphology of a normal cell and will maintain many of the essential properties and markers that are usually observed well *in vivo* (Pan, C., Kumar, Bohl, et al. 2009). Despite these multiple advantages, the primary cell culture is very challenging, and most cell types require particular conditioned culture media. Practices like culturing primary cells on to more physiologically relevant substrates or materials can significantly improve cell attachment, growth and purity. Primary cell culture systems can be an excellent model for studies in cancer research, virology, drug screening, toxicity, vaccine production and tissue engineering. The main advantage of using primary cell culture is that the cells are non-transformed and non-immortalised. Therefore, they are capable of mimicking a living model yielding more physiologically relevant results. In the case of functional activities and experiments, primary cells have a very distinctive receptor profile, express unique enzymes and other signalling pathways that work in a manner not found in non-primary cells (Uysal, Sevimli, Sevimli, et al. 2018). Primary cultures replicate more closely what happens *in vivo*, where cells like neurons stop dividing and undergo differentiation to take on their individual functions. Similarly, when primary cells are cultured in a culture dish, they tend to follow a similar trajectory ([Lab Manager Feb 9<sup>th</sup> 2016](#)).

Recently interest has risen in using primary cells in 3D cell culture models, as they can produce more biologically representative systems showing similar properties as an *in vivo* multicellular environments (Edmondson, Broglie, Adcock, et al. 2014). For example, a study on primary hepatocyte cultures showed that when cultured as a monolayer on plastic the cells

stayed undifferentiated and died within a few days, whereas they survived for almost three weeks and exhibited differentiation when cultured in a 3D culture of collagen gel matrix (Gómez-Lechón, Jover, Donato, et al. 1998). Primary cells cultured in 3D cell culture models are showing better success in attempts to engineer physiologically relevant cells and tissue models (Justice, Badr and Felder 2009). A significant difference is observed between cells cultured in a tissue culture dish versus a 3D culture system, regarding the access to soluble factors and the distribution and types of cell to cell interaction (Hoffman 1993; Schmeichel and Bissell 2003; Yamada, Pankov and Cukierman 2003). Many studies have encountered more of a spherical distribution of cells on a 3D compared to a 2D culture system, and in the case of cells like a primary neuron, it allows them to develop outgrowths in all directions in a 3D culture. One study has shown increased cell viability of neurons harvested from an embryonic brain when cultured in 3D compared to a monolayer culture (Fawcett, Barker and Dunnett 1995). Multiple studies have reported longer neurite outgrowth, longer survival and improved neuronal cell differentiation in 3D compared to 2D cultures (Bellamkonda, Ranieri, Bouche, et al. 1995; Blackshaw, Arkison, Cameron, et al. 1997; Pardo and Honegger 2000). Many other studies have mentioned similar data for multiple primary cell types in 3D culture models (O'Connor, Stenger, Shaffer, et al. 2000; Peretz, Talpalar, Vago, et al. 2007). Primary cell culture research is a critical tool for the future of scientific breakthrough and therapies and combining it with 3D culture; it will become a powerful approach for the achievement of significant advances.

## 5.2 Content of this chapter

In this chapter, we have mainly focused on two different types of cell. These are 1) neural stem cells as modelled by the ReNcell CX human neural progenitor cells line capable of differentiating into neurons and glial cells, 2) primary neurons and glial cells extracted from an embryonic day 18 rat brain hippocampus. The main aim of the work shown in this chapter was to demonstrate our in-house developed random nanofibre model was capable of supporting the growth the two different cell types and had the potential for being used as a suitable model for investigating neurodegenerative and other diseases. The chapter has demonstrated the ability of both cells types to be attached, adapt, proliferate and grow on PAN and PJ fibres. Cell attachment and proliferation was investigated using immunofluorescence microscopy and viability assay. We have also shown some preliminary experiments to investigate the effect of parkinsonism-inducing agents on stem cells. Both stem cell and primary cells were exposed to four different toxins capable of causing different biochemical changes were used. Rotenone and MPTP to induce complex 1 inhibition, MG132 inducing proteasome inhibition and BSO a glutamylcysteine synthetase inhibitor to reduce glutathione levels for a short period, and we studied the possibility for the neurons to recover with the help of glial cells and nanofibres using a co-culture model. Our preliminary experiment of the primary hippocampal cell 3D co-culture model has demonstrated that it can be a suitable model for screening neuroprotective agents and drugs suitable for neuron and related glial disorders.

## 5.3 Results

### 5.3.1 ReNcells CX human neural progenitor cell line

#### 5.3.1.1 Culturing and subculturing

The cells were cultured and maintained in a T25 flask and harvested based on experimental requirements. Prior to culturing, the flasks and TCP were coated with laminin (20 µg/ml) as described in section 2.2.4.2.1. The complete medium for culturing ReNcell CX is made using 500 ml Knockout Dulbecco's modified Eagle's medium (DMEM)/F-12, which was supplemented with 10µg human recombinant FGFb, 10 µg human recombinant EGF, 10 ml StemPro neural supplement, 5 ml of sterile-filtered L-glutamine, 5 ml of sterile-filtered 10000 U/ml penicillin and 100 µg/ml streptomycin. The complete medium was stored at 4 °C and warmed to 37 °C before use. The cells were obtained from the liquid nitrogen storage and thawed and plated by following steps mentioned in section 2.2.4.2.3. Upon reaching 80% confluency, the medium was removed, and the flask was rinsed with PBS. Cells were detached by adding 1-3 ml of accutase and incubation at 37°C for 3-5 minutes, after which the accutase activity was neutralised by adding a complete medium. Cell detachment was confirmed using a light microscope, and cells that had not detached were further detached by either tapping gently on the sides of the flask or by squirting medium using a pipette over the region. The detached cells were then transferred into a tube and pelleted by centrifugation at 300 x g for 5 minutes. The resultant pellet was re-suspended in growth medium, and the required number of cells (250,000 cells in T25 flasks and 1,000,000 cells in T75 flasks) was transferred to a sterile tissue culture flask containing pre-warmed growth medium.

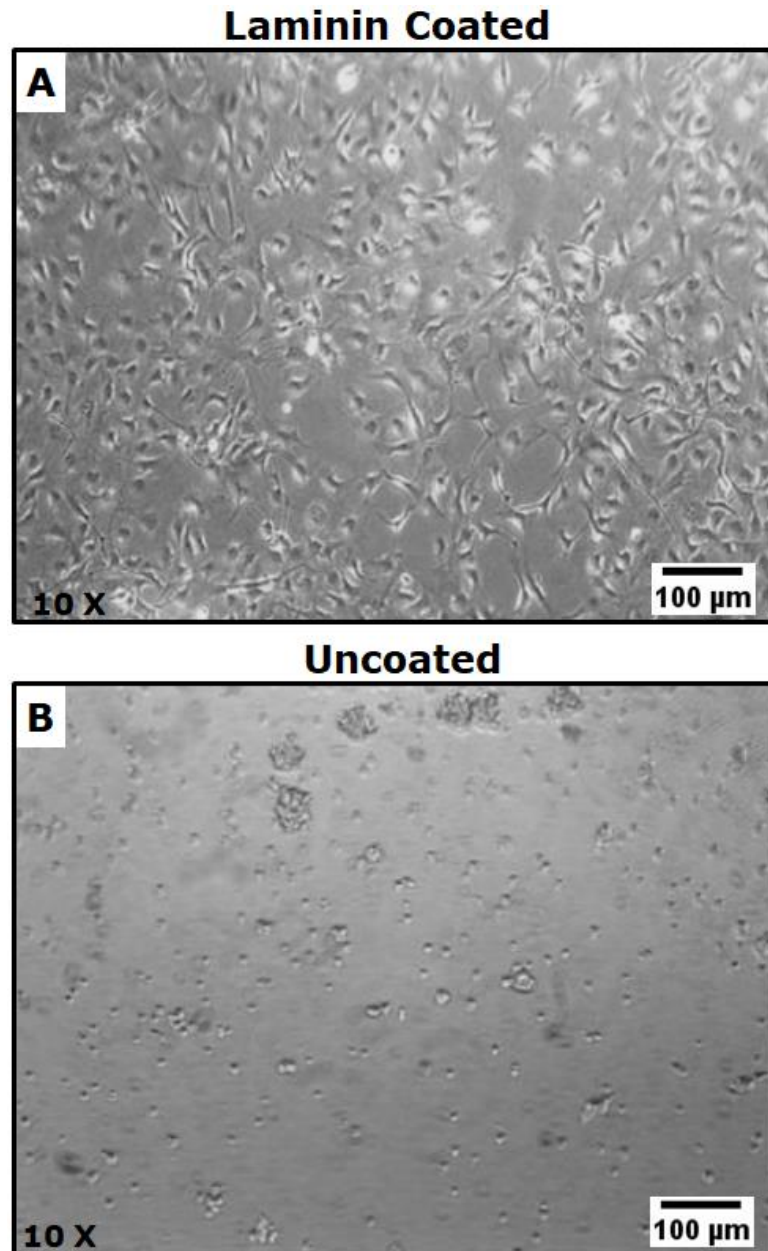


**Figure 5. 1: ReNcell CX cell attachment on laminin-coated and uncoated light microscope image.**

*(A) Represents cells cultured on the laminin-coated surface and (B) shows cells forming spheroidal clusters with no laminin coating.*

The images were obtained after the cells were cultured of 120 hours under regular conditions. Cells cultured on a laminin-coated surface adhered to the surface, proliferated and formed a monolayer, whereas the cells cultured in the uncoated flasks were still viable but stayed floating in the medium forming spheres and clusters.

### 5.3.1.2 Culturing on nanofibre scaffolds

ReNcell culture was performed on both PAN and PJ fibres. Both types of fibre scaffold were sterilised with 70 % v/v ethanol, as explained in section 2.2.5. Random fibres were used to investigate cell attachment, for which the fibres were soaked in 20 µg/ml laminin overnight before cell seeding. Cells were seeded at a density of 50,000 cells/well in each well with nanofibre scaffolds and incubated at 37°C in a humidified atmosphere of 95% air and 5% CO<sub>2</sub> for 48 hours.

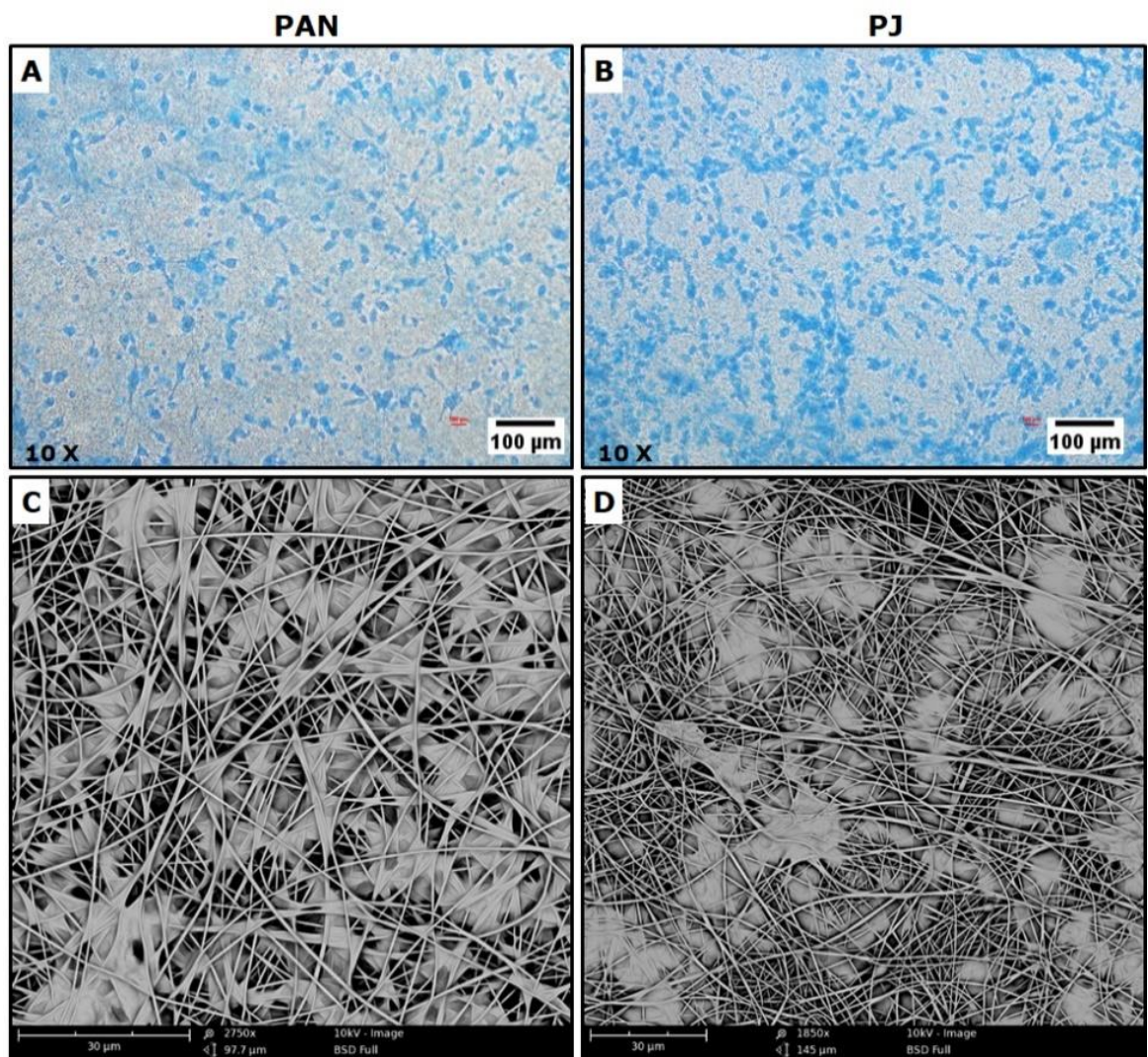


**Figure 5. 2: ReNcell culture on PAN and PJ random fibres.**

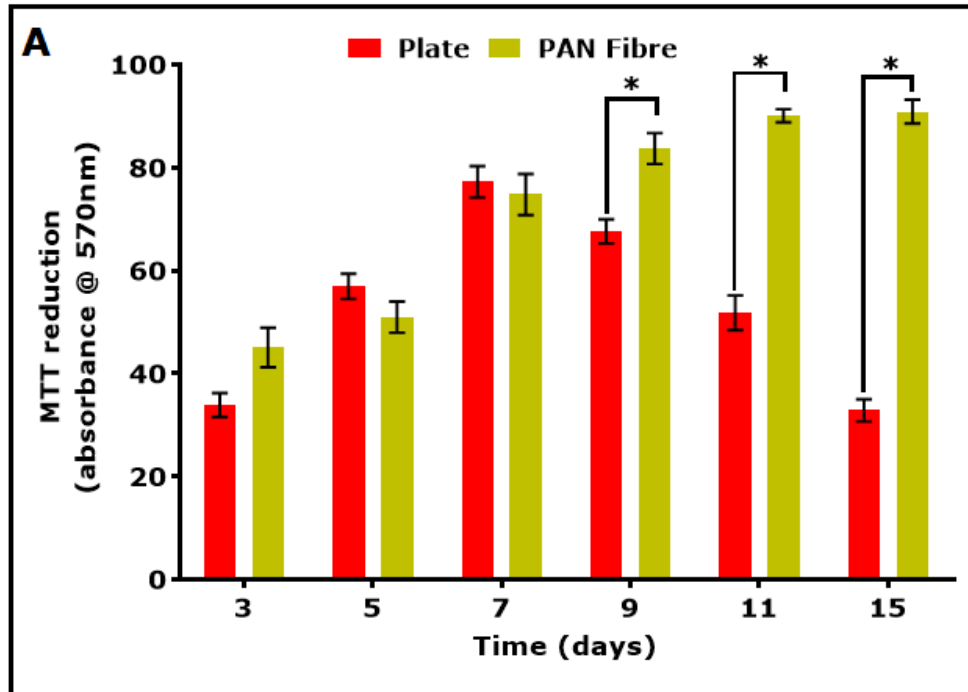
*The cells were incubated for 48 hours and stained using Coomassie blue stain (A and B). The cells were also dehydrated and examined by SEM (C and D). A higher number of cells was found attached to the PJ fibre than to PAN fibres. The image is a representative of n=6 repeats*

Two days later, the cells were stained with Coomassie blue for approximately 10 minutes. The fibres were moved to a new TCP, and both fibres and the TCP were examined using a light microscope. After examining multiple samples, a good number of cells were found attached to both PAN and PJ fibres, with more cells found on PJ compared to PAN. The cells on the fibres were also dehydrated as explained in section 2.2.9.3 and examined by SEM. The cells were found attached on both PAN and PJ; the cells were found wrapped around and growing within the fibres

### **5.3.1.3 ReNcell CX attachment and growth**

Similar to the studies on SH-SY5Y and U-87 MG cell lines, we investigated the ability of ReNcell CX cells to attach to, grow and survive in both PAN and PJ fibres. The experiment was set up as explained in section 2.2.7, and the ability of the cells to survive on fibres compared to the TCP was studied by analysing cell growth and viability by measuring their metabolic activity using MTT reduction assays on both fibres and TCP. Cells were cultured for 15 days on both plastic and fibres with metabolic activity assessed every 48 hours. The data obtained suggested that the cells cultured on both PAN and PJ had a similar growth rate and a steady increase in the metabolic activity was observed. Upon reaching 100% confluency, the cells grown on the TCP slowly started detaching and dying after 7 days in culture. ReNcell CX cells cultured on PAN also expressed a steady increase in cell number similar to that observed in the TCP. The MTT analysis demonstrated that there was no significant difference in a cell in cell growth until day 7 for cells cultured on PAN and TCP. MTT reduction after day 7 remained constant until day 15 for the cell on PAN. In contrast cells culture on PJ fibre showed a very high rate of increase in MTT reduction compared to the cells cultured on TCP increases in MTT reduction continued upto day 15.

### ReNcell CX on plate and PAN fibre



### ReNcell CX on plate and PJ fibre

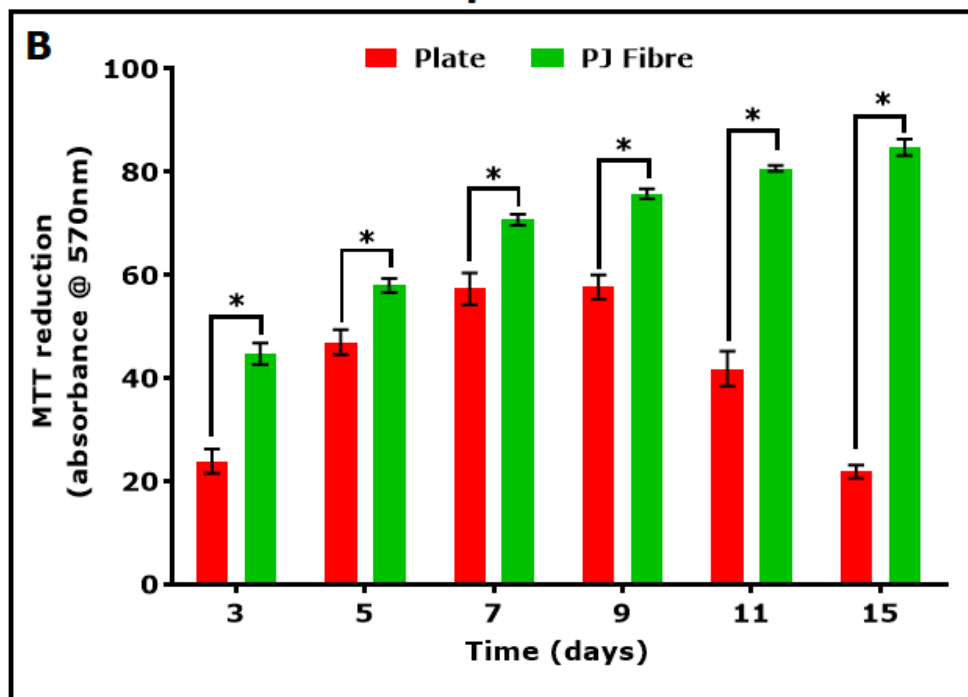


**Figure 5. 3: ReNcell CX MTT metabolic assay on PAN, PJ and TCP.** Panel (A) represents cells cultured on PAN compared to TCP and (B) represents growth on PJ compared to TCP. ReNcell CX showed a gradual increase in cell growth and survived throughout the 15 days on both PAN and PJ fibres. Results are expressed at the mean ratio  $\pm$  SEM  $n=3$  \* $P<0.005$  against TCP vs fibre determined by two-tailed Student-T test and Two-Way ANOVA with Sidak's multiple comparisons tests.

#### 5.3.1.4 Cell differentiation

As described in section 2.2.4.2.6 ReNcell CX cells were induced to differentiate by maintaining the cells in a mitogen-free medium. The cells were cultured for 24 hours, after which the medium was replaced with differentiation medium for 5 days. The ReNcell CX cells are capable of differentiating into neurons and glial cells, which was confirmed with immunofluorescence staining. Undifferentiated control was stained for mouse anti-nestin antibody, which recognises a type VI intermediate filament (IF) protein encoded by the NES gene expressed in progenitor stem cells. When differentiated, the neurons were stained with mouse anti- $\beta$ III tubulin antibody, which recognises a mature neuronal marker. Astrocytes were stained using rabbit anti-glial fibrillary acidic protein (GFAP), which recognises an intermediate filament protein expressed highly in this class of glial cells. Anti-mouse Alexa fluor 568 (red) and anti-rabbit Alexa Fluor 647 (magenta) were used as secondary antibodies. The immunofluorescence images showed that undifferentiated cells exhibited high expression of nestin and that they were spread across the fibres on both PAN and PJ fibre scaffolds. The highest expression for both  $\beta$ III tubulin and GFAP was observed on cells cultured on PJ compared to PAN. A low number of cells was observed on PAN fibre, thus resulting in reduced expression of  $\beta$ III tubulin and GFAP. ReNcell CX cells were therefore capable of differentiating on both PAN and PJ fibres

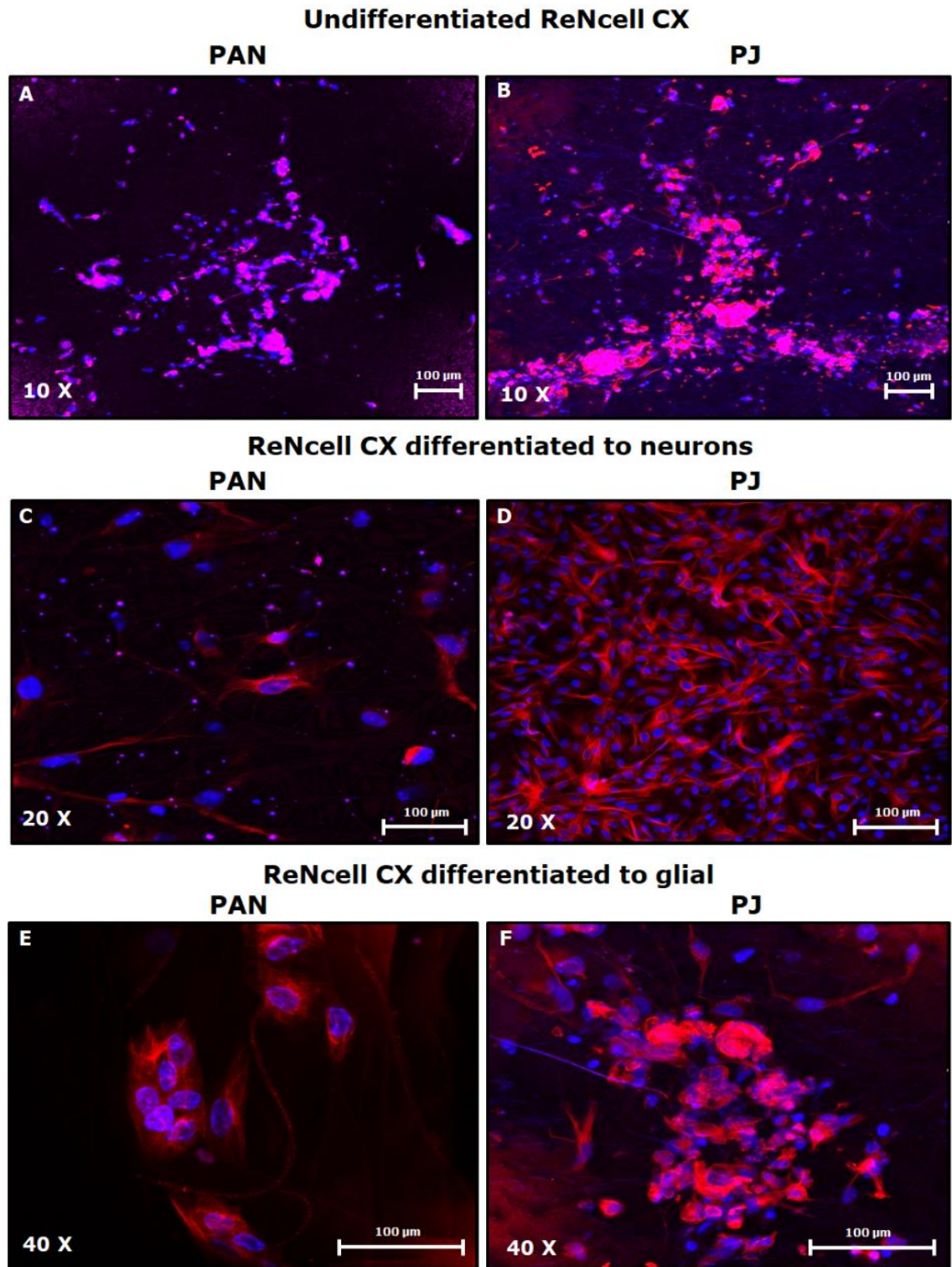


**Figure 5. 4: Immunofluorescence image of undifferentiated and differentiated ReNcells on PAN and PJ fibres.**

Panels A and B represent undifferentiated cells expressing nestin. Panels C and D represent neurons expressing  $\beta$ III tubulin. Panels E and F represent glial cells expressing GFAP.

**5.3.1.5 Effects of toxins on ReNcells CX**

Similar to the SH-SY5Y and U-87MG cells ReNcells was also exposed to toxins that can cause similar neural cell degeneration pathophysiology. ReNcell CX cells (50,000 cells per well) were cultured on PAN, PJ and TCP. After 24 hours, the cells were switched to differentiation medium for 72 hours, which was then replaced with differentiation medium containing rotenone (0.5  $\mu$ M), MPTP (2.5  $\mu$ M), MG132 (10  $\mu$ M) and BSO (2 mM). After a further 72 hours, the effect of the treatments on cells cultured on both nanofibre and TCP were examined by analysing their effect on cell viability using the CellTiter-Glo<sup>®</sup> 3D assay.

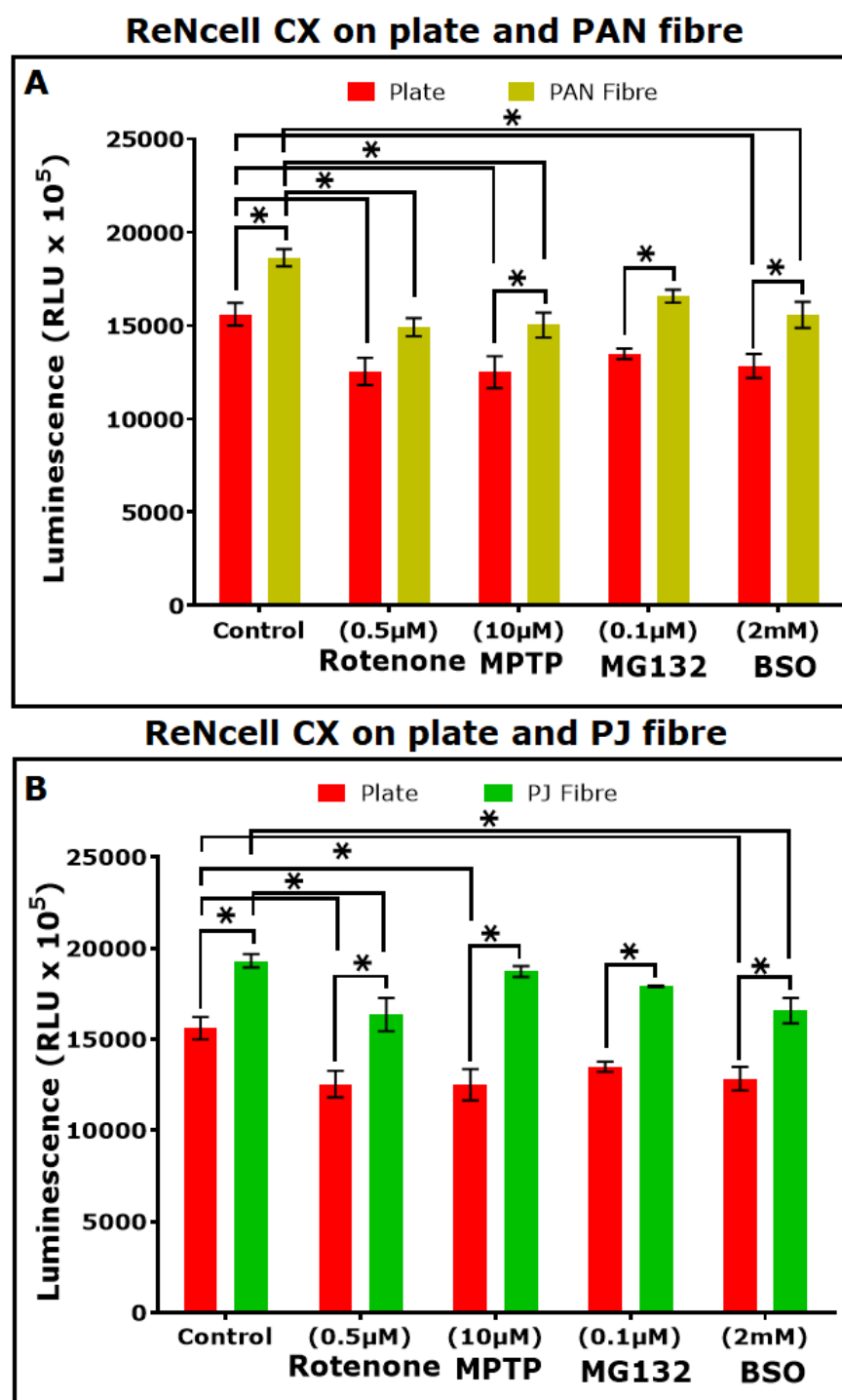


**Figure 5. 5: Effect of toxins on ReNcell CX cells.**

Cells were cultured, differentiated and exposed to low concentrations of rotenone, MPTP MG132 and BSO on PAN, PJ and the TCP for 72 hours and cell viability was measured using CellTiter-Glo® 3D assay. The results are expressed at the mean ratio  $\pm$  SEM  $n=3$  \* $P<0.005$  against TCP vs fibre and control vs treatment for TCP and fibre was determined by Two-Way ANOVA with Sidak's multiple comparisons tests

The CellTiter-Glo<sup>®</sup> 3D assay data showed that cells cultured on both TCP and fibre responded similarly when exposed to the toxins compared to the untreated control on both TCP and fibre. However, after 72 hours of exposure, cells cultured on the TCP showed about a more significant reduction in cell viability compared to both PAN and PJ fibres. The cells cultured on PAN showed a significant reduction in cell viability for rotenone, MPTP and BSO compared to the TCP whereas when treated MG132 cells on PAN expressed similar cell viability as the cells on the TCP (Figure 5.5 A). In contrast, cells cultured on PJ showed better resistance to the treatment. Significantly higher cell viability was observed on PJ for all treatments compared to the TCP (Figure 5.5 B).

### **5.3.2 Primary neurons and glial cells**

#### **5.3.2.1 Culturing of primary cells on TCP and fibres**

Hippocampal tissue from an E18 rat was used to extract neurons and glial cells. The tissue sample was prepared, and the cells were dissociated as explained in sections 2.2.4.3.1 and 2.2.4.3.2. Unlike neuroblastoma, glioblastoma and ReNcell CX, primary cells were extracted and seeded directly on to the nanofibres. Before cell seeding on nanofibres, the scaffolds were immersed in PLL for 1-4 hours at 37°C or 4°C for overnight. Cells were cultured on both PAN and PJ fibres alongside PLL coated coverslips as a corresponding control. The cells obtained from the tissue comprised of a mixed population of neurons and glial cells. Two types of cell culture media were used to promote neuron and astrocyte growth. The cells were cultured in NbActive1 to promote the growth of neurons only, and NbAstro medium was used for glial cells, which promotes the growth of astrocytes. The cells were cultured for over 2 weeks with media changes every four days to remove any dead cells.

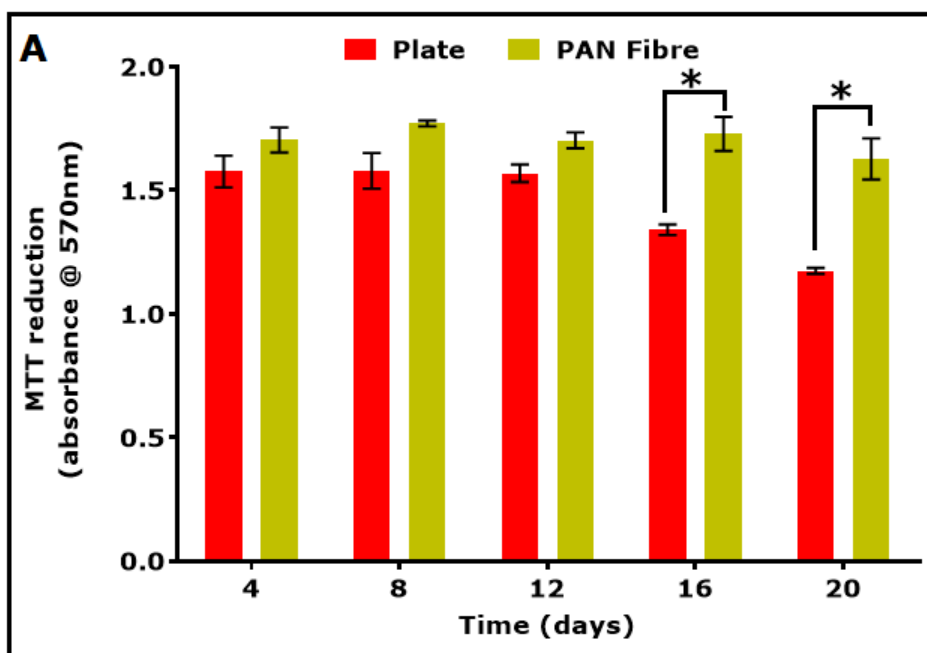
#### **5.3.2.2 Primary cell metabolic activity**

After the cells were dissociated from the primary tissue sample, 50,000 cells/well were seeded on PLL coated PAN, PJ and coverslip and then

incubated at 37 °C in a humidified atmosphere of 95% air and 5% CO<sub>2</sub>. To monitor the level of proliferation and prolonged survival, each cell types was cultured on each fibre type for 21 days alongside control cells cultured on 2D tissue culture plastic surface (control) with media changes every 72 hours. All samples were tested for cell metabolism using MTT reduction assays as explained in section 2.2.6.3. From the data obtained, (Figure 5.6) it can be seen that primary neurons cultured on the TCP and PAN fibre showed a constant level of MTT reduction. A significant decrease in MTT reduction was observed just for the cells grown on the TCP on days 16 and 20 (Figure 5.6 A). In contrast, the cells cultured on PJ fibre scaffolds showed a decrease in MTT reduction with a significant difference being observed between the cells cultured on TCP and PJ fibre (Figure 5.6 B).

Data obtained from culturing primary glial cells on TCP showed that the cells had a steady level of MTT reduction for 12 days and showed a slight progressive decrease after that. However, cells cultured on PAN showed a gradual increase in cell metabolic activity throughout the 20 day incubation period and cells on the TCP decrease in cell viability after day 12 (Figure 5.7 A). A significant difference was observed between the cells on the PAN and TCP through the experiment. A significant difference in the MTT data was seen day 8-20 when compared with day 4 (Figure 5.7 A). Whereas, the cells cultured on PJ showed a very high proliferation rate and continued proliferating for 21 days when the MTT data was analysed between each time points. A highly significant difference in the data was observed when day 4 was compared with day 8-12 (Figure 5.7 B). The cells expressed steady cell viability throughout 21 days with a significant difference when compared to the TCP.

### Primary neurons on plate and PAN fibre



### Primary neurons on plate and PJ fibre

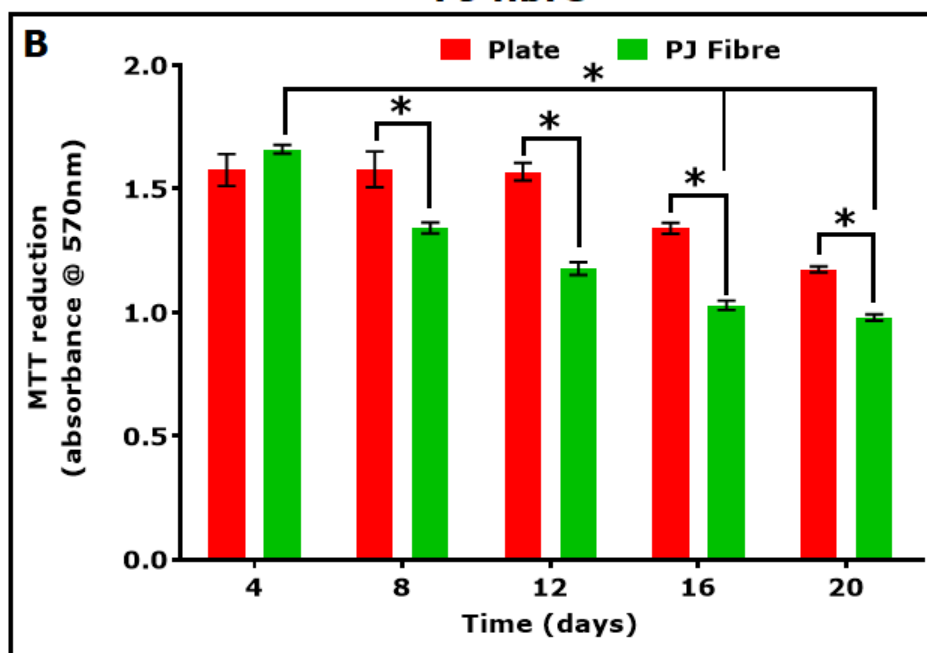
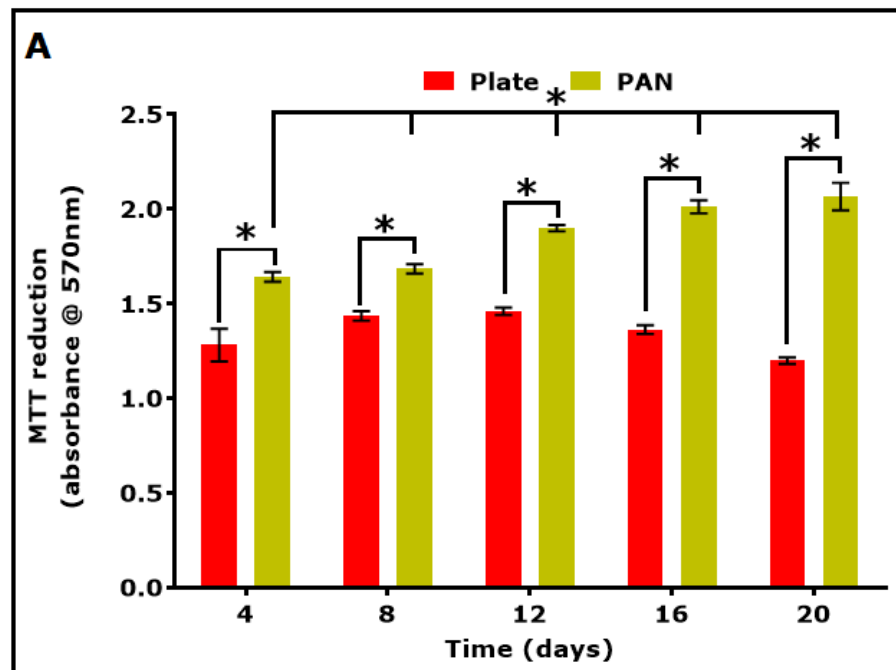


**Figure 5. 6: MTT metabolic assay of primary hippocampal neurons cultured on PAN, PJ fibre compared to TCP.**

The cells were maintained in culture for 21 days, and the metabolic activity was measured every 72 hours using MTT reduction assay. Results are expressed at the mean ratio  $\pm$  SEM  $n=3$  \* $P<0.005$  against TCP vs fibre and between the time points was determined by Two-Way ANOVA with Sidak's multiple comparisons tests.

### Primary Glial cells on plate and PAN fibre



### Primary Glial cells on plate and PJ fibre

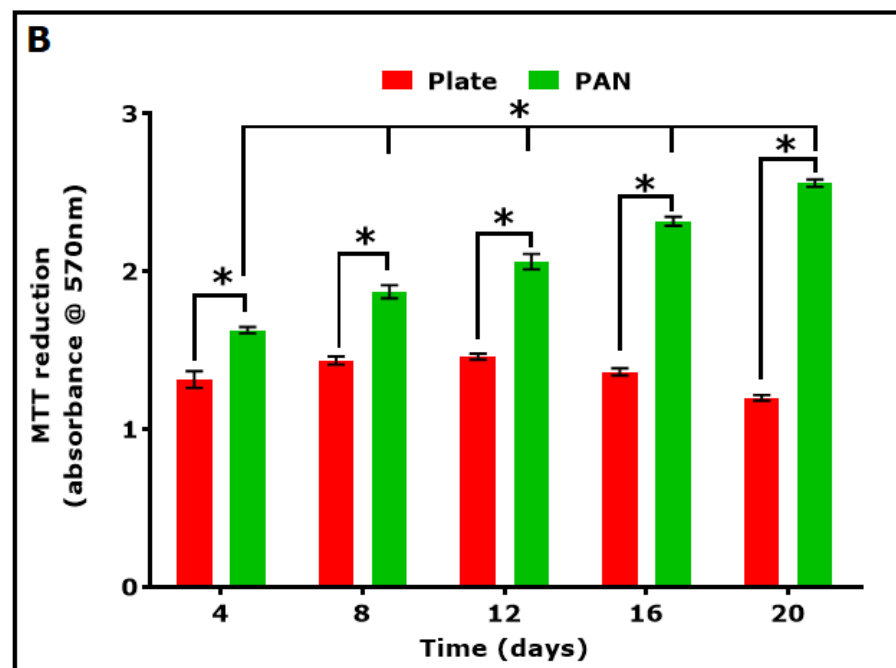


**Figure 5. 7: Primary hippocampal glial cell viability assay on PAN, PJ fibre compared to the TCP.**

The cells were maintained in culture for 21 days, and the cell viability was measured every 72 hours using MTT reduction assay. Results are expressed at the mean ratio  $\pm$  SEM  $n=3$  \* $P<0.005$  against TCP vs fibre and between the time points was determined by Two-Way ANOVA with Sidak's multiple comparisons tests.

### 5.3.2.3 Immunofluorescence

Primary neurons were cultured only on PAN, and glial cells were cultured only on PJ fibres due to the limited number of tissue samples available. A total of 50,000 cells per well were seeded onto each fibre type and incubated with appropriate media at 37°C in a humidified atmosphere of 95% air and 5% CO<sub>2</sub> for 21 days. After 21 days, the cells growing on scaffolds were fixed using 90% v/v methanol in TBS and then stained for immunofluorescence imaging as described in section 2.2.9.2. The primary neurons were incubated with rabbit anti-synaptophysin antibodies to show synaptic activity across the fibres and monoclonal mouse anti- $\beta$ III tubulin antibody to show mature axonal elongation. Glial cells were incubated with rabbit anti-GFAP only to detect astrocytes. Alexa Fluor 532 anti-rabbit Ig was used for detection of synaptophysin, whereas anti-mouse Ig and anti-rabbit Ig Alexa Fluor 568 was used for detection of primary antibodies bound to  $\beta$ III tubulin and GFAP, respectively. Scaffolds were placed on glass slides with anti-fade mountant vectorshield containing DAPI to stain nuclei. When observed with the aid of a confocal microscope, neuronal cells (figure 5.7) showed mature network connections between multiple cells. Axonal projections (red) were observed throughout the fibres (green) in all directions, and a large number of synapses (yellow) were observed throughout the sample (Figure 5.8). The nanofibres were able to support and act as a track to guide axons to connect with neighbouring cells, creating complex systematic network connections. Primary glial cells (figure 5.9) were stained only for GFAP, which is a standard marker that is strongly expressed in astrocytes. A large number of astrocytes (red) was observed. Other glial family cells were also observed within the fibre scaffold which only showed nuclei stain (blue) with no GFAP expression. These cells may have been oligodendrocytes, microglial or ependymal cells.

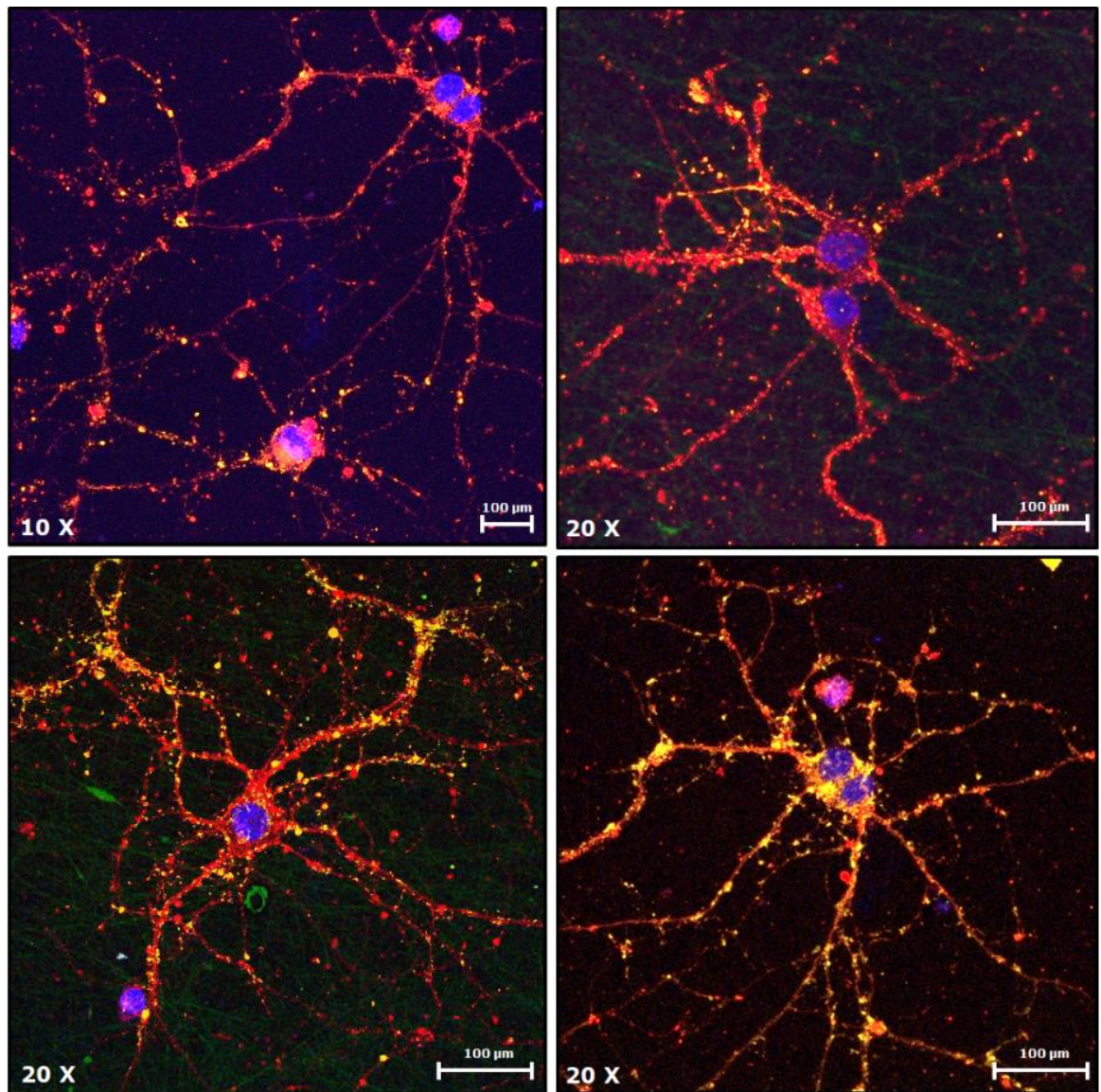


**Figure 5. 8: Immunofluorescence image of primary hippocampal neurons cultured on PAN scaffolds.**

Cells were cultured for 21 days and were stained for  $\beta$ III tubulin (red), synaptophysin (yellow) and nuclei (blue). Green represents the autofluorescence from the fibres.

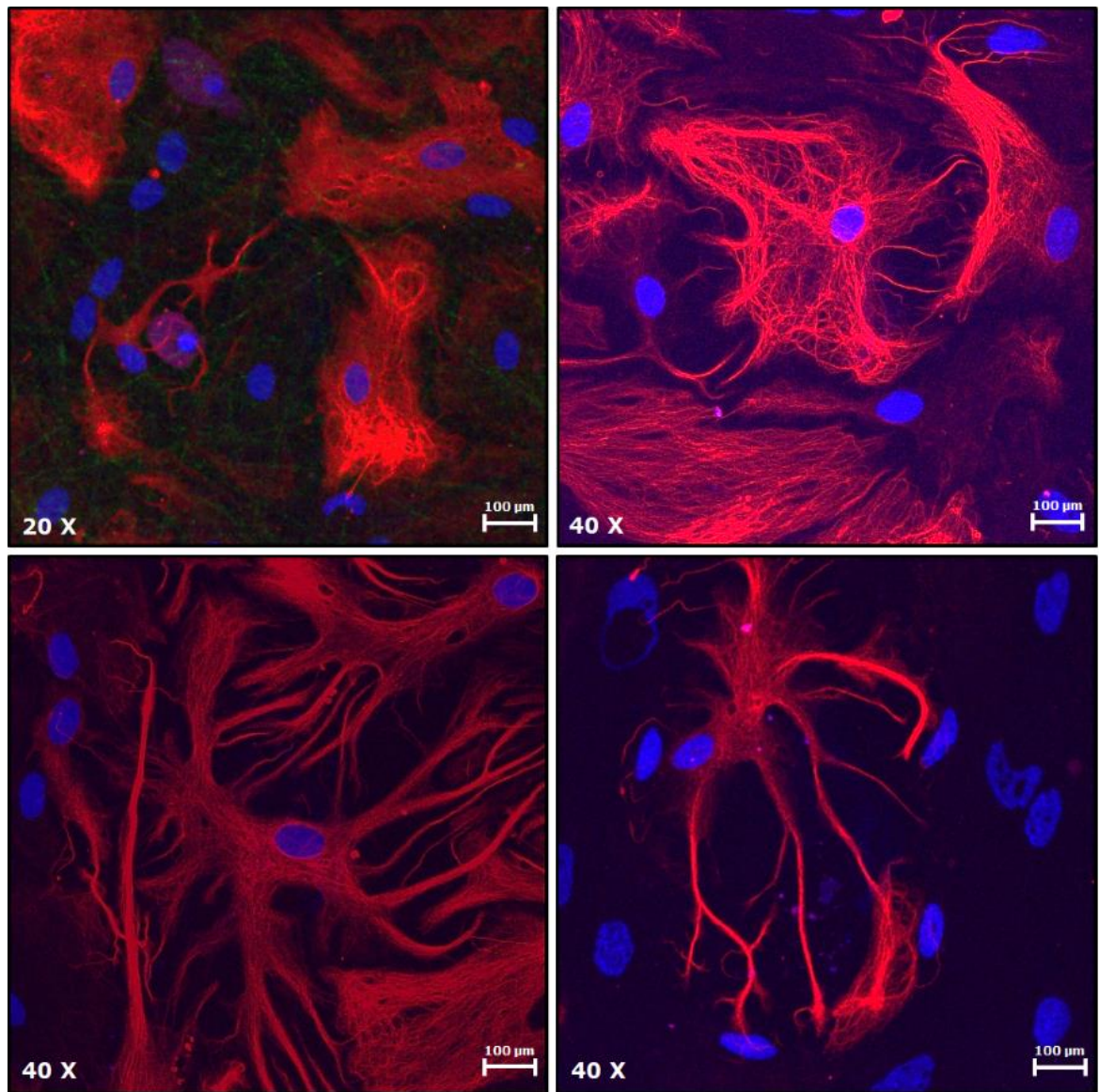


**Figure 5. 9: Immunofluorescence image of primary glial cells from hippocampal tissue.**

*The cells were cultured on PJ scaffolds for 21 days in NbAstro medium, before being fixed and stained for GFAP (red) and nuclei (blue). Green represents the autofluorescence from the fibres. Cells that do not express GFAP showed only the nuclei stain.*

#### **5.3.2.4 3D co-culture model**

This experiment aimed to investigate the recovery of primary neuronal cells on nanofibre scaffolds, after being exposed to low concentrations of toxins in the absence and presence of nanofibre scaffolds containing primary glial cells. The 3D co-culture system was set up as described in section 2.2.12. The co-culture model can be investigated with three

different experimental set. Due to the limitations in the availability of tissue samples the co-culture model was investigated only with multi fibre layered model. Primary neurons were cultured on PAN, and primary glial cells were cultured on PJ fibres. The cells were dissociated from the hippocampal tissue sample and were seeded on to the fibres with the appropriate culture medium to promote either neuronal or glial cell growth. After 7 days in culture, the primary neuronal cells were exposed to rotenone (0.5  $\mu\text{M}$ ), MG132 (10  $\mu\text{M}$ ) and BSO (2 mM) incubated for 3 days, at concentrations causing sub-lethal damage to the cells is caused in subsequent incubation periods. After that, the scaffolds were arranged, as shown in figure 2.11A. The primary neurons exposed to the toxins as layer 1 and PJ fibre containing primary glial cells as layer 2, both layers being separated with a hollow spacer. The co-culture was maintained in medium containing a 50:50 (v/v) mix of NbActive1 and NbAstro culture for 15 days. Cell viability was measured every 48 hours for each layer individually, and the medium was replaced at the same time for remaining wells. Along with the co-culture, simultaneously a separate set of neuronal cells cultured on PAN was treated with toxins for 3 days and replaced with fresh culture medium and cultured individually. The individual culture was also maintained, and viability was measured every 48 hours for 20 days.

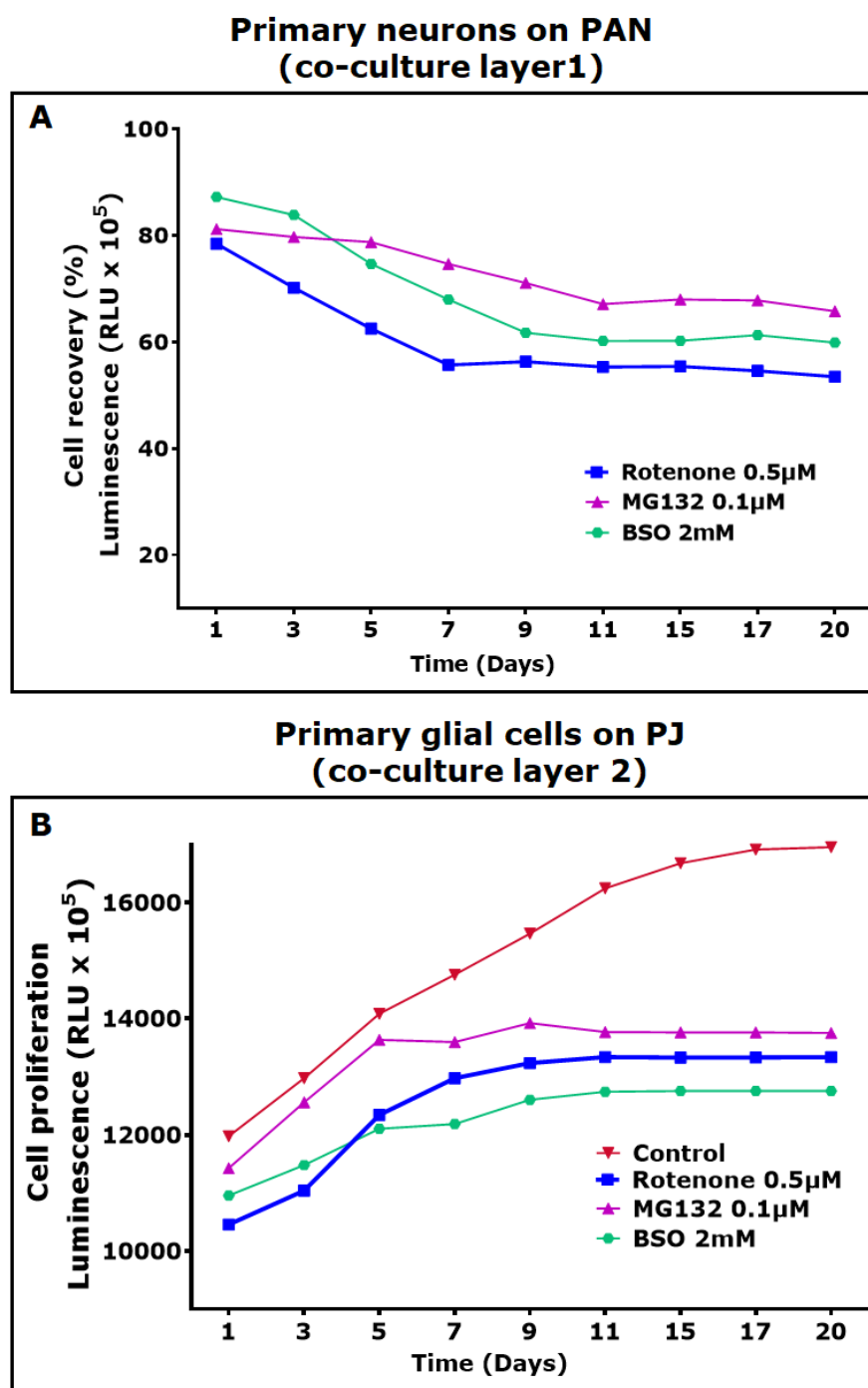


**Figure 5. 10: Primary neurons and glial cell co-culture model.** Neurons were cultured on PAN and treated with toxins for 36 hours. Following the treatment affected neuronal cells were cultured as a co-culture with healthy glial cells on PJ fibre. Every 48 hours, the scaffolds were separated and investigated for cell viability using CellTiter-Glo® 3D assay. Data shown in graph A the obtained values were converted to percentage keeping control at 100% and day 1 was set to 0% to demonstrate post-treatment neuronal recovery, and for graph B raw data was plotted to show post-treatment cell proliferation. No statistical analysis was performed as  $n=1$

The entire experiment was only performed once, and our preliminary findings suggested that the neuronal cells were affected by the toxins and continued to lose viability even after 7 days into co-culture with fresh medium. After the 7<sup>th</sup> day, the rate of cell death was reduced, and the metabolic activity of the cells was stable for the rest of the experiment. Low response to MG132 was observed, and about 50% of cell death was observed when treated with rotenone and BSO. By contrast, the primary glial cells exhibited long term survival and proliferation throughout the experiment and a slower rate of proliferation after day 7. When the primary neurons were exposed to the toxin and cultured individually without the glial cells, the obtained CellTiter-Glo<sup>®</sup> 3D data showed a much more significant decrease in viability (Figure 5.11). After 3 days of exposure, almost 70% of cells were viable, and a continuous decline in cell viability was observed throughout 20 days. By the end of the 20<sup>th</sup> day, viability was reduced to only 10% to 20% of control values for all three treatments.

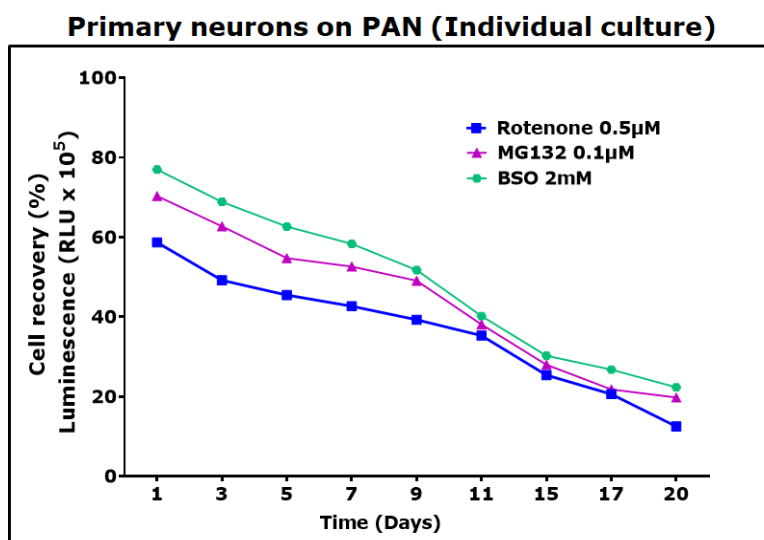


**Figure 5. 11: Primary neuron cultured on PAN and treated with toxins.**

Neurons were cultured on PAN and treated with toxins for 36 hours and then cultured in fresh medium for 20 days. Every 48 hours, each scaffold was tested for cell viability using CellsTiter-Glo<sup>®</sup> 3D viability assay. The obtained values were converted to percentage keeping control at 100% and day 1 was set to 0% to demonstrate post-treatment neuronal recovery. No statistical analysis was performed as  $n=1$

## 5.4 Discussion

This chapter mainly focused on demonstrating that random PAN and PJ nanofibre scaffolds that were manufactured in-house can be suitable to conduct studies that involve other cell types like neural progenitor and primary cells obtained from a tissue sample. Data presented in the two previous chapters have demonstrated that in-house manufactured PAN and PJ nanofibre scaffolds support the attachment and growth of immortalised neurons and glial cells. In the previous chapter, we performed a series of experiments to understand the ability to the two immortalised cell types proliferate, differentiate and react to toxins on nanofibre scaffolds. This results chapter has also followed similar experimental approaches to see if PAN and PJ fibre can be a suitable material for stem cells and primary cell cultures. The study was performed using ReNcell CX, a neural progenitor cell line capable of differentiating into a mixture of neurons and glial cells, and primary neurons and glial cells from E18 rat hippocampal tissue.

The investigation started with analysing if the ReNcell were capable of attaching to the nanofibre. ReNcell cultures require laminin to attach to a surface; therefore, all of the material and surfaces were coated with laminin before culturing the cells. From the Coomassie blue staining (Figure 5.2 A and B), we were able to identify that ReNcells were capable of attaching to both PAN and PJ fibre scaffolds. Further evaluation was made using the SEM imaging (Figure 5.2 C and D). From the SEM analysis, we noticed that on PAN fibre the cells were found attached and holding on to the intersection of two fibre strands whereas on PJ fibre the cells were more growth within the fibre and also was found wrapped around the fibre. On PJ it looks more like the cells have accepted the scaffold as a part of the cell body and used the nanofibres as a support to grow within the mat. A large number of cells were found attached to laminin-coated PCL than tissue culture plastic or uncoated surface /and PJ fibre scaffolds, we investigated their proliferation and survival on both PAN and PJ for 15

days (Figure 5.3). The attachment and proliferation analysis demonstrated that both PAN and PJ was a suitable substrate to support ReNcell CX growth. However, cell cultured on PJ fibres demonstrated a higher rate for proliferation compared to PAN and TCP. The cells cultured on PJ showed a gradual increase in cell viability for 15 days whereas cells on PAN fibre expressed a slower rate of cell proliferation similar to TCP until day 7 and then a gradual increase up to day 15. However, few studies have reported that cells cultured on TCP exhibit a higher rate of proliferation and higher survival compared to a 3D culture (Laco, Grant and Black 2013; Kijeńska, Prabhakaran, Swieszkowski, et al. 2014). In contrast to those studies, the cells cultured on both PAN and PJ showed better survival compared to the cells on TCP. The proliferation assay was only investigated on undifferentiated ReNcells; further investigation on differentiated cells may show the extended survival of neurons and glial based on the choice of material surface.

After we have shown that the ReNcell CX cells are capable of attaching and proliferating on PAN and PJ, we investigated if they were capable of differentiating to neurons and glial cells on both PAN and PJ. The influence of the various nanofibre surfaces on ReNcell CX cell morphology and distribution was investigated through immunofluorescence staining (Figure 5.4). Several studies have shown that many factors can induce differentiation of a neural progenitor cell (Reubinoff, Itsykson, Turetsky, et al. 2001; Dhara and Stice 2008). In this study, we differentiated ReNcell by withdrawing the mitogens from the cell culture medium. In our previous results chapter on SH-SY5Y and U-87MG we were able to demonstrate that neuronal (SH-SY5Y) cells preferred the PAN surface and glial (U-87MG) cells preferred the PJ surface. A similar effect was also expected in ReNcells when differentiated on PAN and PJ; but instead, ReNcell CX cells were capable of differentiating into neurons and glial cells on both PAN and PJ nanofibre scaffolds. Neurons were stained for  $\beta$ III tubulin, and glial cells were stained for GFAP. From the immunofluorescence imaging, it was evident that the ReNcell CX was

capable of differentiating in neurons and glial cells. The imaging also revealed that vast population of the cell was found accumulated in different regions of PJ fibre (Figure 5.4D) whereas cells attached to PAN (figure 5.4 C) was spread across the entire regions. Short extensions of neurite outgrowth were observed expressing  $\beta$ III tubulin a matured neuronal marker (figure 5.4 C and D).

Similarly, GFAP expressing glial cells were found in large clusters on PJ fibre (figure 5.4 F) and a tiny group of cells found in multiple regions on PAN fibres (Figure 5.4 E). Undifferentiated ReNcell CX was examined with nestin protein a standard marker used for ReNcell CX (Lendahl, Zimmerman and McKay 1990; Donato, Miljan, Hines, et al. 2007). The undifferentiated ReNcell CX displays an immature neural morphology (Figure 5.4 A and B). A study on ReNcell CX has reported that on TCP the cells tend to form a small polygonal shape with few processes that develop into a tight cobble-stone pattern when confluent (Donato, Miljan, Hines, et al. 2007). Similarly, clusters of undifferentiated cells were observed in several regions on both PAN and PJ fibres.

ReNcell cell lines have been used to investigate neurodegenerative diseases in several studies (Schüle, Pera and Langston 2009; Gnanasegaran, Govindasamy, Musa, et al. 2016). A study published a decade ago has demonstrated the potential of ReNcell VX cells as a model and showed the association of neurodegeneration with the PINK1 gene. The study used transfected siRNA to target PINK1 gene, and the results indicated that age-dependent neurodegeneration was observed with the reduced long-term viability of the neurons, demonstrating that the effect was triggered through a mitochondrial apoptosis pathway (Wood-Kaczmar, Gandhi, Yao, et al. 2008). ReNcell cell lines have their limitations, being an immortalised cell type, but may still provide a promising model for studying neurodegenerative conditions (Schüle, Pera and Langston 2009). Unlike other models and studies, we investigated toxins on ReNcell CX cells that were cultured on 3D nanofibre scaffolds,

which are capable of providing a robust environment for the cells to respond against the toxins. The differentiated cells were exposed to toxins for 72 hours, and the data showed that the cells on TCPs had lower viability than those on fibres (figure 5.5 A and B). Cells cultured on PJ showed higher viability compared to PAN. In section 5.3.1.3 we have shown that a higher metabolic activity and cell viability was observed on PJ compared to PAN. One possible explanation for this is that, since both cell types were found on fibres, glial cells within the nanofibre scaffolds may have released neurotrophic factors and neuroprotective agents that protected neurons against the effects of the toxins. To validate this phenomenon, further investigation will need to be carried out.

The main source of primary cultures is from either adult or embryonic animal tissue, which is then cultured either as an explant culture, suspension or as monolayer and maintained in vitro. As these cells have undergone very few doublings, they are more representative of the main functional component of the tissue from which they were obtained compared to established cell lines, thus representing a more physiologically relevant model (Alge, Hauck, Priglinger, et al. 2006; Pan, C., Kumar, Bohl, et al. 2009). In the current study, we have used primary cultures of neurons and glial cells derived from E18 embryonic rat hippocampus. The brain was removed and dissected to appropriate tissue by a company named BrianBits, UK. The hippocampal tissue was processed in-house to obtain neurons and glial cells. Preliminary studies showed that the primary cultures were capable of surviving on both PAN and PJ fibres compared to the TCP (Figure 5.6 and 5.7). The primary neurons are not capable of dividing, and the MTT assay showed that primary neurons cultured on PAN expressed a constant metabolic activity for 21 days whereas a decrease in cell metabolism was observed from day 16 on TCP. However, on the viability of neuronal cells cultured on PJ fibre was gradually decreasing. At day 20 almost 50% reduction in cell metabolic activity was observed from the MTT data when compared to the first measurement (figure 5.6 B). The Primary glial cell was capable

of dividing and from the MTT analysis (Figure 5.7) it was evident that glial cells were able to survive and express the increase in cell metabolism up to 21 days in culture on both PAN and PJ. The MTT analysis showed a significant increase and long-term metabolic activity on the fibres compared to the TCP. The cells on TCP expressed an increase in metabolic response until day 12 and gradual decrease after that until day 21.

Cell attachment and differentiation were further confirmed by immunofluorescence imaging. Neurons were stained for  $\beta$ III tubulin, and synaptophysin and glial cells were stained for GFAP. When observed under a confocal microscope the neurons exhibited branches of neurite extensions in contact with neighbouring cells along with evidence of synapse formation (figure 5.8). The cells were presumably using the nanofibres as robust support to extend long axons all over the fibre. The glial cells showed a strong expression of GFAP and star-shaped structured forming a monolayer on the top surface of the fibre, typical of astrocytes (figure 5.9). However, not all cells were positive for GFAP expression; these could be other glial cell types. The cell culture medium supplied by BrainBits for the glial cells was mainly to promote the growth of astrocytes. It was evident that both neurons and glial cells were physically and biochemically capable of growing and differentiating on PAN and PJ fibres, respectively.

A primary aim of the study was to develop a 3D co-culture model to evaluate and neural cell degeneration. The primary neuronal cell cultures grown on PAN scaffolds were exposed to low concentrations of toxins prior to being co-cultured with the glial cell PJ scaffolds in toxin-free conditions to monitor the viability of the neuronal cells. The cell viability data obtained for the neuronal cell scaffolds showed almost 80% of the neuronal viability was lost due to the toxin exposure (Figure 5.10 A). The trend suggested that neurons were dying up to day 7, after which they stabilised up to day 20. A similar effect was seen for all three of the toxins used, among which rotenone caused the most damage. The glial cell data

suggested that these cells remained viable throughout the experiment with a minimal reduction in cell viability compared to the control (figure 5.10 B). However, when the primary neurons were exposed to toxins and subsequently cultured in the absence of glial cells, they exhibited much more significant decreases in cell viability than those in co-cultures (Figure 5.11). Due to the financial and time limitations, the experiment was performed only once and, therefore, to prove the hypothesis of primary neuronal survival in the presence of glial cell scaffolds will require further investigation.

### **5.5 Conclusion**

In summary, this chapter has demonstrated that ReNcell CX cells and primary cultures of cells derived from E18 rat brain tissue can be cultured on both PAN and PJ nanofibres. We have shown with some preliminary experiments that ReNcells are capable of growing on both PAN and PJ but with a higher proliferation rate and survival on PJ compared to PAN. Both PAN and PJ fibre have also shown that they are capable of promoting ReNcell CX cell differentiation to neurons and glial cells. In general, primary cells are complicated to handle and culture. They tend to die due to microbial contamination during the culture period easily. However, in our study model, we were able to manufacture nanofibre scaffolds that were maintained sterile and were also capable of supporting primary neuron and glial cell survival. Both cell types exposed to toxins and demonstrated that it could be a suitable model for investigating neural cell degeneration. Our findings may have shown realistic information compared to other studies performed on 2D tissue culture plastics. Unfortunately, the chronic co-culture model for primary cell study was investigated only once. Nevertheless, our preliminary findings have suggested that the co-culture model is up-and-coming and may be a very suitable candidate for performing chronic studies and high throughput screening of neuroprotective agents and therapeutic drugs for neurodegenerative disease.

## Chapter 6: Main Discussion

### 6.1 Introduction

Neuronal and glial cells have been the main focus for investigating neurodegenerative diseases for several decades (Vila, Jackson-Lewis, Guégan, et al. 2001; Teismann, Tieu, Cohen, et al. 2003; Oh, S. E., Park, He, et al. 2018). Tissue engineering is an ever-expanding field, and a promising strategy for cell therapy. It lies in fixing damaged organs, tissues *in vivo* and also by generating engineered tissue constructs by *in vitro* techniques for subsequent transplantation. For several decades many studies have shown that biomaterials can play a role in the development of functional cells and tissues for the replacement of lost or affected cells and tissues (Kim, B., Baez and Atala 2000; Khan and Tanaka 2018). These replacements are commonly created with combinations for living cells, biomaterial scaffoldings and signalling molecules (Kim, I., Seo, Moon, et al. 2008). Studies have shown when engrafted cells are delivered on a biomaterial scaffold based system benefits have been recorded regarding cell replacement, tissue repair and *in vitro* studies. This may be because well-designed scaffolds are capable of providing structural support and the free flow of essential factors that can enhance the survival and function of the cells (Skop, Calderon, Cho, et al. 2014). When biomaterials are structured to provide an artificial ECM or more natural like habitat for cells, it can elevate the natural biological and mechanical functions of the native ECM of the cells.

Research into 3D cell culture has grown in the last few years. A keyword search in PubMed for 3D cell cultures shows 8872 articles published until February 2019, with the first ever paper on 3D culture published in 1968. The exponential increase publications show the importance and interest among researchers on 3D cell culture techniques. When cells are cultured on a 3D scaffold, they exhibit features that are much closer to *in vivo* conditions (Vinci, Gowan, Boxall, et al. 2012). The 3D culture models have proven to be realistic for translating the study findings for *in vivo*

applications. 3D cell culture studies cover a wide range of topics and have proven to be very suitable for several investigations and studies. Studies such as differentiation studies, drug discovery and pharmacological applications, tumour models, genetic studies, protein expression application, understanding cell physiology, investigating cell proliferation and cell cycle studies, cell cytoskeleton studies, apoptosis, cell adhesion and cell signalling, cell morphology, tissue engineering studies, and co-culture behavioural study have benefited from 3D models. With several advantages of 3D cell cultured, *in vitro* studies are now closer in mimicking a human *in vivo* tissue. A follow-on benefit will be the reduction and replacement of some animal model studies for research and product safety testing. They offer a robust superstructure that can be utilised to understand complex cell interactions that are not possible with 2D cell culture techniques. 3D cultures are more relevant cell models that are capable of better interaction between different cell types promoting integration flow or sometimes used as a barrier tissue. A critical step is a design and the choice of biomaterial used. The biomaterial scaffold must be capable of supporting and controlling the structural and functional integrity of the cell. It must be biocompatible and promote cell survival. In general, it should promote cell adhesion, proliferation, migration and differentiation, but in the case of a barrier, scaffold can restrict migration of cells. Constructing a suitable biomaterial scaffold requires properties like a sizeable surface-area-to-volume ratio making it suitable for a large number of cells, a high degree of porosity, interconnected structures, membrane thickness and individual filament diameters. Several techniques have been used to achieve these cues by using different types of natural and synthetic material to form biocompatible scaffold membranes.

## **6.2 Electrospinning biomaterials scaffolds for in vitro cell culture and tissue engineering.**

Polymer-based nanofibres can be produced by the method of electrospinning and benefits like fibre composition, adjustable fibre diameter, orientation, degradation, physical and mechanical properties, and surface modification can be tailored to specific application making it a very suitable process to produce scaffolds for cell therapy, tissue engineering and 3D cell culture studies (Dahlin, Kasper and Mikos 2011; Thenmozhi, Dharmaraj, Kadirvelu, et al. 2017). A significant number of research projects have been carried out on 3D cell culture methods on electrospun nanofibres using a wide range of natural, synthetic and blended polymers. Nanofibre scaffolds have been produced in different forms and by using many methods but most published work reports that spun fibres are deposited on and in contact with a solid carrier substrate thus making it a pseudo3D or the materials produced are not easily handled in a culture system. In this study, we have designed a production-ready process to create fully suspended correct 3D nanofibre scaffolds. The design allows the delicate nanofibre membrane to be manipulated during cell culture and tissue engineering. The design is very suitable for 6, 12 and 24 well TCP and can be incorporated to hold nanofibres made using suitable polymers.

Suspended 3D scaffold with three orientations was engineered in this study, with each type providing different structural cues for different cell types. The random fibre well plate insert (section 2.2.1.1) consisted of random electrospun nanofibre membranes laid across circular apertures and then held in place or sandwiched between an identical substrate with laser cut circular apertures. The technique has been perfected to create reproducible scaffolds which can be inserted individually into well plates. The aligned fibre scaffold (section 2.2.1.2) uses a unique and patent-pending method to manufacture aligned suspended fibre membranes. Collector drums rotating at high-speed is the principal method to

manufacture aligned nanofibres. This approach requires very high surface speeds of the collector drum, rotor and modification of the existing electrospinning system (Yu, Shao, Xu, et al. 2017). Our method only requires a laser cut sheet with a design that produces regions of aligned and random nanofibre membrane in a single scaffold insert. The design comprises of two rectangular apertures which form pathways for electrostatic discharge and an elliptical aperture which does not have an efficient pathway for electrostatic discharge and the aligned fibres are formed in this region. During electrospinning, an electrostatic field which develops between two rectangular regions forces a charged fibre over one region to travel and stretch to form an aligned fibre and reaches the opposite region which is instantaneously at a lower potential. Based on similar principle we have also developed a radial fibre design (section 2.2.1.3) that comprises of an inner circle and outer circle forming radial fibred between the two. Each scaffold model can be used for various studies like neurodegenerative study, spinal cord study, retinal investigation, wound healing research, orthopaedic research, etc. This study was focused on investigating the ability of random suspended nanofibre 3D scaffolds to support the growth of neuronal and glial cells to establish an improved *in vitro* model.

Currently, there are wide range of natural, synthetic and blended polymers that have been used for manufacturing electrospun nanofibres for various application and studies by different research groups (Zagho and Elzatahry 2016),([Electrospin Tech polymer data](#)). In this study, we have primarily chosen to work with PAN and PJ polymers Jeffamine® ED-2003 was used as an additive to modify PAN forming PJ. Limited comparative information is available on cell-based techniques using PAN and PJ fibres. In general, PAN is a carbon-rich polymer that has been widely used in many different applications, and a few studies have shown it to be a suitable material of *in vitro* cell culture studies. Both PAN and PJ are readily dissolvable in DMF when heated at 50°C overnight with constant stirring. When PAN is completely dissolved, it appears in pale

yellow and adding 5wt% Jeffamine<sup>®</sup> with an absorbance of  $40\% \pm 2\%$  and  $75\% \pm 2\%$  measured at 540nm respectively. Each batch of polymers was prepared and stored at 4°C and heated to room temperature before use. The Rheometer measurements revealed that 10wt% PAN expressed a viscosity of  $7E^{-1} \pm 1$  Pa.s with a calculated breakup time of  $3E^{-1} \pm 0.5$  seconds of PJ at  $7E^{-1} \pm 1$  Pa.s with a calculated breakup time of  $2E^{-1} \pm 0.5$  seconds. Adding 5wt% of jefammine has not altered the extensional viscosity of PAN. The scaffolds made using a blunt-end needle system and a rotating collector in a controlled humidity, and temperature chamber maintained at 65% and 21°C respectively. The polymers were capable of free-flow when pumped at 1ml/hour rate, and the fibres were obtained at 21kv for PAN and 18kv for PJ. When an electrical potential of the surface is increased to a sufficient value, the electrical forces act in opposition to and dominate the surface tension of the fluid causing the jet of the fluid to eject (Reneker and Yarin 2008). Another critical factor is the flow rate during the spinning. Each polymer requires an optimised flow rate based on the polymer properties and the type of fibre required. In this study, both PAN and PJ were spun at 1ml/hour flow rate throughout the study. Fibre diameter and the architecture of the nanofibre surface can influence the growth of cells. Nanofibres were achieved with an average fibre diameter ranging between 500-600nm. Our water contact angle study showed that PAN is hydrophobic, and PJ is hydrophilic. Several studies have confirmed the hydrophobicity properties of PAN as hydrophobic and Jeffamine<sup>®</sup> as hydrophilic (Kobayashi, Nagai, Wang, et al. 1996; Krakovský, Pleštil and Almásy 2006; Alarifi, Alharbi, Khan, et al. 2015). The average membrane thickness used for this study was 33.5µm and 30µm for PAN and PJ respectively. Increase in the total volume of deposition will lead to an increase in the thickness of the membrane. Sterilisation is an essential part of this study. Several techniques are currently available to sterilise nanofibres. Conventional techniques used are gamma treatment, autoclave, dry heat, vacuum, plasma treatment, ethanol, UV and electron beam treatments (Yixiang,

Yong, Liao, et al. 2008; Duszyer, Koral Koc, Hockenberger, et al. 2013; Dai, Ronholm, Tian, et al. 2016; Redigueri, Sassonia, Dua, et al. 2016). In this study, the fibres were tested with 70% ethanol, UV treatment and antibiotic treatment. From further investigating on all three methods of sterilisation, the study was performed using a combination of multiple sterilisation procedures. The study has demonstrated an SOP for sterilisation without causing structural, physical or chemical property damage and developing a contaminant-free nanofibre scaffold suitable for cell-based techniques.

### **6.3 3D scaffolds vs 2D TCP on immortalised cells**

Cell culture techniques are a vital tool in today's biological research and immortalised cells have been the main root of this technique for decades. Culturing these cells on a 2D TCP has been the standard practice for some time now, but a flat and stable surface can never represent or accurately model the *in vivo* nature of human tissue. Many studies have shown that cells cultured in 3D have demonstrated high physiological relevance and improvement in biological response like high cell number, morphology, the rate of proliferation, differentiation and viability. Studies have also shown that cells cultured in 3D responds better to stimuli, drug metabolism, and protein synthesis concerning high relevance to an *in vivo* system (Antoni, Burckel, Josset, et al. 2015). Physiological relevance is a crucial factor for study-related drug discovery, drug testing and cell-based assays.

In this study, we have used two commercially available human cells lines SH-SY5Y neuroblastoma and U-87 MG glioblastoma on both PAN and PJ nanofibre scaffolds. The study was mainly focused on random nanofibre scaffolds of PAN and PJ. Initially, we started with manufacturing nanofibres on a flat surface forming an unsuspended membrane which was more of a pseudo3D scaffold. Cells exposed to those material were found more attached to the edges of the fibre and on losing fibre ends. It was also impossible to maintain the fibres to be intact in lengthy culture

procedures and this led to engineering and manufacturing a fully suspended random scaffold. When the cell was introduced to a full suspended scaffold, most of the cells were found wholly attached throughout the fibre scaffolds, and the fibres were maintained intact throughout the procedure. The cell attachment was confirmed by Coomassie blue staining and immunofluorescence analysis. The results show that PAN and PJ nanofibres are suitable biomaterials to produce random nanofibre constructs that support neuronal and glial cells, respectively. Our investigation of cell proliferation for 11 days showed that PAN was the preferred surface for neuroblastoma and PJ preferred surface of the glioblastoma, but in both cases, cell growth and survival were maintained for longer on nanofibre scaffolds compared to conventional TCP. Several studies have shown that cells cultured on the 3D structure are capable of surviving a more extended period compared to 2D TCP as the cells die due to cell confluency (Antoni, Burckel, Josset, et al. 2015). Comparatively both 3D has double the total surface area compared to a 2D surface. A flat region on a 2D 12 well TCP has a growth region of  $3.8 \text{ cm}^2$  (2D X and Y axis) with a total well diameter of 22.1mm whereas the both scaffolds used in this study is 10mm in diameter and 30micron in thickness providing a total growth surface region of  $6.3 \text{ cm}^2$

The reason behind SH-SY5Y preferring the hydrophobic carbon-rich surface and U-87MG preferring a hydrophilic carbon and amine surface is still unknown. Hypothetically we think the neuronal cell is more prone to migration and extension. Therefore, a hydrophobic surface can support a lighter and flexible cell attachment but may also easily allow the cell body and neurites to roll over the surface for cell-cell contact making it easy for creating complex network connections. Whereas glial cells naturally are supporting cell in the brain and they tend to link firmly to adjacent neuronal cells and provide support and protection. The glial cell may require a hydrophilic surface that may have a better influence on the ECM leading to a firm attachment to the surface. This hypothesis does require

further investigation and explanation to validate the theory behind the mystery of surface preference by each cell type.

After identifying the suitable nanofibre, both cell types were exposed to differentiation inducer RA for SH-SY5Y and dbcAMP for U-87MG (Tiryaki, Ayres, Ahmed, et al. 2015; Korecka, van Kesteren, Blaas, et al. 2013; Fedoroff, McAuley, Houkle, et al. 1984). The B27 supplement is a commercially available product that is commonly used for the survival of primary neurons and differentiation (Roth, Zhang, Chiu, et al. 2010; Kovalevich and Langford 2013) and was used in this study as an alternative differentiating agent. When examined for possible differentiation markers SH-SY5Y cells cultured on PAN showed elevated levels of SMI 34 phosphorylated neurofilament,  $\beta$ III tubulin and synaptophysin and U-87MG showed high levels of GFAP compared to the cells on the plate. The data from confocal imaging and western blot analysis showed that PAN and PJ fibres are capable of supporting SH-SY5Y and U-87MG cell differentiation. Our results on exposure to toxins showed that the cells on fibre exhibited higher sensitivities to the different toxins compared to cells grown on conventional TCP. Cells cultured on both fibres showed a similar effect cell cultured on fibres for more susceptible to toxin than the cell on the plate. However, cells SH-SY5Y cultured on PJ and U-87MG on PAN showed greater damage and a significant decrease in cell viability due to the toxins and also may be due to the non-preferable surface. The increased susceptibility may be due to the increased cell surface in contact with the toxins on fibre compared to cells cultured on a flat culture plate. The ECM plays a central role in the proliferation, differentiation and function of the cells. Glial cells are the primary supporting cells for the neuron in the brain (Takuma, Baba and Matsuda 2004; Barreto, E White, Ouyang, et al. 2011; Cabezas, El-Bachá, González, et al. 2012). Our preliminary investigation on glial ECM on 2D surface revealed the differentiation capabilities of neurons when cultured on glia ECM. The neuronal cells were capable of producing matured axonal elongation with the growth factors from the glial ECM.

The matured axonal growth was confirmed with  $\beta$ III tubulin staining on an immunofluorescence microscope. Due to the limitation in time, this experiment was not performed on nanofibres, but this method could make inhabitable neuronal surfaces like PJ to become a neuron-supporting surface and can provide more natural ways for axonal elongations.

Several studies have shown the role of glial cell and the better development of neurons when cultured as a co-culture. Co-culturing of cells is a commonly used method to understand the response of one type of cell to the presence of another. Neurons and glial cells coexist in nature, and several models are used to co-culture these cells (Berre-Scoul, Chevalier, Oleynikova, et al. 2017). Most co-culture models are 2D based systems where both types of cells are either cultured together in the same dish or one type cultured on the base surface, and others introduced cultures on a glass coverslip or transwell inserts (Skaper and Facci 2018). Either of these methods has various limitations or disadvantages like it is a 2D surface, damage caused by the movement of the coverslip, improper supply of growth factors, challenging to handle, uncontrollable cell habitat.

We investigated our co-culture system with neurons and astrocytes exposed to toxins, and our results indicate that neurons exposed to toxins had a better chance of survival when cultured as a co-culture along with astrocytes on a scaffold-based model. The chronic co-culture model has demonstrated the prolonged survival of cells, and two different types of cell can be cultured on different scaffolds to recreate more realistic chronic models of studying neural cell degeneration. With the presence of astrocytes and nanofibre, the neuronal cells were able to express resistance to the lower concentrations of toxins. Astrocytes provide the neurotrophic factor (Lindahl, Saarma and Lindholm 2017), and the nanofibre provides robust structural support leading to prolonged cell survival. Several studies have also shown that glial cell line-derived neurotrophic factors can support neuronal cell line growth and this is

proving to be very useful in studying neurodegenerative diseases (Nishiguchi, Tokugawa, Yamamoto, et al. 2003; Shishkina, Mishchenko, Mitroshina, et al. 2018). A similar effect of toxins on the undifferentiated cell was also seen when differentiated SH-SY5Y and U-87MG cells were exposed to toxins individually (figure 4.27). Both cell type was sensitive to the inhibitor and showed a higher rate of cell death. They show that both astrocyte and nanofibres play a dual role in longer survival of the cells in the chronic 3D co-culture model.

Our co-culture model can be designed with any choice of electrospinnable polymer and can be made to fit precisely into a well plate. The model can consist of a two-layered co-culture system or can also be a multilayered system. For example, a scaffold with the neuronal cell can be cultured to form one layer and can be sandwiched between different types of glial cells on different layers. In this system, each layer of the scaffold can be placed at very close proximity or can be at a measured specific distance. The system also provides an advantage of measuring the cell viability of individual cell type from each scaffold layer. Cells showing lower viability can be replaced with scaffolds containing healthier cells. Each layer of cells can be easily arranged or separated based on experimental needs. The system opens up a wide range of opportunities to researchers and can be used as a very close model to replicate an *in vivo* system.

#### **6.4 Investigation of stem cell and primary cell on PAN and PJ nanofibre scaffolds**

Stem cell technology and primary cell-based techniques have pioneered the method 3D scaffold-based tissue engineering studies. Carbon-based nanomaterials have revolutionised stem cell and primary cell research (Stout and Webster 2012; Baldrighi, Trusel, Tonini, et al. 2016). Developing scaffolds with nanoscale features which mimics the habitat of cells in tissue is one of the significant challenges in the field of tissue engineering, and electrospinning of nanofibre membranes has shown great potential in overcoming this challenge (Vasita and Katti 2006).

Combination of cell therapy and polymer-based nanofibres material have overcome several obstacles in tissue engineering and regenerative medicines leading to the development of treatment for several medical conditions. As a part of the investigation in this study, we tested the high carbon-rich based PAN and carbon-amine rich PJ nanofibres on stem cell-like neural progenitor cells and primary neuron and glial cells.

As the first part of the investigation first, we tested if the chosen material can support the attachment of ReNcell CX and primary neurons and primary glial cells. As a result of our proliferation study, we were convinced that both ReNcell and the primary cells were capable of attaching and proliferating on both PAN and PJ fibre with only minor setbacks. ReNcell showed better survival and proliferation on PJ compared to PAN, primary neurons better survival on PAN and primary glial showed high survival rate on both PAN and PJ fibres. In both cases, long term survival of the cell on the plate was very questionable compared to fibres. Next, we investigated the ability of these cells to differentiate. ReNcell could differentiate into neurons, and glial cells whereas primary neurons do not divide but the cells are capable of differentiating and producing extend neurite outgrowths, and primary astrocyte growth was promoted from the glial cells. Immunofluorescence imaging revealed the ability of these cells to differentiate on PAN and PJ fibres. Neurons were stained for  $\beta$ III tubulin, and glial cells were stained for GFAP. The high expression on both proteins was expressed for cultures on PAN and PJ fibres. We investigated the expression of nestin protein, which is a standard marker for undifferentiated ReNcell CX (Donato, Miljan, Hines, et al. 2007). In the case of differentiated ReNcells, though neuron and glial cells were found on both PAN and PJ, a high number of cells were found on PJ compared to PAN therefore low expression on  $\beta$ III tubulin, and GFAP was observed on cells cultured on PAN. When stained primary cells were observed under a confocal microscope, the neurons were found growing as a single cell with branches of neurite extensions in contact with neighbouring cells along

with some strong synaptic activity. The 3D nanofibre act as a support for the extension of neurite outgrowth in all direction enabling the cells to create a complex network connection with surrounding cells in its natural form. The glial cells showed a strong expression of GFAP and star-shaped structured forming a monolayer mostly on the top surface of the fibre. Many cells were found with no GFAP expression, and they might have been other glial family of cells.

As per the plan in the study, the cells were investigated with toxins. The differentiated ReNcells were exposed to toxins for 72 hours, and the data showed that the cells on the plate had a lower viability percentage compared to the fibres. Cell cultured on PJ showed higher viability compared to PAN. Introducing healthy ReNcells as co-culture on a different scaffold may have revealed if the damaged cells could recover. Similarly, when we investigated the recovery of primary neurons from the damage caused by the toxins with the co-culture support of healthy glial cells. The neuronal cells were exposed to toxins for 48 hours and co-cultured with glial cells for 15 days in fully healthy conditions. From a preliminary experimental data, the neurons were dying up to day 7, and after day 7, the cells stopped dying and continued to survive up to day 20, and the glial cell was observed as healthy and viable through the experiment. Moreover, when exposed individually the primary neurons showed very poor viability, and the cells continued to die since day one after the exposure. Due to time constraints and financial support, the co-culture model for ReNcells was not investigated, and the co-culture on Primary neurons and glial cells were only performed once. Further experimental repeats are required to understand and validate the survival of primary neurons in the presence of glial cells. Providing an adaptable structure to mimic the native ECM is one of the most significant challenges of 3D based scaffold models. Among all available methods, electrospun nanofibres have shown the most promising results in several studies and therapies.

## 7.0 Conclusion and future work

### 7.1 Conclusion

This thesis has presented data gathered as part of a PhD project "Development of a novel 3D nanofibre co-culture model for characterisation of neural cell degeneration". The investigations shown in this thesis covers an extensive topic on neurodegenerative disease that happens in the human brain. There are number of discovered degenerative disease like amyotrophic lateral sclerosis, Parkinson's disease, Alzheimer's disease, and Huntington's disease. All these diseases share few common factors but still has its uniqueness in the pathophysiology. The model shown and investigated in this study was mainly focused on two significant representatives the neuronal and glial cells. These two types of cells are primarily affected in all neurodegenerative diseases. The slightest change in their regular function and metabolism leads to complications that can become one of the neurodegenerative diseases. Due the limited resource, knowledge and time in this study we have only focused on a small group cell types and materials. The primary focus of the research was to develop a nanofibre scaffold model that may mimic a 3D habitat allowing us to test and understand the behaviour of the two cell types under various conditions. The neural degeneration studies performed in this study shows a broad spectrum of scope for a researcher to choose and tailor it to maybe a specific type of neurodegenerative disorder. The novel co-culture model has also demonstrated that ability to investigate the two-primary type of cells by providing a suitable habitat with benefits of an *in vivo* like *in vitro* environment. The co-culture method has shown the possibilities to investigate several disorders that involve more than one type of cell. The entire study may have revealed a vast topic of neural cell degeneration but with all the findings and the information provided in this study researchers will be able to pick and choose suitable method or a model for much targeted research towards a specific

neurodegenerative disease or any other disease that can benefit in studying on a fully suspended 3D nanofibre scaffold model.

The study was mainly based on nanofibres made using Polyacrylonitrile (PAN) (Mw 150,000) and Jeffamine® ED-2003 as an additive (PJ). In this study, we developed three different engineered designs that may be suitable for a research which uses *in vitro* models. For example, studies which target the development of drugs to treat the disease of the brain and retina, spinal cord damage, and, chronic wounds. In addition, 3D nanofibre scaffolds show potential as acellular scaffolds for soft and hard tissue repair and as a platform for implanting cells as part of a cell-based or regenerative therapy. With the in-house built electrospinning system, using PAN and PJ polymers, we developed a reproducible process to fabricate fully suspended and ultrathin nanofibre fibre scaffolds which were secured between two support substrates which then allowed for easy handling and chronic studies. The SOP for sterilising nanofibre scaffolds demonstrated that the scaffolds could be sterilised with no physical damage or changes to its function and properties. Our various cell-based investigations have shown that both PAN and PJ fibres are capable of supporting cell attachment, proliferation, survival and differentiation.

The cell-based techniques in this study were performed using three different cell types that are commonly used in neurodegenerative related research. The study was conducted using

1. Immortalised cell line human SY-SY5Y neuroblastoma cells and Human U-87 MG glioblastoma cells.
2. Human ReNcell CX neural progenitor cell, and
3. Primary neurons and astrocytes dissociated from an embryonic day 18 rat hippocampus.

Primary investigation on all the three cell types was to investigate if cells are capable of attaching and proliferating on PAN and PJ nanofibres. Our

proliferation assay, which cultured each cell type for more than seven days showed a selective response based on the two kinds of nanofibres used and also expressed a more extended period of survival on fibres than TCP. We differentiated the cell types on both PAN and PJ fibres and showed the expression of several differentiation markers for both neurons and glial cells. Toxins were used to recreate neural cell degeneration pathophysiology for all cell types. An increased response to the toxins from the cells was observed for those grown on PAN and PJ fibres. The immortalised cells appeared more sensitive when exposed individually, and the ReNcell have expressed a minor resistance to the treatment.

Our state-of-the-art multi-stacking co-culture method using scaffolds has shown astonishing preliminary data on the immortalised cells and for the primary cells. High resistance to the inhibitors was observed when the immortalised neurons and astrocytes were cultured as a co-culture on the scaffolds and comparatively when one of the cells was cultured on a 2D based surface reduced cell viability was noticed. The recovery study performed as a co-culture on primary neurons also revealed that when the primary neurons were exposed to the inhibitors for a short time and co-cultured with healthy glial cells, the neurons were able to have prolonged survival. However, when tested without the presence of the astrocytes, the primary neurons exposed to the inhibitors showed reduced cell viability even though the inhibitors were removed from the culture and replaced with nutrient-rich media. This preliminary experiment has been demonstrated that the presence of glial cells and glial-derived neurotrophic factors from the glial cells are essential components for neuronal cell survival. Also, with the help of a robust 3D scaffold the *in vitro* structure resembles the natural *in vivo tissue*. The multi-layered co-culture system presents opportunities to create a wide range of *in vitro* human models using multiple layers of multiple cell types which are better suited to screening for potential drug candidates to improve the chance of drugs having successful clinical trials. This would

help to reduce the reliance on animal testing by the pharmaceutical industry.

Nanofibres can be made with a range of natural and synthetic materials and provides a high surface area with adjustable porosity causing a significant effect of cell attachment, proliferation and differentiation. Although the study has demonstrated several aspects of PAN and PJ nanofibre, both PAN and PJ may not be suitable for all type of cell-based investigations. Our nanofibre design is made to accommodate many different polymers, and these may be chosen to suit separate therapeutic investigations. The work demonstrates for the first time the benefits of using suspended, ultrathin 3D nanofibre scaffolds for in vitro models and justifies further in-depth research to develop models of other diseased or damaged tissue.

## **7.2 Future Work**

### **7.2.1 Polymers and nanofibres**

The study was primarily focused only on nanofibres made using PAN and PJ polymers. An extensive range of polymers are available which can be electrospun to form nanofibre materials, some polymers are derived from animal and plants, while others are synthesised from fossil fuels. One of the main advantages of polymer-based nanofibres is that the polymers can be blended and several additives can be used to dope to the nanofibres to change their functional properties. An area of future work will be to manufacture nanofibre using biodegradable, non-degradable and medical grade polymers to build the bespoke and preferred micro-environments for cells which will lead to manufacturing specific human tissues. However, rather than doping the whole fibre it is possible to coat the outer surface of each fibre using an electrospaying process to provide cells with specific physical and chemical cues. In addition, it has been shown that electrospinnable polymers can be blended with proteins and growth factors to enhance cell growth and maintenance.

In this thesis, only random nanofibre scaffolds were used to progress the development of a neurodegenerative model. But the aligned and radial fibre synthesis techniques developed during this research are being used by other researchers to create new *in vitro* human tissue models.

### 7.2.2 Cells based techniques

Primarily, the study focused on understanding and controlling the morphology of cells on new 3D scaffolds, which involved characterising cell attachment, proliferation and differentiation. In future, the work could be extended to investigate how cells adapt to different habitats, how neuronal elongation can be encouraged or inhibited and whether nanofibre surfaces can control cell division. All of these will benefit from the in-depth molecular biological analysis, such as the mass spectrometry fingerprint of proteins expressed internally or externally during the metabolic process of cells cultured on fibre compared to cells on TCP. GFAP was the only glial cell marker investigated in this work. Follow on studies would look into the expression of other astrocyte markers like EAAT1/GLAST, EAAT2/GLT-1 Glutamine synthetase, S100 beta ALDH1L1.

Using immortalised glial cells, we demonstrated that the glial cell ECM can promote the development of matured neuron and axonal elongation without using any other differentiating agents. This experiment was only performed on the 2D surface; a plan for a future investigation would involve performing the same experiment using nanofibres as the cell culture surface and examine if the nanofibres can promote enhanced neurite extension and direction compared to cells of TCP. Using techniques like qRT-PCR and mass spectrometry analysis it should be possible to identify the key proteins in the glial cell ECM that triggers the differentiation mechanism in neuronal cells.

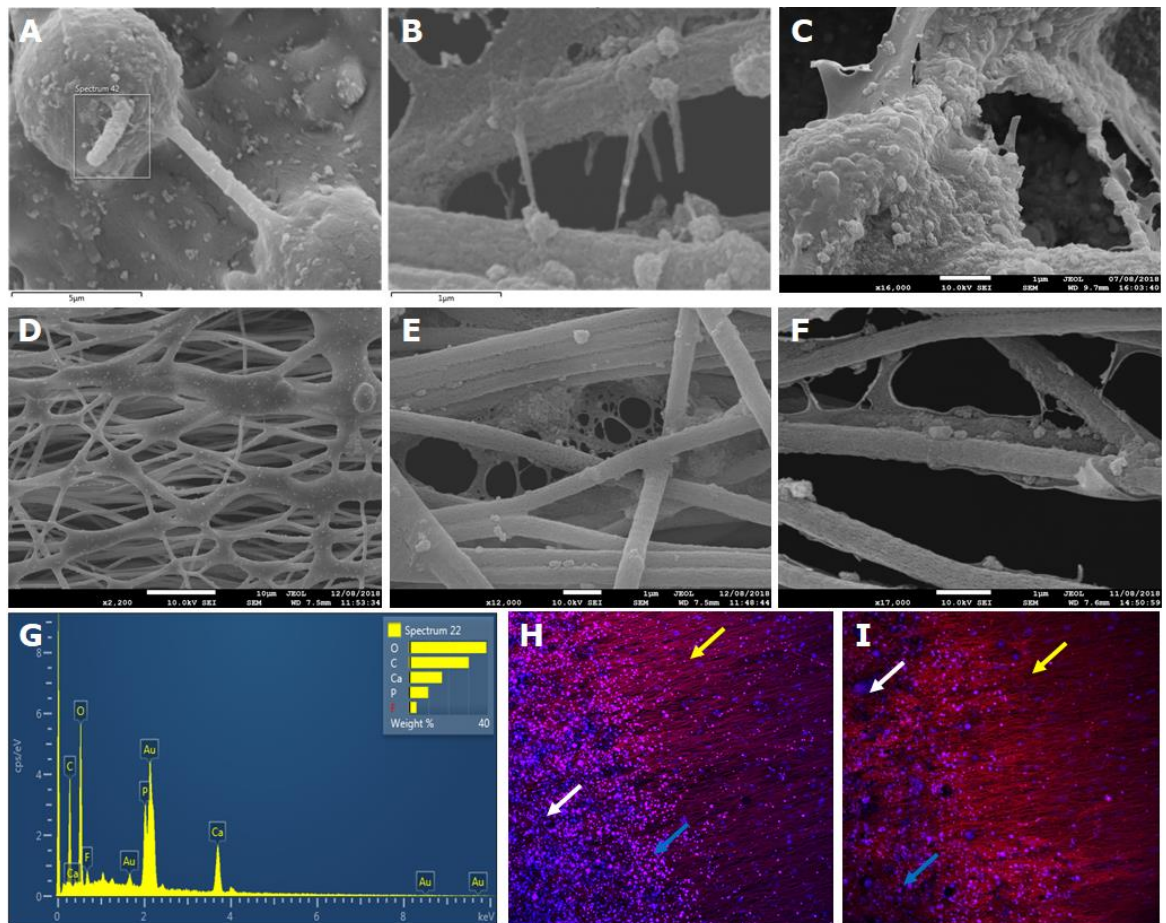
So far the influence of toxins on cell viability have been assessed using the nanofibre model, but further investigations should focus on molecular and genetic-based analysis to improve understanding, with many studies reporting that several genes are associated with neural cell degeneration

pathophysiology. A similar investigation could be carried out using our nanofibre model to analyse the expression of these genes and to understand the difference in the pathway response of each gene expression when cultured on nanofibres and on the plates. The co-culture model can be tested in multiple methods. Current techniques only focused on two-layer based co-culture system. In future, we will be investigating on multiple layered scaffolds to establish *in vitro* tissue which matches the *in vivo* condition.

### 7.2.3 Other nanofibre based studies

The surface of nanofibres can be modified using a number of known and well-established techniques. Several studies have incorporated growth factors, antimicrobial agents and proteins within the nanofibre which has led to better cell attachment and cell growth. An alternative is to coat the surface of the nanofibre with a very thin layer using an electrospray technique.

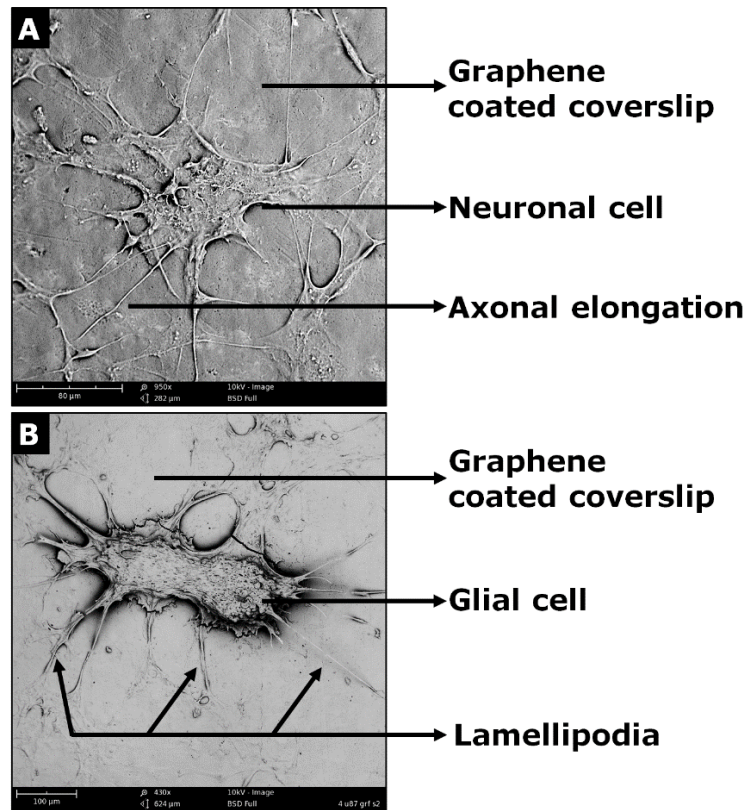
We have experimented on surface modification of nanofibres for several other studies which may also be used in the future for developing an improved neurodegenerative diseases model. One such study which was performed involved using precision robotics and spraying techniques to coat the surface of aligned fibre with hydroxyapatite embedded in a perfluoroelastomer polymer, as shown in Figure 7.1. The coated nanofibres were challenged with primary human tenocyte and osteoblast cells (Figure 7.1 A-F). The results from the study showed high viability and bone spike formation of osteoblast on the coated surface (Figure 7.1 A, B and C) and tenocytes stretched along the uncoated aligned fibre structure forming a collagen-rich monolayer as shown in Figure 7.1 D, E and F. The cells cultured on the aligned fibres were stained for collagen protein (red) and nuclei stain using DAPI (blue) and rich collagen deposition was observed in the uncoated region and high yield of osteoblast with nuclei stain was seen on the coated area, Figure 7.1 H and I.



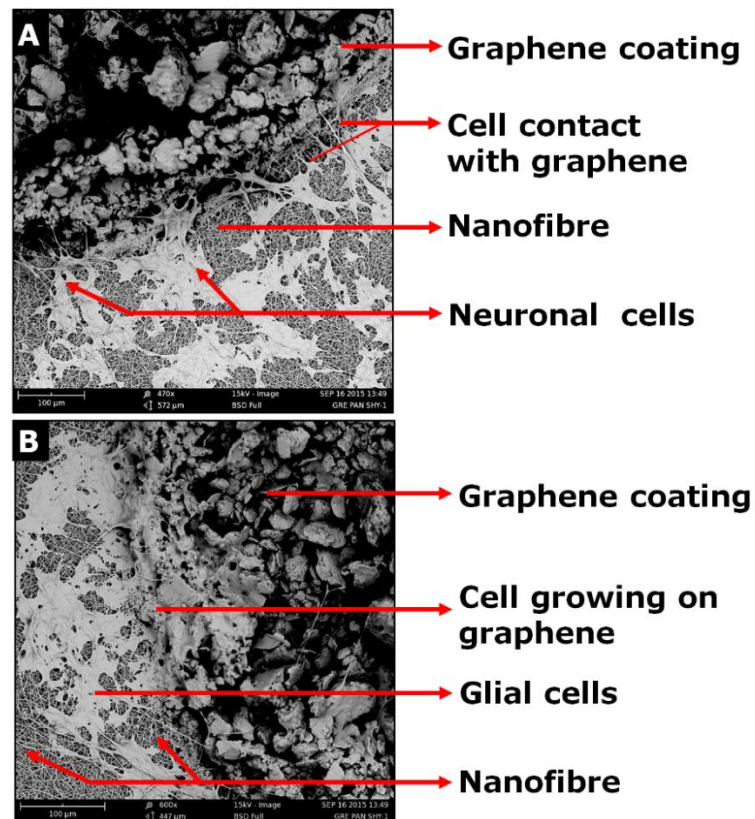
**Figure 7. 1: Human Osteoblast and Tenocyte cultured on hydroxyapatite-coated aligned nanofibre.**

Figure A-C represents osteoblast cells expressing bone spikes. Figure D-F shows tenocytes wrapped and growing along the fibres. Image G shows EDX analysed for different chemical elements. Figure H and I show immunofluorescences imaging expressing collagen and DAPI nuclei stain. The Yellow arrow indicates collagen (red) deposition; blue arrow represents hydroxyapatite coating (magenta) and white show DAPI stain (blue).

Nanofibres seem to create ideal structures for harbouring cells; biodegradable fibres can be used to develop cellular implants to promote cell growth and replace damaged or lost cells in several diseases which are similar to neurodegenerative diseases. We have also tested the ability of neuronal and glial cells to attach and grow on graphene coated surfaces and partial graphene coated nanofibres. Several studies have reported that neuronal cells have shown better attachment and growth when cultured on graphene. Cellular implants which incorporate graphene circuits are the main focus of several research groups.



**Figure 7. 2: Neural cells cultured on graphene-coated coverslips.**  
 (A) Neuronal cells and (B) Glial cells



**Figure 7. 3: Neural cells cultured on graphene-coated nanofibres.**  
 (A) Neuronal cells and (B) Glial cells

Our preliminary experiments on the graphene-coated coverslip (Figure 7.2) and graphene-coated nanofibre (Figure 7.3) demonstrated the ability of neural cells to attach and grow on graphene. The cells cultured on nanofibre and graphene also showed the formation of an integrated network of neural cells and graphene islands along the nanofibres. This work may lead to the development of graphene and nanofibre based biosensors or flexible implants that can monitor cell activity and induce cell response with an electrical impulse.

## Reference

- Abbott, A., 2003. *Biology's New Dimension*, .
- Adem, A., Mattsson, M.E., Nordberg, A. and Pählman, S., 1987. Muscarinic receptors in human SH-SY5Y neuroblastoma cell line: regulation by phorbol ester and retinoic acid-induced differentiation. *Developmental Brain Research*, 33 (2), 235-242.
- Ahmed, Z., and Brown, R.A., 1999. Adhesion, alignment, and migration of cultured Schwann cells on ultrathin fibronectin fibres. *Cell Motility and the Cytoskeleton*, 42 (4), 331-343.
- Alarifi, I.M., Alharbi, A., Khan, W.S., Swindle, A. and Asmatulu, R., 2015. Thermal, electrical and surface hydrophobic properties of electrospun polyacrylonitrile nanofibers for structural health monitoring. *Materials*, 8 (10), 7017-7031.
- Alge, C.S., Hauck, S.M., Priglinger, S.G., Kampik, A. and Ueffing, M., 2006. Differential protein profiling of primary versus immortalized human RPE cells identifies expression patterns associated with cytoskeletal remodeling and cell survival. *Journal of Proteome Research*, 5 (4), 862-878.
- Allen, M., Bjerke, M., Edlund, H., Nelander, S. and Westermark, B., 2016. Origin of the U87MG glioma cell line: Good news and bad news. *Science Translational Medicine*, 8 (354), 354re3.
- Allston-Roberts, C., Barallon, R., Bauer, S., Butler, J., Capes-Davis, A., Dirks, W., Elmore, E., Furtado, M., Kerrigan, L. and Kline, M., 2010. Cell line misidentification: the beginning of the end. *Nat Rev Cancer*, 10, 441-448.
- Alvarez-Fischer, D., Guerreiro, S., Hunot, S., Saurini, F., Marien, M., Sokoloff, P., Hirsch, E.C., Hartmann, A. and Michel, P.P., 2008. Modelling Parkinson-like neurodegeneration via osmotic minipump delivery of MPTP and probenecid. *Journal of Neurochemistry*, 107 (3), 701-711.
- Antoni, D., Burckel, H., Josset, E. and Noel, G., 2015. Three-dimensional cell culture: a breakthrough in vivo. *International Journal of Molecular Sciences*, 16 (3), 5517-5527.
- Attwell, D., Buchan, A.M., Charpak, S., Lauritzen, M., MacVicar, B.A. and Newman, E.A., 2010. Glial and neuronal control of brain blood flow. *Nature*, 468 (7321), 232.
- Aussawasathien, D., Teerawattananon, C. and Vongachariya, A., 2008. Separation of micron to sub-micron particles from water: electrospun

nylon-6 nanofibrous membranes as pre-filters. *Journal of Membrane Science*, 315 (1-2), 11-19.

Avagliano, C., Russo, R., De Caro, C., Cristiano, C., La Rana, G., Piegari, G., Paciello, O., Citraro, R., Russo, E. and De Sarro, G., 2016. Palmitoylethanolamide protects mice against 6-OHDA-induced neurotoxicity and endoplasmic reticulum stress: In vivo and in vitro evidence. *Pharmacological Research*, 113, 276-289.

Awiss, K., Gough, J. and Downes, S., 2010. Aligned electrospun polymer fibres for skeletal muscle regeneration. *Eur Cell Mater*, 19 (1), 193-204.

Avola, R., Graziano, A.C.E., Pannuzzo, G., Albouchi, F. and Cardile, V., 2018. New insights on Parkinson's disease from differentiation of SH-SY5Y into dopaminergic neurons: An involvement of aquaporin4 and 9. *Molecular and Cellular Neuroscience*, 88, 212-221.

Baldrighi, M., Trusel, M., Tonini, R. and Giordani, S., 2016. Carbon nanomaterials interfacing with neurons: an in vivo perspective. *Frontiers in Neuroscience*, 10, 250.

Bang, S., Na, S., Jang, J.M., Kim, J. and Jeon, N.L., 2016. Engineering-Aligned 3D Neural Circuit in Microfluidic Device. *Advanced Healthcare Materials*, 5 (1), 159-166.

Barreto, G., E White, R., Ouyang, Y., Xu, L. and G Giffard, R., 2011. Astrocytes: targets for neuroprotection in stroke. *Central Nervous System Agents in Medicinal Chemistry (Formerly Current Medicinal Chemistry-Central Nervous System Agents)*, 11 (2), 164-173.

Baumann, N., and Pham-Dinh, D., 2001. Biology of oligodendrocyte and myelin in the mammalian central nervous system. *Physiological Reviews*, 81 (2), 871-927.

Bellamkonda, R., Ranieri, J.P., Bouche, N. and Aebischer, P., 1995. Hydrogel-based three-dimensional matrix for neural cells. *Journal of Biomedical Materials Research*, 29 (5), 663-671.

Benarroch, E.E., 2005. Neuron-astrocyte interactions: partnership for normal function and disease in the central nervous system. *In: Mayo Clinic Proceedings*, Elsevier, pp. 1326-1338.

Bergdahl, L., and Ljungqvist, A., 1980. Long-term results after repair of coarctation of the aorta by patch grafting. *The Journal of Thoracic and Cardiovascular Surgery*, 80 (2), 177-181.

Berre-Scoul, C., Chevalier, J., Oleynikova, E., Cossais, F., Talon, S., Neunlist, M. and Boudin, H., 2017. A novel enteric neuron-glia coculture

system reveals the role of glia in neuronal development. *The Journal of Physiology*, 595 (2), 583-598.

Berridge, Michael V., Herst, Patrice M. and Tan, An S., 2005. *Tetrazolium dyes as tools in cell biology: New insights into their cellular reduction*. Elsevier.

Betarbet, R., Sherer, T.B., MacKenzie, G., Garcia-Osuna, M., Panov, A.V. and Greenamyre, J.T., 2000. Chronic systemic pesticide exposure reproduces features of Parkinson's disease. *Nature Neuroscience*, 3 (12), 1301.

Bhatia, S.N., and Ingber, D.E., 2014. Microfluidic organs-on-chips. *Nature Biotechnology*, 32 (8), 760.

Bhattacharjee, S.R., Bhattacharjee, N., Yi, H.K., Hwang, P.H., Cha, D.I. and Kim, H.Y., 2004. Novel biodegradable electrospun membrane: scaffold for tissue engineering. *Biomaterials*, 25 (13), 2595-2602.

Bian, Y., Wang, Y., Aibaidoula, G., Chen, G. and Wu, Q., 2009. Evaluation of poly (3-hydroxybutyrate-co-3-hydroxyhexanoate) conduits for peripheral nerve regeneration. *Biomaterials*, 30 (2), 217-225.

Björklund, A., and Lindvall, O., 2000. Cell replacement therapies for central nervous system disorders. *Nature Neuroscience*, 3 (6), 537.

Björklund, L.M., Sanchez-Pernate, R., Chung, S., Andersson, T., Chen, I.Y., McNaught, K.S., Brownell, A.L., Jenkins, B.G., Wahlestedt, C., Kim, K.S. and Isacson, O., 2002. Embryonic stem cells develop into functional dopaminergic neurons after transplantation in a Parkinson rat model. *Proceedings of the National Academy of Sciences of the United States of America*, 99 (4), 2344-2349.

Blackshaw, S.E., Arkison, S., Cameron, C. and Davies, J.A., 1997. Promotion of regeneration and axon growth following injury in an invertebrate nervous system by the use of three-dimensional collagen gels. *Proceedings Biological Sciences*, 264 (1382), 657-661.

Blesa, J., and Przedborski, S., 2014. Parkinson's disease: animal models and dopaminergic cell vulnerability. *Frontiers in Neuroanatomy*, 8, 155.

Bodaghi, H., and Sinangil, M., 2009. Meltblown nonwoven webs including nanofibers and apparatus and method for forming such meltblown nonwoven webs.

Bogerts, B., Häntsch, J. and Herzer, M., 1983. A morphometric study of the dopamine-containing cell groups in the mesencephalon of normals, Parkinson patients, and schizophrenics. *Biological Psychiatry*, .

Booth, H.D., Hirst, W.D. and Wade-Martins, R., 2017. The role of astrocyte dysfunction in Parkinson's disease pathogenesis. *Trends in Neurosciences*, 40 (6), 358-370.

Bozkurt, A., Brook, G.A., Moellers, S., Lassner, F., Sellhaus, B., Weis, J., Woeltje, M., Tank, J., Beckmann, C. and Fuchs, P., 2007. In vitro assessment of axonal growth using dorsal root ganglia explants in a novel three-dimensional collagen matrix. *Tissue Engineering*, 13 (12), 2971-2979.

Braet, F., De Zanger, R. and Wisse, E., 1997. Drying cells for SEM, AFM and TEM by hexamethyldisilazane: a study on hepatic endothelial cells. *Journal of Microscopy*, 186 (1), 84-87.

Brang, J., Wilkie, A. and Haggard, J., 2008. Method and apparatus for production of meltblown nanofibers. *Method and Apparatus for Production of Meltblown Nanofibers*, .

Brännvall, K., Bergman, K., Wallenquist, U., Svahn, S., Bowden, T., Hilborn, J. and Forsberg-Nilsson, K., 2007. Enhanced neuronal differentiation in a three-dimensional collagen-hyaluronan matrix. *Journal of Neuroscience Research*, 85 (10), 2138-2146.

Bredesen, D.E., Rao, R.V. and Mehlen, P., 2006. Cell death in the nervous system. *Nature*, 443 (7113), 796.

Breedlove, S.M., Rosenzweig, M.R. and Watson, N.V., 2007. *Biological psychology: An introduction to behavioral, cognitive, and clinical neuroscience*. Sinauer Associates Sunderland, MA.

Browne, S., Monaghan, M.G., Brauchle, E., Berrio, D.C., Chantepie, S., Papy-Garcia, D., Schenke-Layland, K. and Pandit, A., 2015. Modulation of inflammation and angiogenesis and changes in ECM GAG-activity via dual delivery of nucleic acids. *Biomaterials*, 69, 133-147.

Brundin, P., Karlsson, J., Emgård, M., Kaminski Schierle, G.S., Hansson, O., Petersén, Å and Castilho, R.F., 2000. Improving the survival of grafted dopaminergic neurons: a review over current approaches. *Cell Transplantation*, 9 (2), 179-195.

Burns, A., and Iliffe, S., 2009. **Alzheimer's disease**. . *Alzheimer's Disease*. *BMJ* 338, b158, .

Cabezas, R., El-Bachá, R.S., González, J. and Barreto, G.E., 2012. Mitochondrial functions in astrocytes: neuroprotective implications from oxidative damage by rotenone. *Neuroscience Research*, 74 (2), 80-90.

Caiazza, M., Okawa, Y., Ranga, A., Piersigilli, A., Tabata, Y. and Lutolf, M.P., 2016. Defined three-dimensional microenvironments boost induction of pluripotency. *Nature Materials*, 15 (3), 344.

Cannon, J.R., Tapias, V., Na, H.M., Honick, A.S., Drolet, R.E. and Greenamyre, J.T., 2009. A highly reproducible rotenone model of Parkinson's disease. *Neurobiology of Disease*, 34 (2), 279-290.

Cassarino, D.S., Parks, J.K., Parker Jr, W.D. and Bennett Jr, J.P., 1999. The parkinsonian neurotoxin MPP<sup>+</sup> opens the mitochondrial permeability transition pore and releases cytochrome c in isolated mitochondria via an oxidative mechanism. *Biochimica Et Biophysica Acta (BBA)-Molecular Basis of Disease*, 1453 (1), 49-62.

Cassie, A., and Baxter, S., 1944. Wettability of porous surfaces. *Transactions of the Faraday Society*, 40, 546-551.

Castañeda, F., and Kinne, R.K., 2000. Short exposure to millimolar concentrations of ethanol induces apoptotic cell death in multicellular HepG2 spheroids. *Journal of Cancer Research and Clinical Oncology*, 126 (6), 305-310.

Cengiz, F., and Jirsak, O., 2009. The effect of salt on the roller electrospinning of polyurethane nanofibers. *Fibers and Polymers*, 10 (2), 177-184.

Chan, B., and Leong, K., 2008. Scaffolding in tissue engineering: general approaches and tissue-specific considerations. *European Spine Journal*, 17 (4), 467-479.

Chan, N.C., Salazar, A.M., Pham, A.H., Sweredoski, M.J., Kolawa, N.J., Graham, R.L., Hess, S. and Chan, D.C., 2011. Broad activation of the ubiquitin-proteasome system by Parkin is critical for mitophagy. *Human Molecular Genetics*, 20 (9), 1726-1737.

Chattopadhyay, S., and Raines, R.T., 2014. Review collagen-based biomaterials for wound healing. *Biopolymers*, 101 (8), 821-833.

Chen, M., Patra, P.K., Warner, S.B. and Bhowmick, S., 2007. Role of fiber diameter in adhesion and proliferation of NIH 3T3 fibroblast on electrospun polycaprolactone scaffolds. *Tissue Engineering*, 13 (3), 579-587.

Chen, Y., Zhang, D., Liao, Z., Wang, B., Gong, S., Wang, C., Zhang, M., Wang, G., Cai, H. and Liao, F., 2015. Anti-oxidant polydatin (piceid) protects against substantia nigral motor degeneration in multiple rodent models of Parkinson's disease. *Molecular Neurodegeneration*, 10 (1), 4.

Chen, J. C., and Harrison, I. R., 2002. *Modification of polyacrylonitrile (PAN) carbon fiber precursor via post-spinning plasticization and stretching in dimethyl formamide (DMF).*

Cheung, Y., Lau, W.K., Yu, M., Lai, C.S., Yeung, S., So, K. and Chang, R.C., 2009. Effects of all-trans-retinoic acid on human SH-SY5Y neuroblastoma as in vitro model in neurotoxicity research. *Neurotoxicology*, 30 (1), 127-135.

Chierchia, Armando, Chirico, Nino, Boeri, Lucia, Raimondi, Ilaria, Riva, Giovanni A., Raimondi, Manuela Teresa, Tunesi, Marta, Giordano, Carmen, Forloni, Gianluigi and Albani, Diego, 2017. *Secretome released from hydrogel-embedded adipose mesenchymal stem cells protects against the Parkinson's disease related toxin 6-hydroxydopamine.*

Chiu, C., Yeh, T., Lai, S., Wu-Chou, Y., Chen, C., Mochly-Rosen, D., Huang, Y., Chen, Y., Chen, C. and Chang, Y., 2015. Neuroprotective effects of aldehyde dehydrogenase 2 activation in rotenone-induced cellular and animal models of parkinsonism. *Experimental Neurology*, 263, 244-253.

Choi, S.H., Kim, Y.H., Quinti, L., Tanzi, R.E. and Kim, D.Y., 2016. 3D culture models of Alzheimer's disease: a road map to a "cure-in-a-dish". *Molecular Neurodegeneration*, 11 (1), 75.

Choi, Y.J., Park, J. and Lee, S., 2013. Size-controllable networked neurospheres as a 3D neuronal tissue model for Alzheimer's disease studies. *Biomaterials*, 34 (12), 2938-2946.

Choi, S.H., Kim, Y.H., Hebisch, M., Sliwinski, C., Lee, S., D'Avanzo, C., Chen, H., Hooli, B., Asselin, C., Muffat, J., Klee, J.B., Zhang, C., Wainger, B.J., Peitz, M., Kovacs, D.M., Woolf, C.J., Wagner, S.L., Tanzi, R.E. and Kim, D.Y., 2014. A three-dimensional human neural cell culture model of Alzheimer's disease. *Nature*, 515 (7526), 274-278.

Chrischilles, E.A., Rubenstein, L.M., Voelker, M.D., Wallace, R.B. and Rodnitzky, R.L., 1998. The health burdens of Parkinson's disease. *Movement Disorders*, 13 (3), 406-413.

Christopherson, G.T., Song, H. and Mao, H., 2009. The influence of fiber diameter of electrospun substrates on neural stem cell differentiation and proliferation. *Biomaterials*, 30 (4), 556-564.

Chuangchote, S., and Supaphol, P., 2006. Fabrication of aligned poly (vinyl alcohol) nanofibers by electrospinning. *Journal of Nanoscience and Nanotechnology*, 6 (1), 125-129.

Chueng, S.D., Yang, L., Zhang, Y. and Lee, K., 2016. Multidimensional nanomaterials for the control of stem cell fate. *Nano Convergence*, 3 (1), 23.

Clarke, L.E., and Barres, B.A., 2013. Emerging roles of astrocytes in neural circuit development. *Nature Reviews Neuroscience*, 14 (5), 311.

Conti, L., Reitano, E. and Cattaneo, E., 2006. Neural stem cell systems: diversities and properties after transplantation in animal models of diseases. *Brain Pathology*, 16 (2), 143-154.

Cooper, J.F., and Van Raamsdonk, J.M., 2018. Modeling Parkinson's Disease in *C. elegans*. *Journal of Parkinson's Disease*, 8 (1), 17-32.

Corey, J.M., Gertz, C.C., Wang, B., Birrell, L.K., Johnson, S.L., Martin, D.C. and Feldman, E.L., 2008. The design of electrospun PLLA nanofiber scaffolds compatible with serum-free growth of primary motor and sensory neurons. *Acta Biomaterialia*, 4 (4), 863-875.

Covell, D., Robinson, J., Akhtar, R., Grossman, M., Weintraub, D., Bucklin, H., Pitkin, R., Riddle, D., Yousef, A. and Trojanowski, J., 2017. Novel conformation-selective alpha-synuclein antibodies raised against different in vitro fibril forms show distinct patterns of Lewy pathology in Parkinson's disease. *Neuropathology and Applied Neurobiology*, 43 (7), 604-620.

Crowder, S.W., Prasai, D., Rath, R., Balikov, D.A., Bae, H., Bolotin, K.I. and Sung, H., 2013. Three-dimensional graphene foams promote osteogenic differentiation of human mesenchymal stem cells. *Nanoscale*, 5 (10), 4171-4176.

Cuende, J., Moreno, S., Bolanos, J. and Almeida, A., 2008. Retinoic acid downregulates Rae1 leading to APC Cdh1 activation and neuroblastoma SH-SY5Y differentiation. *Oncogene*, 27 (23), 3339.

Cui, F., Tian, W., Hou, S., Xu, Q. and Lee, I., 2006. Hyaluronic acid hydrogel immobilized with RGD peptides for brain tissue engineering. *Journal of Materials Science: Materials in Medicine*, 17 (12), 1393-1401.

Dabbeni-sala, F., Di Santo, S., Franceschini, D., Skaper, S.D. and Giusti, P., 2001. Melatonin protects against 6-OHDA-induced neurotoxicity in rats: a role for mitochondrial complex I activity. *The FASEB Journal*, 15 (1), 164-170.

Dahlin, R.L., Kasper, F.K. and Mikos, A.G., 2011. Polymeric nanofibers in tissue engineering. *Tissue Engineering Part B: Reviews*, 17 (5), 349-364.

- Dai, Z., Ronholm, J., Tian, Y., Sethi, B. and Cao, X., 2016. Sterilization techniques for biodegradable scaffolds in tissue engineering applications. *Journal of Tissue Engineering*, 7, 2041731416648810.
- Darice Y, W., Scott J, H., Paul H, K. and Christopher, N., 2007. Poly( $\epsilon$ -Caprolactone) and Poly (L-Lactic-Co-Glycolic Acid) Degradable Polymer Sponges Attenuate Astrocyte Response and Lesion Growth in Acute Traumatic Brain Injury. Volume: 13 (Issue 10), 13(10)-2515-2523.
- Das, A., Karmakar, S., Patel, S.J., Priest, D.G., Banik, N.L. and Ray, S.K., 2005. Differentiation of human glioblastoma U87MG cells with all-trans retinoic acid (ATRA) or 13-cis retinoic acid (13-CRA) down regulated telomerase activity and enhanced sensitivity to interferon-gamma (IFN- $\gamma$ ) or taxol (TXL) for apoptosis.
- Dayalu, P., and Albin, R.L., 2015. Huntington disease: pathogenesis and treatment. *Neurologic Clinics*, 33 (1), 101-114.
- De Lau, L.M., and Breteler, M.M., 2006. Epidemiology of Parkinson's disease. *The Lancet Neurology*, 5 (6), 525-535.
- Defty, C., and Marsden, J., 2012. Melphalan in regional chemotherapy for locally recurrent metastatic melanoma. *Current Topics in Medicinal Chemistry*, 12 (1), 53-60.
- Dhara, S.K., and Stice, S.L., 2008. Neural differentiation of human embryonic stem cells. *Journal of Cellular Biochemistry*, 105 (3), 633-640.
- Dingle, Y.L., Boutin, M.E., Chirila, A.M., Livi, L.L., Labriola, N.R., Jakubek, L.M., Morgan, J.R., Darling, E.M., Kauer, J.A. and Hoffman-Kim, D., 2015. Three-dimensional neural spheroid culture: an in vitro model for cortical studies. *Tissue Engineering Part C: Methods*, 21 (12), 1274-1283.
- Dixon, J.E., Shah, D.A., Rogers, C., Hall, S., Weston, N., Parmenter, C.D., McNally, D., Denning, C. and Shakesheff, K.M., 2014. Combined hydrogels that switch human pluripotent stem cells from self-renewal to differentiation. *Proceedings of the National Academy of Sciences of the United States of America*, 111 (15), 5580-5585.
- Donato, R., Miljan, E.A., Hines, S.J., Aouabdi, S., Pollock, K., Patel, S., Edwards, F.A. and Sinden, J.D., 2007. Differential development of neuronal physiological responsiveness in two human neural stem cell lines. *BMC Neuroscience*, 8 (1), 36.
- Dong, R., Zhang, B., Tai, L., Liu, H., Shi, F. and Liu, N., 2018. The Neuroprotective Role of MiR-124-3p in a 6-Hydroxydopamine-Induced Cell Model of Parkinson's Disease via the Regulation of ANAX5. *Journal of Cellular Biochemistry*, 119 (1), 269-277.

Dorsey, E.R., Constantinescu, R., Thompson, J.P., Biglan, K.M., Holloway, R.G., Kieburtz, K., Marshall, F.J., Ravina, B.M., Schifitto, G., Siderowf, A. and Tanner, C.M., 2007. Projected number of people with Parkinson disease in the most populous nations, 2005 through 2030. *Neurology*, 68 (5), 384-386.

Doshi, J., and Reneker, D.H., 1995. Electrospinning process and applications of electrospun fibers. *Journal of Electrostatics*, 35 (2), 151-160.

Drukarch, B., Schepens, E., Stoof, J.C., Langeveld, C.H. and Van Muiswinkel, F.L., 1998. Astrocyte-enhanced neuronal survival is mediated by scavenging of extracellular reactive oxygen species. *Free Radical Biology and Medicine*, 25 (2), 217-220.

Duszyer, S., Koral Koc, S., Hockenberger, A., Evke, E., Kahveci, Z. and Uguz, A., 2013. Effects of different sterilization methods on polyester surfaces. *Tekstil Ve Konfeksiyon*, 23 (4), 319-324.

Duty, S., and Jenner, P., 2011. Animal models of Parkinson's disease: a source of novel treatments and clues to the cause of the disease. *British Journal of Pharmacology*, 164 (4), 1357-1391.

Edmondson, R., Broglie, J.J., Adcock, A.F. and Yang, L., 2014. Three-dimensional cell culture systems and their applications in drug discovery and cell-based biosensors. *Assay and Drug Development Technologies*, 12 (4), 207-218.

Falck, B., Hillarp, N., Thieme, G. and Torp, A.a., 1962. Fluorescence of catechol amines and related compounds condensed with formaldehyde. *Journal of Histochemistry & Cytochemistry*, 10 (3), 348-354.

Farzaneh, Z., Pournasr, B., Ebrahimi, M., Aghdami, N. and Baharvand, H., 2010. Enhanced functions of human embryonic stem cell-derived hepatocyte-like cells on three-dimensional nanofibrillar surfaces. *Stem Cell Reviews and Reports*, 6 (4), 601-610.

Fawcett, J.W., Barker, R.A. and Dunnett, S.B., 1995. Dopaminergic neuronal survival and the effects of bFGF in explant, three dimensional and monolayer cultures of embryonic rat ventral mesencephalon. *Experimental Brain Research*, 106 (2), 275-282.

Fedoroff, S., McAuley, W., Houkle, J. and Devon, R., 1984. Astrocyte cell lineage. V. Similarity of astrocytes that form in the presence of dBcAMP in cultures to reactive astrocytes in vivo. *Journal of Neuroscience Research*, 12 (1), 15-27.

Feng, L., Li, S., Li, H., Zhai, J., Song, Y., Jiang, L. and Zhu, D., 2002. Super-hydrophobic surface of aligned polyacrylonitrile nanofibers. *Angewandte Chemie International Edition*, 41 (7), 1221-1223.

Ferrigno, A., Vairetti, M., Ambrosi, G., Rizzo, V., Richelmi, P., Blandini, F. and Fuzzati-Armentero, M., 2015. Selective blockade of mGlu5 metabotropic glutamate receptors is protective against hepatic mitochondrial dysfunction in 6-OHDA lesioned Parkinsonian rats. *Clinical and Experimental Pharmacology and Physiology*, 42 (6), 695-703.

Findley, L.J., 2007. The economic impact of Parkinson's disease. *Parkinsonism & Related Disorders*, 13 Suppl, S8-S12.

Förch, R., Schönherr, H., Schonherr, H. and Jenkins, A.T.A., 2009. *Surface design: applications in bioscience and nanotechnology*. John Wiley & Sons.

Fornai, F., Lenzi, P., Ferrucci, M., Lazzeri, G., di Poggio, A.B., Natale, G., Busceti, C.L., Biagioni, F., Giusiani, M. and Ruggieri, S., 2005. Occurrence of neuronal inclusions combined with increased nigral expression of  $\alpha$ -synuclein within dopaminergic neurons following treatment with amphetamine derivatives in mice. *Brain Research Bulletin*, 65 (5), 405-413.

Frantz, C., Stewart, K.M. and Weaver, V.M., 2010. The extracellular matrix at a glance. *Journal of Cell Science*, 123 (Pt 24), 4195-4200.

Freshney, R.I., 2015. *Culture of animal cells: a manual of basic technique and specialized applications*. John Wiley & Sons.

Gai, W. P., Yuan, H. X., Li, X. Q., Power, J. T. H., Blumbergs, P. C. and Jensen, P. H., 2000. *In Situ and in Vitro Study of Colocalization and Segregation of  $\alpha$ -Synuclein, Ubiquitin, and Lipids in Lewy Bodies*.

German, D.C., and Manaye, K.F., 1993. Midbrain dopaminergic neurons (nuclei A8, A9, and A10): three-dimensional reconstruction in the rat. *Journal of Comparative Neurology*, 331 (3), 297-309.

Ghosh, D., Mondal, M., Mohite, G.M., Singh, P.K., Ranjan, P., Anoop, A., Ghosh, S., Jha, N.N., Kumar, A. and Maji, S.K., 2013. The Parkinson's disease-associated H50Q mutation accelerates  $\alpha$ -Synuclein aggregation in vitro. *Biochemistry*, 52 (40), 6925-6927.

Gibrat, C., Saint-Pierre, M., Bousquet, M., Lévesque, D., Rouillard, C. and Cicchetti, F., 2009. Differences between subacute and chronic MPTP mice models: investigation of dopaminergic neuronal degeneration and  $\alpha$ -synuclein inclusions. *Journal of Neurochemistry*, 109 (5), 1469-1482.

- Gnanasegaran, N., Govindasamy, V., Musa, S. and Kasim, N.H.A., 2016. ReNCell VM conditioned medium enhances the induction of dental pulp stem cells into dopaminergic like cells. *Cytotechnology*, 68 (2), 343-353.
- Goldhoff, P., Warrington, N.M., Limbrick, D.D., Jr, Hope, A., Woerner, B.M., Jackson, E., Perry, A., Piwnica-Worms, D. and Rubin, J.B., 2008. Targeted inhibition of cyclic AMP phosphodiesterase-4 promotes brain tumor regression. *Clinical Cancer Research : An Official Journal of the American Association for Cancer Research*, 14 (23), 7717-7725.
- Gómez-Lechón, M.J., Jover, R., Donato, T., Ponsoda, X., Rodriguez, C., Stenzel, K.G., Klocke, R., Paul, D., Guillén, I. and Bort, R., 1998. Long-term expression of differentiated functions in hepatocytes cultured in three-dimensional collagen matrix. *Journal of Cellular Physiology*, 177 (4), 553-562.
- Gomez-Lechon, M., Donato, M., Castell, J. and Jover, R., 2003. Human hepatocytes as a tool for studying toxicity and drug metabolism. *Current Drug Metabolism*, 4 (4), 292-312.
- Gonzalez-Reyes, L.E., Verbitsky, M., Blesa, J., Jackson-Lewis, V., Paredes, D., Tillack, K., Phani, S., Kramer, E.R., Przedborski, S. and Kottmann, A.H., 2012. Sonic hedgehog maintains cellular and neurochemical homeostasis in the adult nigrostriatal circuit. *Neuron*, 75 (2), 306-319.
- Good, C.H., Hoffman, A.F., Hoffer, B.J., Chefer, V.I., Shippenberg, T.S., Bäckman, C.M., Larsson, N., Olson, L., Gellhaar, S. and Galter, D., 2011. Impaired nigrostriatal function precedes behavioral deficits in a genetic mitochondrial model of Parkinson's disease. *The FASEB Journal*, 25 (4), 1333-1344.
- Gopal, R., Kaur, S., Ma, Z., Chan, C., Ramakrishna, S. and Matsuura, T., 2006. Electrospun nanofibrous filtration membrane. *Journal of Membrane Science*, 281 (1-2), 581-586.
- Gordon, G.R., Mulligan, S.J. and MacVicar, B.A., 2007. Astrocyte control of the cerebrovasculature. *Glia*, 55 (12), 1214-1221.
- Gorji, M., Jeddi, A.A. and Gharehaghaji, A., 2012. Fabrication and characterization of polyurethane electrospun nanofiber membranes for protective clothing applications. *Journal of Applied Polymer Science*, 125 (5), 4135-4141.
- Gorshkov, Kirill, Aguisanda, Francis, Thorne, Natasha and Zheng, Wei, 2018. *Astrocytes as targets for drug discovery*.
- Gray, E., Rice, C., Nightingale, H., Ginty, M., Hares, K., Kemp, K., Cohen, N., Love, S., Scolding, N. and Wilkins, A., 2013. Accumulation of cortical

hyperphosphorylated neurofilaments as a marker of neurodegeneration in multiple sclerosis. *Multiple Sclerosis Journal*, 19 (2), 153-161.

Greiner, A., and Wendorff, J.H., 2007. Electrospinning: a fascinating method for the preparation of ultrathin fibers. *Angewandte Chemie International Edition*, 46 (30), 5670-5703.

Gu, Z., and Xu, Q., Cosmetic mask based on electrospinning nanometer fiber for skin, comprises electrospinning nanometer fiber nonwoven fabric or nonwoven felt.

Guo, J., Leung, K.K.G., Su, H., Yuan, Q., Wang, L., Chu, T., Zhang, W., Pu, J.K.S., Ng, G.K.P. and Wong, W.M., 2009. Self-assembling peptide nanofiber scaffold promotes the reconstruction of acutely injured brain. *Nanomedicine: Nanotechnology, Biology and Medicine*, 5 (3), 345-351.

Gupta, A., Paliwal, D. and Bajaj, P., 1998. Melting behavior of acrylonitrile polymers. *Journal of Applied Polymer Science*, 70 (13), 2703-2709.

Haider, S., Al-Zeghayer, Y., Ali, F.A.A., Haider, A., Mahmood, A., Al-Masry, W.A., Imran, M. and Aijaz, M.O., 2013. Highly aligned narrow diameter chitosan electrospun nanofibers. *Journal of Polymer Research*, 20 (4), 1-11.

Han, Y.H., Moon, H.J., You, B.R. and Park, W.H., 2009. The effect of MG132, a proteasome inhibitor on HeLa cells in relation to cell growth, reactive oxygen species and GSH. *Oncology Reports*, 22 (1), 215.

Hanani, M., 2005. Satellite glial cells in sensory ganglia: from form to function. *Brain Research Reviews*, 48 (3), 457-476.

Haycock, J.W., 2011. 3D cell culture: a review of current approaches and techniques. *In: 3D cell culture: a review of current approaches and techniques. 3D cell culture*. Springer, 2011, pp. 1-15.

Heffernan, John M., McNamara, James B., Borwege, Sabine, Vernon, Brent L., Sanai, Nader, Mehta, Shwetel and Sirianni, Rachael W., 2017. *PNIPAAm-co-Jeffamine® (PNJ) scaffolds as in vitro models for niche enrichment of glioblastoma stem-like cells*.

Hegazy, M.A., Maklad, H.M., Samy, D.M., Abdelmonsif, D.A., El Sabaa, B.M. and Elnozahy, F.Y., 2017. Cerium oxide nanoparticles could ameliorate behavioral and neurochemical impairments in 6-hydroxydopamine induced Parkinson's disease in rats. *Neurochemistry International*, 108, 361-371.

- Herculano-Houzel, S., 2014. The glia/neuron ratio: how it varies uniformly across brain structures and species and what that means for brain physiology and evolution. *Glia*, 62 (9), 1377-1391.
- Herculano-Houzel, S., 2009. The human brain in numbers: a linearly scaled-up primate brain. *Frontiers in Human Neuroscience*, 3, 31.
- Hillen, A.E., Burbach, J.P.H. and Hol, E.M., 2018. Cell adhesion and matricellular support by astrocytes of the tripartite synapse. *Progress in Neurobiology*, .
- Hinz, B., 2015. The extracellular matrix and transforming growth factor- $\beta$ 1: Tale of a strained relationship. *Matrix Biology*, 47, 54-65.
- Hirsch, E.C., and Hunot, S., 2009. Neuroinflammation in Parkinson's disease: a target for neuroprotection? *The Lancet Neurology*, 8 (4), 382-397.
- Hoffman, R.M., 1993. To do tissue culture in two or three dimensions? That is the question. *Stem Cells*, 11 (2), 105-111.
- Höglinger, G.U., Féger, J., Prigent, A., Michel, P.P., Parain, K., Champy, P., Ruberg, M., Oertel, W.H. and Hirsch, E.C., 2003. Chronic systemic complex I inhibition induces a hypokinetic multisystem degeneration in rats. *Journal of Neurochemistry*, 84 (3), 491-502.
- Hovakimyan, M., Müller, J., Wree, A., Ortinau, S., Rolfs, A. and Schmitt, O., 2012. Survival of transplanted human neural stem cell line (ReNcell VM) into the rat brain with and without immunosuppression. *Annals of Anatomy-Anatomischer Anzeiger*, 194 (5), 429-435.
- Hu, J., Kai, D., Ye, H., Tian, L., Ding, X., Ramakrishna, S. and Loh, X.J., 2017. Electrospinning of poly (glycerol sebacate)-based nanofibers for nerve tissue engineering. *Materials Science and Engineering: C*, 70, 1089-1094.
- Hu, X., Liu, S., Zhou, G., Huang, Y., Xie, Z. and Jing, X., 2014. Electrospinning of polymeric nanofibers for drug delivery applications. *Journal of Controlled Release*, 185, 12-21.
- Huang, T., Marshall, L.R., Armantrout, J.E., Yembrick, S., Dunn, W.H., Oconnor, J.M., Mueller, T., Avgousti, M. and Wetzel, M.D., 2012. Production of nanofibers by melt spinning.
- Hwang, O., 2013. Role of oxidative stress in Parkinson's disease. *Experimental Neurobiology*, 22 (1), 11-17.

Innamorato, N.G., Jazwa, A., Rojo, A.I., García, C., Fernández-Ruiz, J., Grochot-Przeczek, A., Stachurska, A., Jozkowicz, A., Dulak, J. and Cuadrado, A., 2010. Different susceptibility to the Parkinson's toxin MPTP in mice lacking the redox master regulator Nrf2 or its target gene heme oxygenase-1. *PLoS One*, 5 (7), e11838.

Irons, H.R., Cullen, D.K., Shapiro, N.P., Lambert, N.A., Lee, R.H. and LaPlaca, M.C., 2008. Three-dimensional neural constructs: a novel platform for neurophysiological investigation. *Journal of Neural Engineering*, 5 (3), 333.

Itano, Y., Ito, A., Uehara, T. and Nomura, Y., 1996. Regulation of Bcl-2 protein expression in human neuroblastoma SH-SY5Y cells: positive and negative effects of protein kinases C and A, respectively. *Journal of Neurochemistry*, 67 (1), 131-137.

Ivanov, D.P., Parker, T.L., Walker, D.A., Alexander, C., Ashford, M.B., Gellert, P.R. and Garnett, M.C., 2014. Multiplexing spheroid volume, resazurin and acid phosphatase viability assays for high-throughput screening of tumour spheroids and stem cell neurospheres. *PloS One*, 9 (8), e103817.

Ivascu, A., and Kubbies, M., 2006. Rapid generation of single-tumor spheroids for high-throughput cell function and toxicity analysis. *Journal of Biomolecular Screening*, 11 (8), 922-932.

Jackson-Lewis, V., Blesa, J. and Przedborski, S., 2012. Animal models of Parkinson's disease. *Parkinsonism & Related Disorders*, 18 Suppl 1, S183-5.

Jacque, C., Vinner, C., Kujas, M., Raoul, M., Racadot, J. and Baumann, N., 1978. Determination of glial fibrillary acidic protein (GFAP) in human brain tumors. *Journal of the Neurological Sciences*, 35 (1), 147-155.

Jäkel, S., and Dimou, L., 2017. Glial cells and their function in the adult brain: a journey through the history of their ablation. *Frontiers in Cellular Neuroscience*, 11, 24.

Jensen, S.S., Petterson, S.A., Halle, B., Aaberg-Jessen, C. and Kristensen, B.W., 2017. Effects of the lysosomal destabilizing drug siramesine on glioblastoma in vitro and in vivo. *BMC Cancer*, 17 (1), 178.

Jeong, G.S., Chang, J.Y., Park, J.S., Lee, S., Park, D., Woo, J., An, H., Lee, C.J. and Lee, S., 2015. Networked neural spheroid by neuro-bundle mimicking nervous system created by topology effect. *Molecular Brain*, 8 (1), 17.

Jessen, K.R., and Mirsky, R., 2005. The origin and development of glial cells in peripheral nerves. *Nature Reviews Neuroscience*, 6 (9), 671.

Jessen, K.R., and Mirsky, R., 1980. Glial cells in the enteric nervous system contain glial fibrillary acidic protein.

Johansson, C.B., Momma, S., Clarke, D.L., Risling, M., Lendahl, U. and Frisén, J., 1999. Identification of a neural stem cell in the adult mammalian central nervous system. *Cell*, 96 (1), 25-34.

Jung, B., 2004. Preparation of hydrophilic polyacrylonitrile blend membranes for ultrafiltration. *Journal of Membrane Science*, 229 (1-2), 129-136.

Justice, B.A., Badr, N.A. and Felder, R.A., 2009. 3D cell culture opens new dimensions in cell-based assays. *Drug Discovery Today*, 14 (1-2), 102-107.

Kalia, Lorraine V., and Lang, Anthony E., 2015. *Parkinson's disease*.

Kaneko, N., Kako, E. and Sawamoto, K., 2011. Prospects and limitations of using endogenous neural stem cells for brain regeneration. *Genes*, 2 (1), 107-130.

Kato-Negishi, M., Morimoto, Y., Onoe, H. and Takeuchi, S., 2013. Millimeter-Sized Neural Building Blocks for 3D Heterogeneous Neural Network Assembly. *Advanced Healthcare Materials*, 2 (12), 1564-1570.

Katta, P., Alessandro, M., Ramsier, R. and Chase, G., 2004. Continuous electrospinning of aligned polymer nanofibers onto a wire drum collector. *Nano Letters*, 4 (11), 2215-2218.

Kaur, G., and Dufour, J.M., 2012. Cell lines. *Spermatogenesis*, 2 (1), 1-5.

Khajavi, R., Abbasipour, M. and Bahador, A., 2016. Electrospun biodegradable nanofibers scaffolds for bone tissue engineering. *Journal of Applied Polymer Science*, 133 (3).

Khamforoush, M., and Mahjob, M., 2011. Modification of the rotating jet method to generate highly aligned electrospun nanofibers. *Materials Letters*, 65 (3), 453-455.

Khan, F., and Tanaka, M., 2018. Designing smart biomaterials for tissue engineering. *International Journal of Molecular Sciences*, 19 (1), 17.

Kijeńska, E., Prabhakaran, M.P., Swieszkowski, W., Kurzydłowski, K.J. and Ramakrishna, S., 2014. Interaction of Schwann cells with laminin

encapsulated PLCL core-shell nanofibers for nerve tissue engineering. *European Polymer Journal*, 50, 30-38.

Kikuchi, T., Morizane, A., Doi, D., Magotani, H., Onoe, H., Hayashi, T., Mizuma, H., Takara, S., Takahashi, R. and Inoue, H., 2017. Human iPS cell-derived dopaminergic neurons function in a primate Parkinson's disease model. *Nature*, 548 (7669), 592-596.

Kim, B., Baez, C.E. and Atala, A., 2000. Biomaterials for tissue engineering. *World Journal of Urology*, 18 (1), 2-9.

Kim, I., Seo, S., Moon, H., Yoo, M., Park, I., Kim, B. and Cho, C., 2008. Chitosan and its derivatives for tissue engineering applications. *Biotechnology Advances*, 26 (1), 1-21.

Kim, J.I., Kim, J.Y. and Park, C.H., 2018. Fabrication of transparent hemispherical 3D nanofibrous scaffolds with radially aligned patterns via a novel electrospinning method. *Scientific Reports*, 8 (1), 3424.

Kim, Y.H., Choi, S.H., D'Avanzo, C., Hebisch, M., Sliwinski, C., Bylykbashi, E., Washicosky, K.J., Klee, J.B., Brüstle, O. and Tanzi, R.E., 2015. A 3D human neural cell culture system for modeling Alzheimer's disease. *Nature Protocols*, 10 (7), 985.

Kim, D., Kim, S. and Li, G.C., 1999. Proteasome Inhibitors MG132 and Lactacystin Hyperphosphorylate HSF1 and Induce hsp70 and hsp27 Expression. *Biochemical and Biophysical Research Communications*, 254 (1), 264-268.

Kim, S.J., Sung, J.Y., Um, J.W., Hattori, N., Mizuno, Y., Tanaka, K., Paik, S.R., Kim, J. and Chung, K.C., 2003. Parkin cleaves intracellular alpha-synuclein inclusions via the activation of calpain. *The Journal of Biological Chemistry*, 278 (43), 41890-41899.

Kimelberg, Harold K., and Nedergaard, Maiken, 2010. *Functions of Astrocytes and their Potential As Therapeutic Targets*.

Kinmonth, J.B., Taylor, G.W. and Lee, R.H., 1955. Arteriol replacement by orlon cloth; a preliminary report of its experimental and clinical use. *British Medical Journal*, 1 (4927), 1406-1409.

Kizildag, N., Ucar, N. and Onen, A., 2018. Nanocomposite polyacrylonitrile filaments with titanium dioxide and silver nanoparticles for multifunctionality. *Journal of Industrial Textiles*, 47 (7), 1716-1738.

Knight, E., and Przyborski, S., 2014. Advances in 3D cell culture technologies enabling tissue-like structures to be created in vitro. *Journal of Anatomy*, .

Kobayashi, T., Nagai, T., Wang, H.Y. and Fujii, N., 1996. Charged ultrafiltration membranes of polyacrylonitrile covalently binding amphiphilic quaternary ammonium group: effect of aliphatic hydrophobic groups on the filtration properties. *Journal of Membrane Science*, 112 (2), 219-228.

Kolb, B., and Whishaw, I.Q., 2009. *Fundamentals of human neuropsychology*. Macmillan.

Korecka, J.A., van Kesteren, R.E., Blaas, E., Spitzer, S.O., Kamstra, J.H., Smit, A.B., Swaab, D.F., Verhaagen, J. and Bossers, K., 2013. Phenotypic characterization of retinoic acid differentiated SH-SY5Y cells by transcriptional profiling. *PLoS One*, 8 (5), e63862.

Koroleva, A., Gill, A., Ortega, I., Haycock, J., Schlie, S., Gittard, S., Chichkov, B. and Claeysens, F., 2012. Two-photon polymerization-generated and micromolding-replicated 3D scaffolds for peripheral neural tissue engineering applications. *Biofabrication*, 4 (2), 025005.

Kothapalli, C.R., and Kamm, R.D., 2013. 3D matrix microenvironment for targeted differentiation of embryonic stem cells into neural and glial lineages. *Biomaterials*, 34 (25), 5995-6007.

Kovalevich, J., and Langford, D., 2013. Considerations for the use of SH-SY5Y neuroblastoma cells in neurobiology. *In: Considerations for the use of SH-SY5Y neuroblastoma cells in neurobiology. Neuronal Cell Culture*. Springer, 2013, pp. 9-21.

Kowalczyk, T., Nowicka, A., Elbaum, D. and Kowalewski, T.A., 2008. Electrospinning of bovine serum albumin. Optimization and the use for production of biosensors. *Biomacromolecules*, 9 (7), 2087-2090.

Krakovský, Ivan, Pleštil, Josef and Almásy, László, 2006. *Structure and swelling behaviour of hydrophilic epoxy networks investigated by SANS*.

Kumbar, S., James, R., Nukavarapu, S. and Laurencin, C., 2008. Electrospun nanofiber scaffolds: engineering soft tissues. *Biomedical Materials*, 3 (3), 034002.

Kume, T., Kawato, Y., Osakada, F., Izumi, Y., Katsuki, H., Nakagawa, T., Kaneko, S., Niidome, T., Takada-Takatori, Y. and Akaike, A., 2008. Dibutyryl cyclic AMP induces differentiation of human neuroblastoma SH-SY5Y cells into a noradrenergic phenotype. *Neuroscience Letters*, 443 (3), 199-203.

Kunze, A., Giugliano, M., Valero, A. and Renaud, P., 2011. Micropatterning neural cell cultures in 3D with a multi-layered scaffold. *Biomaterials*, 32 (8), 2088-2098.

Kusamoto, N., and Tajima, T., Fiber comprises an eggshell membrane component useful for producing a fiber assembly, which is used as a wound dressing or a cosmetic sheet. *US Patent, US2009031691-A1*, .

Laco, F., Grant, M.H. and Black, R.A., 2013. Collagen–nanofiber hydrogel composites promote contact guidance of human lymphatic microvascular endothelial cells and directed capillary tube formation. *Journal of Biomedical Materials Research Part A*, 101 (6), 1787-1799.

Lancaster, M.A., Renner, M., Martin, C., Wenzel, D., Bicknell, L.S., Hurles, M.E., Homfray, T., Penninger, J.M., Jackson, A.P. and Knoblich, J.A., 2013. Cerebral organoids model human brain development and microcephaly. *Nature*, 501 (7467), 373.

Langley, M., Ghosh, A., Charli, A., Sarkar, S., Ay, M., Luo, J., Zielonka, J., Brenza, T., Bennett, B. and Jin, H., 2017. Mito-apocynin prevents mitochondrial dysfunction, microglial activation, oxidative damage, and progressive neurodegeneration in mitopark transgenic mice. *Antioxidants & Redox Signaling*, 27 (14), 1048-1066.

Lee, J., Cuddihy, M.J. and Kotov, N.A., 2008. Three-dimensional cell culture matrices: state of the art. *Tissue Engineering Part B: Reviews*, 14 (1), 61-86.

Lee, S., and Kay Obendorf, S., 2006. Developing protective textile materials as barriers to liquid penetration using melt-electrospinning. *Journal of Applied Polymer Science*, 102 (4), 3430-3437.

Lee, T.T., Chana, G., Gorry, P.R., Ellett, A., Bousman, C.A., Churchill, M.J., Gray, L.R. and Everall, I.P., 2015. Inhibition of catechol-O-methyl transferase (COMT) by tolcapone restores reductions in microtubule-associated protein 2 (MAP2) and synaptophysin (SYP) following exposure of neuronal cells to neurotropic HIV. *Journal of Neurovirology*, 21 (5), 535-543.

Lee, Y., and Livingston Arinzeh, T., 2011. Electrospun nanofibrous materials for neural tissue engineering. *Polymers*, 3 (1), 413-426.

Lei, S., and Powers, R., 2013. NMR metabolomics analysis of Parkinson's Disease. *Current Metabolomics*, 1 (3), 191-209.

Lendahl, U., Zimmerman, L.B. and McKay, R.D., 1990. CNS stem cells express a new class of intermediate filament protein. *Cell*, 60 (4), 585-595.

Levenberg, S., Huang, N.F., Lavik, E., Rogers, A.B., Itskovitz-Eldor, J. and Langer, R., 2003. Differentiation of human embryonic stem cells on three-dimensional polymer scaffolds. *Proceedings of the National*

*Academy of Sciences of the United States of America*, 100 (22), 12741-12746.

LF Nascimento, M., S Araujo, E., R Cordeiro, E., HP de Oliveira, A. and P de Oliveira, H., 2015. A literature investigation about electrospinning and nanofibers: historical trends, current status and future challenges. *Recent Patents on Nanotechnology*, 9 (2), 76-85.

Li, H., Ke, Y. and Hu, Y., 2006. Polymer nanofibers prepared by template melt extrusion. *Journal of Applied Polymer Science*, 99 (3), 1018-1023.

Li, J., Darabi, M., Gu, J., Shi, J., Xue, J., Huang, L., Liu, Y., Zhang, L., Liu, N. and Zhong, W., 2016. A drug delivery hydrogel system based on activin B for Parkinson's disease. *Biomaterials*, 102, 72-86.

Li, W., Tuli, R., Huang, X., Laquerriere, P. and Tuan, R.S., 2005. Multilineage differentiation of human mesenchymal stem cells in a three-dimensional nanofibrous scaffold. *Biomaterials*, 26 (25), 5158-5166.

Li, H., Labean, T.H. and Leong, K.W., 2011. Nucleic acid-based nanoengineering: novel structures for biomedical applications. *Interface Focus*, 1 (5), 702-724.

Liang, D., Hsiao, B.S. and Chu, B., 2007. Functional electrospun nanofibrous scaffolds for biomedical applications. *Advanced Drug Delivery Reviews*, 59 (14), 1392-1412.

Lincoln, L., Fisher, R., Jackson, M.J., Jenner, P., Neumeyer, J., Sromek, A.W., Lees, A.J. and Rose, S., 2016. Oral r(-)-11-o-valeryl-n-n-propylnoraporphine reverses motor deficits in mptp-treated marmosets. *Movement Disorders*, 31 (9), 1381-1388.

Lindahl, M., Saarma, M. and Lindholm, P., 2017. Unconventional neurotrophic factors CDNF and MANF: Structure, physiological functions and therapeutic potential. *Neurobiology of Disease*, 97, 90-102.

Liu, G., Qiao, L. and Guo, A., 1996. Diblock copolymer nanofibers. *Macromolecules*, 29 (16), 5508-5510.

Liu, Y., and He, J., 2007. Bubble electrospinning for mass production of nanofibers. *International Journal of Nonlinear Sciences and Numerical Simulation*, 8 (3), 393-396.

Lloyd, L.F., Gallay, O.S., Akins, J. and Zeikus, J.G., 1994. Crystallization and preliminary X-ray diffraction studies of xylose isomerase from *Thermoanaerobacterium thermosulfurigenes* strain 4B. *Journal of Molecular Biology*, 240 (5), 504-506.

Lohr, K.M., Bernstein, A.I., Stout, K.A., Dunn, A.R., Lazo, C.R., Alter, S.P., Wang, M., Li, Y., Fan, X., Hess, E.J., Yi, H., Vecchio, L.M., Goldstein, D.S., Guillot, T.S., Salahpour, A. and Miller, G.W., 2014. Increased vesicular monoamine transporter enhances dopamine release and opposes Parkinson disease-related neurodegeneration in vivo. *Proceedings of the National Academy of Sciences of the United States of America*, 111 (27), 9977-9982.

Lopes, F.M., da Motta, L.L., De Bastiani, M.A., Pfaffenseller, B., Aguiar, B.W., de Souza, L.F., Zanatta, G., Vargas, D.M., Schönhofen, P. and Londero, G.F., 2017. RA differentiation enhances dopaminergic features, changes redox parameters, and increases dopamine transporter dependency in 6-hydroxydopamine-induced neurotoxicity in SH-SY5Y cells. *Neurotoxicity Research*, 31 (4), 545-559.

Lopes, F.M., Schröder, R., da Frota Júnior, Mário Luiz Conte, Zanotto-Filho, A., Müller, C.B., Pires, A.S., Meurer, R.T., Colpo, G.D., Gelain, D.P. and Kapczinski, F., 2010. Comparison between proliferative and neuron-like SH-SY5Y cells as an in vitro model for Parkinson disease studies. *Brain Research*, 1337, 85-94.

Lopez-Carballo, G., Moreno, L., Masia, S., Perez, P. and Baretino, D., 2002. Activation of the phosphatidylinositol 3-kinase/Akt signaling pathway by retinoic acid is required for neural differentiation of SH-SY5Y human neuroblastoma cells. *The Journal of Biological Chemistry*, 277 (28), 25297-25304.

Lorsch, J.R., Collins, F.S. and Lippincott-Schwartz, J., 2014. Cell Biology. Fixing problems with cell lines. *Science (New York, N.Y.)*, 346 (6216), 1452-1453.

Low, W.C., Rujitanaroj, P., Wang, F., Wang, J. and Chew, S.Y., 2013. Nanofiber-mediated release of retinoic acid and brain-derived neurotrophic factor for enhanced neuronal differentiation of neural progenitor cells. *Drug Delivery and Translational Research*, , 1-12.

Lowry, O.H., Rosebrough, N.J., Farr, A.L. and Randall, R.J., 1951. Protein measurement with the Folin phenol reagent. *Journal of Biological Chemistry*, 193, 265-275.

Lozano, K., and Sarkar, K., 2009. Methods and apparatuses for making superfine fibers. *Methods and Apparatuses for Making Superfine Fibers*, .

Lu, T., Chen, X., Shi, Q., Wang, Y., Zhang, P. and Jing, X., 2008. The immobilization of proteins on biodegradable fibers via biotin-streptavidin bridges. *Acta Biomaterialia*, 4 (6), 1770-1777.

Lu, Y., Zhang, X., Zhao, L., Yang, C., Pan, L., Li, C., Liu, K., Bai, G., Gao, H. and Yan, Z., 2018. Metabolic disturbances in the striatum and substantia nigra in the onset and progression of MPTP-induced Parkinsonism model. *Frontiers in Neuroscience*, 12, 90.

Ma, Y., Zhan, M., OuYang, L., Li, Y., Chen, S., Wu, J., Chen, J., Luo, C. and Lei, W., 2014. The effects of unilateral 6-OHDA lesion in medial forebrain bundle on the motor, cognitive dysfunctions and vulnerability of different striatal interneuron types in rats. *Behavioural Brain Research*, 266, 37-45.

Macdonald, C., 1990. Development of new cell lines for animal cell biotechnology. *Critical Reviews in Biotechnology*, 10 (2), 155-178.

MacVicar, B.A., and Newman, E.A., 2015. Astrocyte regulation of blood flow in the brain. *Cold Spring Harbor Perspectives in Biology*, 7 (5), 10.1101/cshperspect.a020388.

Mahairaki, V., Lim, S.H., Christopherson, G.T., Xu, L., Nasonkin, I., Yu, C., Mao, H. and Koliatsos, V.E., 2010. Nanofiber matrices promote the neuronal differentiation of human embryonic stem cell-derived neural precursors in vitro. *Tissue Engineering Part A*, 17 (5-6), 855-863.

Malagelada, C., Jin, Z.H., Jackson-Lewis, V., Przedborski, S. and Greene, L.A., 2010. Rapamycin protects against neuron death in in vitro and in vivo models of Parkinson's disease. *The Journal of Neuroscience : The Official Journal of the Society for Neuroscience*, 30 (3), 1166-1175.

Manning-Bog, A.B., McCormack, A.L., Li, J., Uversky, V.N., Fink, A.L. and Di Monte, D.A., 2002. The herbicide paraquat causes up-regulation and aggregation of alpha-synuclein in mice: paraquat and alpha-synuclein. *The Journal of Biological Chemistry*, 277 (3), 1641-1644.

Mathiasen, J.R., McKenna, B.A.W., Saporito, M.S., Ghadge, G.D., Roos, R.P., Holskin, B.P., Wu, Z., Trusko, S.P., Connors, T.C. and Maroney, A.C., 2004. Inhibition of mixed lineage kinase 3 attenuates MPP -induced neurotoxicity in SH-SY5Y cells. *Brain Research*, 1003 (1-2), 86-97.

McCann, J.T., Marquez, M. and Xia, Y., 2006. Melt coaxial electrospinning: a versatile method for the encapsulation of solid materials and fabrication of phase change nanofibers. *Nano Letters*, 6 (12), 2868-2872.

McNaught, K.S.P., Thull, U., Carrupt, P., Altomare, C., Cellamare, S., Carotti, A., Testa, B., Jenner, P. and Marsden, C.D., 1996. Nigral cell loss produced by infusion of isoquinoline derivatives structurally related to 1-methyl-4-phenyl-1, 2, 3, 6-tetrahydropyridine. *Neurodegeneration*, 5 (3), 265-274.

McPherson, A., 1992. Two approaches to the rapid screening of crystallization conditions. *Journal of Crystal Growth*, 122 (1-4), 161-167.

Min, S.K., Jung, S., Kim, S.H., Kim, C.R. and Shin, H.S., 2013. Implications of the oxygenated electrospun poly ( $\epsilon$ -caprolactone) nanofiber for the astrocytes activities. *Journal of Biomedical Materials Research Part B: Applied Biomaterials*, 101 (7), 1267-1274.

Miyazaki, I., Asanuma, M., Murakami, S., Takeshima, M., Torigoe, N., Kitamura, Y. and Miyoshi, K., 2013. Targeting 5-HT<sub>1A</sub> receptors in astrocytes to protect dopaminergic neurons in parkinsonian models. *Neurobiology of Disease*, 59 (0), 244-256.

Mladenova, Rosica, Ignatova, Milena, Manolova, Nevena, Petrova, Tsvetanka and Rashkov, Iliya, 2002. *Preparation, characterization and biological activity of Schiff base compounds derived from 8-hydroxyquinoline-2-carboxaldehyde and Jeffamines ED®*.

Moriarty, N., Pandit, A. and Dowd, E., 2017. Encapsulation of primary dopaminergic neurons in a GDNF-loaded collagen hydrogel increases their survival, re-innervation and function after intra-striatal transplantation. *Scientific Reports*, 7 (1), 16033.

Mosmann, Tim, 1983. *Rapid colorimetric assay for cellular growth and survival: Application to proliferation and cytotoxicity assays*.

Muthukumaran, K., Leahy, S., Harrison, K., Sikorska, M., Sandhu, J.K., Cohen, J., Keshan, C., Lopatin, D., Miller, H. and Borowy-Borowski, H., 2014. Orally delivered water soluble Coenzyme Q 10 (Ubisol-Q 10) blocks on-going neurodegeneration in rats exposed to paraquat: potential for therapeutic application in Parkinson's disease. *BMC Neuroscience*, 15 (1), 21.

Nayak, R., Padhye, R., Kyratzis, I.L., Truong, Y.B. and Arnold, L., 2012. Recent advances in nanofibre fabrication techniques. *Textile Research Journal*, 82 (2), 129-147.

Nguyen-Vu, T.B., Chen, H., Cassell, A.M., Andrews, R.J., Meyyappan, M. and Li, J., 2007. Vertically aligned carbon nanofiber architecture as a multifunctional 3-D neural electrical interface. *IEEE Transactions on Biomedical Engineering*, 54 (6), 1121-1128.

Nishiguchi, M., Tokugawa, K., Yamamoto, K., Akama, T., Nozawa, Y., Chaki, S., Ueki, T., Kameo, K. and Okuyama, S., 2003. Increase in secretion of glial cell line-derived neurotrophic factor from glial cell lines by inhibitors of vacuolar ATPase. *Neurochemistry International*, 42 (6), 493-498.

Noriega, S.E., Hasanova, G.I., Schneider, M.J., Larsen, G.F. and Subramanian, A., 2012. Effect of fiber diameter on the spreading, proliferation and differentiation of chondrocytes on electrospun chitosan matrices. *Cells, Tissues, Organs*, 195 (3), 207-221.

Novikova, L.N., Pettersson, J., Brohlin, M., Wiberg, M. and Novikov, L.N., 2008. Biodegradable poly- $\beta$ -hydroxybutyrate scaffold seeded with Schwann cells to promote spinal cord repair. *Biomaterials*, 29 (9), 1198-1206.

Nussbaum, R.L., and Ellis, C.E., 2003. Alzheimer's disease and Parkinson's disease. *New England Journal of Medicine*, 348 (14), 1356-1364.

O'Connor, S.M., Stenger, D.A., Shaffer, K.M., Maric, D., Barker, J.L. and Ma, W., 2000. Primary neural precursor cell expansion, differentiation and cytosolic Ca<sup>2</sup> response in three-dimensional collagen gel. *Journal of Neuroscience Methods*, 102 (2), 187-195.

Ogata, N., Yamaguchi, S., Shimada, N., Lu, G., Iwata, T., Nakane, K. and Ogihara, T., 2007. Poly (lactide) nanofibers produced by a melt-electrospinning system with a laser melting device. *Journal of Applied Polymer Science*, 104 (3), 1640-1645.

Oh, J., Jung, C., Lee, M., Kim, J. and Son, M., 2018. Comparative analysis of human embryonic stem cell-derived neural stem cells as an in vitro human model. *International Journal of Molecular Medicine*, 41 (2), 783-790.

Oh, S.E., Park, H., He, L., Skibieli, C., Junn, E. and Mouradian, M.M., 2018. The Parkinson's disease gene product DJ-1 modulates miR-221 to promote neuronal survival against oxidative stress. *Redox Biology*, 19, 62-73.

Ohara, P.T., Vit, J., Bhargava, A. and Jasmin, L., 2008. Evidence for a role of connexin 43 in trigeminal pain using RNA interference in vivo. *Journal of Neurophysiology*, 100 (6), 3064-3073.

Okrongly, D.A., Lamons, D. and Okarma, T.B., 1994. Stabilization of sterilized surfaces for research and medical use.

Orive, G., Anitua, E., Pedraz, J.L. and Emerich, D.F., 2009. Biomaterials for promoting brain protection, repair and regeneration. *Nature Reviews Neuroscience*, 10 (9), 682.

Ortinou, S., Schmich, J., Block, S., Liedmann, A., Jonas, L., Weiss, D.G., Helm, C.A., Rolfs, A. and Frech, M.J., 2010. Effect of 3D-scaffold

formation on differentiation and survival in human neural progenitor cells. *Biomed Eng Online*, 9 (1), 70.

Påhlman, S., Ruusala, A., Abrahamsson, L., Mattsson, M.E. and Esscher, T., 1984. Retinoic acid-induced differentiation of cultured human neuroblastoma cells: a comparison with phorbol ester-induced differentiation. *Cell Differentiation*, 14 (2), 135-144.

Pampaloni, F., Reynaud, E.G. and Stelzer, E.H., 2007. The third dimension bridges the gap between cell culture and live tissue. *Nature Reviews Molecular Cell Biology*, 8 (10), 839.

Pan, C., Kumar, C., Bohl, S., Klingmueller, U. and Mann, M., 2009. Comparative proteomic phenotyping of cell lines and primary cells to assess preservation of cell type-specific functions. *Molecular & Cellular Proteomics*, 8 (3), 443-450.

Pan, H., Jiang, H. and Chen, W., 2006. Interaction of dermal fibroblasts with electrospun composite polymer scaffolds prepared from dextran and poly lactide-co-glycolide. *Biomaterials*, 27 (17), 3209-3220.

Papuć, E., Kurzepa, J., Kurys-Denis, E., Grabarska, A., Krupski, W. and Rejdak, K., 2014. Humoral response against glial derived antigens in Parkinson's disease. *Neuroscience Letters*, 566, 77-81.

Parameswaran, S., and Verma, R.S., 2011. Scanning electron microscopy preparation protocol for differentiated stem cells. *Analytical Biochemistry*, 416 (2), 186-190.

Pardo, B., and Honegger, P., 2000. Differentiation of rat striatal embryonic stem cells in vitro: monolayer culture vs. three-dimensional coculture with differentiated brain cells. *Journal of Neuroscience Research*, 59 (4), 504-512.

Park, J., Lee, B.K., Jeong, G.S., Hyun, J.K., Lee, C.J. and Lee, S., 2015. Three-dimensional brain-on-a-chip with an interstitial level of flow and its application as an in vitro model of Alzheimer's disease. *Lab on a Chip*, 15 (1), 141-150.

Park, S.H., and Yang, D., 2011. Fabrication of aligned electrospun nanofibers by inclined gap method. *Journal of Applied Polymer Science*, 120 (3), 1800-1807.

Park, S.E., Song, K., Kim, H., Chung, S. and Youn, I., 2018. Graded 6-OHDA-induced dopamine depletion in the nigrostriatal pathway evokes progressive pathological neuronal activities in the subthalamic nucleus of a hemi-parkinsonian mouse. *Behavioural Brain Research*, 344, 42-47.

- Patino, M.G., Neiders, M.E., Andreana, S., Noble, B. and Cohen, R.E., 2002. Collagen as an implantable material in medicine and dentistry. *Journal of Oral Implantology*, 28 (5), 220-225.
- Pedron, S., Becka, E. and Harley, B.A., 2015. Spatially gradated hydrogel platform as a 3D engineered tumor microenvironment. *Advanced Materials*, 27 (9), 1567-1572.
- Peng, J., Oo, M.L. and Andersen, J.K., 2010. Synergistic effects of environmental risk factors and gene mutations in Parkinson's disease accelerate age-related neurodegeneration. *Journal of Neurochemistry*, 115 (6), 1363-1373.
- Peretz, H., Talpalar, A.E., Vago, R. and Baranes, D., 2007. Superior survival and durability of neurons and astrocytes on 3-dimensional aragonite biomatrices. *Tissue Engineering*, 13 (3), 461-472.
- Pillay, V., Dott, C., Choonara, Y.E., Tyagi, C., Tomar, L., Kumar, P., du Toit, L.C. and Ndesendo, V.M., 2013. A review of the effect of processing variables on the fabrication of electrospun nanofibers for drug delivery applications. *Journal of Nanomaterials*, 2013.
- Prajapati, S.K., Garabadu, D. and Krishnamurthy, S., 2017. Coenzyme Q10 prevents mitochondrial dysfunction and facilitates pharmacological activity of atorvastatin in 6-OHDA induced dopaminergic toxicity in rats. *Neurotoxicity Research*, 31 (4), 478-492.
- Purisai, M.G., McCormack, A.L., Langston, W.J., Johnston, L.C. and Di Monte, D.A., 2005.  $\alpha$ -Synuclein expression in the substantia nigra of MPTP-lesioned non-human primates. *Neurobiology of Disease*, 20 (3), 898-906.
- Purves, D., Augustine, G., Fitzpatrick, D., Katz, L., LaMantia, A., McNamara, J. and Williams, S., 2001. Neuroscience 2nd Edition. Sunderland (MA) Sinauer Associates.
- Rabey, J., and Hefti, F., 1990. Neuromelanin synthesis in rat and human substantia nigra. *Journal of Neural Transmission-Parkinson's Disease and Dementia Section*, 2 (1), 1-14.
- Rappold, Phillip M., and Tieu, Kim, 2010. *Astrocytes and Therapeutics for Parkinson's Disease*.
- Ravenstijn, P.G., Merlini, M., Hameetman, M., Murray, T.K., Ward, M.A., Lewis, H., Ball, G., Mottart, C., de Goyet, Christine de Ville and Lemarchand, T., 2008. The exploration of rotenone as a toxin for inducing Parkinson's disease in rats, for application in BBB transport and PK-PD

experiments. *Journal of Pharmacological and Toxicological Methods*, 57 (2), 114-130.

Redigueri, C.F., Sassonia, R.C., Dua, K., Kikuchi, I.S. and Pinto, Terezinha de Jesus Andreoli, 2016. Impact of sterilization methods on electrospun scaffolds for tissue engineering. *European Polymer Journal*, 82, 181-195.

Ren, M., Du, C., Acero, E.H., Tang-Schomer, M. and Özkucur, N., 2016. A biofidelic 3D culture model to study the development of brain cellular systems. *Scientific Reports*, 6, 24953.

Ren, J.P., Zhao, Y.W. and Sun, X.J., 2009. Toxic influence of chronic oral administration of paraquat on nigrostriatal dopaminergic neurons in C57BL/6 mice. *Chinese Medical Journal*, 122 (19), 2366-2371.

Reneker, D.H., and Chun, I., 1996. Nanometre diameter fibres of polymer, produced by electrospinning. *Nanotechnology*, 7 (3), 216.

Reneker, D.H., Chun, I. and Ertley, D., 2002. Process and apparatus for the production of nanofibers. *Process and Apparatus for the Production of Nanofibers*, .

Reneker, D.H., and Yarin, A.L., 2008. Electrospinning jets and polymer nanofibers. *Polymer*, 49 (10), 2387-2425.

Restrepo, A., Smith, C.A., Agnihotri, S., Shekarforoush, M., Kongkham, P.N., Seol, H.J., Northcott, P. and Rutka, J.T., 2010. Epigenetic regulation of glial fibrillary acidic protein by DNA methylation in human malignant gliomas. *Neuro-Oncology*, 13 (1), 42-50.

Reubinoff, B.E., Itsykson, P., Turetsky, T., Pera, M.F., Reinhartz, E., Itzik, A. and Ben-Hur, T., 2001. Neural progenitors from human embryonic stem cells. *Nature Biotechnology*, 19 (12), 1134.

Rieger, K.A., Birch, N.P. and Schiffman, J.D., 2013. Designing electrospun nanofiber mats to promote wound healing—a review. *Journal of Materials Chemistry B*, 1 (36), 4531-4541.

Risher, W.C., and Eroglu, C., 2012. Thrombospondins as key regulators of synaptogenesis in the central nervous system. *Matrix Biology*, 31 (3), 170-177.

Rojas, R., and Pinto, N.J., 2008. Using electrospinning for the fabrication of rapid response gas sensors based on conducting polymer nanowires. *IEEE Sensors Journal*, 8 (6), 951-953.

Rossi, F., and Cattaneo, E., 2002. Neural stem cell therapy for neurological diseases: dreams and reality. *Nature Reviews Neuroscience*, 3 (5), 401.

Roth, S., Zhang, S., Chiu, J., Wirth, E.K. and Schweizer, U., 2010. Development of a serum-free supplement for primary neuron culture reveals the interplay of selenium and vitamin E in neuronal survival. *Journal of Trace Elements in Medicine and Biology*, 24 (2), 130-137.

Rubert Sánchez, D., 2018. New hypothesis and treatment of Amyotrophic lateral sclerosis: a holistic point of view of the key evidence.

Rubinsztein, D.C., 2006. The roles of intracellular protein-degradation pathways in neurodegeneration. *Nature*, 443 (7113), 780.

Sadek, R.M., Mohammed, S.A., Abunbehan, A.R.K., Ghattas, Abdul Karim H Abdul, Badawi, M.R., Mortaja, M.N., Abu-Nasser, B.S. and Abu-Naser, S.S., 2019. Parkinson's Disease Prediction Using Artificial Neural Network.

Saeed, Y., Xie, B., Xu, J., Rehman, A., Hong, M., Hong, Q. and Deng, Y., 2015. Glial U87 cells protect neuronal SH-SY5Y cells from indirect effect of radiation by reducing oxidative stress and apoptosis. *Acta Biochimica Et Biophysica Sinica*, 47 (4), 250-257.

Sanchez, S., Jimenez, C., Carrera, A., Diaz-Nido, J., Avila, J. and Wandosell, F., 2004. A cAMP-activated pathway, including PKA and PI3K, regulates neuronal differentiation. *Neurochemistry International*, 44 (4), 231-242.

Sang, Q., Liu, X., Wang, L., Qi, L., Sun, W., Wang, W., Sun, Y. and Zhang, H., 2018. Curcumin Protects an SH-SY5Y Cell Model of Parkinson's Disease Against Toxic Injury by Regulating HSP90. *Cellular Physiology and Biochemistry : International Journal of Experimental Cellular Physiology, Biochemistry, and Pharmacology*, 51 (2), 681-691.

Sargetis, J., 2016. *Evaluation of Particulate Metal and Noise Exposures at a Foundry and Recommended Control Strategies*, .

Sayas, C.L., Moreno-Flores, M.T., Avila, J. and Wandosell, F., 1999. The neurite retraction induced by lysophosphatidic acid increases Alzheimer's disease-like Tau phosphorylation. *The Journal of Biological Chemistry*, 274 (52), 37046-37052.

Schmeichel, K.L., and Bissell, M.J., 2003. Modeling tissue-specific signaling and organ function in three dimensions. *Journal of Cell Science*, 116 (Pt 12), 2377-2388.

- Schnell, E., Klinkhammer, K., Balzer, S., Brook, G., Klee, D., Dalton, P. and Mey, J., 2007. Guidance of glial cell migration and axonal growth on electrospun nanofibers of poly- $\epsilon$ -caprolactone and a collagen/poly- $\epsilon$ -caprolactone blend. *Biomaterials*, 28 (19), 3012-3025.
- Schousboe, A., Bak, L.K. and Waagepetersen, H.S., 2013. Astrocytic control of biosynthesis and turnover of the neurotransmitters glutamate and GABA. *Frontiers in Endocrinology*, 4, 102.
- Schousboe, I., and Winther-Lindqvist, D., 2013. Introduction: children's play and development. *In: Introduction: children's play and development. Children's Play and Development*. Springer, 2013, pp. 1-11.
- Schreuder-Gibson, H., Gibson, P., Senecal, K., Sennett, M., Walker, J., Yeomans, W., ZIEGLER, D. and TSAI, P.P., 2002. Protective textile materials based on electrospun nanofibers. *Journal of Advanced Materials*, 34 (3), 44-55.
- Schüle, B., Pera, R.A.R. and Langston, J.W., 2009. Can cellular models revolutionize drug discovery in Parkinson's disease? *Biochimica Et Biophysica Acta (BBA)-Molecular Basis of Disease*, 1792 (11), 1043-1051.
- Schultz, W., 2007. Multiple dopamine functions at different time courses. *Annu.Rev.Neurosci.*, 30, 259-288.
- Schurr, M.J., Foster, K.N., Centanni, J.M., Comer, A.R., Wicks, A., Gibson, A.L., Thomas-Virnig, C.L., Schlosser, S.J., Faucher, L.D., Lokuta, M.A. and Allen-Hoffmann, B.L., 2009. Phase I/II clinical evaluation of StrataGraft: a consistent, pathogen-free human skin substitute. *The Journal of Trauma*, 66 (3), 866-73; discussion 873-4.
- Scott,Laura, Dawson,Valina L. and Dawson,Ted M., 2017. *Trumping neurodegeneration: Targeting common pathways regulated by autosomal recessive Parkinson's disease genes*.
- Seidel, D., Krinke, D., Jahnke, H., Hirche, A., Kloß, D., Mack, T.G., Striggow, F. and Robitzki, A., 2012. Induced tauopathy in a novel 3D-culture model mediates neurodegenerative processes: A real-time study on biochips. *PLoS One*, 7 (11), e49150.
- Sen, A., Bedding, J. and Gu, B., 2005. Process for forming polymeric micro and nanofibers.
- Shang, S., Yang, F., Cheng, X., Walboomers, X.F. and Jansen, J.A., 2010. The effect of electrospun fibre alignment on the behaviour of rat periodontal ligament cells.

Shen, J., Li, D., Jiang, F., Qiu, J. and Gao, C., 2009. Purification and concentration of collagen by charged ultrafiltration membrane of hydrophilic polyacrylonitrile blend. *Separation and Purification Technology*, 66 (2), 257-262.

Sheng, W.S., Hu, S., Feng, A. and Rock, R.B., 2013. Reactive oxygen species from human astrocytes induced functional impairment and oxidative damage. *Neurochemical Research*, 38 (10), 2148-2159.

Sherer, T.B., Betarbet, R., Stout, A.K., Lund, S., Baptista, M., Panov, A.V., Cookson, M.R. and Greenamyre, J.T., 2002. An in vitro model of Parkinson's disease: linking mitochondrial impairment to altered alpha-synuclein metabolism and oxidative damage. *The Journal of Neuroscience : The Official Journal of the Society for Neuroscience*, 22 (16), 7006-7015.

Sherer, T.B., Betarbet, R., Testa, C.M., Seo, B.B., Richardson, J.R., Kim, J.H., Miller, G.W., Yagi, T., Matsuno-Yagi, A. and Greenamyre, J.T., 2003. Mechanism of toxicity in rotenone models of Parkinson's disease. *The Journal of Neuroscience : The Official Journal of the Society for Neuroscience*, 23 (34), 10756-10764.

Shi, L., Huang, C., Luo, Q., Xia, Y., Liu, H., Li, L., Liu, W., Ma, W., Fang, J. and Tang, L., 2017. Pilot study: molecular risk factors for diagnosing sporadic Parkinson's disease based on gene expression in blood in MPTP-induced rhesus monkeys. *Oncotarget*, 8 (62), 105606.

Shi, Q., Chen, X., Lu, T. and Jing, X., 2008. The immobilization of proteins on biodegradable polymer fibers via click chemistry. *Biomaterials*, 29 (8), 1118-1126.

Shi, Z., Lou, M., Zhao, Y., Zhang, Q., Cui, D. and Wang, K., 2013. Effect of all-trans retinoic acid on the differentiation of U87 glioma stem/progenitor cells. *Cellular and Molecular Neurobiology*, 33 (7), 943-951.

Shimoji, M., Zhang, L., Mandir, A.S., Dawson, V.L. and Dawson, T.M., 2005. Absence of inclusion body formation in the MPTP mouse model of Parkinson's disease. *Molecular Brain Research*, 134 (1), 103-108.

Shiono, K., and Usukura, K., 1994. Stretch fabric for medical use.

Shishkina, T.V., Mishchenko, T.A., Mitroshina, E.V., Shirokova, O.M., Pimashkin, A.S., Kastalskiy, I.A., Mukhina, I.V., Kazantsev, V.B. and Vedunova, M.V., 2018. Glial cell line-derived neurotrophic factor (GDNF) counteracts hypoxic damage to hippocampal neural network function in vitro. *Brain Research*, 1678, 310-321.

Sill, T.J., and von Recum, H.A., 2008. Electrospinning: applications in drug delivery and tissue engineering. *Biomaterials*, 29 (13), 1989-2006.

Silva, G.A., Czeisler, C., Niece, K.L., Beniash, E., Harrington, D.A., Kessler, J.A. and Stupp, S.I., 2004. Selective differentiation of neural progenitor cells by high-epitope density nanofibers. *Science (New York, N.Y.)*, 303 (5662), 1352-1355.

Simao, D., Pinto, C., Piersanti, S., Weston, A., Peddie, C.J., Bastos, A.E., Licursi, V., Schwarz, S.C., Collinson, L.M. and Salinas, S., 2014. Modeling human neural functionality in vitro: three-dimensional culture for dopaminergic differentiation. *Tissue Engineering Part A*, 21 (3-4), 654-668.

Sisson, K., Zhang, C., Farach-Carson, M.C., Chase, D.B. and Rabolt, J.F., 2010. Fiber diameters control osteoblastic cell migration and differentiation in electrospun gelatin. *Journal of Biomedical Materials Research Part A*, 94 (4), 1312-1320.

Skaper, S.D., and Facci, L., 2018. Central Nervous System Neuron-Glia co-Culture Models and Application to Neuroprotective Agents. *In: Central Nervous System Neuron-Glia co-Culture Models and Application to Neuroprotective Agents. Neurotrophic Factors*. Springer, 2018, pp. 63-80.

Skop, N.B., Calderon, F., Cho, C.H., Gandhi, C.D. and Levison, S.W., 2014. Improvements in biomaterial matrices for neural precursor cell transplantation. *Molecular and Cellular Therapies*, 2 (1), 19.

Smeyne, M., and Smeyne, R.J., 2013. Glutathione metabolism and Parkinson's disease. *Free Radical Biology and Medicine*, 62, 13-25.

Sofroniew, M.V., and Vinters, H.V., 2010. Astrocytes: biology and pathology. *Acta Neuropathologica*, 119 (1), 7-35.

Speranskaya, Elena S., Beloglazova, Natalia V., Lenain, Pieterjan, De Saeger, Sarah, Wang, Zhanhui, Zhang, Suxia, Hens, Zeger, Knopp, Dietmar, Niessner, Reinhard, Potapkin, Dmitry V. and Goryacheva, Irina Yu, 2014. *Polymer-coated fluorescent CdSe-based quantum dots for application in immunoassay*.

Srivastava, Y., Loscertales, I., Marquez, M. and Thorsen, T., 2008. Electrospinning of hollow and core/sheath nanofibers using a microfluidic manifold. *Microfluidics and Nanofluidics*, 4 (3), 245-250.

Stockert, J.C., Blázquez-Castro, A., Cañete, M., Horobin, R.W. and Villanueva, Á, 2012. MTT assay for cell viability: Intracellular localization of the formazan product is in lipid droplets. *Acta Histochemica*, 114 (8), 785-796.

Stockert, J.C., Horobin, R.W., Colombo, L.L. and Blazquez-Castro, A., 2018. Tetrazolium salts and formazan products in Cell Biology: Viability assessment, fluorescence imaging, and labeling perspectives. *Acta Histochemica*, 120 (3), 159-167.

Stork, P.J., and Schmitt, J.M., 2002. Crosstalk between cAMP and MAP kinase signaling in the regulation of cell proliferation. *Trends in Cell Biology*, 12 (6), 258-266.

Stout, D.A., and Webster, T.J., 2012. Carbon nanotubes for stem cell control. *Materials Today*, 15 (7-8), 312-318.

Subramanian, A., Krishnan, U.M. and Sethuraman, S., 2011. Fabrication of uniaxially aligned 3D electrospun scaffolds for neural regeneration. *Biomedical Materials*, 6 (2), 025004.

Sundaray, B., Subramanian, V., Natarajan, T., Xiang, R., Chang, C. and Fann, W., 2004. Electrospinning of continuous aligned polymer fibers. *Applied Physics Letters*, 84 (7), 1222-1224.

Sveinbjornsdottir, S., 2016. The clinical symptoms of Parkinson's disease. *Journal of Neurochemistry*, 139 (S1), 318-324.

Takuma, K., Baba, A. and Matsuda, T., 2004. Astrocyte apoptosis: implications for neuroprotection. *Progress in Neurobiology*, 72 (2), 111-127.

Tanner, C.M., Kamel, F., Ross, G.W., Hoppin, J.A., Goldman, S.M., Korell, M., Marras, C., Bhudhikanok, G.S., Kasten, M. and Chade, A.R., 2011. Rotenone, paraquat, and Parkinson's disease. *Environmental Health Perspectives*, 119 (6), 866.

Taylor, T.N., Alter, S.P., Wang, M., Goldstein, D.S. and Miller, G.W., 2014. Reduced vesicular storage of catecholamines causes progressive degeneration in the locus ceruleus. *Neuropharmacology*, 76, 97-105.

Teismann, P., Tieu, K., Cohen, O., Choi, D., Wu, D.C., Marks, D., Vila, M., Jackson-Lewis, V. and Przedborski, S., 2003. Pathogenic role of glial cells in Parkinson's disease. *Movement Disorders*, 18 (2), 121-129.

Teraoka, A.A., and Teraoka, I., 2002. *Polymer solutions: an introduction to physical properties*. John Wiley & Sons.

Terrasso, A.P., Pinto, C., Serra, M., Filipe, A., Almeida, S., Ferreira, A.L., Pedrosa, P., Brito, C. and Alves, P.M., 2015. Novel scalable 3D cell based model for in vitro neurotoxicity testing: Combining human differentiated neurospheres with gene expression and functional endpoints. *Journal of Biotechnology*, 205, 82-92.

- Terron, A., Bal-Price, A., Pains, A., Monnet-Tschudi, F., Bennekou, S.H., Leist, M. and Schildknecht, S., 2018. An adverse outcome pathway for parkinsonian motor deficits associated with mitochondrial complex I inhibition. *Archives of Toxicology*, , 1-42.
- Thenmozhi,S., Dharmaraj,N., Kadirvelu,K. and Kim,Hak Yong, 2017. *Electrospun nanofibers: New generation materials for advanced applications*.
- Theron, A., Zussman, E. and Yarin, A., 2001. Electrostatic field-assisted alignment of electrospun nanofibres. *Nanotechnology*, 12 (3), 384.
- Timmins, N., Harding, F., Smart, C., Brown, M. and Nielsen, L., 2005. Method for the generation and cultivation of functional three-dimensional mammary constructs without exogenous extracellular matrix. *Cell and Tissue Research*, 320 (1), 207-210.
- Tiryaki, V.M., Ayres, V.M., Ahmed, I. and Shreiber, D.I., 2015. Differentiation of reactive-like astrocytes cultured on nanofibrillar and comparative culture surfaces. *Nanomedicine*, 10 (4), 529-545.
- Tong, J., Ang, L., Williams, B., Furukawa, Y., Fitzmaurice, P., Guttman, M., Boileau, I., Hornykiewicz, O. and Kish, S.J., 2015. Low levels of astroglial markers in Parkinson's disease: Relationship to  $\alpha$ -synuclein accumulation. *Neurobiology of Disease*, 82, 243-253.
- Tong, L., and Mazur, E., 2008. Glass nanofibers for micro-and nano-scale photonic devices. *Journal of Non-Crystalline Solids*, 354 (12-13), 1240-1244.
- Tovote, P., Esposito, M.S., Botta, P., Chaudun, F., Fadok, J.P., Markovic, M., Wolff, S.B., Ramakrishnan, C., Fenno, L. and Deisseroth, K., 2016. Midbrain circuits for defensive behaviour. *Nature*, 534 (7606), 206.
- Towbin, H., Staehelin, T. and Gordon, J., 1979. Electrophoretic transfer of proteins from polyacrylamide gels to nitrocellulose sheets: procedure and some applications. *Proceedings of the National Academy of Sciences of the United States of America*, 76 (9), 4350-4354.
- Tucker, N., Stanger, J., Staiger, M., Razzaq, H. and Hofman, K., 2012. The history of the science and technology of electrospinning from 1600 to 1995. *Journal of Engineered Fibers and Fabrics*, 7, 63-73.
- Tuin, S., Pourdeyhimi, B. and Lobo, E., 2016. Creating tissues from textiles: scalable nonwoven manufacturing techniques for fabrication of tissue engineering scaffolds. *Biomedical Materials*, 11 (1), 015017.

Tysseling-Mattiace, V.M., Sahni, V., Niece, K.L., Birch, D., Czeisler, C., Fehlings, M.G., Stupp, S.I. and Kessler, J.A., 2008. Self-assembling nanofibers inhibit glial scar formation and promote axon elongation after spinal cord injury. *The Journal of Neuroscience : The Official Journal of the Society for Neuroscience*, 28 (14), 3814-3823.

Ushiro, S., Takahashi, H. and Ueno, Y., 2018. Copolymer and medical device, separation membrane module for medical use, and blood purifier including the same.

Uysal, Onur, Sevimli, Tugba, Sevimli, Murat, Gunes, Sibel and Eker Sariboyaci, Ayla, 2018. *Chapter 17 - Cell and Tissue Culture: The Base of Biotechnology*. Academic Press.

van Duinen, V., Trietsch, S.J., Joore, J., Vulto, P. and Hankemeier, T., 2015. Microfluidic 3D cell culture: from tools to tissue models. *Current Opinion in Biotechnology*, 35, 118-126.

Varabhas, J., Chase, G.G. and Reneker, D., 2008. Electrospun nanofibers from a porous hollow tube. *Polymer*, 49 (19), 4226-4229.

Vasita, R., and Katti, D.S., 2006. Nanofibers and their applications in tissue engineering. *International Journal of Nanomedicine*, 1 (1), 15-30.

Venkatesh, K., Srikanth, L., Vengamma, B., Chandrasekhar, C., Sanjeevkumar, A., Mouleshwara Prasad, B.C. and Sarma, P.V., 2013. In vitro differentiation of cultured human CD34+ cells into astrocytes. *Neurology India*, 61 (4), 383-388.

Vergani, L., Grattarola, M. and Nicolini, C., 2004. Modifications of chromatin structure and gene expression following induced alterations of cellular shape. *The International Journal of Biochemistry & Cell Biology*, 36 (8), 1447-1461.

Verkhatsky, A., and Butt, A., 2013. Numbers: how many glial cells are in the brain? *Glial Physiology and Pathophysiology*, , 93-96.

Vila, M., Jackson-Lewis, V., Guégan, C., Teismann, P., Choi, D., Tieu, K. and Przedborski, S., 2001. The role of glial cells in Parkinson's disease. *Current Opinion in Neurology*, 14 (4), 483-489.

Vinci, M., Gowan, S., Boxall, F., Patterson, L., Zimmermann, M., Lomas, C., Mendiola, M., Hardisson, D. and Eccles, S.A., 2012. Advances in establishment and analysis of three-dimensional tumor spheroid-based functional assays for target validation and drug evaluation. *BMC Biology*, 10 (1), 29.

- Vizzeri, G., Weinreb, R.N., Gonzalez-Garcia, A.O., Bowd, C., Medeiros, F.A., Sample, P.A. and Zangwill, L.M., 2009. Agreement between spectral-domain and time-domain OCT for measuring RNFL thickness. *The British Journal of Ophthalmology*, 93 (6), 775-781.
- Wang, F., Ni, J., Wang, X., Xie, B., Feng, C., Zhao, S., Saeed, Y., Qing, H. and Deng, Y., 2015. Salsolinol damaged neuroblastoma SH-SY5Y cells induce proliferation of human monocyte THP-1 cells through the mTOR pathway in a co-culture system. *Neurochemical Research*, 40 (5), 932-941.
- Wang, X., Um, I.C., Fang, D., Okamoto, A., Hsiao, B.S. and Chu, B., 2005. Formation of water-resistant hyaluronic acid nanofibers by blowing-assisted electro-spinning and non-toxic post treatments. *Polymer*, 46 (13), 4853-4867.
- Wangxi, Z., Jie, L. and Gang, W., 2003. Evolution of structure and properties of PAN precursors during their conversion to carbon fibers. *Carbon*, 41 (14), 2805-2812.
- Weightman, A., Jenkins, S., Pickard, M., Chari, D. and Yang, Y., 2014. Alignment of multiple glial cell populations in 3D nanofiber scaffolds: Toward the development of multicellular implantable scaffolds for repair of neural injury. *Nanomedicine: Nanotechnology, Biology and Medicine*, 10 (2), 291-295.
- Wolosker, H., Dumin, E., Balan, L. and Foltyn, V.N., 2008. D-amino acids in the brain: D-serine in neurotransmission and neurodegeneration. *The FEBS Journal*, 275 (14), 3514-3526.
- Wood-Kaczmar, A., Gandhi, S., Yao, Z., Abramov, A.S., Miljan, E.A., Keen, G., Stanyer, L., Hargreaves, I., Klupsch, K. and Deas, E., 2008. PINK1 is necessary for long term survival and mitochondrial function in human dopaminergic neurons. *PloS One*, 3 (6), e2455.
- Wu, Q., Chen, X., Wan, L. and Xu, Z., 2012. Interactions between polyacrylonitrile and solvents: density functional theory study and two-dimensional infrared correlation analysis. *The Journal of Physical Chemistry B*, 116 (28), 8321-8330.
- Xie, H., Hu, L. and Li, G., 2010. sh-sy5y human neuroblastoma cell line: in vitro cell model of dopaminergic neurons in Parkinson's disease. *Chinese Medical Journal*, 123 (8), 1086-1092.
- Xie, J., MacEwan, M.R., Ray, W.Z., Liu, W., Siewe, D.Y. and Xia, Y., 2010. Radially aligned, electrospun nanofibers as dural substitutes for wound closure and tissue regeneration applications. *ACS Nano*, 4 (9), 5027-5036.

- Xing, F., Luan, Y., Cai, J., Wu, S., Mai, J., Gu, J., Zhang, H., Li, K., Lin, Y. and Xiao, X., 2017. The anti-warburg effect elicited by the cAMP-PGC1 $\alpha$  pathway drives differentiation of glioblastoma cells into astrocytes. *Cell Reports*, 18 (2), 468-481.
- Xing, X., Wang, Y. and Li, B., 2008. Nanofiber drawing and nanodevice assembly in poly (trimethylene terephthalate). *Optics Express*, 16 (14), 10815-10822.
- Xu, C., Inai, R., Kotaki, M. and Ramakrishna, S., 2004. Electrospun nanofiber fabrication as synthetic extracellular matrix and its potential for vascular tissue engineering. *Tissue Engineering*, 10 (7-8), 1160-1168.
- Xu, X., Li, X., Peng, S., Xiao, J., Liu, C., Fang, G., Chen, K.C. and Chen, G., 2010. The behaviour of neural stem cells on polyhydroxyalkanoate nanofiber scaffolds. *Biomaterials*, 31 (14), 3967-3975.
- Yamada, K., Pankov, R. and Cukierman, E., 2003. Dimensions and dynamics in integrin function. *Brazilian Journal of Medical and Biological Research*, 36 (8), 959-966.
- Yan, M.H., Wang, X. and Zhu, X., 2013. Mitochondrial defects and oxidative stress in Alzheimer disease and Parkinson disease. *Free Radical Biology and Medicine*, 62, 90-101.
- Yang, L., Jackson, E., Woerner, B.M., Perry, A., Piwnica-Worms, D. and Rubin, J.B., 2007. Blocking CXCR4-mediated cyclic AMP suppression inhibits brain tumor growth in vivo. *Cancer Research*, 67 (2), 651-658.
- Yarin, A., and Zussman, E., 2004. Upward needleless electrospinning of multiple nanofibers. *Polymer*, 45 (9), 2977-2980.
- Yixiang, D., Yong, T., Liao, S., Chan, C.K. and Ramakrishna, S., 2008. Degradation of electrospun nanofiber scaffold by short wave length ultraviolet radiation treatment and its potential applications in tissue engineering. *Tissue Engineering Part A*, 14 (8), 1321-1329.
- Yoo, H.S., Kim, T.G. and Park, T.G., 2009. Surface-functionalized electrospun nanofibers for tissue engineering and drug delivery. *Advanced Drug Delivery Reviews*, 61 (12), 1033-1042.
- Yovcheva, T.A., Avramova, I.A., Mekishev, G.A. and Marinova, T.S., 2007. Corona-charged polypropylene electrets analyzed by XPS. *Journal of Electrostatics*, 65 (10-11), 667-671.
- Yu, L., Shao, Z., Xu, L. and Wang, M., 2017. High throughput preparation of aligned nanofibers using an improved bubble-electrospinning. *Polymers*, 9 (12), 658.

Zagho, M.M., and Elzatahry, A., 2016. Recent Trends in Electrospinning of Polymer Nanofibers and their Applications as Templates for Metal Oxide Nanofibers Preparation. *In: Recent Trends in Electrospinning of Polymer Nanofibers and their Applications as Templates for Metal Oxide Nanofibers Preparation. Electrospinning-Material, Techniques, and Biomedical Applications.* InTech, 2016, .

Zahedi, P., Rezaeian, I., Ranaei-Siadat, S., Jafari, S. and Supaphol, P., 2010. A review on wound dressings with an emphasis on electrospun nanofibrous polymeric bandages. *Polymers for Advanced Technologies*, 21 (2), 77-95.

Zeng, X., Geng, W. and Jia, J., 2018. Neurotoxin-induced animal models of Parkinson disease: Pathogenic mechanism and assessment. *ASN Neuro*, 10, 1759091418777438.

Zeng, X., Jia, J., Kwon, Y., Wang, S. and Bai, J., 2014. The role of thioredoxin-1 in suppression of endoplasmic reticulum stress in Parkinson disease. *Free Radical Biology and Medicine*, 67, 10-18.

Zhang, L., Le, W., Xie, W. and Dani, J.A., 2012. Age-related changes in dopamine signaling in Nurr1 deficient mice as a model of Parkinson's disease. *Neurobiology of Aging*, 33 (5), 1001. e7-1001. e16.

Zhou, H., Green, T.B. and Joo, Y.L., 2006. The thermal effects on electrospinning of polylactic acid melts. *Polymer*, 47 (21), 7497-7505.

Zhuang, P., Sun, A.X., An, J., Chua, C.K. and Chew, S.Y., 2018. 3D neural tissue models: From spheroids to bioprinting. *Biomaterials*, 154, 113-133.

Zimmermann, Jörg, Bittner, Katharina, Stark, Björn and Mülhaupt, Rolf, 2002. *Novel hydrogels as supports for in vitro cell growth: poly(ethylene glycol)- and gelatine-based (meth)acrylamido peptide macromonomers.*

Zotter, S., Pircher, M., Götzinger, E., Torzicky, T., Yoshida, H., Hirose, F., Holzer, S., Kroisamer, J., Vass, C. and Schmidt-Erfurth, U., 2013. Measuring retinal nerve fiber layer birefringence, retardation, and thickness using wide-field, high-speed polarization sensitive spectral domain OCT. *Investigative Ophthalmology & Visual Science*, 54 (1), 72-84.

<https://www.nhs.uk/conditions/parkinsons-disease/#treating-parkinsons-disease>

[https://www.ageuk.org.uk/globalassets/age-uk/documents/reports-and-publications/late\\_life\\_uk\\_factsheet.pdf?dtrk=true](https://www.ageuk.org.uk/globalassets/age-uk/documents/reports-and-publications/late_life_uk_factsheet.pdf?dtrk=true)

<http://www.imperial.ac.uk/news/126466/cost-brain-disorders-uk-estimated-112/>

<http://www.parkinson.org/Understanding-Parkinsons/Treatment/Surgical-Treatment-Options/Deep-Brain-Stimulation>

<https://www.qiagen.com/gb/shop/genes-and-pathways/pathway-details/?pwid=345>

<https://www.sigmaaldrich.com/catalog/product/sigma/r8875?lang=en&region=GB>

<https://www.sigmaaldrich.com/catalog/product/sigma/m0896?lang=en&region=GB>

<https://www.sigmaaldrich.com/catalog/product/sigma/m8699?lang=en&region=GB>

<https://www.sigmaaldrich.com/catalog/product/sigma/b2515?lang=en&region=GB>

[https://www.huntsman.com/performance\\_products/Media%20Library/a\\_MC348531CFA3EA9A2E040EBCD2B6B7B06/Products\\_MC348531D0B9FA9A2E040EBCD2B6B7B06/Amines\\_MC348531D0BECA9A2E040EBCD2B6B7B06/Polyetheramines%20%20%20JE\\_MC348531D0E07A9A2E040EBCD2B6B7B06/files/JEFFAMINE%20Polyetheramines%20booklet%20-%2010-12R1\\_2.pdf](https://www.huntsman.com/performance_products/Media%20Library/a_MC348531CFA3EA9A2E040EBCD2B6B7B06/Products_MC348531D0B9FA9A2E040EBCD2B6B7B06/Amines_MC348531D0BECA9A2E040EBCD2B6B7B06/Polyetheramines%20%20%20JE_MC348531D0E07A9A2E040EBCD2B6B7B06/files/JEFFAMINE%20Polyetheramines%20booklet%20-%2010-12R1_2.pdf)

[https://hamptonresearch.com/tip\\_detail.aspx?id=203](https://hamptonresearch.com/tip_detail.aspx?id=203)

<https://www.thermofisher.com/order/catalog/product/398-0001>

<https://www.labmanager.com/insights/2016/02/the-case-for-primary-cells#.XJEPsyj7SM8>

<https://medicalxpress.com/news/2019-01-defective-glia-cells-neurons-parkinson.html>